

# **Structural and Biochemical Characterization of the Rod-Zwilch-Zw10 complex**

## **Dissertation**

Zur Erlangung des Doktorgrades  
(Dr. rer. Nat.)  
der Fakultät Chemie an der  
Technischen Universität Dortmund

angefertigt am  
Max-Planck-Institut für molekulare Physiologie, Dortmund,

vorgelegt von  
M.Sc. Anika Altenfeld  
geboren am 19.09.1986 in Hattingen

September 2015

The work described in this dissertation was carried out between January 2012 and June 2015 under the guidance of H. Prof. Dr. Andrea Musacchio at the Max-Planck-Institute for molecular Physiology, Dortmund in the Department of Mechanistic Cell Biology.

First supervisor: Prof. Dr. Roland Winter

Second supervisor: H. Prof. Dr. Andrea Musacchio

Die vorliegende Arbeit wurde in der Zeit von Januar 2012 bis Juli 2015 am Max-Planck-Institut für molekulare Physiologie in der Abteilung für mechanistische Zellbiologie angefertigt.

# Index

|                                                                                                |            |
|------------------------------------------------------------------------------------------------|------------|
| List of Figures .....                                                                          | v          |
| <b>1 Abstract and Zusammenfassung .....</b>                                                    | <b>10</b>  |
| Abstract.....                                                                                  | 10         |
| Zusammenfassung.....                                                                           | 12         |
| <b>2 Introduction .....</b>                                                                    | <b>14</b>  |
| 2.1 Mitosis, the key event of the cell cycle .....                                             | 14         |
| 2.2 Kinetochore organization and assembly .....                                                | 21         |
| 2.3 Regulation of kinetochore microtubule attachments .....                                    | 24         |
| 2.4 The spindle assembly checkpoint .....                                                      | 29         |
| 2.5 The RZZ complex.....                                                                       | 36         |
| 2.6 Functions of the RZZ complex .....                                                         | 41         |
| <b>3 Objective.....</b>                                                                        | <b>46</b>  |
| <b>4 Results.....</b>                                                                          | <b>48</b>  |
| 4.1 Characterization of the RZZ complex.....                                                   | 48         |
| 4.1.1 Purification of the full length RZZ complex.....                                         | 48         |
| 4.1.2 Analytical Ultracentrifugation.....                                                      | 51         |
| 4.1.3 Thermofluor Analysis .....                                                               | 53         |
| 4.1.4 Limited Proteolysis .....                                                                | 54         |
| 4.1.5 Crystallogenesi.....                                                                     | 56         |
| 4.1.6 Data Collection and processing .....                                                     | 59         |
| 4.1.7 Self Rotation Function.....                                                              | 62         |
| 4.2 Electron microscopy analysis of the RZZ complex .....                                      | 63         |
| 4.2.1 Cryo EM of the RZZ complex.....                                                          | 63         |
| 4.2.2 Protein labeling for negative stain EM.....                                              | 64         |
| 4.2.3 Cross-Linking Analysis.....                                                              | 66         |
| 4.2.4 Fitting of crystal structures and homology models into the 3D density EM map of RZZ..... | 70         |
| 4.2.5 Model Validation –Mini RZZ.....                                                          | 73         |
| 4.2.6 Model Validation -Mini-Rod.....                                                          | 77         |
| 4.3 Functional Assays .....                                                                    | 80         |
| 4.3.1 Zw10 forms a complex with Knl1/Zwint-1 but not with the KMN complex.....                 | 80         |
| 4.3.2 Does the RZZ complex bind any kinetochore proteins? .....                                | 85         |
| 4.3.3 Microinjection of the RZZ complex into human cells.....                                  | 88         |
| 4.3.4 Spindly interaction.....                                                                 | 90         |
| <b>5 Discussion .....</b>                                                                      | <b>105</b> |
| 5.1 Structural organization of the RZZ complex.....                                            | 105        |
| 5.2 RZZ kinetochore recruitment.....                                                           | 109        |
| 5.3 RZZ function in SAC activation .....                                                       | 110        |
| 5.3.1 RZZ function in SAC silencing .....                                                      | 111        |
| 5.3.2 Dynein/Dynactin interaction .....                                                        | 112        |
| 5.4 Model of RZZ function.....                                                                 | 113        |
| <b>6 Materials and Methods .....</b>                                                           | <b>115</b> |
| 6.1 Methods .....                                                                              | 115        |
| 6.1.1 Chemicals .....                                                                          | 115        |
| 6.1.2 Kits .....                                                                               | 115        |

|        |                                                                             |     |
|--------|-----------------------------------------------------------------------------|-----|
| 6.1.3  | <i>Markers</i>                                                              | 116 |
| 6.1.4  | <i>Microorganisms and cell lines</i>                                        | 117 |
| 6.1.5  | <i>Vectors and constructs</i>                                               | 118 |
| 6.1.6  | <i>Enzymes</i>                                                              | 119 |
| 6.1.7  | <i>Media, antibiotics and transfection reagents</i>                         | 120 |
| 6.1.8  | <i>Columns</i>                                                              | 121 |
| 6.1.9  | <i>Laboratory Equipment</i>                                                 | 122 |
| 6.1.11 | <i>Frequently used buffers</i>                                              | 124 |
| 6.2    | <b>Methods Molecular Biology</b>                                            | 126 |
| 6.2.1  | <i>Plasmid Purification</i>                                                 | 126 |
| 6.2.2  | <i>Polymerase Chain Reaction</i>                                            | 126 |
| 6.2.3  | <i>Agarose Gel Electrophoresis</i>                                          | 127 |
| 6.2.4  | <i>Restriction Digest</i>                                                   | 127 |
| 6.2.5  | <i>Ligation</i>                                                             | 127 |
| 6.2.6  | <i>Transformation of DNA into E. coli cells</i>                             | 128 |
| 6.2.7  | <i>Colony PCR</i>                                                           | 128 |
| 6.2.8  | <i>DNA sequencing</i>                                                       | 129 |
| 6.2.9  | <i>Baculo-Transfection and Virus Amplification in sf9 cells</i>             | 130 |
| 6.3    | <b>Methods Biochemistry</b>                                                 | 132 |
| 6.3.1  | <i>Protein Expression test (insect cells)</i>                               | 132 |
| 6.3.2  | <i>Protein Expression</i>                                                   | 132 |
| 6.3.3  | <i>Cell lysis</i>                                                           | 132 |
| 6.3.4  | <i>Immobilized Metal Ion Affinity Chromatography (IMAC)</i>                 | 133 |
| 6.3.5  | <i>Ion Exchange Chromatography</i>                                          | 133 |
| 6.3.6  | <i>Concentration of protein samples</i>                                     | 133 |
| 6.3.7  | <i>Dialysis of protein samples</i>                                          | 134 |
| 6.3.8  | <i>Determination of protein concentrations</i>                              | 134 |
| 6.3.9  | <i>Size Exclusion Chromatography (SEC)</i>                                  | 134 |
| 6.3.10 | <i>Sodiumdodecylsulfate-Polyacrylamide Gelelectrophoresis (SDS-PAGE)</i>    | 134 |
| 6.3.11 | <i>Western Blot Analysis</i>                                                | 136 |
| 6.3.12 | <i>Expression and purification of Zw10</i>                                  | 136 |
| 6.3.13 | <i>Expression and purification of Spindly</i>                               | 137 |
| 6.3.14 | <i>Expression and purification of RZZ</i>                                   | 137 |
| 6.3.15 | <i>Expression and purification of Mini-RZZ</i>                              | 138 |
| 6.3.16 | <i>Expression and purification of Mini-Rod/Zwilch</i>                       | 138 |
| 6.3.17 | <i>Analytical SEC migration shift assay</i>                                 | 138 |
| 6.3.18 | <i>Limited proteolysis</i>                                                  | 139 |
| 6.3.19 | <i>In-gel digestion for mass spectrometric characterization of proteins</i> | 139 |
| 6.3.20 | <i>Analytical Ultracentrifugation</i>                                       | 140 |
| 6.3.21 | <i>Thermofluor Assay</i>                                                    | 140 |
| 6.3.22 | <i>Cross-linking Analysis coupled with mass spectrometry</i>                | 141 |
| 6.3.23 | <i>SILAC Immunoprecipitation experiments</i>                                | 141 |
| 6.3.24 | <i>Microinjection of human cells with recombinant proteins</i>              | 142 |
| 6.3.25 | <i>Crystallogenesis</i>                                                     | 143 |
| 6.3.26 | <i>Data Collection and Processing</i>                                       | 147 |
| 7      | <b>References</b>                                                           | 148 |
| 8      | <b>Supplementary Information</b>                                            | 163 |

## List of Figures

|                                                                                                                                         |     |
|-----------------------------------------------------------------------------------------------------------------------------------------|-----|
| Figure 1: Overview of the six phases during mitosis.....                                                                                | 16  |
| Figure 2: The anaphase promoting complex .....                                                                                          | 18  |
| Figure 3: The mitotic Spindle .....                                                                                                     | 19  |
| Figure 4: Dynamic instability of microtubules.....                                                                                      | 20  |
| Figure 5: Centromere organization .....                                                                                                 | 22  |
| Figure 6: Schematic of kinetochore organization.....                                                                                    | 23  |
| Figure 7: Kinetochore-microtubule attachment.....                                                                                       | 25  |
| Figure 10: Crystal structure of Zwilch .....                                                                                            | 38  |
| Figure 11: Model of RZZ function .....                                                                                                  | 45  |
| Figure 12: Nickel resin affinity column purification of the RZZ complex .....                                                           | 49  |
| Figure 13: Size exclusion chromatography of the RZZ complex .....                                                                       | 50  |
| Figure 14: Analytical Ultracentrifugation of the RZZ complex.....                                                                       | 52  |
| Figure 15: Thermofluor analysis of the RZZ complex.....                                                                                 | 53  |
| Figure 16: Limited proteolysis of the full length RZZ complex .....                                                                     | 55  |
| Figure 17: Obtained RZZ crystals.....                                                                                                   | 57  |
| Figure 18: SDS PAGE analysis of RZZ crystals .....                                                                                      | 58  |
| Figure 19: Diffraction pattern of the RZZ crystals .....                                                                                | 61  |
| Figure 20: Self-rotation functions of three sections.....                                                                               | 62  |
| Figure 21: Representative views of the 3D structure of the RZZ complex.....                                                             | 64  |
| Figure 22: Antibody labeling studies on the RZZ complex.....                                                                            | 65  |
| Figure 23: Visualization of the cross-links within the RZZ complex .....                                                                | 67  |
| Figure 24: Zwilch and Zw10 do not show interaction is SEC.....                                                                          | 68  |
| Figure 25: Cartoon representation of the RZZ domain organization and<br>cross-links.....                                                | 69  |
| Figure 26: Rigid body fit of subunits into the RZZ 3D density.....                                                                      | 72  |
| Figure 27: Cartoon representation of the Mini-RZZ complex.....                                                                          | 73  |
| Figure 28: Size exclusion chromatography of the Mini-RZZ complex.....                                                                   | 74  |
| Figure 29: Representative negative stain class averages of the Mini-RZZ<br>complex .....                                                | 75  |
| Figure 30: Representative views of Mini-RZZ.....                                                                                        | 75  |
| Figure 31: Comparison of Mini-RZZ and RZZ.....                                                                                          | 76  |
| Figure 32: Cartoon representation of the Mini-Rod/Zwilch construct.....                                                                 | 77  |
| Figure 33: Coexpression of Mini-Rod with Zw10 or Zwilch.....                                                                            | 78  |
| Figure 34: The Mini-Rod/Zwilch complex does not interact with Zw10.....                                                                 | 79  |
| Figure 35: Knl1/Zwint-1 does interact with Zw10 .....                                                                                   | 81  |
| Figure 36: Zw10 does not interact with the KMN network .....                                                                            | 83  |
| Figure 37: Knl1/Zwint-1 does not interact with the RZZ complex .....                                                                    | 84  |
| Figure 38: Recombinant RZZ localizes to kinetochores in mitotic HeLa cells .....                                                        | 89  |
| Figure 39: Schematic view of the SILAC experiment.....                                                                                  | 91  |
| Figure 40: Identification of RZZ interacting under the influence of detergents .....                                                    | 93  |
| Figure 41: LFQ intensities of heavy peaks of the detergent free and detergent<br>containing experiment plotted against each other ..... | 95  |
| Figure 42: The RZZ complex interacts with farnesylated Spindly.....                                                                     | 97  |
| Figure 43: Cdk1 phosphorylation does not influence the interaction of RZZ with<br>farnesylated Spindly .....                            | 99  |
| Figure 44: Zw10 does not interact with farnesylated Spindly.....                                                                        | 101 |
| Figure 45: Zwilch does not interact with farnesylated Spindly .....                                                                     | 102 |
| Figure 46: The Mini-Rod/Zwilch complex does not interact with farnesylated<br>Spindly .....                                             | 103 |

|                                                                               |     |
|-------------------------------------------------------------------------------|-----|
| Figure 47: The Mini RZZ complex does interact with farnesylated Spindly ..... | 104 |
| Figure 48: Membrane-coating scaffolds of the NPC and vesicle coats .....      | 107 |
| Figure 49: Model for the functions of RZZ at kinetochores .....               | 114 |
| Figure 53: Thermofluor analysis of the Mini-RZZ complex .....                 | 168 |
| Figure 54: Final step of Spindly purification .....                           | 169 |
| Figure 55: Spindly farnesylation after FTase and FPP incubation .....         | 170 |

## List of Tables

|                                                                                                          |     |
|----------------------------------------------------------------------------------------------------------|-----|
| Table 1: Data collection and processing .....                                                            | 60  |
| Table 2: Statistics of the Matthews Calculation .....                                                    | 60  |
| Table 3: Overview of RZZ interaction trials with other kinetochore proteins or<br>protein complexes..... | 86  |
| Table 4: List of all used Kits .....                                                                     | 115 |
| Table 5: List of all used markers .....                                                                  | 116 |
| Table 6: List of all used microorganisms.....                                                            | 117 |
| Table 7: List of all used vectors and designed constructs .....                                          | 118 |
| Table 8: List of all used enzymes.....                                                                   | 119 |
| Table 9: List of all used media, antibiotics and transfection reagents.....                              | 120 |
| Table 10: List of all used columns and beads.....                                                        | 121 |
| Table 11: List of the laboratory equipment.....                                                          | 122 |
| Table 12: List of frequently used buffers .....                                                          | 124 |
| Table 13: PCR pipetting scheme .....                                                                     | 126 |
| Table 14: PCR program .....                                                                              | 127 |
| Table 15: Colony-PCR pipetting scheme .....                                                              | 128 |
| Table 16: Colony-PCR program.....                                                                        | 128 |
| Table 17: Pipetting scheme for 4 SDS gels .....                                                          | 135 |
| Table 18: Overview crystallogensis attempts.....                                                         | 145 |
| Table 21: List of all crosslinks within the RZZ complex .....                                            | 163 |
| Table 22: Confidence values for structural models of RZZ domains .....                                   | 168 |

## List of abbreviations

|                |                                                      |
|----------------|------------------------------------------------------|
| 3C             | PreScission (Protease)                               |
| Å              | Angström ( $10^{-10}$ m)                             |
| ADP            | Adenosindiphosphate                                  |
| al.            | Lat.: alii                                           |
| Amp            | Ampicilline                                          |
| APC/C          | Anaphase promoting complex / cyclosome               |
| APS            | Ammoniumpersulfate                                   |
| ATP            | Adenosintriphosphate                                 |
| AU             | Absorbance units                                     |
| β-ME           | β-Mercapto ethanole                                  |
| BAC            | Bacterial artificial chromosome                      |
| bp             | Base pair                                            |
| Bub            | Budding uninhibited by benomyl                       |
| CCAN           | Constitutive centromere associated network           |
| Cdk            | Cyclin dependent kinase                              |
| cpm            | Counts per minutes                                   |
| C-Terminus     | Carboxy-Terminus                                     |
| Cyc            | Cyclin                                               |
| Da             | Dalton                                               |
| DNA            | Deoxyribonucleic acid                                |
| dNTP           | Desoxy nucleotide triphosphate                       |
| DMSO           | Dimethyl sulfoxide                                   |
| DTE            | Dithioerythritole                                    |
| DTT            | Dithioerythritole                                    |
| <i>E. coli</i> | <i>Escherichia coli</i>                              |
| EDTA           | Ethylenediaminetetraacetic acid                      |
| ER             | Endoplasmatic Reticulum                              |
| ESI-MS         | Electrospray ionisation mass spectrometry            |
| GFP            | Green fluorescent protein                            |
| GST            | Glutathione S transferase                            |
| GTP            | Guanosine triphosphate                               |
| H3             | Histone 3                                            |
| HEPES          | N-(2-hydroxyethyle) piperazine-2-ethanesulfonic acid |
| HPLC           | High performance liquid chromatography               |
| IP             | Immuno precipitation                                 |
| IPTG           | Isopropyl β-D-1-thiogalactopyranosid                 |
| ITC            | Isothermal titration calorimetry                     |
| Kan            | Kanamycine                                           |
| kb             | Kilo base                                            |
| KMN            | Kn1 complex - Mis12 complex - Ndc80 complex          |
| LB             | Lysogeny broth                                       |
| Mad            | Mitotic arrest deficient                             |
| MCC            | Mitotic checkpoint complex                           |
| mCherry        | Monomeric cherry                                     |
| Mg             | Magnesium                                            |
| RNAi           | Ribonucleic acid interference                        |
| Ni-NTA         | Nickel-nitrilotriacetic acid                         |
| nt             | Nucleotide                                           |
| N-Terminus     | Amino-Terminus                                       |
| ODx            | Optic density at wavelength x                        |
| PAGE           | Polyacrylamide gel electrophoresis                   |
| PBS            | Phosphate buffered saline                            |
| PCR            | Polymerase chain reaction                            |



|                      |                                   |
|----------------------|-----------------------------------|
| PDB                  | Protein data base                 |
| PEG                  | Polyethyleneglycole               |
| Plk                  | Polo-like kinase                  |
| pSer                 | Phosphoserine                     |
| pThr                 | Phosphothreonine                  |
| pTyr                 | Phosphotyrosine                   |
| RNA                  | Ribonucleic acid                  |
| Rod                  | Rough deal                        |
| rpm                  | Revolutions per minute            |
| RT                   | Room temperature                  |
| RZZ                  | Rod-Zw10-Zwilch                   |
| SAC                  | Spindle assembly checkpoint       |
| <i>S. cerevisiae</i> | <i>Saccharomyces cerevisiae</i>   |
| SDS                  | Sodium dodecyl sulfate            |
| SEC                  | Size exclusion chromatography     |
| SN                   | Supernatant                       |
| TCEP                 | Tris-(2-carboxyethyl)phosphine    |
| TEMED                | Tetramethylethylenediamine        |
| TEV                  | Tobacco Etch Virus                |
| TOF                  | Time of flight                    |
| TFA                  | Trifluoroacetic acid              |
| T <sub>m</sub>       | Melting temperture                |
| Tris                 | Tris-(hydroxymethyl)-aminomethane |
| v/v                  | Volume per volume                 |
| w/v                  | Weight per volume                 |
| WCE                  | Whole cell extract                |
| wt                   | Wildtype                          |
| Zw10                 | Zeste white 10                    |

Amino acids are abbreviated as recommended in the international union of pure and applied chemistry (IUPAC) and international union of biochemistry and molecular biology (IUB).

# 1 Abstract and Zusammenfassung

## Abstract

The 3-subunit Rod-Zwilch-Zw10 (RZZ) complex is a crucial component of the spindle assembly checkpoint (SAC) in higher eukaryotes. It is required for kinetochore localization of the Mad1/Mad2 checkpoint complex and of the microtubule motor Dynein, thus contributing to kinetochore-microtubule attachment as well as to the Dynein-dependent stripping of SAC components upon checkpoint satisfaction. How the RZZ fulfills these different roles and integrates signals from the kinetochore-microtubule interface remains unclear.

In my doctoral thesis, I report the successful recombinant production and a preliminary crystallographic analysis of the 813 kDa RZZ complex from co-expression of its three subunits Rod, Zwilch, and Zw10. Additionally the organization and function of the RZZ complex was studied by using a multidisciplinary approach that combines structural biology and biochemistry. Cryo electron microscopy combined with cross-linking mass spectrometry analysis provided insight into the structural organization of the RZZ complex. The resulting molecular model shows that the RZZ complex is a 2:2:2 hexamer in which the two Rod molecules form an elongated antiparallel dimer. At either end of the structure the Rod heads interact with Zwilch, using both the N-terminal beta-propeller domain, and its C-terminal region. Zw10 bridges the middle parts of both Rod molecules. Together, Rod, Zwilch and Zw10 create a very extensive dimerization interface that explains the stoichiometry of the complex. Furthermore, I describe an extensive series of interaction studies of the RZZ complex with other kinetochore components that have been suggested to be involved in the RZZ function. I demonstrate for the first time a direct interaction between the RZZ complex and Spindly that strictly depends on farnesylation of the C-terminal CAAX-box of Spindly.

Our studies pave the way to a detailed structural and functional characterization of the RZZ complex and support a model by which Spindly farnesylation promotes its interaction with kinetochores and mediates its biological function. We propose that upon SAC activation Spindly becomes farnesylated by a Farnesyltransferase and binds to the RZZ complex. This in turn enables further recruitment of Dynein/Dynactin to the kinetochore. Upon binding of the minus-end directed motor

## Abstract

protein Dynein, checkpoint proteins are transported away from kinetochores towards the spindle poles.

## Zusammenfassung

In höher entwickelten Eukaryoten ist der aus drei Proteinen bestehende Rod-Zwilch-Zw10 (RZZ) Komplex essentieller Bestandteil des "spindle assembly checkpoint" (SAC). Der RZZ-Komplex wird für die Lokalisation des Mad1/Mad2 SAC Komplexes sowie des Microtubuli Motorproteins Dynein benötigt. Dadurch trägt der RZZ-Komplex zur Ausbildung von Kinetochor-Microtubuli-Bindungen bei. Außerdem ist der RZZ-Komplex in den Prozess involviert bei dem SAC Proteine in Abhängigkeit von Dynein vom Kinetochor weg zu den Spindelpolen transportiert werden, sobald der SAC zufrieden gestellt ist („kinetochore shedding“). Wie genau der RZZ-Komplex diese unterschiedlichen Funktionen erfüllt und Signale von der Kinetochor-Microtubuli Schnittstelle integriert ist bislang nicht bekannt.

In meiner Doktorarbeit beschreibe ich die erfolgreiche Aufreinigung des rekombinant hergestellten, 813 kDa großen RZZ-Komplexes sowie dessen vorläufige kristallographische Analyse. In einem multidisziplinären Ansatz bestehend aus strukturbioologischen und biochemischen Methoden habe ich die strukturelle Organisation und Funktion des RZZ-Komplexes untersucht. Eine Kombination aus Kryo Elektronenmikroskopie und quervernetzender Massenspektroskopie Analyse führte zu Erkenntnissen über die strukturelle Organisation des RZZ-Komplexes. Das herausgearbeitete Modell zeigt, dass der RZZ-Komplex ein Hexamer mit einer 2:2:2 Stöchiometrie bildet. Darin formen zwei Rod Moleküle ein längliches antiparalleles Dimer. An beiden Enden der Struktur betten der C-Terminus und der N-Terminale beta-propeller von zwei unterschiedlichen Rod Molekülen ein Zwilch Molekül zwischen sich ein. Zw10 verbindet die zentralen Bereiche von beiden Rod Molekülen miteinander. Zusammen bilden Rod, Zwilch und Zw10 eine extensive Dimer-Berührungsfläche aus. Außerdem beschreibe ich in meiner Arbeit umfangreiche Interaktionsuntersuchungen zwischen dem RZZ-Komplex und anderen Kinetochor Proteinen, welche möglicherweise die RZZ Funktionen beeinflussen. Ich zeige in meiner Arbeit erstmals, dass eine direkte Binding zwischen dem RZZ-Komplex und Spindly stattfindet und dass diese von der Farnesylierung der C-terminalen CAAX-Box von Spindly abhängt.

Diese Untersuchungen ebnen den Weg zu einer detaillierten strukturellen und funktionalen Untersuchung des RZZ-Komplexes und favorisieren ein Modell, in welchem der Prozess des „kinetochore shedding“ Farnesylierung von Spindly

## Zusammenfassung

erfordert. Unser Modell schlägt vor, dass nach SAC Aktivierung Spindly farnesyliert wird und daraufhin an RZZ bindet. Das wiederum ermöglicht die Bindung von Dynein/Dynactin. Durch die Bindung des zum Minus-Ende gerichteten Motorproteins Dynein werden SAC Proteine vom Kinetochore weg und zu den Spindelpolen hin transportiert.

## 2 Introduction

My PhD thesis focuses on the RZZ complex, which is a key regulator of the cell division process named mitosis. In order to elucidate its role within this process I will begin with a short introduction to mitosis. As the RZZ complex is part of multi-protein assemblies called kinetochores, I will next explain the organization, assembly and function of kinetochores. One of their functions is to serve as a platform for the spindle assembly checkpoint, a surveillance mechanism for proper cell division in which the RZZ complex is engaged. I will therefore continue by outlining the current state of knowledge on the spindle assembly checkpoint. To highlight why it is important to gain a better understanding of the RZZ functions I will then describe what is known about the RZZ complex, including its discovery, structure, kinetochore recruitment and function during mitosis.

### 2.1 Mitosis, the key event of the cell cycle

The process of mitosis has gained particular scientific attention after the pioneering work of Walther Flemming (Paweletz, 2001), who has studied cell division combining an aniline dye with microscopy and has been the first to describe chromosomes as rod-like structures. During mitosis cells are in a very fragile state. Inaccurate chromosome segregation can cause aneuploidy (aberrations in chromosome number) and chromosomal instability, a common occurrence in cancer (Weaver & Cleveland, 2006), (Kolodner *et al*, 2011), (Hartwell, 1992). Mitosis is the process of eukaryotic somatic cell division and it generates two daughter cells with identical genomes. Cell division in multicellular organisms ensures growth and regeneration of damaged tissue (Morgan, 2007). A series of complex and highly regulated events, collectively known as the cell cycle, guarantees proper cell reproduction. In eukaryotic cells the cell cycle consists of four distinct phases: the first gap phase G1, the synthesis phase S, the second gap phase G2, and mitosis or M phase. The time between the end of one M phase and the beginning of the next is called interphase. In G1 the cell grows and prepares for DNA replication. In S phase the DNA is being replicated and results in duplicated chromosomes. Cohesin ring complexes retained on chromosomal *loci* called centromeres mediate a tight linkage between the duplicated chromosomes (sister chromatids) (Nasmyth, 2011). During the second gap phase the cell grows and prepares for the key event of the cell cycle, mitosis, by duplication of its

## Introduction

protein and organelle masses. In mitosis the sister chromatids are separated and eventually two daughter cells are formed.

Mitosis can be divided in the following events: prophase, prometaphase, metaphase, anaphase, telophase, and cytokinesis (Morgan, 2007) (Figure 1). In prophase, the DNA, having been duplicated in S-phase, is condensed. The sister chromatids, each containing a copy of the DNA, are held together by the “protein glue” cohesin. In prometaphase, the nuclear envelope breaks down and microtubules, which are attached at one end to centrosomes, nucleate out and start to attach to kinetochores forming the mitotic spindle. During metaphase sister chromatids align at the metaphase plate, at the equator of the cell. When all chromosomes are bi-oriented, which means that they are attached to microtubules emanating from opposite spindle poles, the cell progresses into anaphase. Bi-orientation on the mitotic spindle is the only possible configuration of sister chromatid attachment that allows an even distribution of the genome to the newly forming daughter cells. At the metaphase-to-anaphase transition, centromeric cohesin is cleaved and the sister chromosomes are pulled apart. In telophase, polar microtubules become elongated and nuclear envelopes are formed around each set of daughter chromosomes. The process of mitosis is followed by cytokinesis in which the cell membrane, the cytoplasm and cell organelles are divided in two complete new daughter cells.

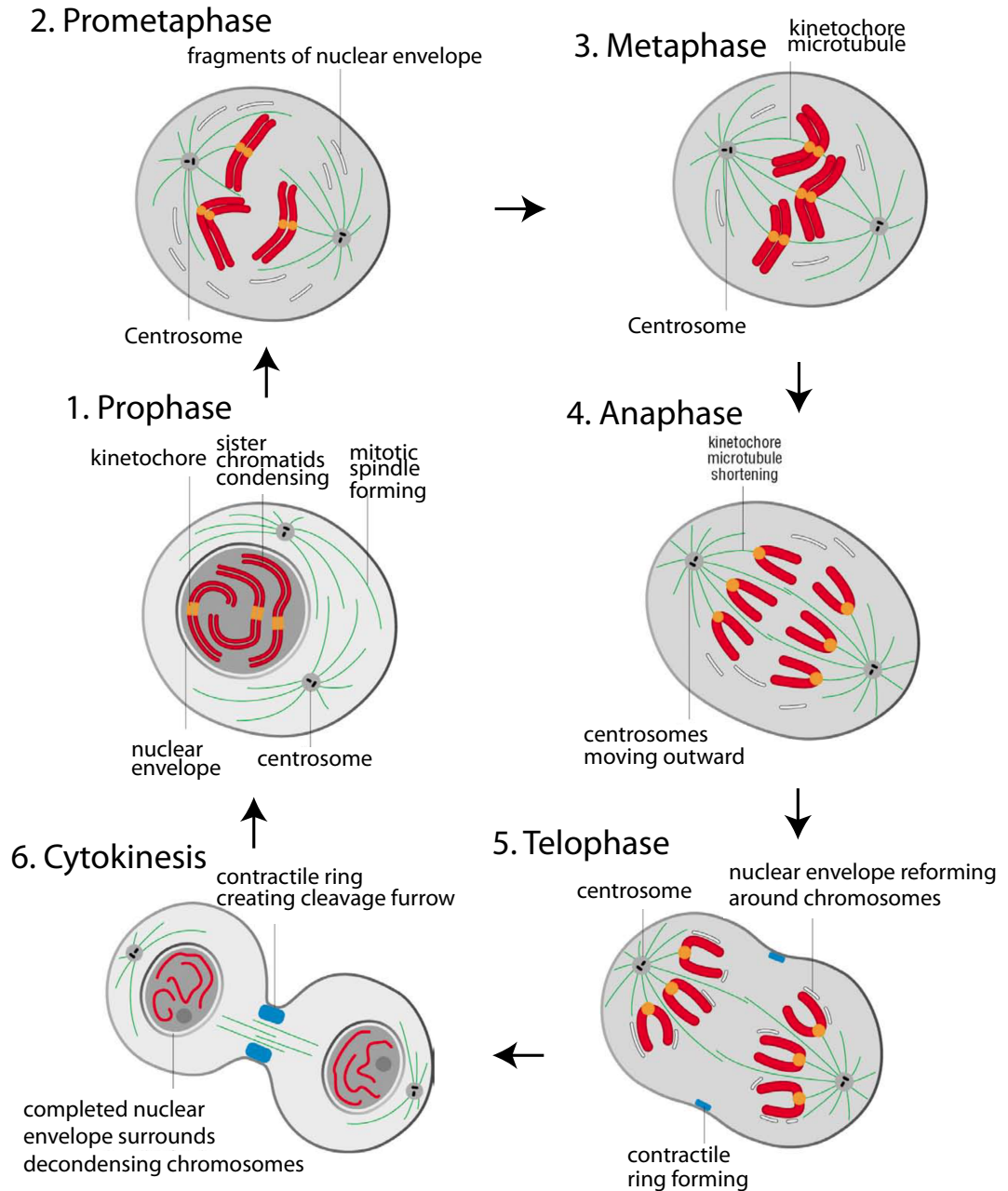


**Figure 1: Overview of the six phases during mitosis**

The six phases of mitosis (prophase, prometaphase, metaphase, anaphase, telophase and cytokinesis) are illustrated.

Adapted from (Morgan, 2007)



## Introduction

The main regulators of the cell cycle are Cyclin dependent kinases (Cdks). The concentration of Cdks remains constant throughout the cell cycle. However, association with their regulatory subunits, which are the Cyclins, controls the activity of Cdks. Cyclin levels oscillate during the cell cycle due to protein synthesis and degradation (reviewed in (Morgan, 2007)). Oscillating levels of specific Cyclins allow temporally regulated activation of Cdks, therefore promoting transitions between different phases through the cell cycle. For example mitotic entry is triggered by formation of the Cdk1-Cyclin B complex and mitotic exit is triggered by Cyclin B degradation. More specifically, Cyclin B is synthesized during S- and G2-phases and after having reached a threshold, Cdk1 is sufficiently active and phosphorylates a variety of substrates resulting in nuclear envelope break down and additional mitotic events (Nigg, 2001), (Pomerening *et al*, 2003), (Morgan, 2007).

Mitotic exit is mediated by proteasome-dependent Cyclin B degradation, which is controlled by the RING E3 ubiquitin-protein ligase anaphase promoting complex or cyclosome (APC/C) (reviewed in (Primorac & Musacchio, 2013)) (Figure 2). The APC/C contains 19 subunits and its activity requires association with one of its coactivators Cdc20 or Cdc20 homologue1 (Cdh1) (Chang *et al*, 2015). Cdks phosphorylate the APC/C, which promotes Cdc20 association and inhibits Cdh1 association. The APC/C polyubiquitinylates the proteins Securin and Cyclin B (and other substrates) for ordered proteasomal degradation. Cyclin B and Securin are recognized by the APC/C through a destruction box sequence (D-box) that is present in each of these targets (Foley & Kapoor, 2013). The APC/C subunit APC10 forms, together with Cdc20, the recognition site for the D-box (Foley & Kapoor, 2013). Degradation of Securin results in activation of Separase, which removes Cohesin, the glue between sister chromatids, thus enabling their physical separation. The degradation of Cyclin B inactivates Cdk1, initiating telophase followed by cytokinesis and mitotic exit (Musacchio & Salmon, 2007).

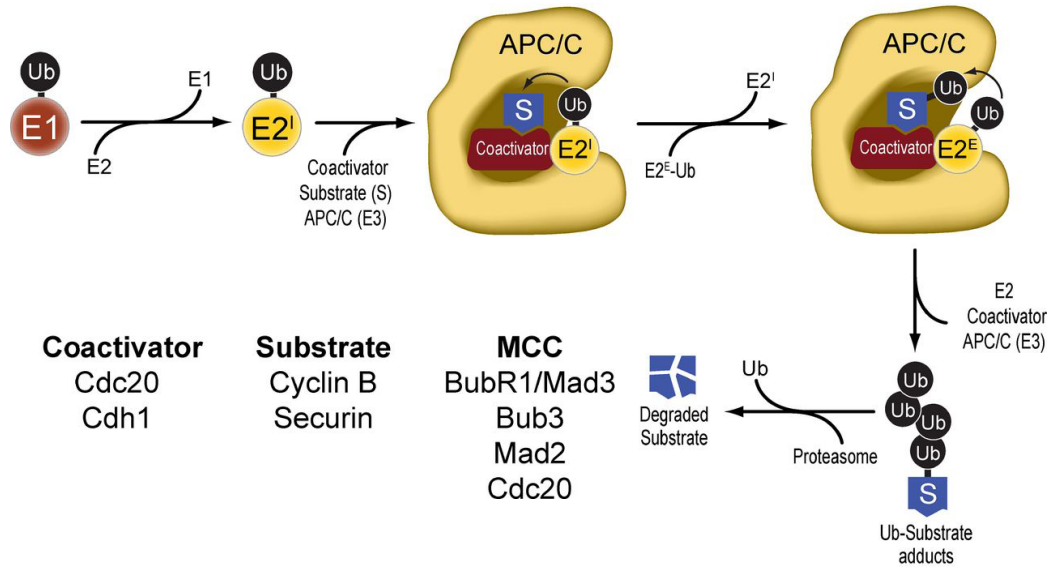


**Figure 2: The anaphase promoting complex**

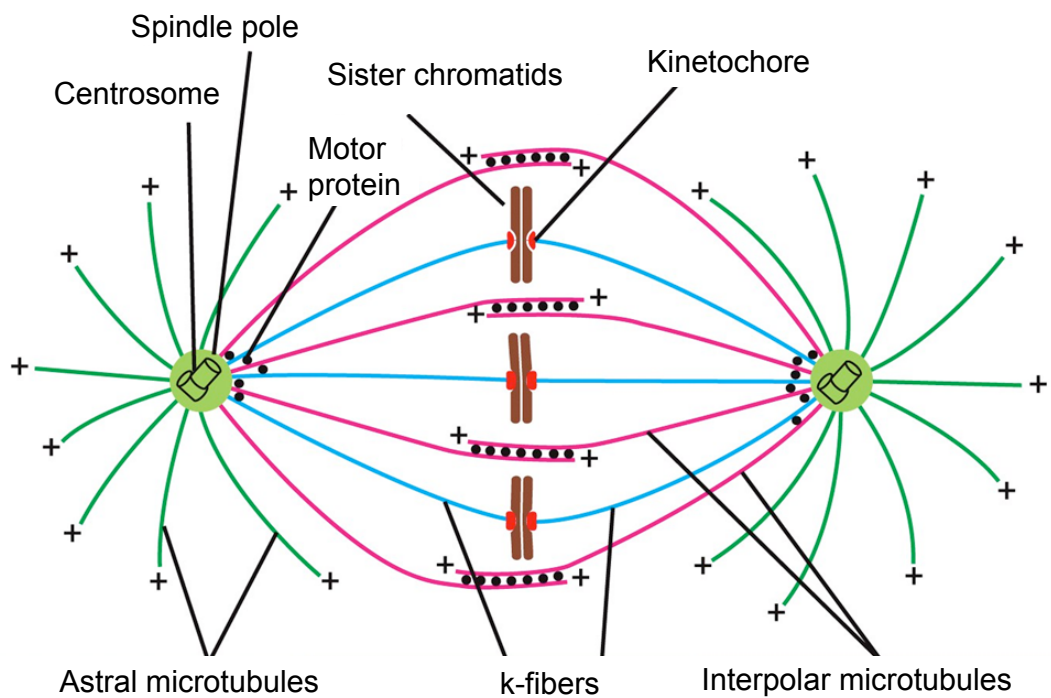
Ubiquitin (Ub) is first activated by an E1 enzyme, transferred to a chain-initiating E2 (E2<sup>I</sup>), and transferred to a substrate (S). The creation of poly-Ub chains by the APC/C requires an elongating E2 (E2<sup>E</sup>). The substrate is presented to the RING-E3 ligase APC/C by a coactivator.

Figure adapted from (Primorac & Musacchio, 2013).

The main microtubule-organizing center in the cell is the centrosome, which is found at the poles of the spindle. It promotes microtubule nucleation during interphase and mitotic division. Abundant microtubule nucleation within the mitotic spindle, mediated by complexes such as Augmin, is also possible. The spindle is a molecular machine consisting of microtubules, motor proteins, and other molecules and its crucial function is the distribution of the genome to the daughter cells (Karsenti & Vernos, 2001)) (Figure 3). The main structural elements of the mitotic spindle are antiparallel arrays of microtubules with their minus ends anchored at the spindle poles and their plus ends projecting towards the chromosomes. Microtubules are polar polymers consisting of  $\alpha\beta$ -tubulin dimers with a slow growing minus end and a fast growing plus end. The plus ends of kinetochore microtubules expose  $\beta$ -tubulin, while the minus ends expose  $\alpha$ -tubulin (Euteneuer & McIntosh, 1981). Microtubule ends undergo stochastic changes from a polymerizing to a depolymerizing state driven by the binding, hydrolysis and exchange of a guanine nucleotide on the  $\beta$ -tubulin monomer, a phenomenon known as dynamic instability (Desai & Mitchison, 1997) (Figure 4). The cross-linking interaction of microtubule plus ends emanating from opposite spindle poles establishes the spindle midzone. Other microtubule plus ends are bound to large protein structures called kinetochores. The latter are located at specific *loci* on

## Introduction

each sister chromatid named the centromere (Section 2.2). Such kinetochore bound microtubules are called k-fibers. While most spindle microtubules have relatively short half-lives, k-fibers have a half-life in the order of minutes. They become stabilized when tension is applied upon proper chromosome alignment in the midzone of the mitotic spindle (Akiyoshi *et al*, 2010), (Nicklas, 1997), (Dewar *et al*, 2004). The convergence from a highly dynamic spindle to a more stabilized one is the basis of error correction, which will be discussed later in this dissertation (Section 2.3). The polar microtubule lattice serves as a path for the microtubule dependent motor proteins of the Dynein and kinesin superfamilies. These proteins convert energy from ATP hydrolysis into movement along microtubules (Hirokawa *et al*, 1998).



**Figure 3: The mitotic Spindle**

Schematic representation of a mitotic spindle.

Figure adapted from <http://imgarcade.com/1/mitotic-spindle-diagram/>.

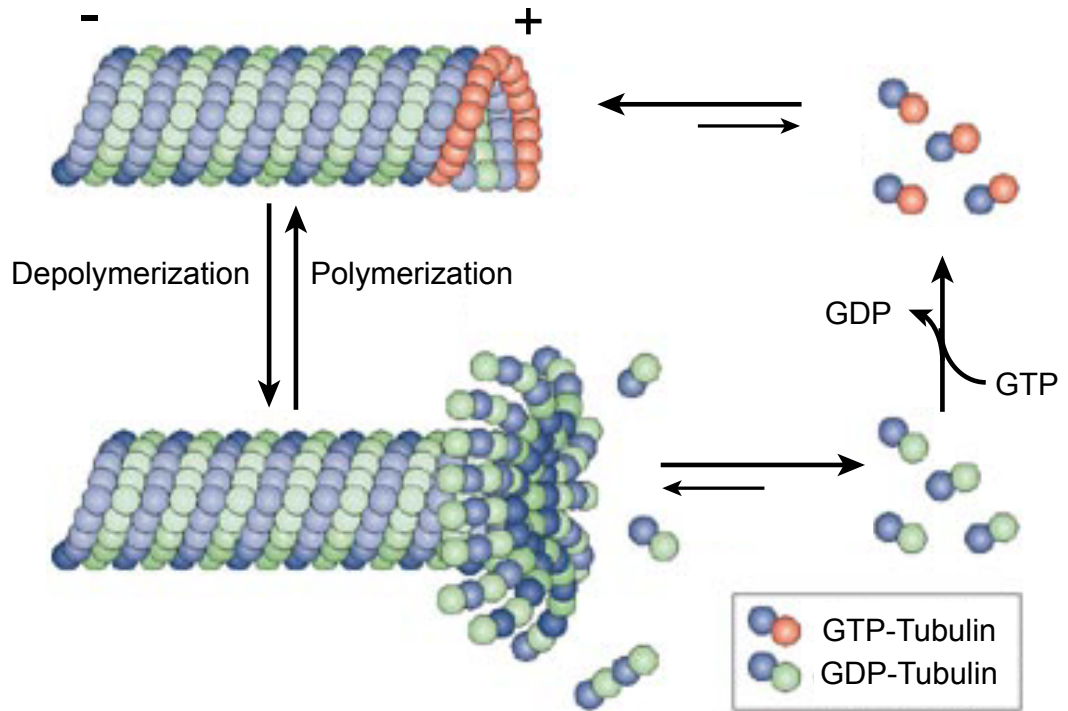


**Figure 4: Dynamic instability of microtubules**

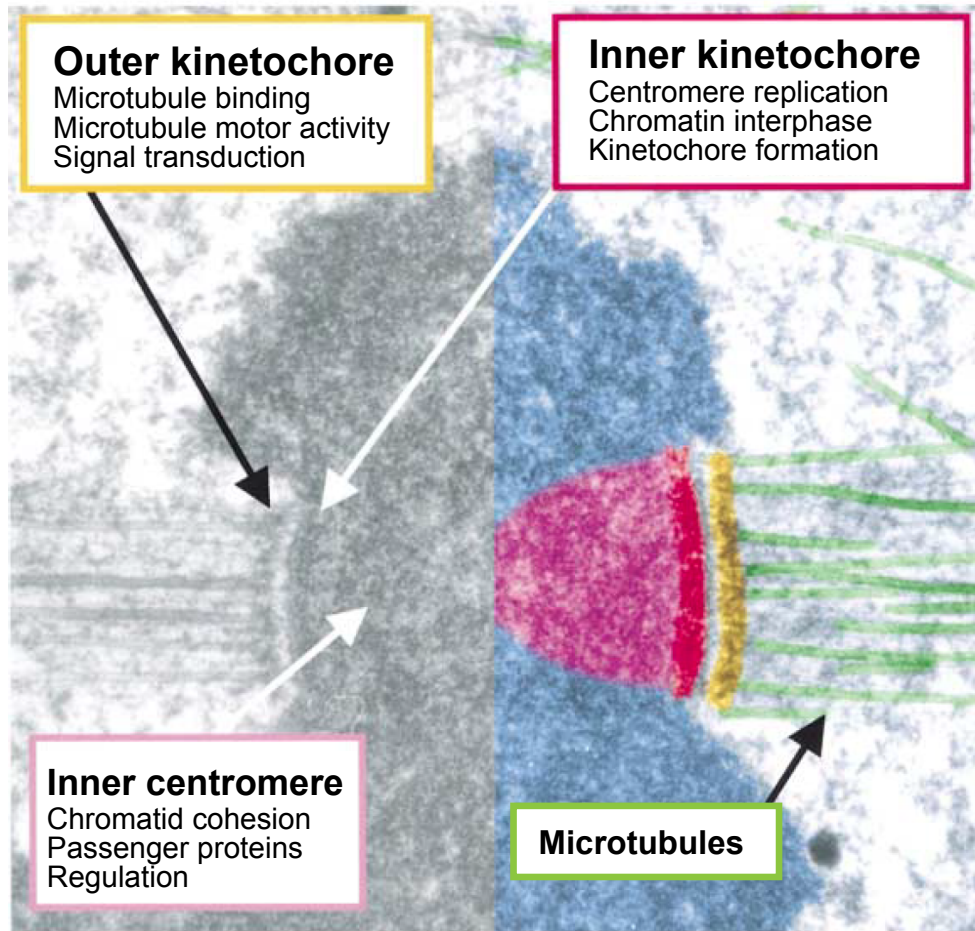
Polymerization (assembly) and depolymerization (disassembly) of microtubules is driven by the binding, hydrolysis and exchange of a guanine nucleotide on the  $\beta$ -tubulin monomer.

Figure adapted from (Cheeseman & Desai, 2008).

### 2.2 Kinetochores organization and assembly

Kinetochores are multiprotein complexes built on centromeres and they are responsible for the establishment of load bearing attachments between chromosomes and microtubules during mitosis (reviewed in (Santaguida & Musacchio, 2009)). The simplest kinetochores in budding yeast bind a single microtubule (reviewed in (McAinsh *et al*, 2003)) They contain approximately 60 proteins which are conserved from yeast to human with few exceptions. This suggests that the larger kinetochores of higher eukaryotes, binding multiple microtubules, are assembled from the repetition of the basic microtubule-binding module of budding yeast (Zinkowski *et al*, 1991), (Santaguida & Musacchio, 2009). Transmission electron microscopy studies have revealed that vertebrate kinetochores appear as trilaminar plates with a dense inner and outer plate and a less dense middle layer (McEwen *et al*, 1998), (Cleveland *et al*, 2003), (Santaguida & Musacchio, 2009).

Human kinetochores are composed of more than 100 proteins (Cheeseman & Desai, 2008), which can be schematically subdivided into three distinct functional modules (Figure 5). The inner kinetochores mainly containing the Constitutive Centromere-Associated Network (CCAN) is the interface with centromeric chromatin and is built on centromeres around a specialized nucleosome containing the histone H3 variant CENP-A (Warburton *et al*, 1997), (Santaguida & Musacchio, 2009), (Hori & Fukagawa, 2012), (Tanaka, 2013). The outer kinetochores provides the core microtubule-binding interface and its most prominent component is the 10-protein complex called the KMN network (reviewed in (Cheeseman *et al*, 2006)). The third module, the fibrous corona contains in contrast to the inner and outer kinetochores proteins that are not constitutive kinetochores components, but become recruited in distinct phases of mitosis to fulfill their regulatory functions (reviewed in (Cleveland *et al*, 2003)). The fibrous corona is only formed upon mitotic entry when the outer layer of kinetochores is enlarged. It becomes compacted again after the formation of end-on microtubule attachments (Magidson *et al*, 2015). This third module is implicated in the control of the state of kinetochores-microtubule attachment and contains among others, proteins of the spindle assembly checkpoint, which detects the lack of kinetochores-microtubule attachment, and the chromosomal passenger complex, which is involved in detection and correction of erroneous kinetochores-microtubule attachments (Santaguida & Musacchio, 2009).



**Figure 5: Centromere organization**

A mitotic chromosome has been sectioned along the plane of the spindle axis and was analysed by transmission electron microscopy. The inner centromere (pink) is a heterochromatin domain that is a focus for cohesins and regulatory proteins. The inner kinetochore (red) creates an interface with centromeric chromatin. The outer kinetochore (yellow) is composed of proteins that interact with the plus ends of microtubules. Adapted from (Cleveland *et al*, 2003).

The investigation of interdependencies of individual kinetochore proteins has led to the development of a scheme describing how the kinetochore might be assembled (Liu *et al*, 2006), (Cheeseman, 2014) (Figure 6). The inner kinetochore assembles on the histone H3 variant CENP-A (Kingwell & Rattner, 1987). In vertebrates, CENP-A is neighbored by a group of at least 16 inner kinetochore proteins, collectively has been identified as the CCAN (Foltz *et al*, 2006), (Foley & Kapoor, 2013), (Obuse *et al*, 2004), (Izuta *et al*, 2006). The CCAN forms the scaffolding link between nucleosomes and the outer kinetochore, playing an important role in kinetochore assembly. Within the CCAN there exist at least four sub complexes. CENP-C and the CENP-N/L complex bind directly to CENP-A, (Kato *et al*, 2013), (Carroll *et al*, 2009). This forms the molecular basis of kinetochore assembly. The

## Introduction

recently discovered CENP-HIKM complex (Basilico *et al*, 2014) has been shown to bind directly to the CENP-TWSX complex and is required for its recruitment to kinetochores (Basilico *et al*, 2014). The CENP-TWSX complex contains histone fold proteins that assemble in a nucleosome like structure. It contributes to outer kinetochore assembly by directly interacting with centromeric DNA and the Mis12 and Ndc80 complexes (Hori *et al*, 2008a), (Gascoigne *et al*, 2011), (Schleiffer *et al*, 2012), (Nishino *et al*, 2013), (Foley & Kapoor, 2013). Finally, the CENP-OPQU/R complex has been implicated in microtubule binding and checkpoint control (Hori *et al*, 2008b), (Perpelescu & Fukagawa, 2011).

The outer kinetochore contains the 10-subunit KMN network (Figure 6). It is composed of three sub complexes, the Knl1 complex, the Mis12 complex and the Ndc80 complex. The KMN network provides a platform for the spindle assembly checkpoint, as explained later in this dissertation (Section 2.4). The Ndc80 and Knl1 subunits enable kinetochore attachment to spindle microtubules (Cheeseman & Desai, 2008).

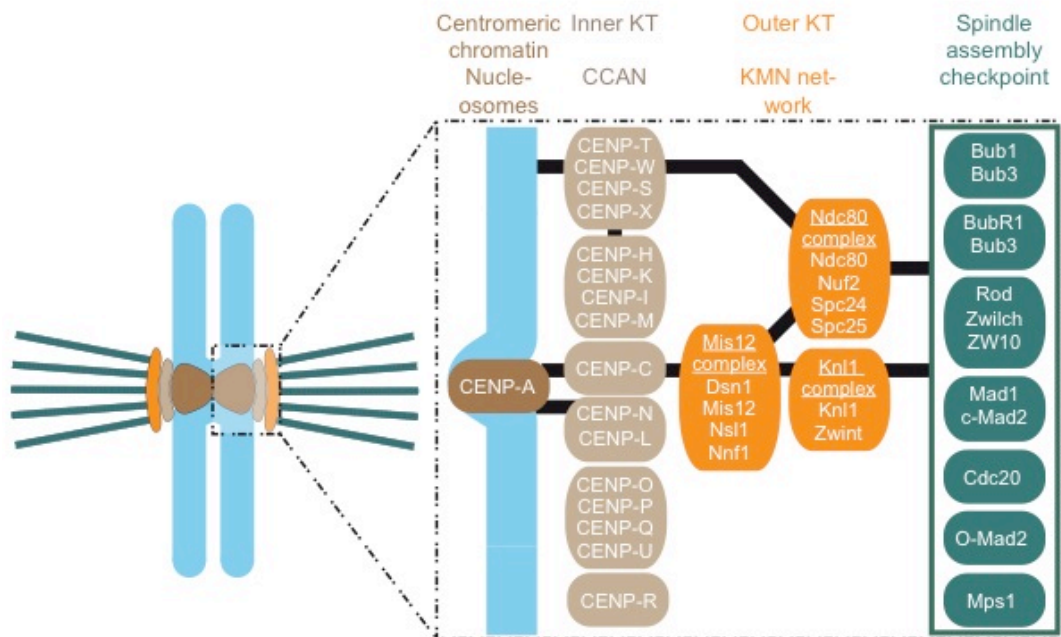


**Figure 6: Schematic of kinetochore organization**

Model of kinetochore assembly. The inner kinetochore, composed by the centromeric chromatin interacting network (CCAN) is depicted in beige, the outer kinetochore, composed of the KMN network, is shown in orange and the spindle assembly checkpoint proteins are represented in green.

Figure adapted from (Basilico *et al*, 2014).

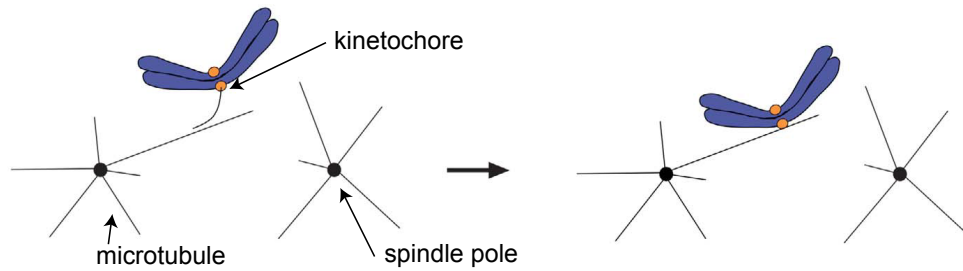
### 2.3 Regulation of kinetochore microtubule attachments

To enable faithful chromosome segregation, kinetochores must capture spindle microtubules to properly align along the mitotic spindle (bi-orientation) before cells progress into anaphase. The kinetochore initially interacts with the lateral surface of a single spindle-pole microtubule (Hayden *et al*, 1990), (Rieder & Alexander, 1990), (Tanaka, 2010) (step 1 Figure 7). The kinetochore then slides along the lateral surface of its bound microtubule towards a spindle pole (Hayden *et al*, 1990), (Rieder & Alexander, 1990) (step 2 Figure 7). In vertebrates this transport is promoted by the minus-end directed microtubule motor protein Dynein (King *et al*, 2000). After being transported towards a spindle pole, both sister kinetochores attach to microtubules. If both sister kinetochores attach to microtubules from the same spindle pole the attachment is turned over until bi-orientation is established with a microtubule from the opposing pole (error correction) (Nicklas, 1997), (Tanaka, 2010) (step 3 Figure 7). The turnover of the kinetochore microtubule attachment stops once tension is generated across sister kinetochores upon the establishment of bi-orientation (Nicklas, 1997), (Dewar *et al*, 2004) (step 4 Figure 7) (see Section 2.1).

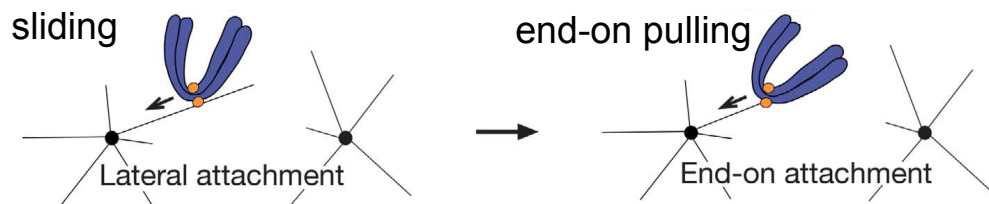


## Introduction

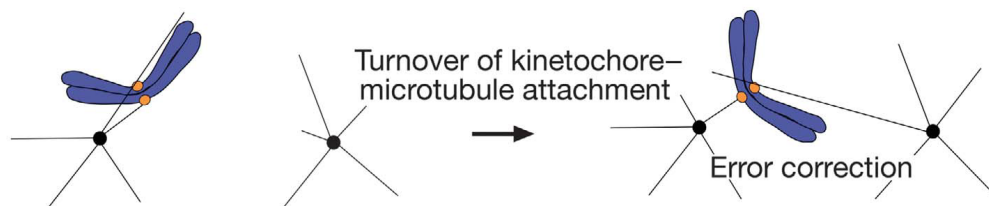
- 1.) Kinetochore initially interacts with the lateral surface of a microtubule from a spindle pole



- 2.) Microtubule dependent kinetochore transport towards a spindle pole



- 3.) Interaction of sister kinetochores with microtubules from the same or opposite spindle poles



- 4.) Sister kinetochore bi-orientation

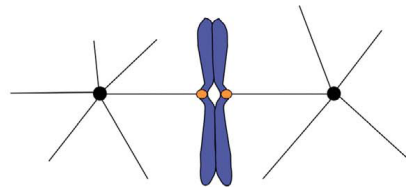


**Figure 7: Kinetochore-microtubule attachment**

The figure shows the development of kinetochore-microtubule interactions during prometaphase (steps 1–3) and metaphase (step 4). Step 1: The kinetochore initially interacts with the lateral surface of a single microtubule. Step 2: Once loaded on a spindle-pole microtubule, the kinetochore is transported along the microtubule lateral surface towards a spindle pole. Step 3: Following the kinetochore transport towards a spindle pole, both sister kinetochores could attach to microtubules. If both sister kinetochores attach to microtubules from the same spindle pole the attachment must be turned over until proper bi-orientation is established with a microtubule from the opposing pole (error correction). Step 4: The turnover of the kinetochore microtubule attachment stops once tension is generated across sister kinetochores upon the establishment of bi-orientation. Figure adapted from (Tanaka, 2010).

## Introduction

### Error correction

The geometry of sister kinetochores and of the mitotic spindle allow most chromosomes to reach bi-orientation spontaneously (Tanaka, 2010). However, the process of establishing kinetochore microtubule attachments is highly regulated and an essential process called error correction is in place to destabilize erroneous attachments and stabilize amphitelic attachments (bi-orientation). Famous experiments by Nicklas and colleagues, which have been performed in 1969, demonstrate that tension applied artificially on incorrectly attached (syntelic) chromosomes stabilizes kinetochore microtubule attachments (Nicklas & Koch, 1969). The same authors have shown many years later that artificially generated tension is sufficient to promote anaphase onset (Li & Nicklas, 1995), suggesting that kinetochores measure microtubule-generated tension, rather than the mere presence of microtubules. Aurora B kinase inhibition can artificially stabilize attachment errors (Hauf *et al*, 2003), (Ditchfield *et al*, 2003), (Lampson *et al*, 2004), (Cimini *et al*, 2006). This implicates Aurora B as an important factor in error correction. In more detail, phosphorylation of the KMN network by Aurora B interferes with its binding to microtubules. Phosphorylation of the N-terminal tail of Hec1 neutralizes its positive charge and decreases the Ndc80 binding affinity for microtubules (Cheeseman *et al*, 2006), (DeLuca *et al*, 2006). Additionally, Aurora B phosphorylation impairs association of the Ska complex with the Ndc80 complex and microtubules to avoid stabilization of erroneous attachments (Chan *et al*, 2012). Aurora B phosphorylation is counterbalanced by PP2A-B56 dephosphorylation (Meppelink *et al*, 2015), (Foley *et al*, 2011). It has been demonstrated that the generation of stable k-fibres depends on the B56-PP2A phosphatase, which is enriched at unattached kinetochores. B56-PP2A depletion results in destabilized k-fibers and increases the level of phosphorylation of Aurora B kinetochore substrates. Chemical inhibition of Aurora B restores k-fibres in B56-PP2A-depleted cells (Foley *et al*, 2011).

Initial kinetochore interactions are established with the lateral surface of microtubules (Tanaka, 2010). The maturation from lateral to end-on attachments produces tension, increasing the intra kinetochore stretch and therefore the distance between Aurora B and the KMN network. As a result of this, the substrates of Aurora B are out of the reach of the kinase domain, which is tethered to nucleosomes via interaction with additional subunits of a chromosome passenger complex (CPC) of which Aurora B is the catalytic subunit (Liu *et al*, 2009), (Santaguida & Musacchio, 2009), (Tanaka, 2010). A “dog-leash” model has

## Introduction

been proposed, to provide a hypothetical molecular description of this process (Santaguida & Musacchio, 2009). The idea behind this model is that the distance of Aurora B (the dog) can reach away from its kinetochore anchor (the dog's owner, represented by the Survivin and Borealin subunits of the CPC) is limited by the length of INCENP (which defines the maximal stretch of the leash), the fourth subunit of the CPC. Recent work has provided evidence in favor of the dog-leash model (Monda & Cheeseman, 2015), but other models have also been proposed. For instance, it has been proposed that the decrease of Aurora B target modification as a function of intra-kinetochore stretch may be generated by a diffusible gradient of the kinase (Lampson & Cheeseman, 2011). A complete understanding of the molecular mechanisms of error correction remains elusive. Dissecting the molecular details of the regulation of the antagonistic relationship of Aurora B and PP2A-B56 is one fundamental topic of research for the future.

### Interface of the kinetochore microtubule attachment

The core microtubule attachment site at kinetochores, for end-on attachments, is the KMN network (Tanaka, 2010). The KMN network is one of the most evolutionarily conserved feature of kinetochores, which emphasizes its fundamental importance in ensuring proper dynamic interaction of kinetochores with the mitotic spindle during mitosis (Foley & Kapoor, 2013).

The Ndc80 complex is the main microtubule end-on attachment site at kinetochores (Cheeseman *et al*, 2006). The 170 kDa Ndc80 complex is a heterotetramer of Hec1, Nuf2, Spc24 and Spc25 (Ciferri *et al*, 2005). Within the Ndc80 complex heterodimers of Spc24/Spc25 and Hec1/Nuf2 partake distinct functionalities. The globular domains of Spc24 and Spc25 are essential for kinetochore targeting of the Ndc80 complex, as they interact directly with the Mis12 complex and the CCAN (Petrovic *et al*, 2014). Structural and biochemical studies revealed that the globular calponin homology (CH) domains of Hec1 and Nuf2 mediate microtubule binding (Cheeseman *et al*, 2006), (Wei *et al*, 2007), (Ciferri *et al*, 2008). The interaction between microtubules and Hec1/Nuf2 is initially facilitated by an electrostatic interaction of the basic N-terminal tail of Hec1 with the acidic C-terminal tails of tubulin (the E-hooks) (Wei *et al*, 2007), (Ciferri *et al*, 2008), (Alushin *et al*, 2012). On microtubules, the Ndc80 complexes bind at the  $\alpha\beta$ -tubulin and  $\beta\alpha$ -tubulin interfaces, and therefore every 4 nm in the longitudinal direction of the microtubule (Alushin *et al*, 2010). The interaction with microtubules mediates oligomerization of the Ndc80 complex and oligomerization has been

## Introduction

proposed to maintain processive association to the dynamic microtubules (Alushin *et al*, 2010). The isolated Ndc80 complex does not bind to growing and shrinking microtubules, as the bending of microtubules (Figure 4) disrupts the  $\alpha\beta$ -tubulin and  $\beta\alpha$ -tubulin interface (Alushin *et al*, 2012). Multiple Ndc80 complexes, cooperatively bound to a single microtubule, allow persistent association of kinetochores with dynamic microtubules (Alushin *et al*, 2010), (Alushin *et al*, 2012), (reviewed in (Foley & Kapoor, 2013)).

High affinity kinetochore microtubule interactions are retained during microtubule growth and shrinkage (Foley & Kapoor, 2013), (Santaguida & Musacchio, 2009). In yeast, the Ndc80 and Dam1 complexes together mediate connections to microtubules, with the Dam1 complex facilitating processive interactions of the Ndc80 complex with microtubules (Lampert *et al*, 2010), (Tien *et al*, 2010). However, the Dam1 complex is absent in metazoans and it has been suggested that the Ska complex may functionally replace it. The latter is required to maintain Ndc80 complex monomers on polymerizing and depolymerizing microtubule tips and the Ndc80 complex can exclusively make load-bearing processive attachments when associated with the Ska complex (Welburn *et al*, 2009), (Schmidt *et al*, 2012). Consistent with this, depletion of the Ska complex results in chromosome segregation defects (Welburn *et al*, 2009), (Gaitanos *et al*, 2009). Moreover, by using k-fiber stability assays it has been demonstrated that depletion of the Ska complex results in compromised k-fiber stability (Gaitanos *et al*, 2009). However, a more detailed picture about this regulatory mechanism is missing.

Within the KMN network the protein Knl1 provides another binding site for the plus ends of microtubules (Espeut *et al*, 2012a). The very N-terminal end of Knl1 harbors a conserved microtubule-binding domain. It has been shown that this short positive patch enhances binding of the KMN with microtubules *in vitro* (Espeut *et al*, 2012b), (Cheeseman *et al*, 2006) (Pagliuca *et al*, 2009). Understanding the mechanism and function of Knl1 microtubule binding remains elusive, due to a lack of structural information.

### 2.4 The spindle assembly checkpoint

Besides being attachment sites on chromosomes, kinetochores also serve as a platform for the spindle assembly checkpoint (SAC). The SAC is an evolutionary conserved surveillance mechanism that monitors attachment of sister chromatids and delays the metaphase-anaphase transition until every single sister kinetochore pair is bi-oriented at the mitotic spindle (Foley & Kapoor, 2013), (Santaguida & Musacchio, 2009). Proteins involved in the spindle assembly checkpoint have been initially discovered in two independent genetic screens in budding yeast which identified mutations that disable cells to arrest in mitosis in the presence of spindle poisons (Li & Murray, 1991), (Hoyt *et al*, 1991). This checkpoint was named spindle assembly checkpoint based on the observation that it is activated upon interference with spindle assembly in the presence of spindle poisons (Minshull *et al*, 1994). Today we know that it does not monitor spindle assembly but rather interaction of kinetochores with microtubules (Musacchio & Salmon, 2007).

The core spindle assembly checkpoint proteins, that are conserved throughout species are the kinases Monopolar spindle protein 1 (Mps1), Budding uninhibited by benomyl 1 (Bub1) and Aurora B, as well as the non catalytic proteins Mitotic arrest deficient 1 (Mad1), Mad2, Bub1 related 1 (BubR1) and Cell division cycle 20 (Cdc20) (Foley & Kapoor, 2013). In higher eukaryotes additional proteins regulate the SAC activity including the Rod-Zw10-Zwilch (RZZ) complex, p31 comet, the microtubule motors CENP-E and Dynein. Dynein-associated proteins (for example Spindly), as well as several protein kinases including mitogen-activated protein kinase (MAPK), Cdk1-Cyclin B, Nek2, Haspin and polo-like kinase-1 (Plk1) are also involved (Musacchio & Salmon, 2007).

During prometaphase SAC proteins are recruited to unattached kinetochores where they generate a diffusible “wait signal” (Musacchio & Salmon, 2007). Premature chromosome segregation is delayed through the inactivation of Cdc20, which is a cofactor of the anaphase promoting complex/cyclosome (APC/C) (see Section 2.1). Mitotic entry requires the activity of the most important kinase during mitosis, Cyclin-dependent-kinase-1 (Cdk1). Cdk1 phosphorylates many key proteins for mitotic entry and maintenance (Morgan, 2007), (Musacchio & Salmon, 2007). The activity of Cdk1 depends on Cyclin B binding. Exit from mitosis cannot occur until Cyclin B has been degraded and Cdk1 has been inactivated (Musacchio & Salmon, 2007). Progression into anaphase is mediated by the ubiquitin-protein ligase APC/C activation that tags the protein Securin for

## Introduction

destruction. Securin destruction liberates and activates Separase. Separase is a protease that cleaves the Kleisin subunit of the Cohesin complex, which links sister chromatids together (represented as yellow dots between the sister chromatids in (Figure 8) at the onset of the metaphase to anaphase transition (Oliveira & Nasmyth, 2010), (Foley & Kapoor, 2013), (Lara-Gonzalez *et al*, 2012).

Unattached kinetochores trigger the sequestration of Cdc20 by Mad2 in the mitotic checkpoint complex (MCC), the SAC effector, which inhibits the APC/C. The MCC is a hetero-tetramer formed of the Mad2-Cdc20 complex bound to BubR1 and Bub3 (Sudakin *et al*, 2001) (described in more detail later in this Section). Without Cdc20 the APC/C cannot become activated and anaphase is not triggered. Once all sister chromatids have reached bi-orientation, Cdc20 is released from the MCC, activating the APC/C. Subsequently the APC/C polyubiquitinylates its substrates Securin and Cyclin B, initiating their proteolytic degradation. Degradation of Securin results in activation of Separase, which removes Cohesin, and enables the physical separation of sister chromatids. The degradation of Cyclin B inactivates Cdk1, initiating telophase followed by cytokinesis and mitotic exit (Musacchio & Salmon, 2007), (Foley & Kapoor, 2013), (Lara-Gonzalez *et al*, 2012).

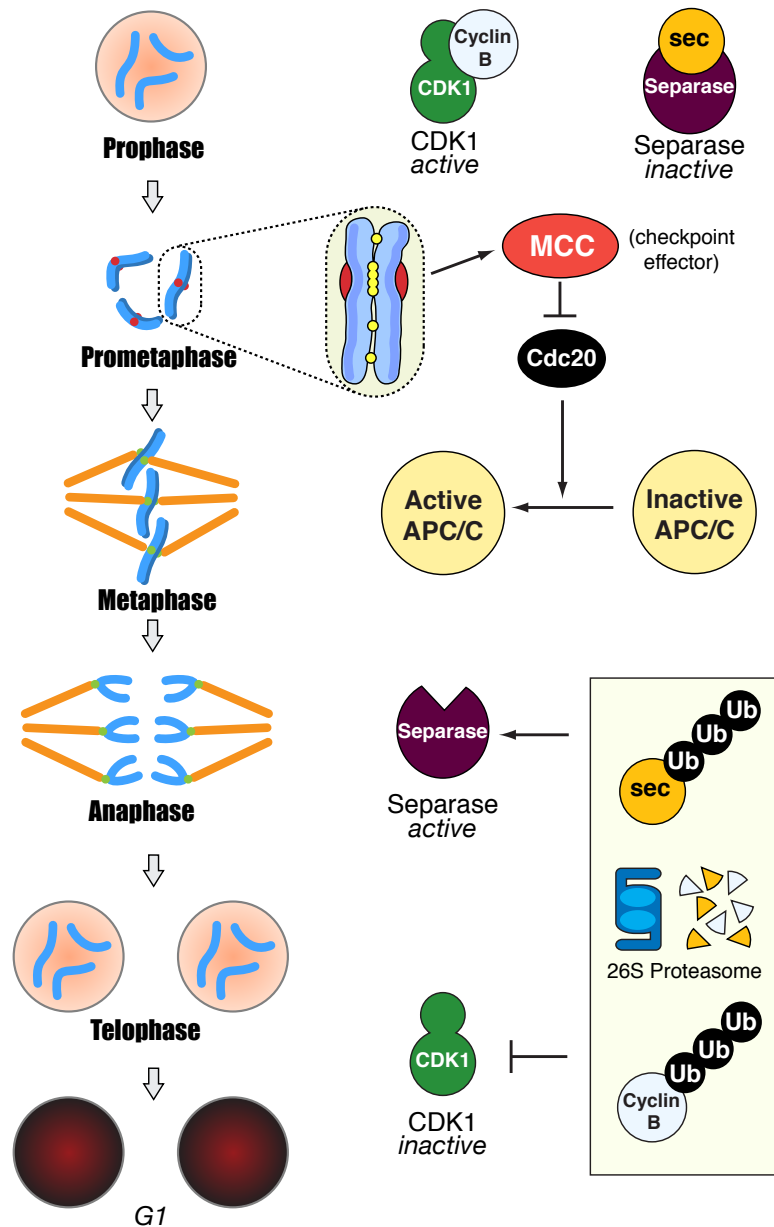


**Figure 8: Relationship between the spindle assembly checkpoint and the cell cycle**

Mitotic entry requires the activity of the most important kinase during mitosis, Cyclin-dependent-kinase-1 (Cdk1), which is dependent on its binding to Cyclin B. The protease separase is required to remove cohesion (represented in yellow between the sister chromatids) from sister chromatids at the onset of anaphase. Until anaphase onset separase is kept inactive by binding of securing (SEC). Unattached kinetochores are involved in formation of the mitotic checkpoint complex (MCC). The MCC inhibits Cdc20, a cofactor of the ubiquitin ligase anaphase promoting complex/cyclosome (APC/C) inactivating the APC/C. The spindle assembly checkpoint is negatively regulated in the absence of unattached kinetochores. Only when all sister chromatids have reached bi-orientation, Cdc20 is released from the MCC and activates the APC/C. The APC/C polyubiquitinylates its substrates securin and Cyclin B, thus initiating their proteolytic degradation by the proteasome. Degradation of securin results in activation of separase, which removes cohesion and enables their physical separation. The degradation of Cyclin B inactivates Cdk1, initiating cytokinesis and mitotic exit. (Adopted from {Musacchio:2007jx})

## Introduction

The mitotic checkpoint complex (MCC) is the main effector of the SAC and consists of the Mad2-Cdc20 complex bound to BubR1 and Bub3 (Sudakin *et al*, 2001). Within the MCC Mad2 and BubR1 bind to two distinct binding sites on Cdc20 (Hwang *et al*, 1998), (Hardwick *et al*, 2000) and have a synergistic effect on APC/C inhibition (Fang, 2002), (Davenport *et al*, 2006), (Han *et al*, 2013). In the last years structural and biochemical studies have resulted in a good understanding of the protein-protein interactions involved in MCC formation (Luo *et al*, 2000), (Luo *et al*, 2002), (Luo *et al*, 2004), (De Antoni *et al*, 2005), (Mapelli *et al*, 2007), (Chao *et al*, 2012). The Mad2-Cdc20 and BubR1-Bub3 subcomplexes assemble the MCC. Mad2 binds to a 10-residue motif in the N-terminal region of Cdc20, which has been named the Mad2 interaction motif (MIM) (Hwang *et al*, 1998), (Luo *et al*, 2002), (Primorac & Musacchio, 2013). BubR1 contains two K-E-N sequences (where K, E, and N are single-letter codes for the amino acids Lysine, Glutamic acid, and Asparagine) (KEN1 and KEN2) and both of them are essential for SAC signaling (Burton & Solomon, 2007), (King *et al*, 2007), (Primorac & Musacchio, 2013). KEN1 is required for incorporation of BubR1 in a complex with Mad2-Cdc20 subcomplex and for its binding to the APC/C (Primorac & Musacchio, 2013). The reason why KEN1 is necessary was revealed recently with the crystal structure of the fission yeast MCC (Chao *et al*, 2012). This structure revealed that KEN1 binds to the KEN box-binding pocket of Cdc20, thus directly competing with Cdc20 substrates. Therefore BubR1 is a pseudosubstrate inhibitor of the APC/C (Lara-Gonzalez *et al*, 2011). KEN2 is also required for mitotic arrest, but not for the association of the MCC and the APC/C (Burton & Solomon, 2007), (King *et al*, 2007), (Lara-Gonzalez *et al*, 2011). More specifically, KEN2 is required to prevent the D-box- and Cdc20-dependent binding of Cyclin B to the APC/C (Lara-Gonzalez *et al*, 2011). Mechanistically, its function is exercised through the interaction with a second molecule of Cdc20 (Izawa & Pines, 2015). Thus, MCC contains two molecules of Cdc20, rather than one as previously proposed (Sudakin *et al*, 2001).

## Recruitment of SAC proteins

Spindle assembly checkpoint activation requires the recruitment of checkpoint proteins to kinetochores. A complete picture of recruitment mechanisms remains elusive but there has been remarkable progress in the elucidation of many aspects of this process. Mps1 and Aurora B kinase activity is essential for the recruitment



## Introduction

of all checkpoint components to kinetochores, as the chemical inhibition of these two kinases impairs the kinetochore localization of checkpoint proteins (Maciejowski *et al*, 2010), (Hewitt *et al*, 2010), (Kwiatkowski *et al*, 2010), (Santaguida *et al*, 2010), (Santaguida *et al*, 2011), (Ditchfield *et al*, 2003), (Emanuele *et al*, 2008). Mps1 and Aurora B contribute to SAC signaling after Mad1-Mad2 recruitment by controlling MCC formation and the MCC-APC/C interaction (Funabiki & Wynne, 2013). Aurora B kinetochore localization is mediated by Haspin phosphorylation of H3 nucleosomes, which recruits the CPC via its subunits Borealin and Survivin (Carmena *et al*, 2012). Mps1 kinetochore localization depends on the Ndc80 complex, but the exact mechanism is currently unclear (Martin-Lluesma *et al*, 2002), (Stucke *et al*, 2004), (Funabiki & Wynne, 2013). Knl1 plays an important role in Mps1 dependent checkpoint activation. It has been identified as a substrate of Mps1 and mutations of the respective phosphorylation sites impair SAC function (Shepperd *et al*, 2012), (Yamagishi *et al*, 2012). It has also been reported that phosphorylation of Knl1 at so-called MELT motifs (where M, E, L and T are single-letter codes for the amino acids Methionine, Glutamic acid, Leucine, and Threonine) create a binding site for the SAC kinase Bub1 (London *et al*, 2012) (Shepperd *et al*, 2012), (Yamagishi *et al*, 2012), (Primorac *et al*, 2013). It has been shown that Bub3 binds directly to Knl1 through a region that contains multiple MELT motifs and that this interaction only happens if these MELT have been phosphorylated by Mps1. Moreover, once bound to Knl1, Bub3 then recruits Bub1 to the kinetochore (Primorac *et al*, 2013). Bub1 is important for recruitment of Bub3, BubR1 and Mad1 (Rischitor *et al*, 2007), (Vanoosthuyse *et al*, 2004). Bub1 can be recruited to kinetochores independently of BubR1, but BubR1 kinetochore localization depends on Bub1 binding (Overlack *et al*, 2015).

A more downstream event in the recruitment process of checkpoint proteins is the activation of Mad2 at kinetochores. Structural analysis of Mad2 clarified that it exists in two different topologies, now generally referred as open and closed Mad2 (O- and C-Mad2) (Luo *et al*, 2002), (Sironi *et al*, 2002). O-Mad2, also referred to as inactive Mad2, predominates when the SAC is inactive, and is eminently cytosolic. C-Mad2, also referred as active Mad2, signals SAC activation. Mad2 adopts this conformation when bound to Mad1 or to Cdc20. Closed Mad2/Mad1 recruits o-Mad2 to kinetochores by forming a dimeric O-Mad2/C-Mad2 structural heterodimer (De Antoni *et al*, 2005). This leads to the closure of O-Mad2 and to its conversion to C-Mad2, which binds Cdc20. The two complexes Mad1/c-Mad2 and Cdc20/c-

## Introduction

Mad2 are structural copies of one another, as they both contain Mad2 in its closed conformation and Cdc20 and Mad1 share a Mad2 binding motif. Thus, the reaction of activation of O-Mad2 that precedes its conversion to C-Mad2 is templated by Mad1/c-Mad2, which justifies the name “template model” for the Mad2 activation mechanism. The Cdc20/Mad2 complex, once it has formed at kinetochores, dissociates away into the cytosol where it mimics the Mad1/c-Mad2 complex and may convert more o-Mad2 into c-Mad2 bound to Cdc20 in a positive feedback loop (De Antoni *et al*, 2005).

## Introduction

### SAC silencing

For faithful chromosome segregation not only the activation of the SAC is essential, but also SAC silencing. Upon microtubule attachment, checkpoint proteins are depleted from kinetochores (Musacchio & Salmon, 2007). This removal of SAC proteins at properly attached kinetochores is important in switching off the SAC. Microtubule binding to kinetochores produces changes in kinetochore and SAC chemistry, most notably their state of phosphorylation. It has been shown that SAC silencing depends on the phosphatase PP1, which is targeted to kinetochores via Knl1 (Pinsky *et al*, 2009), (Vanoosthuyse & Hardwick, 2009). Mutations within the PP1 binding motif in the yeast homologue of Knl1 disables SAC silencing, which is eventually lethal (Rosenberg *et al*, 2011). The impaired SAC can be rescued by fusing PP1, but not a catalytically dead mutant, to mutant Knl1. Thus, kinetochore recruitment of PP1 may be crucial for SAC silencing in yeast. Similar effects could be observed in *C. elegans* (Espeut *et al*, 2012b).

There may also exist Knl1-independent silencing mechanisms. One mechanism that has been linked to SAC silencing is Dynein dependent kinetochore stripping (Gassmann *et al*, 2010), (Howell, 2001). The microtubule motor Dynein removes SAC proteins from kinetochores in a minus end directed movement along microtubules. Among the SAC proteins removed by Dynein are Mad1, Mad2, the RZZ complex and Spindly which is required for kinetochore recruitment of Dynein and Dynactin (Barisic & Geley, 2011). In Spindly depleted cells, there exists an alternative mechanism for Mad1/Mad2 removal from kinetochores that is probably KMN network dependent (Gassmann *et al*, 2010). However, in Spindly motif mutants cells that abrogate recruitment of Dynein/Dynactin to kinetochores, there is no additional mechanism to remove Mad1/Mad2 (Gassmann *et al*, 2010). Spindly is likely involved in the transition from lateral attachments to end-on attachments at kinetochores (Gassmann *et al*, 2008), (Varma *et al*, 2008), (Barisic & Geley, 2011) (Section 2.6).

Ultimately, SAC silencing likely requires the disassembly of Cdc20 from the MCC in order to activate the APC/C. P31<sup>comet</sup>, which is an additional binding partner of c-Mad2, extracts Mad2 from the MCC (Westhorpe *et al*, 2011). Polyubiquitylation of Cdc20 in the MCC also leads to MCC disassembly (Reddy *et al*, 2007).

## 2.5 The RZZ complex

### Discovery

The RZZ complex is an important regulator of the SAC in higher eukaryotes and it contains the three proteins rough deal (Rod), zeste white 10 (Zw10) and Zwiich (Karess, 2005). Initially Rod and Zw10 have been independently identified in genetic screens in *Drosophila* (Smith *et al*, 1985), (Karess & Glover, 1989), (Williams *et al*, 1992) and later in human cells (Starr *et al*, 1997). Rod and Zw10 were later shown to function together in an evolutionary conserved complex in higher eukaryotes (Scaërou *et al*, 2001). The last component of the complex, Zwiich, has been discovered by immune affinity chromatography on Zw10 in *Drosophila* and further characterized biochemically (Williams *et al*, 2003). The three-protein complex has then been renamed the Rod-Zwiich-Zw10 (RZZ) complex. The three proteins co-elute from size exclusion chromatography (SEC) in a single peak of approximately 800 kDa (Williams *et al*, 2003). The combined mass of the three proteins Rod (250 kDa), Zw10 (89 kDa) and Zwiich (67 kDa) is about half of the apparent mass of the complex, suggesting that the complex formed a stable dimer (Karess, 2005). Null mutations or depletion by siRNA of any RZZ gene cause severe chromosome segregation defects (Starr *et al*, 1997), (Scaërou *et al*, 2001), (Williams *et al*, 2003). It has been shown that the RZZ complex is part of the spindle assembly checkpoint as cells lacking the RZZ complex no longer arrest in M phase in response to spindle damage, but go on to separate sister chromatids, degrade Cyclin B and exit mitosis, which is the same phenotype that other checkpoint proteins reveal (Chan *et al*, 2000). Mutations in RZZ encoding genes are frequently identified in cancers (Wang, 2004).

### Dynamics during mitosis

The kinetochore and spindle dynamics of the RZZ complex have been studied extensively, and found to be the same across tissues and species (Karess, 2005). In interphase, all three proteins are cytoplasmic (Williams *et al*, 1992) (Basto *et al*, 2004), (Karess, 2005). In late prophase they enter the nucleus and accumulate at kinetochores during nuclear envelope breakdown (Williams *et al*, 1992), (Williams *et al*, 2003), (Basto *et al*, 2004), (Karess, 2005). Once kinetochore microtubules have attached, the RZZ redistributes away from kinetochores, as other checkpoint proteins, and relocates along the kinetochore attached microtubules predominantly

## Introduction

towards the spindle poles (Williams *et al*, 1992), (Scaërou *et al*, 1999), (Karess, 2005). This process is called kinetochore shedding (Section 2.4).

### Structural organization

A structural analysis of the RZZ complex, carried out in the Musacchio laboratory, revealed a common ancestry with the Nag-Rint-Zw10 (NRZ) complex which acts as a tethering complex for retrograde trafficking of COPI vesicles between the Golgi apparatus and the endoplasmic reticulum (ER) (Aoki *et al*, 2009), (Çivril *et al*, 2010). Human Zw10 is not only a subunit of the RZZ complex but also of the NRZ complex (Çivril *et al*, 2010). Among the RZZ subunits, Zw10 is the only one that has a homologue in yeast, namely Dsl1 (Andag & Schmitt, 2003). Dsl1 is incorporated into the Dsl1/Sec39/Tip20 complex and similarly to the NRZ complex, is involved in membrane trafficking of COPI-coated vesicles (Andag & Schmitt, 2003). Thus, the Dsl1/Sec39/Tip20 complex is the yeast equivalent of the NRZ complex (Andag & Schmitt, 2003), (Tripathi *et al*, 2009), (Menant & Karess, 2010). Unlike Zw10, Dsl1 is not involved in mitosis (Çivril *et al*, 2010). Probably (or at least partly) due to its double life, Zw10 is the most thoroughly studied protein of the RZZ complex. Bioinformatic comparison of the NRZ and RZZ complexes showed that Rod and Nag are both large proteins (2209 and 2371 amino acids respectively) predicted to fold into an N-terminal  $\beta$ -propeller followed by an extensive  $\alpha$ -solenoid (Çivril *et al*, 2010). This extensive  $\alpha$ -solenoid includes a domain, which is very conserved between Rod and Nag, named the Nag Rod homology domain (NRH), which is followed by a domain homologous to the Sec39 motif (Figure 9) (Çivril *et al*, 2010). The combination of a  $\beta$ -propeller with an  $\alpha$ -solenoid is rather rare, and occurs in transport proteins at the nuclear pore complexes (NPC) or in vesicle coat proteins such as COPII or clathrin (Çivril *et al*, 2010).

Functionally, Nag and Rod are different. Immunofluorescence analysis shows that Nag is located at the Golgi and ER and not at kinetochores, whereas Rod is a known component of kinetochores and does not localize to the Golgi and ER.

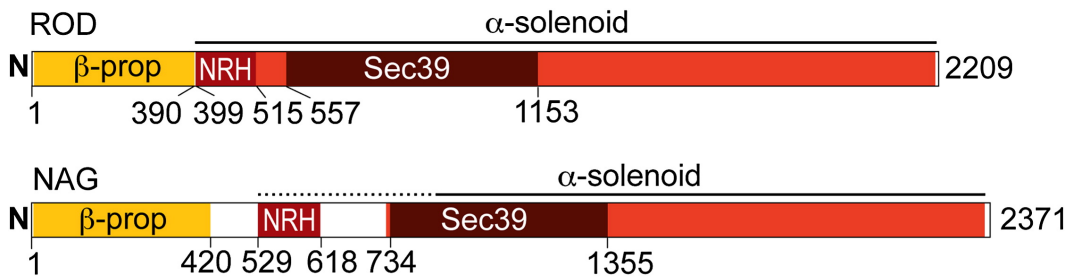


**Figure 9: Domain organization of Rod and Nag**

Rod and Nag are both predicted to fold into a N-terminal terminal  $\beta$ -propeller (yellow) followed by an extensive  $\alpha$ -solenoid (orange) that contains the Nag Rod homology domain (NRH) (red) and the Sec39 homology motif (dark red).

Figure adopted from (Çivril *et al*, 2010).

The crystal structure of Zwilch has been solved in the Mussachio laboratory (Figure 10) (Çivril *et al*, 2010). The crystal structure of Tip20 (the yeast homologue of Rint) has previously been solved in the Hughson laboratory (Ren *et al*, 2009). A comparison between the two structures revealed that Zwilch with Rint have no similar features. Additionally, Zwilch also forms a novel fold with no equivalent in the protein database (PDB) (Çivril *et al*, 2010).

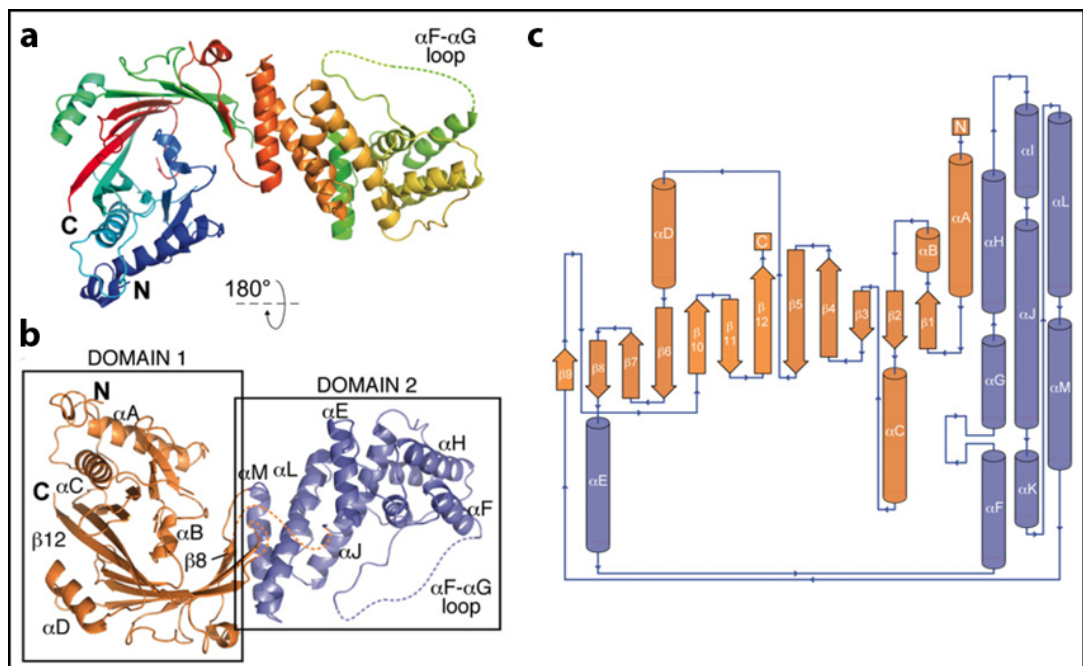


**Figure 10: Crystal structure of Zwilch**

(A) A cartoon model of Zwilch. The structure is colored blue to red from the N to the C-terminus as if it were not split into two segments. Some disordered loops are drawn as dashed lines. (B) Cartoon model after a 180° rotation relative to (A) illustrates two structural domains of Zwilch described in the text (PDB ID:3IF8). (C) Topology diagram of Zwilch.

Figure adopted from (Çivril *et al*, 2010).

## Introduction

The topology of the NRZ and RZZ complexes reveal significant differences. In the NRZ complex (as in the Dsl1/Sec39/Tip20 complex) Zw10 may bridge Nag and Rint, suggesting that Nag may not contact Rint directly. This is different in the RZZ complex, where Zw10 and Zwlch both bind directly to Rod (Çivril *et al*, 2010). In conclusion, the RZZ and NRZ have a common ancestor, but how this reflects on their function remains elusive.

### Recruitment of the RZZ complex to kinetochores

The fundamental question of how the RZZ becomes recruited to kinetochores and how it operates there remains unanswered. There are controversies in the literature whether the Zw10 interacting protein-1 (Zwint-1) is the kinetochore receptor of RZZ. Zwint-1 has been identified in a yeast two hybrid screen for proteins that interact with Zw10 (Starr *et al*, 2000). Zwint-1 is part of the KMN network (Kops, 2005). It has been initially suggested to be required and sufficient for Kinetochore localization of Zw10 and thus the RZZ complex in HeLa cells (Wang *et al*, 2004). In agreement with this, the knockdown of Zwint-1 by RNAi depletes Zw10 from kinetochores (Wang *et al*, 2004), (Welburn *et al*, 2010). A study from the Cleveland laboratory also support the idea that Zwint-1 is required for kinetochore recruitment of the RZZ complex and revealed that the Zw10-Zwint-1 interaction is of low affinity (Kops, 2005). Another study reported that Zwint-1 is not required for Zw10 recruitment but for its stable residency at kinetochores (Famulski *et al*, 2008). Attempts to dissect the binding domain within Zw10 that promotes kinetochore localization as well as Zwint-1 binding led to conflicting results. Initially the binding domain of Zw10 that promotes Zwint-1 interactions have been mapped to its C-terminal region (468-779 aa) (Starr *et al*, 2000). Another study has mapped the Zwint-1 binding domain to the first 80 residues of Zw10 and claims that this segment is sufficient for its kinetochore localization (Wang *et al*, 2004). Yet, another study has mapped the Zwint-1 interacting domain to residues 30-82 and identified a C-terminal kinetochore localization domain (536-686 aa). Thus, both regions of Zw10 may be required for kinetochore localization (Famulski *et al*, 2008).

Hec1, which is part of the Ndc80 complex, has also been implicated in RZZ recruitment to kinetochores (Chan, 2009). Hec1 may act upstream of Zwint-1, and therefore it may be only indirectly required for Zw10 recruitment to kinetochores. In agreement with this idea, no direct interaction between Hec1 and Zw10 could be detected (Lin *et al*, 2006). In contrast, a study from the Salmon laboratory reported that in HeLa cells Zwint-1 localizes to kinetochores before Hec1, and that depletion

## Introduction

of Hec1 in nocodazole-treated HeLa cells does not decrease the levels of Zwint-1 at kinetochores (Varma *et al*, 2013). More recently, the Salmon laboratory reported the partial interdependency of Knl1 and Zwint-1 for their kinetochore localization in HeLa cells. They demonstrate that Knl1 kinetochore localization is reduced upon Zwint-1 depletion and Zwint-1 does not localize at kinetochores in Knl1 depleted cells. Consistently Zwint-1 deletion cause a 60% reduction of RZZ levels at kinetochores, while Knl1 depletion results in a complete loss of the RZZ complex at kinetochores (Varma *et al*, 2013). This points to Knl1 as the receptor of the RZZ at kinetochores rather than Zwint-1.

A very recent set of experiments by the Nilsson laboratory reports that the effects on RZZ localization caused by Knl1 depletion may be due to the loss of Bub1 at kinetochores (Zhang *et al*, 2015). The authors further identify a central domain within Bub1 (residues 437-521) as being responsible for RZZ recruitment (Zhang *et al*, 2015). However, studies by Dr. Veronica Krenn and Katharina Overlack in our laboratory demonstrate normal RZZ localization upon Bub1 depletion (data not shown).

Additional evidence exists that Aurora B phosphorylation may be involved in the Zwint-1 mediated Zw10 recruitment to kinetochores (Kasuboski *et al*, 2011). However, despite extensive attempts, this could not be reproduced in our laboratory (data not shown). Furthermore the Stukenberg laboratory proposed that in the absence of Aurora B activity, the inner kinetochore protein CENP-I is required to recruit and maintain RZZ at kinetochores. This proposal is based on the finding that in HeLa cells depleted of both Aurora B and Cenp-I, RZZ levels are greatly reduced (Matson & Stukenberg, 2014). However, the reduction in RZZ upon depletion of CENP-I may be a very indirect effect, caused by a concomitant reduction in the levels of the KMN network components upon depletion of CENP-I. Also, it has been shown that Mps1 knockdown by RNAi or inhibition of its kinase activity by Reversine leads to a drastic reduction of RZZ at kinetochores (~80%) (Santaguida *et al*, 2010).

Collectively, these data fall short of providing a unifying view of the recruitment mechanism of the RZZ complex to kinetochores.



## 2.6 Functions of the RZZ complex

### SAC activation

Since the discovery of the RZZ in genetic screens, it has been known that the RZZ complex is required for proper cell division in mitosis and that “null mutations” in any RZZ gene lead to chromosome segregation defects (Karess & Glover, 1989), (Williams *et al*, 1992), (Smith *et al*, 1985), (Williams *et al*, 2003). The RZZ complex has been identified as a checkpoint protein already in 2000 (Chan *et al*, 2000). However its exact function in the SAC remains poorly characterized. It has been established that the RZZ complex is involved in the activation of the SAC by recruiting, and/or stabilizing the presence of Mad1/Mad2 at kinetochores, which is directly involved in SAC activation (Section 2.4). In Zw10-depleted HeLa cells, Mad1/Mad2 localization at kinetochores is diminished (Kops, 2005). However, despite various attempts, Mad1/Mad2 and RZZ do not appear to interact strongly (Kops, 2005), (Williams *et al*, 2003), (Starr *et al*, 2000), (Buffin *et al*, 2005). This could indicate a more indirect link between the RZZ complex and Mad1/Mad2. The RZZ complex could promote Mad1/Mad2 stabilization at kinetochores rather than being its recruitment anchor (Karess, 2005). Indeed, it has been shown that Mad1/Mad2 kinetochore localization depends on several other proteins whose requirement for RZZ kinetochore recruitment remains uncertain, for example the Ndc80 complex (Lin *et al*, 2006), (Varma *et al*, 2013), (DeLuca *et al*, 2003), (Cheerambathur *et al*, 2013), (Chan, 2009). In *C. elegans* an additional protein, Spindly is required for Mad1/Mad2 localization at kinetochores (Gassmann *et al*, 2008), but Spindly homologs in other organisms are not required for Mad1/Mad2 recruitment. A superresolution approach developed by the Salmon laboratory positioned Zwint-1, RZZ, Mad1/Mad2 and the C-terminus of Spindly in close physical proximity to one another (Maresca & Salmon, 2009), (Varma *et al*, 2013). In conclusion, deciphering the mechanism by which RZZ stabilizes Mad1/Mad2 at unattached kinetochores will be important to gain insight into the function of the RZZ complex in SAC activation, but at present a unifying view of the mechanism of RZZ recruitment is missing.

### SAC silencing

The RZZ complex is not only involved in SAC activation but plays also a role in SAC silencing in a Spindly and Dynein dependent manner. Dynein is a minus-end directed microtubule motor protein, which is involved in many intracellular transport

## Introduction

processes (Höök & Vallee, 2006) and it consists of two heavy chains (DHC), two intermediate chains (DIC) and two light intermediate chains (DLIC). The DHCs mediate microtubule binding while the DLICs mediate binding to accessory binding partners of the motor complex, for example Dynactin, RZZ or Bicaudal D (Höök & Vallee, 2006), (Kardon & Vale, 2009). These accessory proteins regulate Dynein. In different Dynein complexes (i.e. complexes with different accessory complexes) Dynein can function differently (Kardon & Vale, 2009). In mitosis Dynein function depends on kinetochore microtubule attachments. The regulation of Dynein dependent removal of the RZZ-Spindly complex from kinetochores depends on tension and has been suggested to require Aurora B kinase activity (Kasuboski *et al*, 2011). However, the molecular basis for this dependency is currently poorly understood (Barisic *et al*, 2010), (Famulski & Chan, 2007), (Chan *et al*, 2009).

In early mitosis kinetochores form lateral attachments with microtubules and Dynein, together with other motors such as CENP-E, might contribute to this process. Once the lateral attachments are converted to end-on attachments, Dynein leaves the kinetochores and moves on microtubules towards spindle poles, taking checkpoint proteins, such as the RZZ complex and Mad2, with it (Howell, 2001), (Wojcik *et al*, 2001), (Basto *et al*, 2004), (Griffis *et al*, 2007), (Varma *et al*, 2008), (Sivaram *et al*, 2009). The removal of the checkpoint proteins is a part of the mechanism to silence the SAC (Karess, 2005).

The RZZ complex and Dynein have a two way relationship as the RZZ is also required for Dynein recruitment to kinetochores (Scaërou *et al*, 1999). More precisely, Zw10 acts as a putative anchor for Dynein at the kinetochore, which may indicate a more general and unifying function of Zw10 extending to its role in intracellular transport. Initially Zw10 has been found to interact with Dynamitin (P50), a subunit of Dynactin, in a yeast two hybrid screen. Residues 468-779 of Zw10 bind to P50 (Starr *et al*, 1997), (Starr *et al*, 1998). However, another study reports that residues 1-316 of Zw10 are sufficient to promote interaction with P50 (Inoue *et al*, 2008). A further interaction between Zw10 and the phosphorylated DIC motif of Dynein was detected, which seems to be important for Dynein kinetochore localization. Interestingly upon dephosphorylation of the DIC region/motif, Dynein binding to Dynactin is promoted and poleward streaming is induced (Whyte *et al*, 2008).

In mitosis Spindly acts as an adaptor between RZZ and the Dynein motor complex and is important for chromosome alignment and checkpoint signaling (Barisic *et al*, 2010). Spindly was first identified in *Drosophila* (Griffis *et al*, 2007). Like the RZZ complex, Spindly is only conserved in higher eukaryotes, although with weak

## Introduction

sequence conservation. One conserved feature is that Spindly is a functional regulator of Dynein in mitosis (Barisic & Geley, 2011). Spindly co-localizes with RZZ and Dynein at kinetochores in early prometaphase and at spindle poles in metaphase (Chan *et al*, 2009), (Gassmann *et al*, 2008), (Griffis *et al*, 2007). Spindly localization at kinetochores requires the RZZ complex. Co-immunoprecipitation experiments have detected a weak interaction between Spindly and the RZZ complex, that could only be observed in detergent free conditions (Barisic *et al*, 2010), (Chan *et al*, 2009), (Gassmann *et al*, 2008). Very recently, two groups independently showed that Spindly localization at kinetochore requires farnesylation of the Spindly C-terminal CAAX-box (Moudgil *et al*, 2015), (Holland *et al*, 2015). Spindly farnesylation likely contributes to its interaction with RZZ, and this would explain why RZZ proteins in Spindly precipitates can only be detected in the absence of detergents (Barisic *et al*, 2010). In human cells Spindly is required for the localization of Dynein and Dynactin to kinetochores (Barisic *et al*, 2010), (Gassmann *et al*, 2008), (Griffis *et al*, 2007), (Barisic & Geley, 2011). Localization dependencies and RNAi experiments suggest that RZZ and Spindly act in a linear manner. In this linear recruitment, one could imagine Spindly to act as a protein adaptor between the RZZ and the Dynein/Dynactin motor complex (Figure 11). However, no direct interaction between Spindly and Dynein or Dynactin could be detected so far (Chan *et al*, 2009), (Barisic & Geley, 2011). Thus, it remains to be elucidated if Spindly interacts directly with Dynein or indirectly by controlling the binding of Dynein to RZZ (Barisic & Geley, 2011).

There are some interesting differences in Spindly between species. For instance, in *Drosophila* Spindly is not required for Dynein localization to kinetochores and Spindly deletion leads to accumulation of Mad2 on bi-oriented kinetochores (Griffis *et al*, 2007). In contrast, in *C. elegans* Spindly interacts directly with Mad1 and is required for localization of the Mad1/Mad2 checkpoint proteins (Gassmann *et al*, 2008). However, in human cells neither Mad2 recruitment to kinetochores nor its removal upon bi-orientation is affected by Spindly depletion (Barisic *et al*, 2010). One possible explanation for this is the observed differences in kinetochore structures among species colluding with the finding that Spindly sequences are poorly conserved among species.

In addition to the loss of Dynein and Dynactin, Spindly depletion in human cells leads to a chromosome congression defect. Cells depleted of Spindly accumulate in prometaphase and establish irregular spindles, resulting in misaligned chromosomes. The strength of the Spindly deletion phenotype cannot be

## Introduction

explained by the loss of Dynein function alone, because it is partially rescued by concomitant RZZ depletion, suggesting that the phenotype results from a dominant effect of Spindly at kinetochores when Dynein cannot remove it (Barisic *et al*, 2010). Co-depletion of Spindly and RZZ, however, induces a more severe chromosome segregation defect and more severe irregularities in spindle formation. These defects could, at least in part, be explained by a failure, in the absence of Dynein, to establish lateral microtubule attachments and subsequent poleward movement, which is believed to promote establishment of stable end-on attachments (Gassmann *et al*, 2008), (Varma *et al*, 2008), (Barisic & Geley, 2011). The possible role for Spindly in formation of lateral kinetochore microtubule attachments is also strongly supported by the finding that co-depletion of Ndc80 and Spindly induces a stronger non-attachment phenotype than the individual RNAi phenotypes alone (Barisic *et al*, 2010), (Barisic & Geley, 2011). Point mutations in Spindly, which only prevent Dynein/Dynactin binding but retain the other functions of Spindly, rescue the Spindly depletion phenotype causing a subsequent arrest of cells in metaphase due to a failure in checkpoint silencing in the absence of Dynein/Dynactin (Gassmann *et al*, 2010). Taken together these studies indicate that Spindly is not only involved in Dynein recruitment to kinetochores but also in the formation of correct metaphase plates (Barisic *et al*, 2010).

Besides recruiting Spindly to kinetochores, RZZ might also contribute to the Spindly-dependent formation of microtubule attachments, but the function of RZZ in this process is poorly understood. It was suggested, and recently supported, that in *C. elegans* the RZZ complex negatively regulates the microtubule binding activity of Ndc80 at unattached kinetochores, and that the loss of Spindly exacerbates this suppressive function by preventing the removal of RZZ from kinetochores or by modulating this suppressive function of RZZ on Ndc80 function in a more direct manner (Gassmann *et al*, 2008), (Cheerambathur *et al*, 2013). It is worth noting that functions of the Ndc80 complex, RZZ and Spindly differ significantly among species. Whether human RZZ inhibits Ndc80 microtubule binding in a similar way remains elusive at this point.

In conclusion, the RZZ complex is a key regulator of mitosis, and is important for SAC activation as well as its inactivation. Whether or not the human RZZ complex is additionally important in formation of lateral kinetochore-microtubule attachments remains speculative at this point. The molecular mechanisms of RZZ function in the activation and in the silencing of the SAC are of great interest and represent an important question in RZZ research.

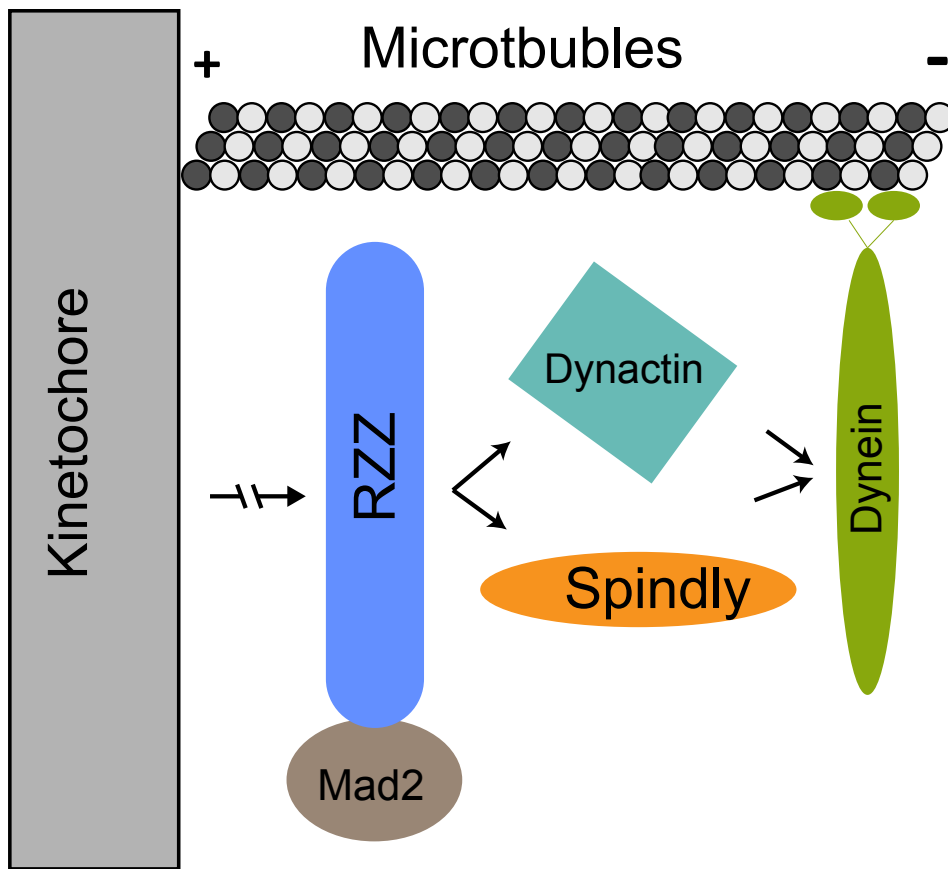


**Figure 11: Model of RZZ function**

During mitosis, the RZZ complex binds to the kinetochore and is involved in stable Mad2 binding to the kinetochore as well as Spindly and Dynactin recruitment. Spindly and Dynactin then together recruit Dynein to the kinetochore, which then transports the whole complex toward the spindle pole and silences SAC signaling. Adapted from (Griffis *et al*, 2007).

### 3 Objective

The RZZ complex is a key regulator of mitosis and mutations in any of its subunits result in chromosome segregation defects that can lead to cancer (Karess, 2005). However very little is known about the structure and function of this crucial component of the kinetochore. Previous work in Musacchio's laboratory resulted in the crystal structure of Zwilch, the smallest subunit of the RZZ complex (67 kDa) (Çivril *et al*, 2010). Additional work in Musacchio's laboratory also established that the N-terminal domain of the largest subunit, Rod (240 kDa), interacts directly with Zwilch (Çivril *et al*, 2010). The aim of my PhD project was to extend these previous findings by gaining a better biochemical, structural and functional understanding of the RZZ complex.

Therefore my work revolved around two main objectives. First, I wanted to investigate structurally how the RZZ complex is organized in terms of inter-subunit interactions. For this, it was crucial to generate a recombinant form of the RZZ complex. For this purpose I tried to express and purify full length versions of the RZZ subunits as well as several constructs of domains and sub-complexes. I tried to obtain the crystal structure of the full-length RZZ complex and of relevant domains and sub-complexes. Besides this, I also contributed to an ongoing collaboration with the laboratory of Dr. Stefan Raunser, aiming to perform 3D negative-stain and cryo-electron reconstitutions of the RZZ complex. These reconstitutions, which were carried out by Dr. Shyamal Mosalaganti, were used to identify the position of the subunits within the complex, for instance through specific antibody labeling. In collaboration with Professor Franz Herzog at the Gene Center in Munich (Leitner *et al*, 2010), (Grimm *et al*, 2015), I also carried out a cross-linking-mass spectrometry analysis to identify inter-subunit contacts.

Second, I wanted to gain a better understanding of how the RZZ becomes recruited to the kinetochore and what its function is at the kinetochore. Specific subunits of the KMN network have been implicated in the recruitment of RZZ to the kinetochore. To investigate the mechanism of kinetochore recruitment of RZZ, I carried out interaction studies between recombinant versions of the RZZ and of the KMN network subunits. For these interaction studies the potential role of additional recruitment factors, such as protein kinases (i.e. Mps1, Aurora B, Bub1, Plk1, Cdk1) was considered. To study the role of the RZZ complex in SAC activation I investigated whether there is a direct interaction of the RZZ complex with

## Objective

Mad1/Mad2, to understand how the RZZ complex stabilizes Mad1/Mad2 at kinetochores. To dissect the role of RZZ in SAC silencing I aimed to gain a better understanding of how the RZZ contributes to the recruitment of Dynein/Dynactin. As neither Dynein/Dynactin nor Spindly were available in the Musacchio laboratory, I first wanted to generate recombinant Spindly and investigate the interactions between the RZZ complex and Spindly, the putative adaptor for Dynein/Dynactin. Individual subunits of Dynein and Dynactin also became available in the Musacchio laboratory and were subjected to interaction studies with the RZZ complex, or with Zw10 individually, given Zw10's proposed role as a Dynein/Dynactin anchor within the RZZ complex.

## 4 Results

### 4.1 Characterization of the RZZ complex

Despite extensive attempts, we were initially unable to express and purify stable domains and deletion mutants of Rod and Zw10. Co-expression of full-length versions of the RZZ subunits turned out to be a successful strategy to obtain stable and well behaving recombinant versions of the RZZ complex. Therefore, I will focus in this chapter on the successful generation of the recombinant RZZ full-length complex and two additional sub-complexes, as well as its characterization and a preliminary crystallographic study.

#### 4.1.1 Purification of the full length RZZ complex

The cDNA sequences of human Zw10, Zwilch and Rod were sub-cloned into pACEbac1 or pFL vectors for expression in insect cells (ATG Biosynthetics, Merzhausen, Germany). Expression of Zwilch with two His residues at its N-terminus considerably enhanced its expression levels. Rod was expressed with an N-terminal hexa-histidine tag with a linker and a TEV protease cleavage site, leading to 18 additional residues between the hexa-histidine tag and the Rod sequence. Zw10 was expressed without any tag. The expression and purification of the RZZ complex is described in Section 6.3.14

The recombinant full length RZZ complex was purified in a two-step approach, using a nickel resin affinity column followed by size-exclusion chromatography (SEC) (Figure 12 and Figure 13). After the second step of the purification procedure the RZZ complex was >90% pure, based on SDS-PAGE analysis (Figure 13). The SEC elution profile (Figure 13) shows an apparent molecular weight of 800 kDa, which is consistent with earlier publications (Scaërou *et al*, 2001), (Williams *et al*, 2003).



## Results

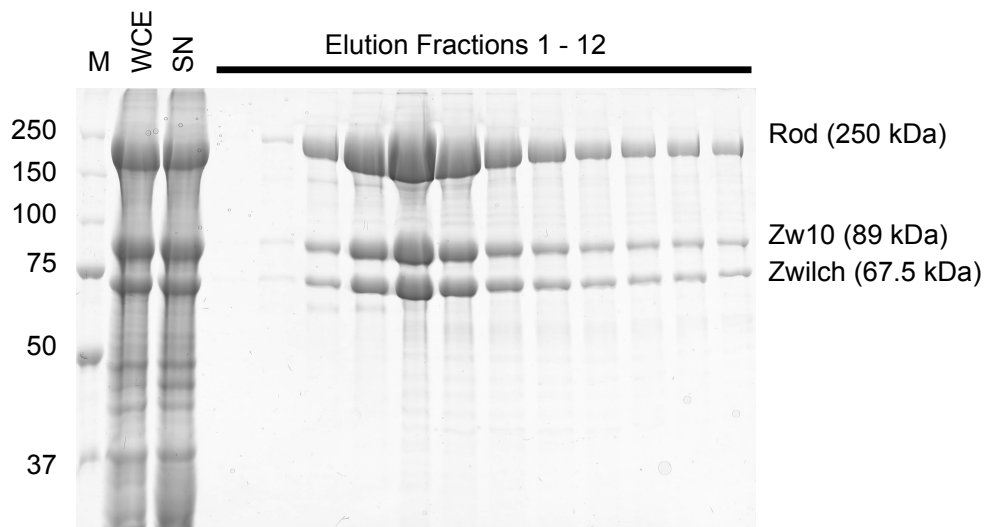


**Figure 12: Nickel resin affinity column purification of the RZZ complex**

A HisTrap Crude FF 5 ml column (GE Healthcare, Germany) was used and a step elution with 250 mM Imidazole was performed (WCE = whole cell extract; SN = supernatant).

## Results

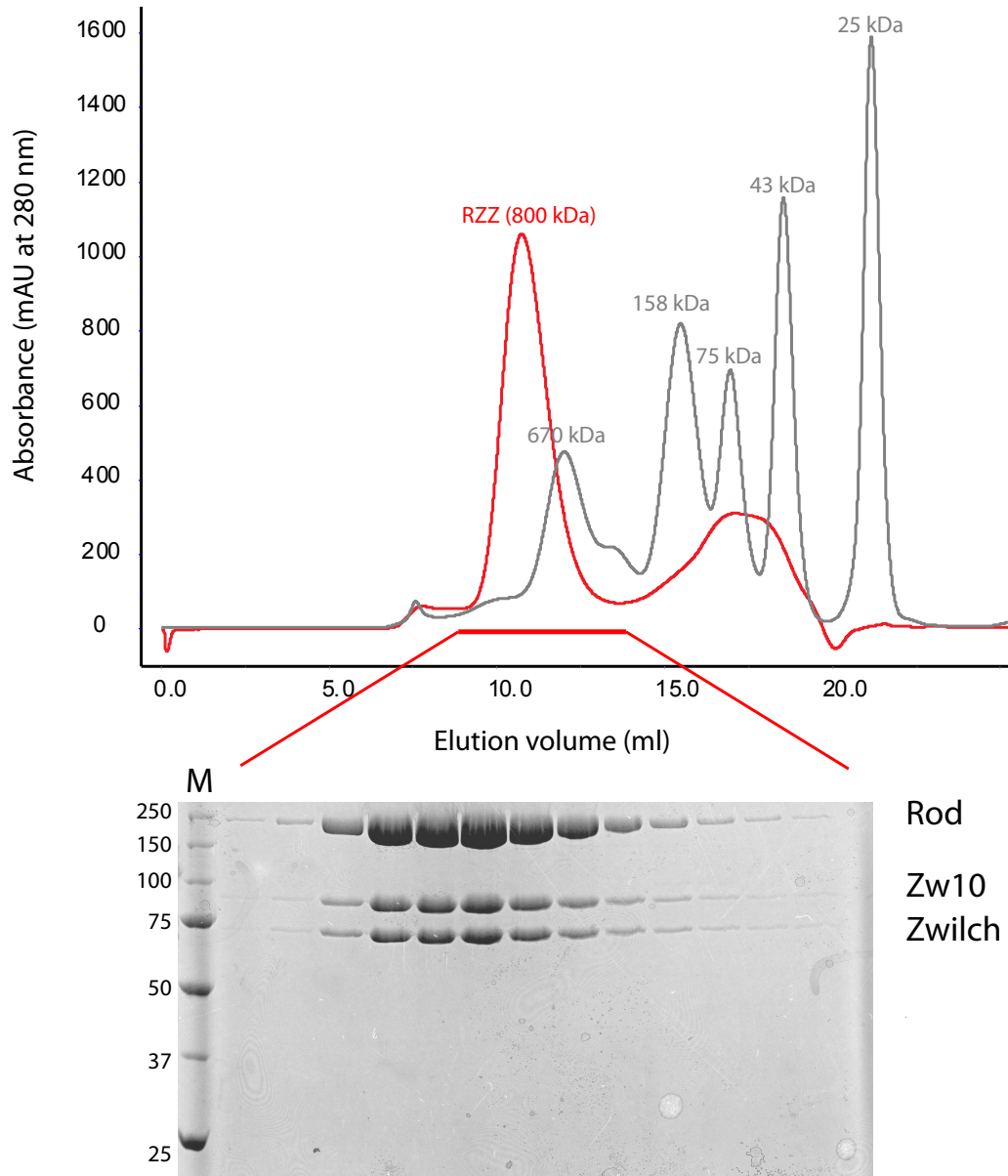


**Figure 13: Size exclusion chromatography of the RZZ complex**

Size exclusion chromatography of the RZZ complex using a Superose 6 10/300 column (GE Healthcare, Germany). The chromatogram of the RZZ purification is overlaid with a control molecular weight marker run.

## Results

### 4.1.2 Analytical Ultracentrifugation

Two studies showed that the RZZ members associate in a large complex of approximately 800 kDa and proposed the RZZ complex subunits (which have an overall molecular mass of 400 kDa) to further assemble in a dimeric arrangement (Scaërrou *et al*, 2001), (Williams *et al*, 2003). The SEC experiment showed that the recombinant RZZ complex elutes at a molecular weight higher than 670 kDa (Figure 13) suggesting a possible oligomerization of the complex. To characterize its hydrodynamic parameters and to derive stoichiometries of RZZ, we subjected the recombinant RZZ complex to analytical ultracentrifugation (AUC) (Section 6.3.20). AUC also provided information about the aggregation propensity of a sample. The purified RZZ complex was used in three different concentrations ranging from 0.1 mg/ml to 0.6 mg/ml to investigate if the oligomerization of the complex is concentration dependent. The Sedfit (Schuck, 2000) software was used for data analysis, which was performed by Dr. Arsen Petrovic. The data analysis of the analytical ultracentrifugation resulted in a major peak containing 69.6 % of the total mass (Figure 14). This peak, which contained the bulk of the RZZ complex, showed a sedimentation coefficient of 15.65 S corresponding to a molecular weight of 812 kDa, which validated the RZZ complex to be a dimer of trimer (Figure 14) as the expected molecular weight of the heterodimeric RZZ complex is 813 kDa.

## Results

MW experimental= 812 kDa  
MW theoretical= 813 kDa  
Percentage of main peak= 69.6 %  
 $S\omega(20,\omega)=15.65$  S  
 $f/f_0= 1.99$

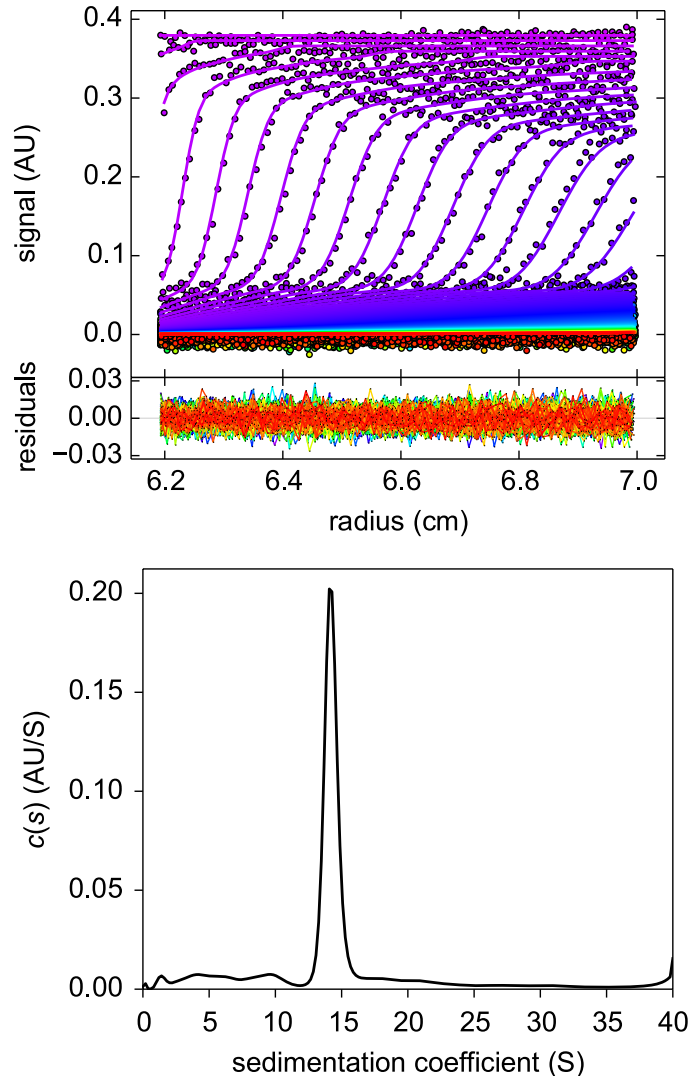


**Figure 14: Analytical Ultracentrifugation of the RZZ complex**

Analytical ultracentrifugation sedimentation velocity measurements of the RZZ complex were analyzed as a distribution of sedimentation coefficients. Fringes were collected by absorbance measurements at 285 nm (top panel) and resultant continuous  $c(S)$  distributions in the range of 1–15 S (bottom panel). Data fitting (using Sedfit (Schuck, 2000)) showed a mean sedimentation coefficient of 15.65 S, best fit by assuming a frictional ratio ( $f/f_0$ ) of 1.99 and calculated mean molecular weight of 812 kDa. Interpreted species account for 69.6% of total. Its theoretical size is 813 kDa.

## Results

### 4.1.3 Thermofluor Analysis

To analyze the thermal stability of the RZZ complex, a thermofluor assay (Boivin *et al*, 2013) was performed (Figure 15) during a P-Cube training at EMBL in Hamburg (Section 6.3.21). The analysis shows a single melting curve for the RZZ complex with a  $T_m$  (melting temperature) of  $\sim 43^\circ\text{C}$ , suggesting a cooperative disruption of the complex. . Melting curve of protein complexes, in which the proteins composing the complex interact with modest affinity often result in overlays of the melting curves of the individual denaturing events, often preventing a clear interpretation of melting curves. For example, a non-interpretable curve was obtained for the Mini-RZZ complex (Figure 50), which is described later in this thesis (Section 4.2.5)

The apparent melting temperature ( $T_m$ ) of  $43^\circ\text{C}$ , is moderately high for a human protein complex (Bischof & He, 2005). Given that the fluorophore used in this analysis is known to destabilize the protein samples slightly (Boivin *et al*, 2013), it is likely that the measured  $T_m$  is lower than the real  $T_m$ . Thus the  $T_m$  of  $43^\circ\text{C}$  for the RZZ complex implies a high sample stability. We carried out crystallogenesis of the RZZ complex at  $20^\circ\text{C}$ , which is about  $25^\circ\text{C}$  lower than its  $T_m$ , an optimal condition for crystallogenesis (Dupeux *et al*, 2011).

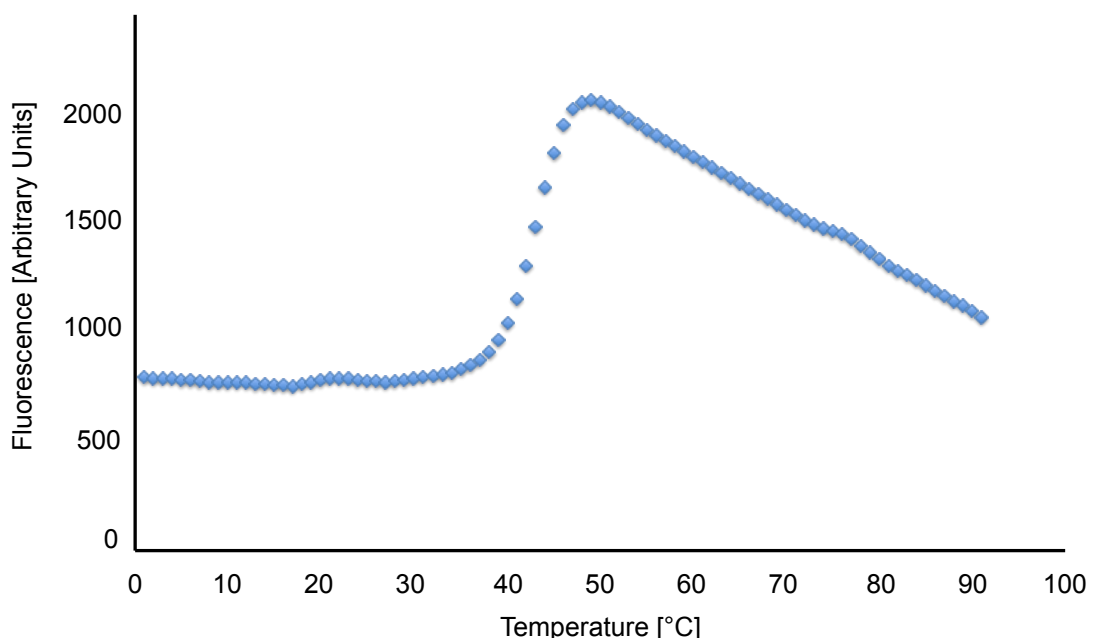


**Figure 15: Thermofluor analysis of the RZZ complex**

Thermofluor based protein-unfolding curve of the RZZ complex. The resulting melting temperature ( $T_m$ ) is  $43^\circ\text{C}$ . This assay was performed in RZZ SEC buffer (25 mM Hepes pH 8.5, 250 mM NaCl, 2 mM TCEP).

## Results

### 4.1.4 Limited Proteolysis

We applied limited proteolysis to the full length RZZ complex to identify any existing stable sub-complexes. Specifically, the protease Trypsin was mixed with the RZZ complex in a 1:100 ratio and incubated at 37°C for one hour (Section 6.3.18). Protein samples were taken at several time points and initially visualized by SDS-PAGE (Figure 16). A selected number of bands were later analyzed by a limited in-gel digest followed by mass spectrometry (performed by Dr. Petra Janning) as described in Section 6.3.19. This experiment enabled us to determine that the 250 kDa subunit Rod became cleaved into two halves, of approximately 130 kDa (N-terminal) and 120 kDa (C-terminal) (Figure 16). The 89 kDa protein Zw10 was proteolyzed into a stable segment migrating with an apparent molecular mass of 75 kDa in SDS-PAGE. However, the most N-terminal peptide that could be detected by mass spectrometry analysis of this band started from amino acid 242, which suggested a fragment of 61 kDa might be formed during limited proteolysis. Possibly this segment showed abnormal migration in SDS-PAGE, or alternatively peptides corresponding to the N-terminal region of ZW10 remained undetected in the mass spectrometry experiment. The 67 kDa protein Zwilch was also sensitive to proteolytic digestion and we identified an N-terminal segment of approximately 40 kDa corresponding to the N-terminal part of the protein and a C-terminal segment corresponding to amino acids 335-591. These two segments of Zwilch (1-334 and 335-591) correspond exactly to the split Zwilch construct used to determine the crystal structure of Zwilch (Çivril *et al*, 2010) and which was designed based on limited proteolysis of the isolated Zwilch subunit.

## Results

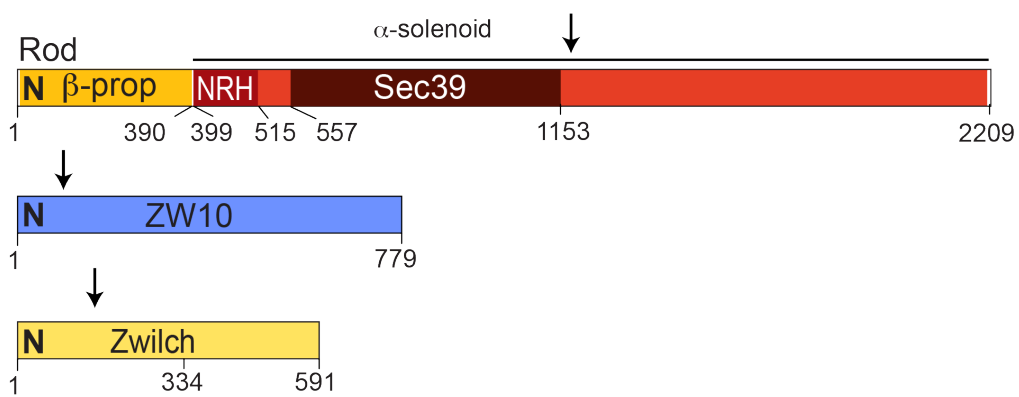
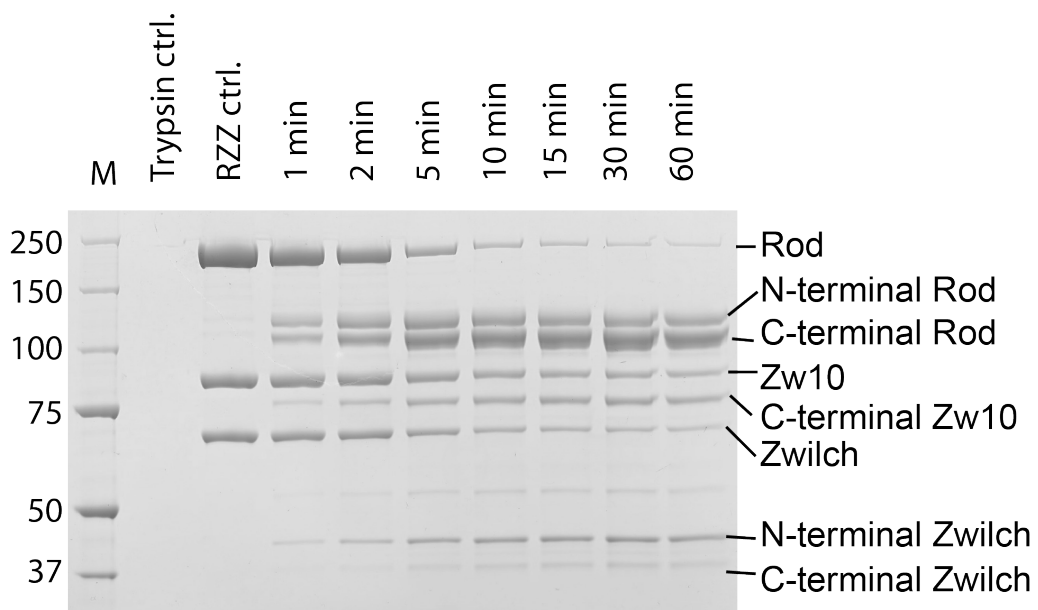


**Figure 16: Limited proteolysis of the full length RZZ complex**

The full-length RZZ complex was subjected to limited proteolysis using the Trypsin protease in a 1:100 ratio (37°C, 1 h). Selected protein bands were analyzed by mass spectrometry (following limited in gel digest). Arrows indicate in the sequence representations of Rod (red), Zw10 (blue) and Zwilch (yellow) the protease cleavage sites.

This analysis prompted us to design a Mini-RZZ complex, which is described later in this dissertation (Section 4.2.5).

## Results

### 4.1.5 Crystallogenesi

The ultimate goal of this project was to determine the structure of the RZZ complex at atomic resolution. Thus the full-length RZZ complex was subjected to various crystallogenesi approaches. Initially screenings in 96-well plates using commercially available Masterblocks were performed varying the protein concentration and the protein to precipitant ratio. Initial crystals were obtained using condition No. 69 (1 M ammonium sulfate, 0.1 M MES pH 6.5) of the ProComplex Suite (Qiagen, Hilden, Germany) and the sitting-drop vapour diffusion method as described in Table 18. These initial crystals did not diffract. To achieve and improve diffraction we attempted a wide range of options including improvement of sample quality, crystallogenesi conditions and post crystallization treatments (Table 18).

#### Sample quality improvement

To reduce flexibility of the sample the N-terminal hexahistidine tag of Rod was removed using PreScission protease during elution from a Ni-NTA column. Evidence from mass-spectrometric analyses showed that the RZZ complex is phosphorylated during expression in insect cells (data not shown). Thus, to further improve the homogeneity of the sample we performed dephosphorylation using  $\lambda$ -phosphatase. Finally, the purity of the sample increased through a third purification step in which the sample, after Ni-NTA affinity purification, was subjected to an anion exchange column (Resource Q, GE Healthcare, Germany).

#### Optimization of the crystallization conditions

A detailed table with the individual steps that were exploited to optimize the crystallization conditions can be found in Section 6.3.25.

#### Post-crystallization treatment

Because the diffraction of the obtained crystals was poor, we also varied post-crystallization treatments. Therefore, dehydration (reduction of the solvent content) of the crystals was attempted by either serial addition of glycerol to the reservoir solution or by increasing the precipitant concentration of the reservoir in 2–5% increments every two days. It is well known that reduction of solvent content can produce more closely packed and better ordered crystals, therefore improving diffraction (Heras & Martin, 2005). However in our case this did not lead to better diffracting RZZ crystals. Additionally, we tried to anneal the crystals by re-warming of a flash-cooled crystal to reduce mosaicity and potentially increase resolution by reducing the crystals solvent content (Harp *et al*, 1999), (Yeh & Hol, 1998).



## Results

Therefore we briefly interrupted the nitrogen stream that usually keeps the crystals at 100 K. Annealing did not result in better diffracting crystals.

Data-collection experiments at room temperature were also performed to avoid the freezing step and investigate whether flash cooling might be compromising the diffraction quality of the crystals. As this did not improve the diffraction quality, we concluded that the limited diffraction results from problems in crystallogenesis that precede freezing (Heras & Martin, 2005).

Best diffracting crystals (Figure 17) were grown against a reservoir buffer consisting of 380 mM ammonium sulfate, 0.1 M MES pH 6.3. The data set was collected on the crystals shown in Figure 17.

### Crystal content

To test if the crystals contained all subunits of the full-length RZZ complex, they were washed extensively with reservoir solution to separate them from soluble protein in the crystallization drop dissolved, and analyzed by SDS-PAGE. The SDS-PAGE gels (Figure 18) revealed that all three individual subunits of the RZZ complex are present, each devoid of apparent signs of degradation (Figure 18).

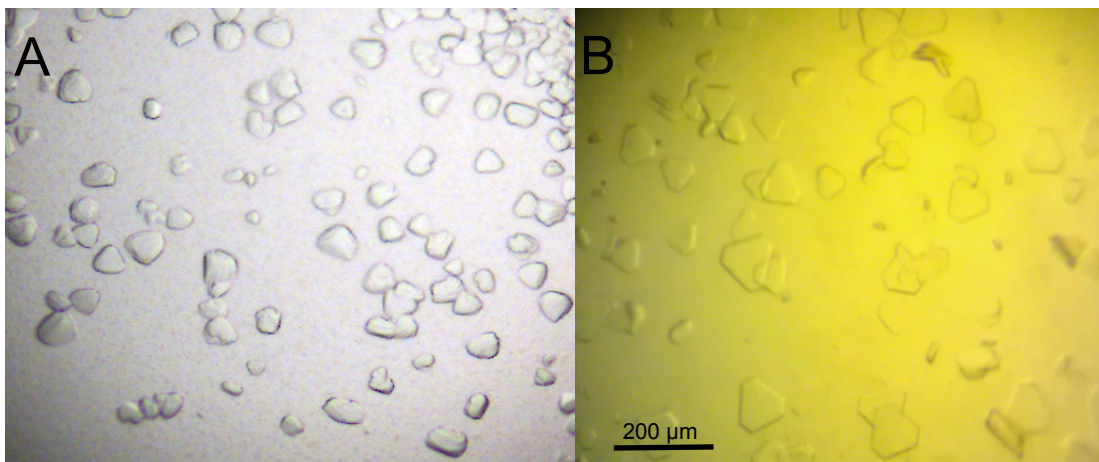


**Figure 17: Obtained RZZ crystals**

A) Initial crystals (0.5 M ammonium sulfate, 0.1 M MES pH 6.5, grown at 20 °C)

B) Crystals after optimization (0.38 M ammonium sulfate, 0.1 M MES pH 6.5, grown at 12 °C).

## Results

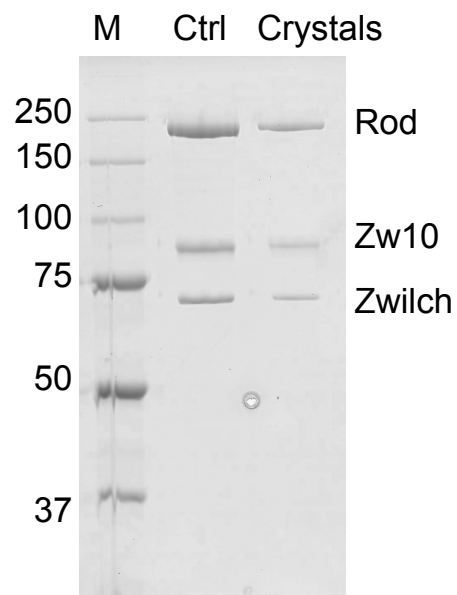


**Figure 18: SDS PAGE analysis of RZZ crystals**

RZZ crystals (washed and dissolved) contained all three RZZ subunits unaltered with respect to the original sample (*Ctrl*).

## Results

### 4.1.6 Data Collection and processing

Crystals grown against a reservoir buffer consisting of 380 mM ammonium sulfate, 0.1 M MES pH 6.3 were soaked in cryoprotecting solution (0.5 M ammonium sulfate, 0.1 M MES pH 6.3 and 20% ethylene glycol). A data set (collected on the crystals shown in Figure 16) was collected at beamline X10SA at the Swiss Light Source, Villigen, Switzerland (Table 1). The crystals showed a clean diffraction pattern to 18 Å resolution with additional reflections extending to a 14 Å resolution limit. Processing of the data (indexing, integration and scaling using XDS and XSCALE (Kabsch, 2010)) (Section 6.3.26) revealed symmetry and systematic absences (the structure factor of distinct positions equals zero due to screw or glide axis elements or due to lattice centering) typical of the trigonal space groups  $P3_1$  or  $P3_2$  (Figure 19). Analysis of the unit cell volume predicts the packing of two RZZ complexes, each consisting of two heterodimers, in the crystals' asymmetric unit, with a Matthews parameter (defined by the cell volume divided by the molecular mass) of 3.78 Å<sup>3</sup>/Da corresponding to a solvent content of 68% (Table 2) (Alternatively, with three heterodimers in the asymmetric unit, the Matthews parameter was expected to be 2.52 Å<sup>3</sup>/Da corresponding to a solvent content of 51%). To calculate the Matthews coefficient we use the program Matthews-Cell Content Analysis from the CCP4 program suite (Winn *et al*, 2011), (Kantardjieff & Rupp, 2003), (Matthews, 1968).

## Results

**Table 1: Data collection and processing**

Values in parentheses are for the outer shell.

|                                   |                                                        |
|-----------------------------------|--------------------------------------------------------|
| Diffraction source                | X10SA, SLS                                             |
| Wavelength (Å)                    | 0.9789                                                 |
| Temperature (K)                   | 100                                                    |
| Detector                          | Pilatus 6M                                             |
| Crystal-to-detector-distance (mm) | 1080                                                   |
| Rotation range per image (°)      | 0.25                                                   |
| Total rotation range (°)          | 180                                                    |
| Exposure time per image (s)       | 0.25                                                   |
| Space group                       | P3 <sub>1</sub> [No. 144] or P3 <sub>2</sub> [No. 145] |
| Unit-cell parameters (Å, °)       | a=b=215.4, c=458.7, α=β=90, γ=120                      |
| Mosaicity (°)                     | 0.213                                                  |
| Resolution range (Å)              | 60-18                                                  |
| Total No. of reflections          | 10804                                                  |
| No. of unique reflections         | 2073                                                   |
| Completeness (%)                  | 94.8 (100)                                             |
| Multiplicity                      | 5.21 (5.47)                                            |
| <I/σ(I)>                          | 8.8 (2.29)                                             |
| R <sub>meas</sub> (%)             | 14.5 (96.3)                                            |
| CC <sub>1/2</sub>                 | 99.5 (73.4)                                            |

**Table 2: Statistics of the Matthews Calculation**

| Number of molecules per asymmetric unit | Matthews coefficient (Å <sup>3</sup> /Da) | Solvent content (%) |
|-----------------------------------------|-------------------------------------------|---------------------|
| 1                                       | 7.56                                      | 83.74               |
| 2                                       | 3.78                                      | 67.48               |
| 3                                       | 2.52                                      | 51.22               |
| 4                                       | 1.89                                      | 34.96               |
| 5                                       | 1.51                                      | 18.7                |
| 6                                       | 1.26                                      | 2.45                |

## Results

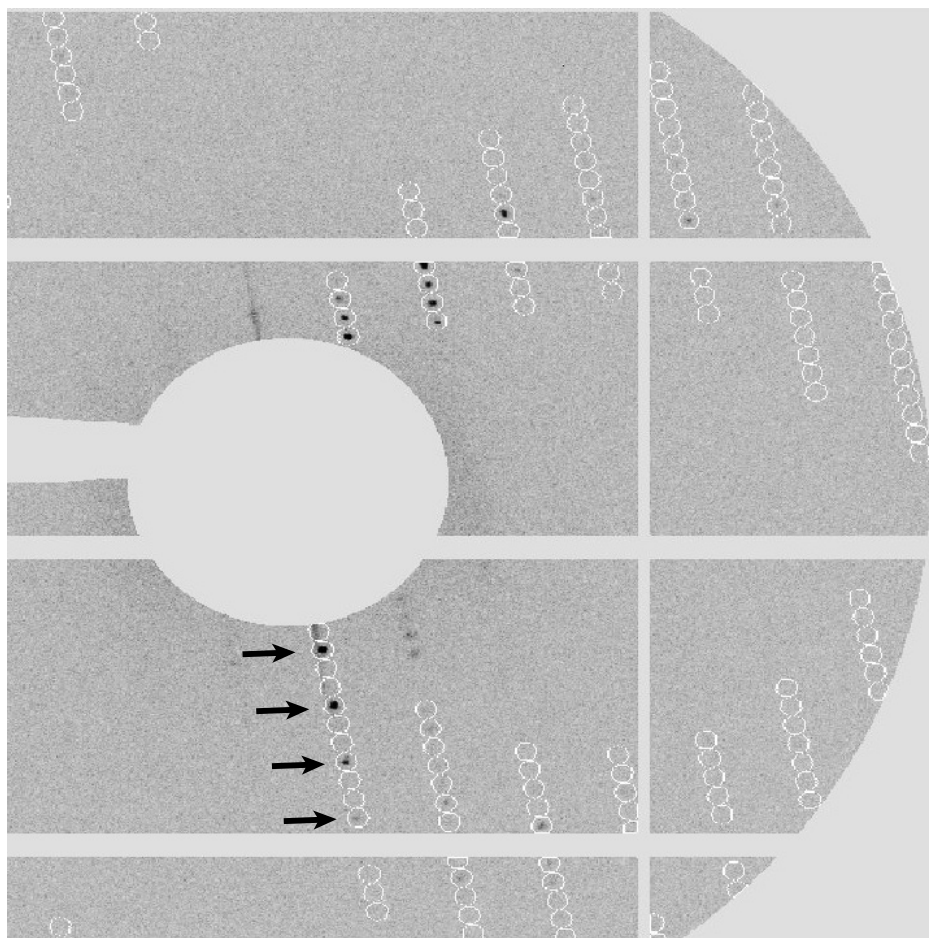


**Figure 19: Diffraction pattern of the RZZ crystals**

Diffraction pattern showing diffraction peaks (indicated by black arrowheads) alternating with two ( $2n$ ) absences along the  $c$  axis.

## Results

### 4.1.7 Self Rotation Function

A self-rotation function may be utilized to identify the rotational component of a non-crystallographic symmetry axis relating identical objects in the asymmetric unit. The largest peaks in the self-rotation function (Figure 20) indicated the presence of non-crystallographic two-fold axes (section  $\kappa=180^\circ$ ) orthogonal to the crystallographic threefold (visible in the section  $\kappa=120^\circ$ ) and likely relate the two RZZ complexes in the asymmetric unit. Two additional two fold symmetry axes might correspond to internal symmetry elements of one RZZ complex, perhaps reflecting the 2:2:2 stoichiometry of the complex.

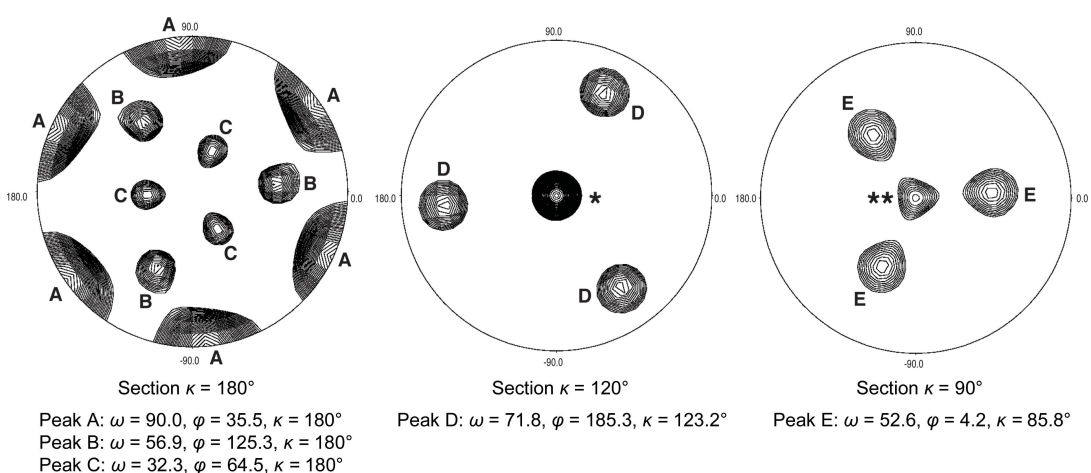


**Figure 20: Self-rotation functions of three sections**

The self-rotation function is shown for the indicated sections. Polar angles of the main noncrystallographic symmetry axes are reported. The two fold axes in the  $\kappa=180^\circ$  section may be generated by internal twofold symmetry of the RZZ complex (which is likely to form a 2:2:2 hexamer) as well as the likely presence of two RZZ complexes in the asymmetric unit of the crystal. The single asterisk in the central panel marks the crystallographic threefold axis. The double asterisk in the right panel marks the 'bleed-through' of the threefold axis in the  $90^\circ$  section. Peaks B and D and peaks C and E are symmetry related. The relative heights of the peaks (origin peak = 100) were as follows: peak A=98.8, peak B=56.4, peak C= 50.2 and 'bleed-through' peak of the crystallographic threefold axis = 49.

### 4.2 Electron microscopy analysis of the RZZ complex

A major goal of my PhD project was to investigate the structural organization of the RZZ complex. As the determination of a high-resolution structure of the RZZ complex by X-ray crystallography was not possible due to insufficient crystal quality, we used as an alternative approach electron microscopy combined with different other techniques to understand the structural organization of the RZZ complex.

#### 4.2.1 Cryo EM of the RZZ complex

The electron microscopy (EM) analysis of the RZZ complex was done in collaboration with Dr. Shyamal Mosalaganti from Professor Stefan Raunser's group. Details about data collection and processing are described in his PhD thesis (shyamal, 2014). The front of the peak fraction of a SEC separation of the RZZ complex at a concentration of 3.0 mg/ml was used for cryo EM grid preparation. 35404 particles were selected for data processing. This eventually yielded a 10.5 Å 3D density map of the RZZ complex. The density map revealed that the RZZ complex is rigid and elongated and shows a clear 2-fold symmetry perpendicular to its long axis, in agreement with the AUC analysis demonstrating that RZZ is a dimer (Section 4.1.2). The complex is 42 nm in length and about 10 nm in width.

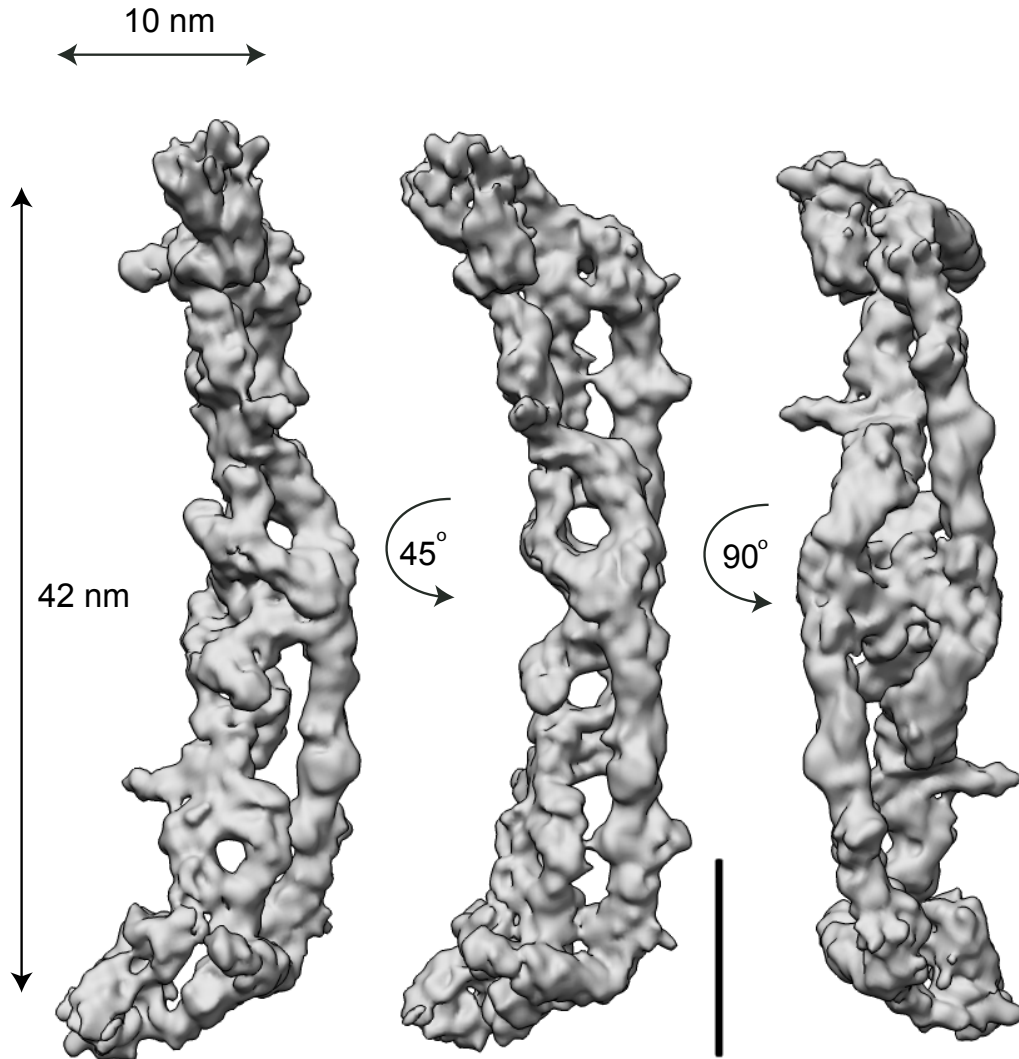


**Figure 21: Representative views of the 3D structure of the RZZ complex**

Scale bar, 10 nm.

#### 4.2.2 Protein labeling for negative stain EM

To identify the position of the RZZ subunits we used a combination of antibody labeling and protein fusions. A first attempt was the labeling of the N-terminal hexahistidine tag of Rod with a monoclonal anti-hexahistidine antibody. The RZZ complex was incubated with the antibody and immediately subjected to negative stain electron microscopy. In another approach, GFP-fusion versions of RZZ, including GFP-Zw10 and Zw10-GFP were subjected to negative stain electron microscopy. From these negative stain experiments we learned that the N-terminus of Rod is located almost at the longitudinal tip of the RZZ complex (Figure 22c). Zw10 localizes in the middle of the RZZ complex (Figure 22b and d).



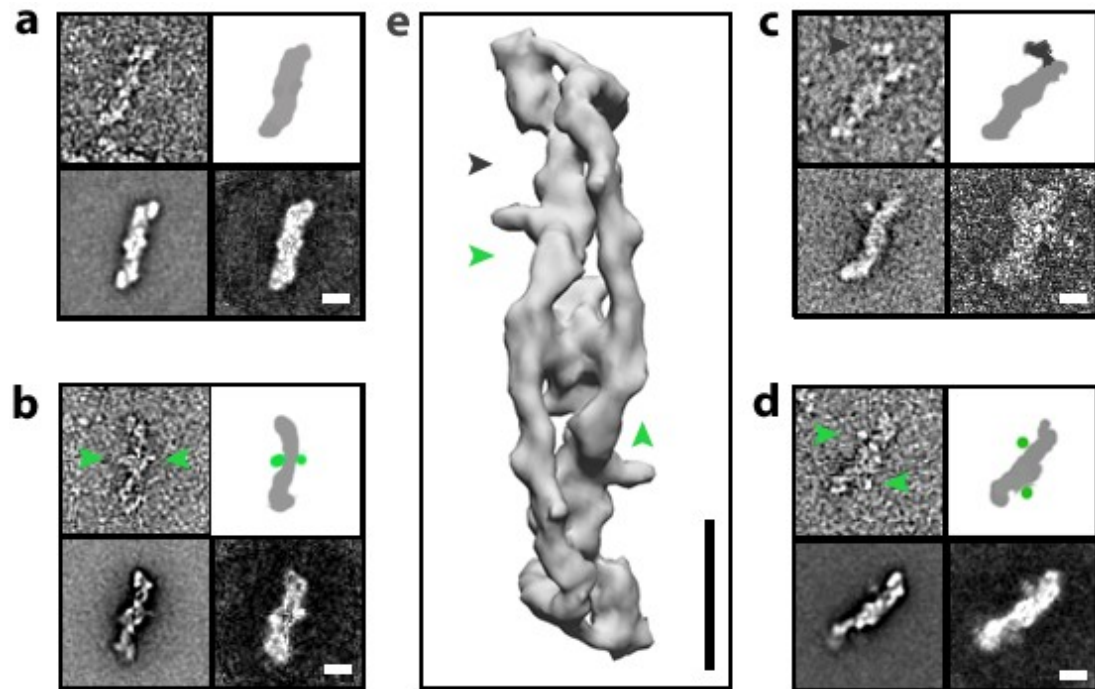


**Figure 22: Antibody labeling studies on the RZZ complex**

(a) Shows the RZZ complex, (b) the (c)RZZ complex with Zw10-GFP, (c) the RZZ complex labeled with a monoclonal anti-hexahistidine antibody and (d) the (n)RZZ complex with GFP-Zw10. Each of the different RZZ samples (a, b, c and d) is depicted as a raw particle (top left), a cartoon of the raw particle (top right), a representative average classification (bottom left) and the corresponding variance (bottom right). (e) A summary of the positions of the labels is indicated. Green arrowheads represent the GFP labels of Zw10 and the grey arrowhead represents the hexahistidine tag. (Figure provided by Dr. Shyamal Mosalaganti)

## Results

### 4.2.3 Cross-Linking Analysis

In addition to labeling individual RZZ subunits, we investigated the inter- and intramolecular interactions within the RZZ complex by cross-linking analysis. Chemical cross-linking coupled with mass spectrometry enables low-resolution analysis of the architecture of protein complexes (Maiolica *et al*, 2007). Primary amines within a distance compatible with the length of the chemical compound Disuccinimidyl Suberate (DSS) (11.4 Å) become covalently cross-linked. This method provides positional information on lysine residues in protein complexes in solution. The mass spectrometric analysis was performed by Prof. Franz Herzog's laboratory at the Ludwig Maximilian University in Munich. The result of this cross-linking analysis is depicted in Figure 23 and a table of all cross-links is shown in the supplementary (**Error! Reference source not found.**). Positions of the cross-links supported the hypothesis that Rod forms an antiparallel dimer rather than a parallel dimer (Figure 25 and Figure 23). Intermolecular cross-links of Zwilch with both the N- and C-terminal region of Rod were found. These cross-links are consistent with previous work in Musacchio's laboratory (Çivril *et al*, 2010) showing that Zwilch interacts with the N-terminal part of Rod. Additionally, Zwilch residues were cross-linked with the C-terminal part of Rod, indicating that it forms a more extensive interface with the longitudinal tip of Rod. Several cross-links found between Zw10 and the central region of Rod, were consistent with our mapping studies described in the previous section (Figure 22). A closer analysis of the intermolecular cross-links between Zw10 and Rod indicated that Zw10 bridges the two Rod molecules, because it seems unlikely that single amino acids of Zw10 cross-link with two amino acids far from another in the same Rod molecule.

Interestingly, there were no cross-links detected between Zw10 and Zwilch. We tested a possible interaction of these proteins in an analytical SEC comigration shift assay. In line with the absence of cross-links between these proteins, Zw10 and Zwilch did not form a complex in the absence of Rod (Figure 24). Combination of cross-linking analysis and electron microscopy analysis indicates that most likely Rod forms an antiparallel dimer where Zwilch is trapped between the N-terminus of one monomer and the C-terminus of the second monomer. Zw10 bridges the two Rod molecules in the central region of the complex (Figure 25).

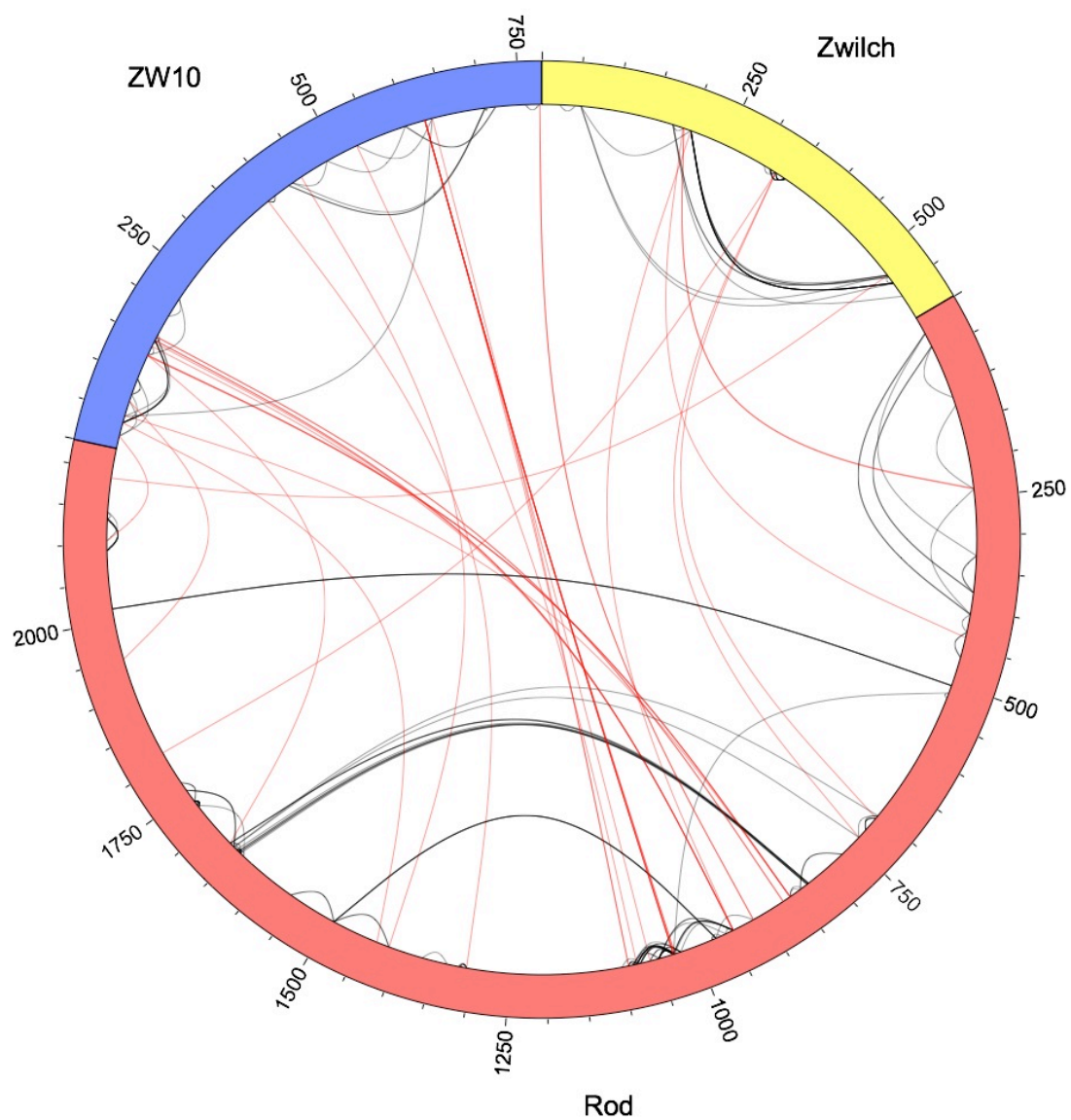


**Figure 23: Visualization of the cross-links within the RZZ complex**

The software xVis (Grimm *et al*, 2015) was used for the visualization of cross-links. Intramolecular cross-links are depicted in black and intermolecular cross-links are depicted in red.

## Results

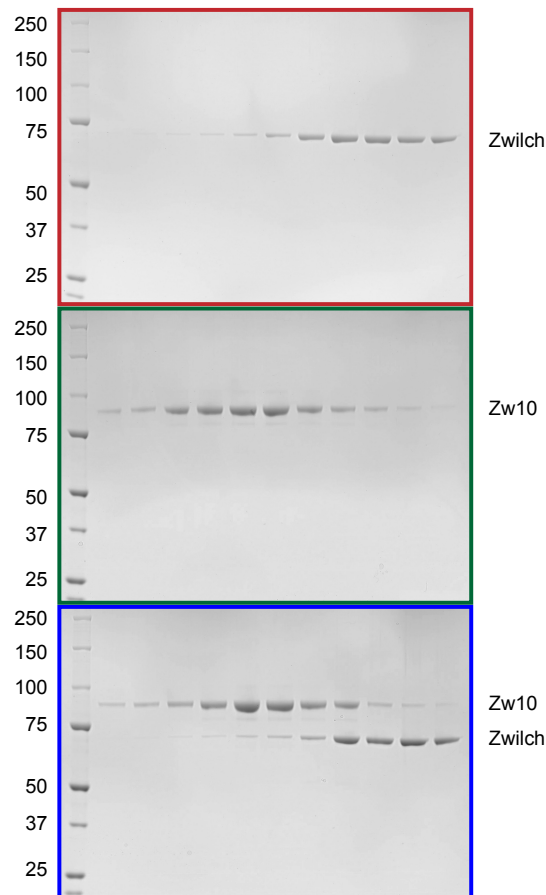
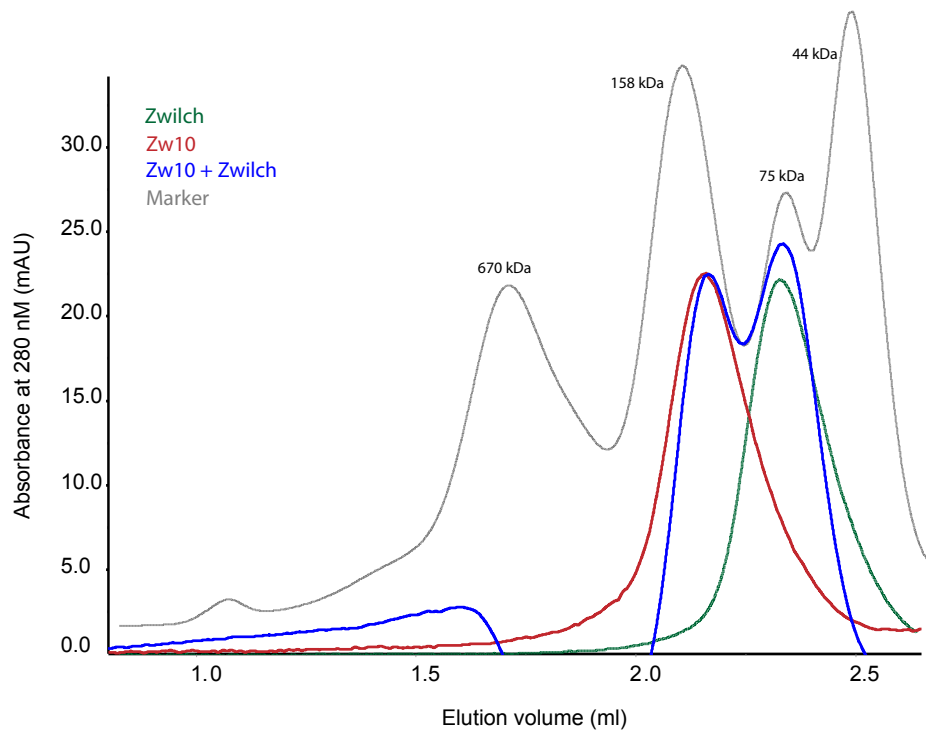


**Figure 24: Zwilch and Zw10 do not show interaction is SEC**

SEC elution profiles and SDS-PAGE analyses of Zwilch (red), Zw10 (green) and their stoichiometric combination (blue). No interaction of Zw10 and Zwilch was detected. The proteins were used at 5  $\mu$ M in 50  $\mu$ l and a Superose 6 5/15 column (GE Healthcare, Munich) was used.

## Results

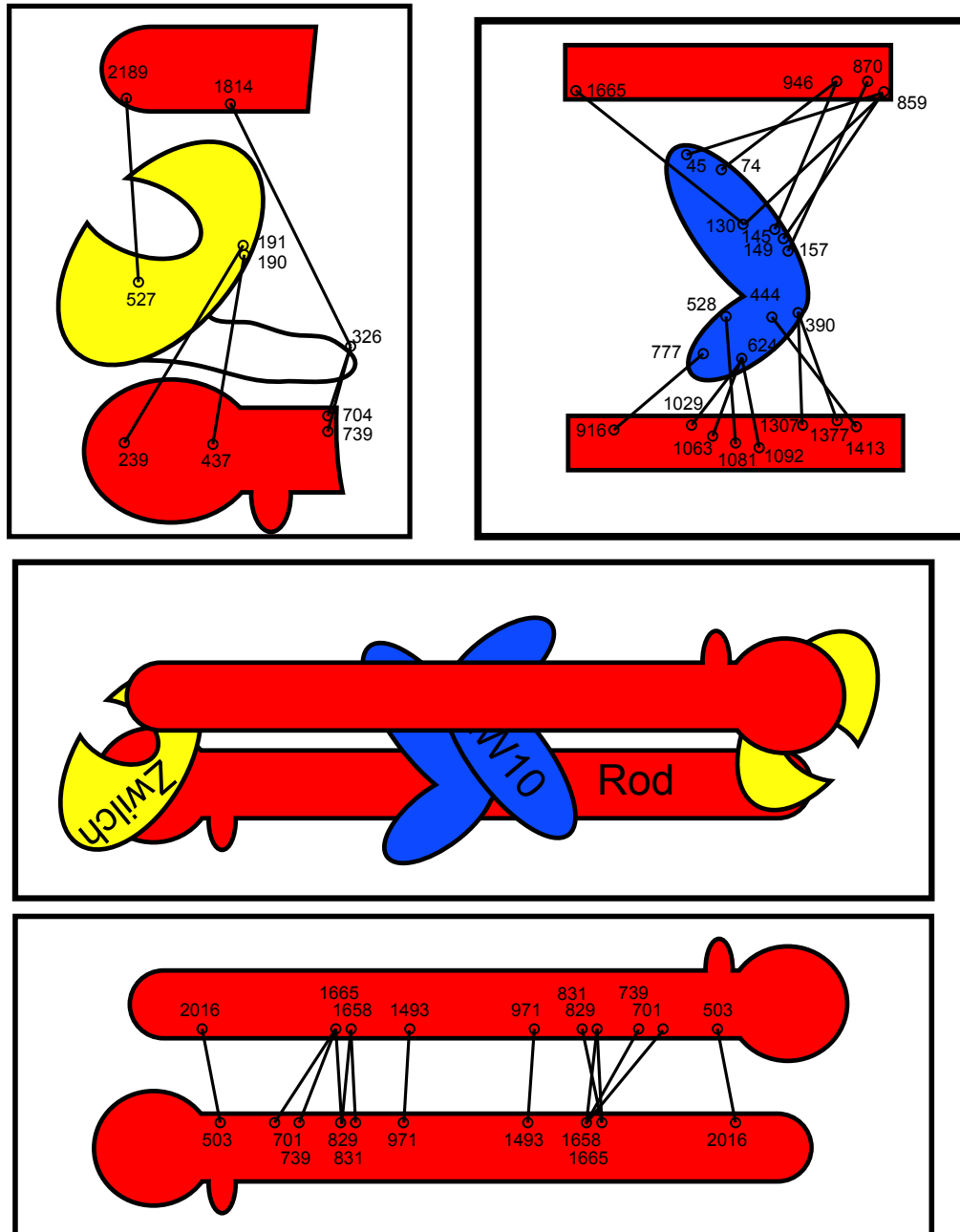


**Figure 25** Cartoon representation of the RZZ domain organization and cross-links

Rod is shown in red, Zwilch is shown in yellow and Zw10 is shown in blue. Relevant cross-links within Rod, between Rod and Zwilch and between Rod and Zw10 are highlighted. Several intra-Rod crosslinks, numerous cross-links of the central region of Rod with Zw10 and distinct cross-links of Zwilch both with the very N-terminal and with the C-terminal regions of Rod illustrate the extensive dimer interface of the RZZ complex.

## Results

### 4.2.4 Fitting of crystal structures and homology models into the 3D density EM map of RZZ

Next, we aimed to combine our 10.5 Å 3D density map of the RZZ complex from cryo EM analysis (Section 4.2.1 & Figure 21) with the information about the inter domain organization from protein labeling experiments (Section 4.2.2) and with cross-linking analysis. In collaboration with Dr. Jenny Keller (Musacchio laboratory), structural models of the individual subunits or sub complexes were fitted into the 3D density map. Previously, the crystal structure of Zwilch has been solved (Musacchio laboratory) (Çivril *et al*, 2010) (PDB ID: 3IF8). For the remaining components of the RZZ complex (Rod and Zw10), we created structure homology models using Phyre2 (Kelley *et al*, 2015). As Zw10 has a homologous yeast protein, Dsl1, of which crystal structures have been published (PDB ID's: 3ETU and 3K8P) (Tripathi *et al*, 2009), (Ren *et al*, 2009), we generated high-confidence homology models of the N-terminal half of Zw10 (residues 73-388) and the C-terminal half of Zw10 (residues 475-779) (C-scores of 100% for both in Phyre2). For Rod, four structure homology models were generated, each covering a different domain. The first homology model (residues 49-365) covered the N-terminal  $\beta$ -propeller of Rod, which is similar to several other  $\beta$ -propellers found in transport proteins, such as Sec31. The second homology model covered the Nag-Rod homology (NRH) domain (Çivril *et al*, 2010) (residue 396-496). The third homology model covered the Sec39 homology domain of Rod (residues 584-1174) and the final homology model was created for the C-terminal part of Rod (residues 1798-2192), which is very similar to the C-terminal domains found in both transport proteins Sec31 and Nup145.

These models also had high confidence scores (C-scores ranging from 75% to 100%, see supplementary Table 20). It was not possible to create structural homology models with a sufficiently high confidence for residue 1175 to 1798 of Rod. Thus we decided not to include this region into the density. In order to fit the crystal structure of Zwilch and the generated structure homology models of Rod and Zw10 into the 3D density map, the rigid body fitting function of Chimera was utilized. Placement of the Zw10 and Rod models and the Zwilch structure in the density map was guided by previous experiments (Figure 25) and resulted in a very good fit with confidence values of 0.82 to 0.97 (Table 20). The result of the rigid body fit is represented in the upper panel of Figure 26. Two monomers of Rod (depicted in red and pink) were positioned as antiparallel dimers. The two Zwilch molecules (illustrated in orange and yellow) were placed so that one Zwilch molecule contacts

## Results

the N-terminal  $\beta$ -propeller of one of the Rod monomers and the C-terminus of the second Rod monomer (see third and bottom panel of Figure 26). Both Zw10 molecules (shown in dark and light blue) were positioned in the central region of the density. Each monomer of Zw10 was positioned to account for the observed distance measurements with both Rod protomers (bottom panel of Figure 26).

Overall, the results presented here provide the first structural information of the full length RZZ complex by cryo electron microscopy. Based on low-resolution information, we were able to fit known crystal structures and structure homology models of Zw10 and the RZZ subunits, into this 3D density with high confidence. Next, we aimed to validate our model of the inter domain organization within the RZZ complex biochemically.

## Results

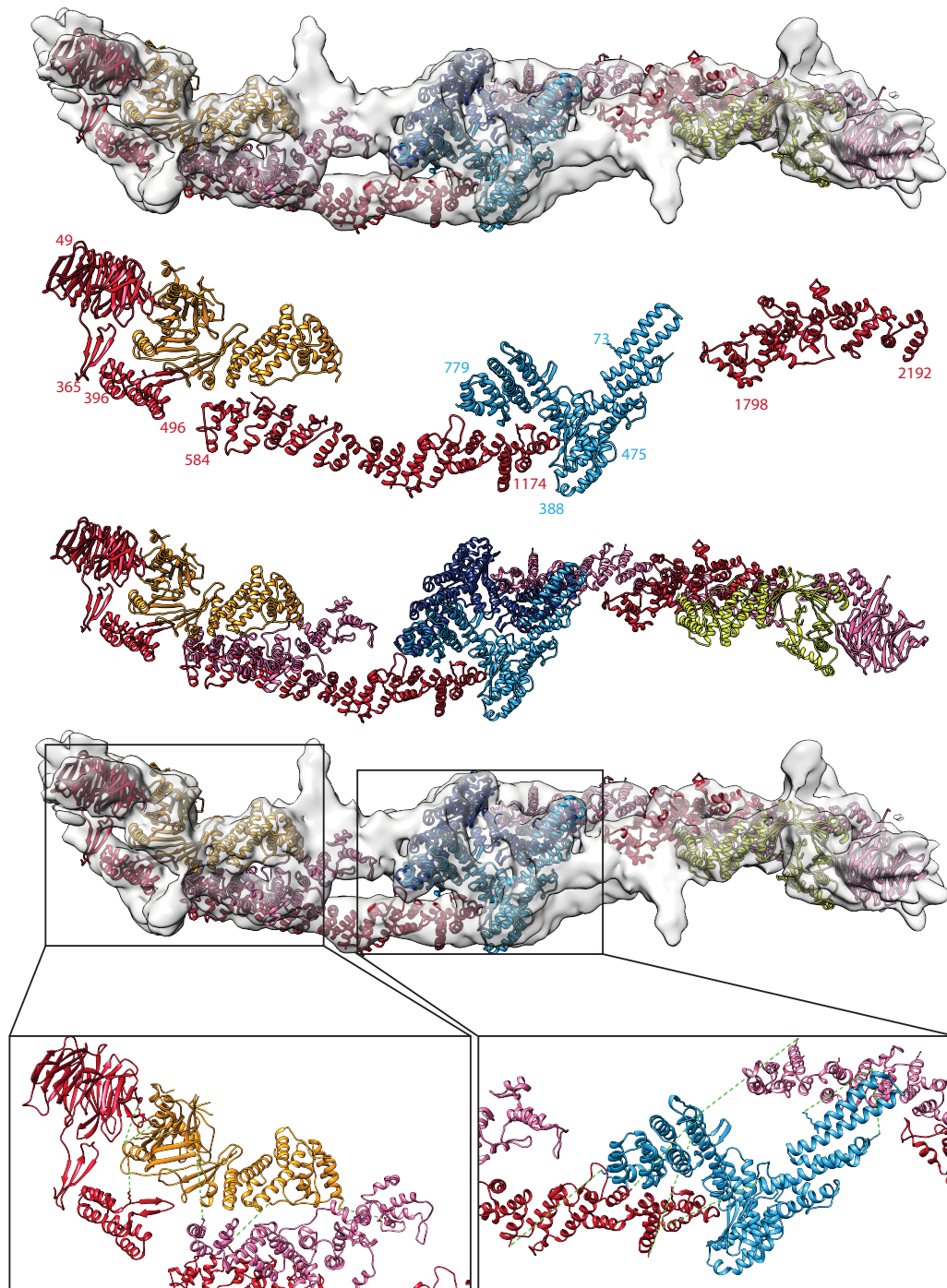


**Figure 26: Rigid body fit of subunits into the RZZ 3D density**

Structural models of Rod (molecule 1: red, molecule 2: pink) and Zw10 (molecule 1: dark blue, molecule 2: light blue) and the crystal structure of Zwilch (molecule 1: orange, molecule 2: yellow) were fitted into the 10.5 Å density map of the RZZ complex. The upper panel shows the overall fit (rigid body fit) of RZZ molecular models in the EM density maps. The second panel shows one molecule of each structural model or crystal structure (Zwilch) in the orientation within the fit. Numbers indicate amino acid boundaries. Residues 1175 to 1799 were not included due to poor confidence of the models. The third panel shows the fit of two RZZ molecules, in the absence of the EM density. The bottom panel highlights the short distances between residues within Rod with Zwilch (left) or Zw10 (right), which were also found to be in close proximity to one another by cross-linking analysis.



## Results

### 4.2.5 Model Validation –Mini RZZ

A first attempt to validate our model of the RZZ domain organization was to design a monomeric version of the RZZ complex by disrupting its predicted mechanism of dimerization. For this, we designed a complex containing a shortened version of Rod, inspired by the limited proteolysis experiment (Figure 16), which indicated that Rod can be cleaved into two stable moieties, including an N-terminal one. The Mini-RZZ complex contains the first 1250 amino acids of Rod (Rod\_1-1250) and full-length versions of Zw10 and Zwilch.

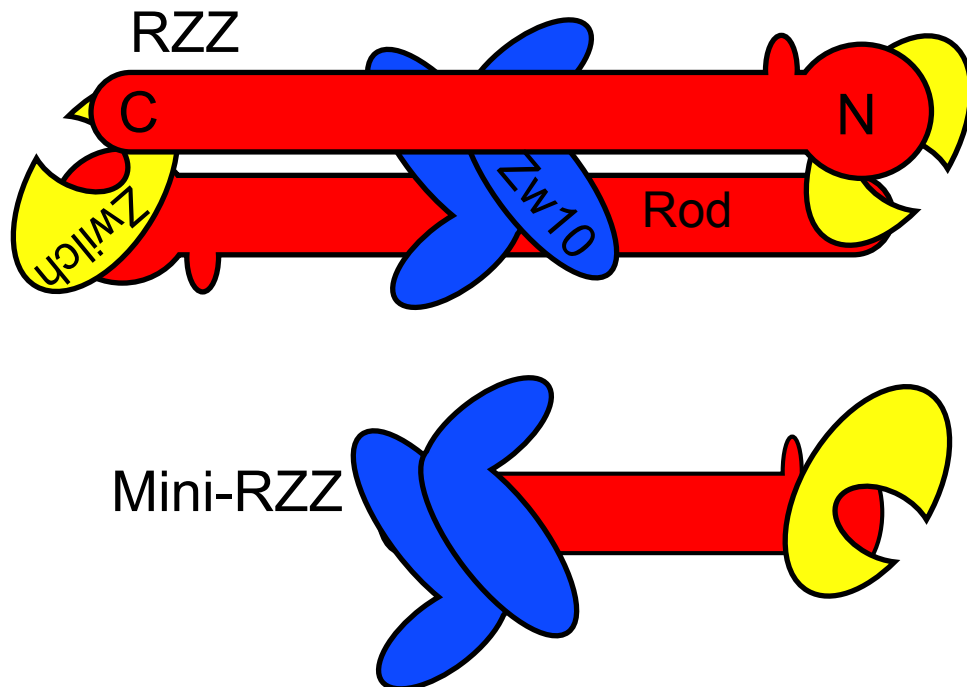


**Figure 27: Cartoon representation of the Mini-RZZ complex**

Schematic representation of the Mini-RZZ construct, based on the cartoon model of the RZZ complex (Figure 25). Rod is shown in red, Zwilch is represented in yellow and Zw10 is depicted in blue.

The Mini-RZZ complex was expressed and purified using the same protocol as for the RZZ complex (Figure 28). Mini-RZZ eluted with an apparent molecular weight under 400 kDa from a size exclusion chromatography experiment (Figure 28), suggesting that the Mini-RZZ has lost the ability to dimerize but may still be able to bind two Zw10 molecules. The expected molecular weight of an arrangement consisting of Mini-Rod, Zwilch, and two Zw10 molecules would be about 385 kDa.

## Results

The Mini-RZZ complex was significantly less stable than the full-length RZZ complex (see supplementary **Error! Reference source not found.**) with a high tendency to form aggregates.

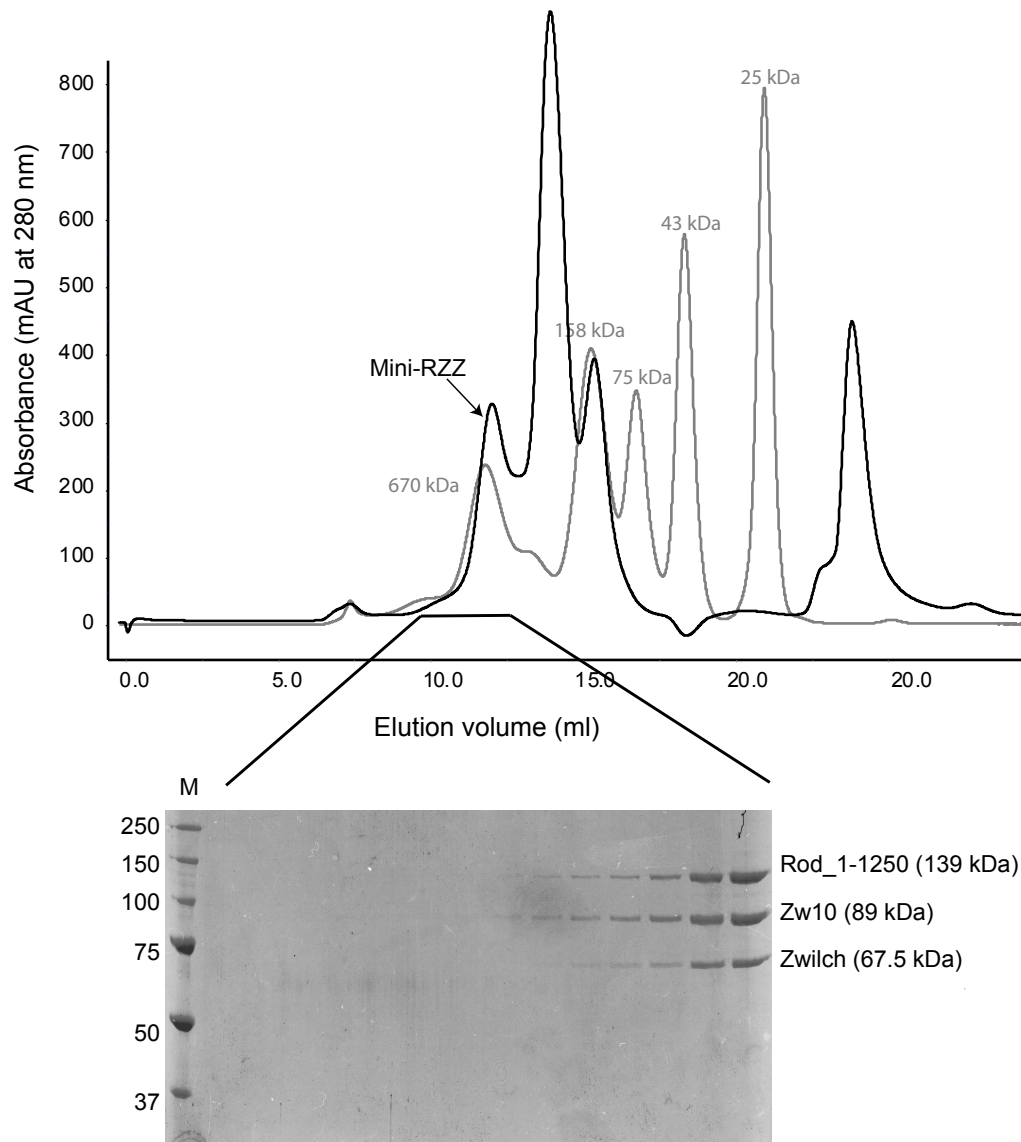


**Figure 28: Size exclusion chromatography of the Mini-RZZ complex**

SEC elution profile and SDS-PAGE analysis of the Mini-RZZ complex. The complex eluted as a monomer and is pure without apparent degradation products. A Superose 6 10/300 column (GE Healthcare, Munich) was used.

## Results

We subjected this Mini-RZZ complex to negative stain electron microscopy and calculated class averages of the particles, which are depicted in Figure 29.

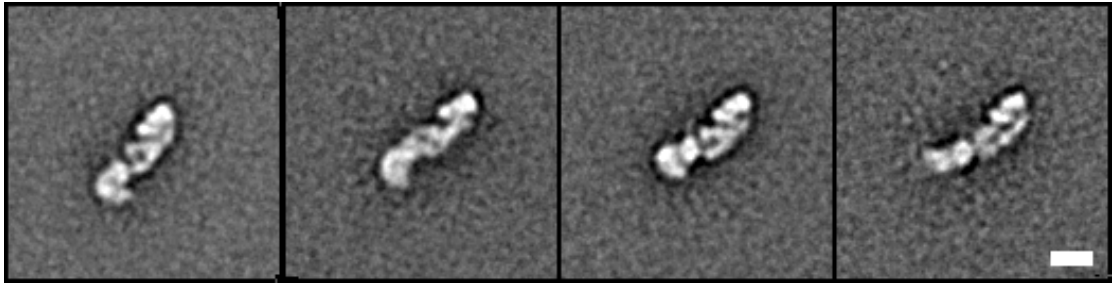


**Figure 29: Representative negative stain class averages of the Mini-RZZ complex**

Scale bar, 10 nm.

From these class averages it is evident that the Mini-RZZ complex is notably shorter than the RZZ complex and does not exhibit any symmetry elements. We calculated a 24 Å 3D density map of the Mini-RZZ complex (Figure 30). This density map of the Mini-RZZ complex has a length of 26 nm, which is significantly shorter than the full-length RZZ complex (42 nm). This density map is in agreement with our hypothesis that Mini-RZZ is monomeric, and supports our proposed model of the domain organization of the RZZ complex (Figure 25 and Figure 26).

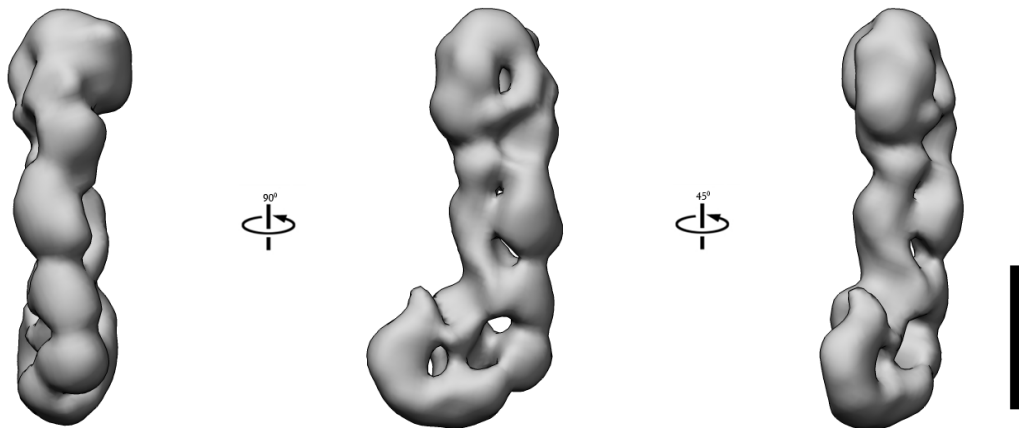


**Figure 30: Representative views of Mini-RZZ**

Scale bar, 10 nm. The length of the complex is 26 nm.

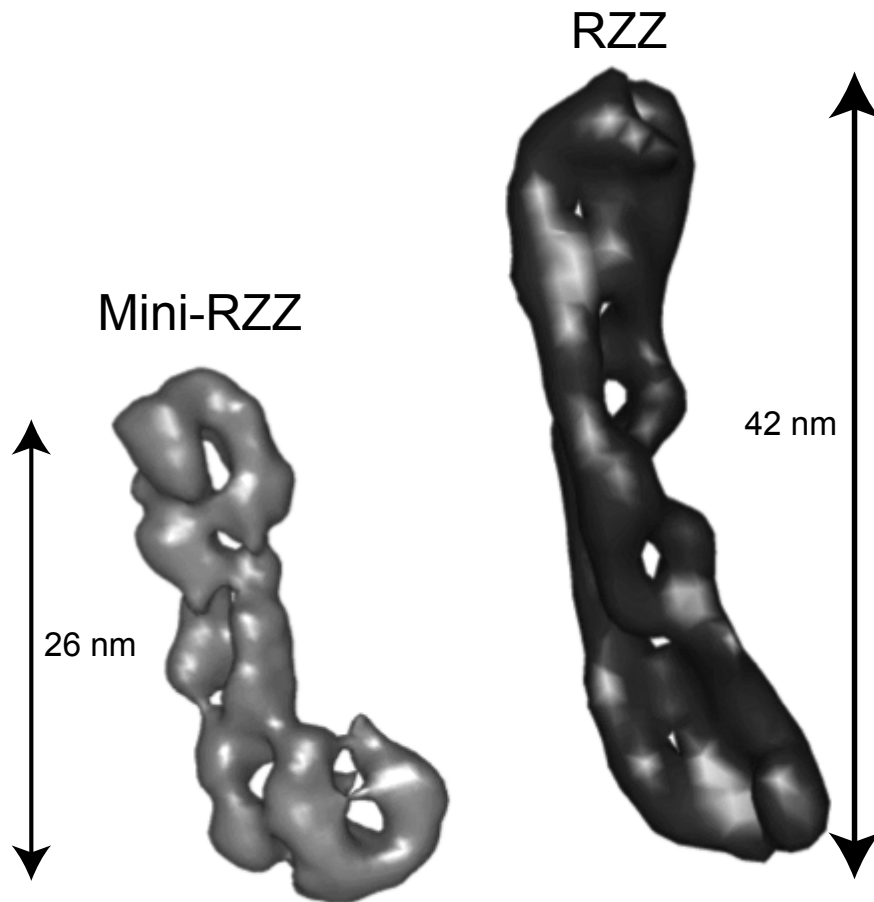


**Figure 31: Comparison of Mini-RZZ and RZZ**

3D density maps from negative stain EM of the Mini-RZZ in comparison with RZZ at the same resolution (24 Å).

#### 4.2.6 Model Validation -Mini-Rod

We also designed the construct Rod\_1-753\_(GGSG)<sub>4</sub>\_1797\_2209, which lacks the central region of Rod. The purpose of this Mini-Rod (not to be confused with the previous construct, called Mini-RZZ) construct was to further validate our model of the domain organization of the RZZ complex. To be consistent with our model, this construct should form a complex with Zwilch, but be unable to bind to Zw10 (Figure 32)

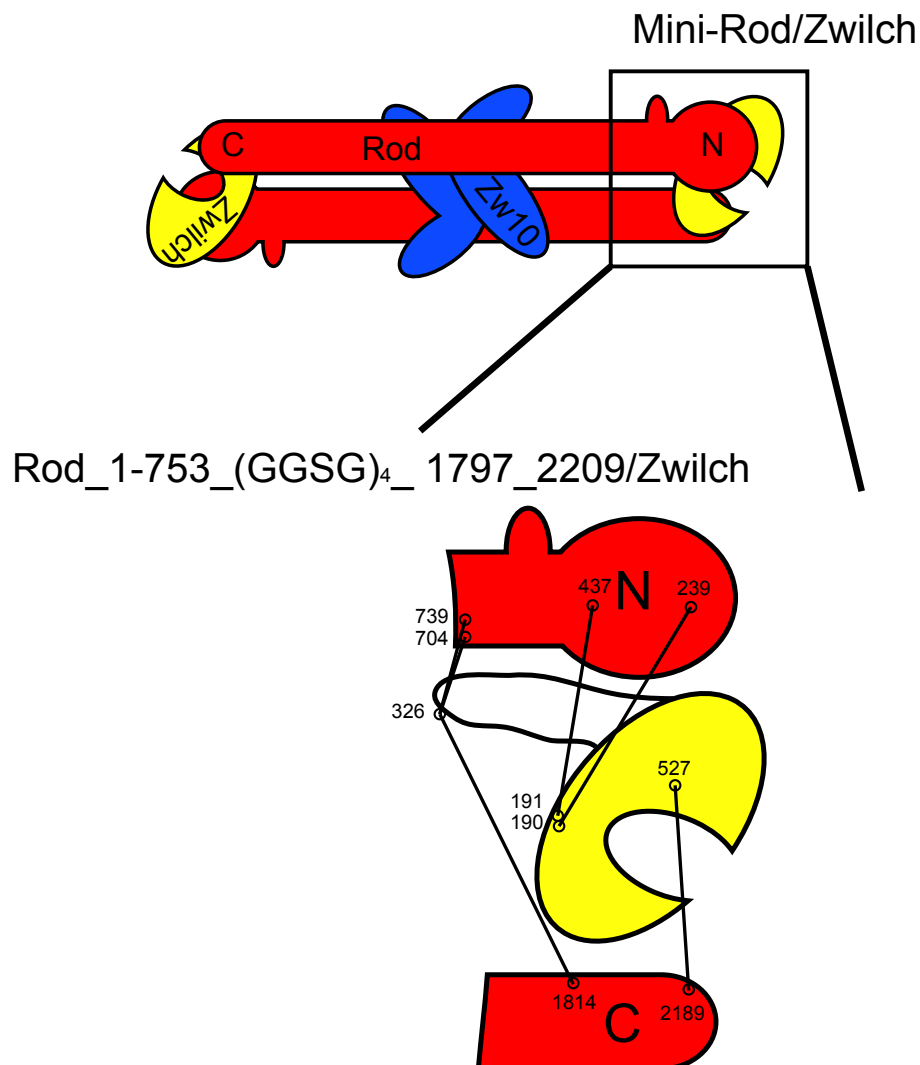


**Figure 32: Cartoon representation of the Mini-Rod/Zwilch construct**

Schematic representation of the Mini-Rod/Zwilch construct, based on the cartoon model of the RZZ complex (Figure 25). Rod is shown in red, Zwilch is represented in yellow and Zw10 is depicted in blue.

## Results

This construct was expressed in insect cells. Expression tests already partly validated our hypothesis, that Mini-Rod forms a complex with Zwilch, as it was insoluble when co expressed with Zw10, but it became soluble when co expressed with Zwilch (Figure 33).

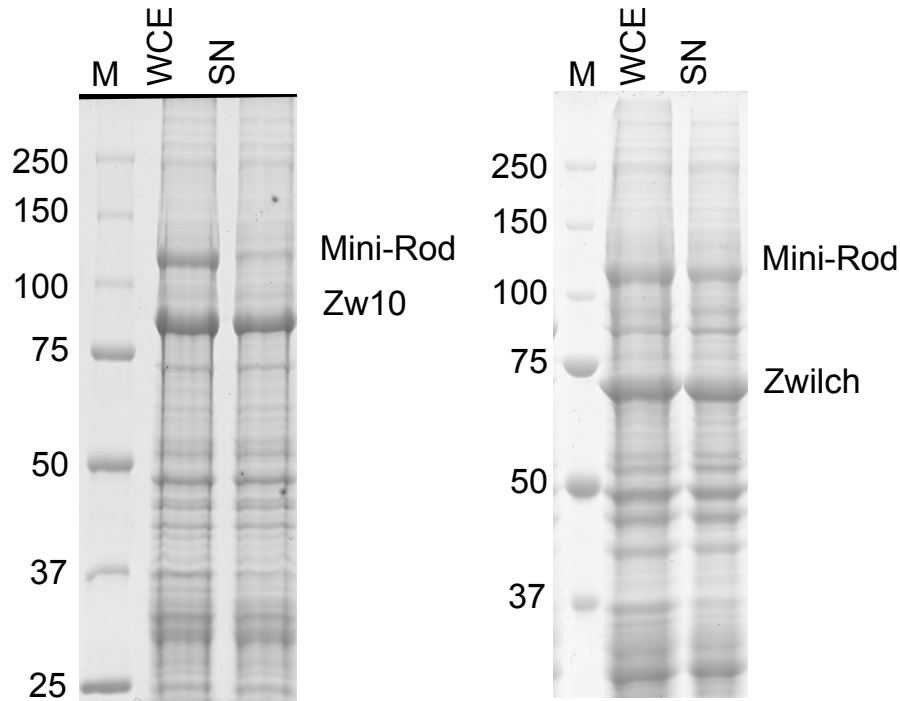


**Figure 33: Coexpression of Mini-Rod with Zw10 or Zwilch**

The gels show the whole cell extract (WCE) and supernatant (SN) samples of Mini-Rod co-expressions in TnaO38 cells with either Zw10 (left gel) or Zwilch (right gel). Mini-Rod co-expressed with Zw10 was apparently not soluble, while it became soluble when co-expressed with Zwilch.

Like the Mini-RZZ complex, the Mini-Rod/Zwilch complex was remarkably less stable than the full-length RZZ complex. In order to test if the Mini-Rod/Zwilch complex was able to form a complex with Zw10 we performed an analytical SEC assay. This revealed the Mini-Rod/Zwilch complex is unable to form a complex with Zw10, thus validating our hypothesis that the binding site for Zw10 engages the central domain of Rod.

## Results

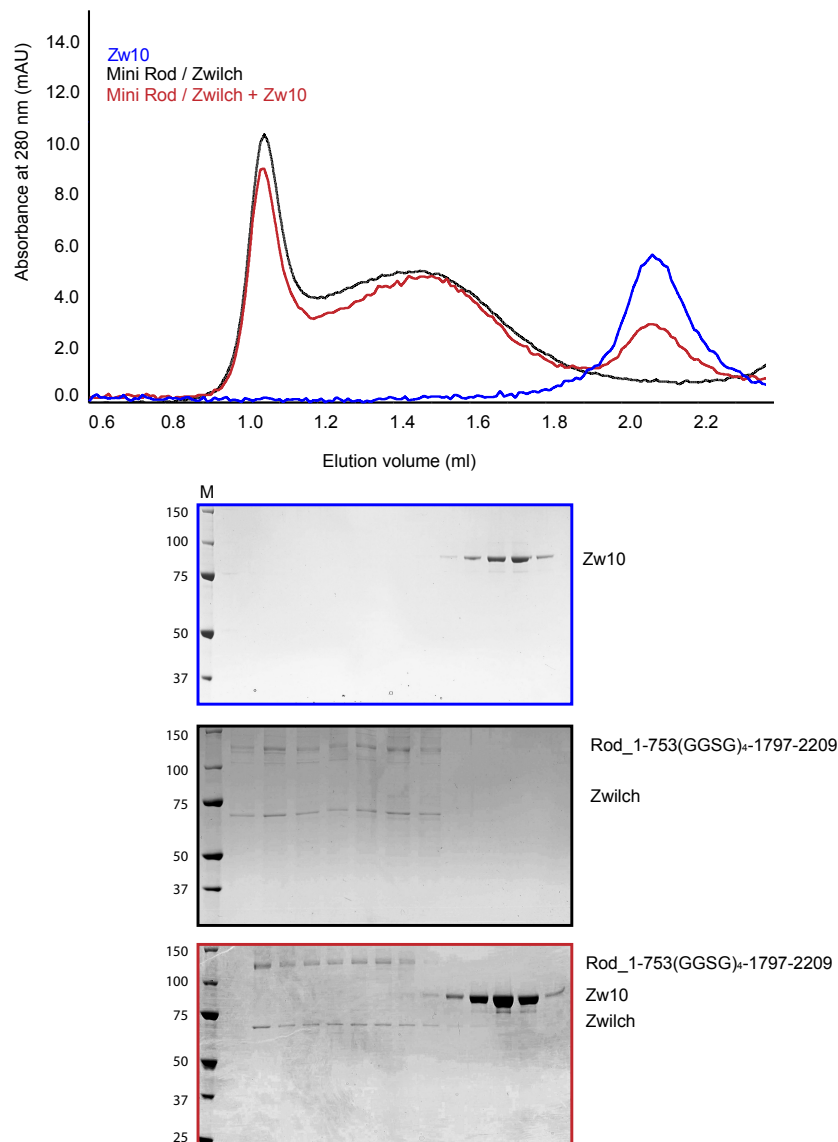


**Figure 34: The Mini-Rod/Zwilch complex does not interact with Zw10**

SEC elution profiles and SDS-PAGE analyses of Zw10 (blue), the Mini-Rod/Zwilch complex (black) and their stoichiometric combination (red). No interaction of Zw10 and the Mini-Rod/Zwilch complex was detected. The proteins were used at 3  $\mu$ M in 50  $\mu$ l and a Superose 6 5/15 column (GE Healthcare, Munich) was used.

Collectively, the findings that the Mini-RZZ complex lacks the ability to dimerize, and that the Mini-Rod construct forms a complex with Zwilch, but not with Zw10, corroborate the proposed model of the domain organization within the RZZ complex. This is further supported by the discovery that both the Mini-RZZ complex and the Mini-Rod/Zwilch complex are less stable than the full length RZZ complex, which could be explained by the disruption of an extensive dimer interface of the RZZ complex formed by the antiparallel dimer of Rod plus additional influence of Zw10 bridging these two Rod molecules.

## Results

### 4.3 Functional Assays

In this section we will describe our attempts to achieve a better understanding of how the RZZ becomes recruited to the kinetochore and what its functions are. In particular we focused on interactions of the RZZ complex with the KMN network, Spindly, and the Dynein/Dynactin complex.

#### 4.3.1 Zw10 forms a complex with Knl1/Zwint-1 but not with the KMN complex

Zwint-1 and Knl1 have been proposed to be the receptor for the RZZ complex at the kinetochore (Starr *et al*, 2000), (Wang *et al*, 2004), (Welburn *et al*, 2010), (Kops, 2005), (Famulski *et al*, 2008), (Varma *et al*, 2013) (Section 2.5). In a first attempt to investigate possible interactions between the KMN network and the RZZ complex, we studied the interactions of Zw10 and Zwint-1. Zw10 and Zwint-1 were subjected to an analytical SEC co-elution assay but we could not detect a direct interaction of Zw10 and Zwint-1. Previous work in the Musacchio laboratory demonstrated that Zwint-1 forms a stable complex with the C-terminal construct of Knl1<sup>2000-2311</sup>. Therefore we repeated our binding experiment with the Knl1<sup>2000-2311</sup>/Zwint-1 complex and Zw10 and observed a distinct shift of the peak resulting from the Knl1<sup>2000-2311</sup>/Zwint-1 + Zw10 sample compared to the individual ones (Figure 34). This experiment showed that Zw10 interacted with the Knl1<sup>2000-2311</sup>/Zwint-1 complex. The three proteins form a tight complex with a predicted stoichiometry of Knl1/Zwint-1/Zw10 (KZZ) 1:2:1, based on SEC co-elution experiments in which the proteins were mixed in different ratios (data not shown).

The result that Zw10 binds to the Knl1<sup>2000-2311</sup>/Zwint-1 complex but not to Zwint-1 individually prompted us to test if Knl1<sup>2000-2311</sup> is able to bind to Zw10 in the absence of Zwint-1. We performed the same assay with Knl1<sup>2000-2311</sup> and Zw10 and did not observe any peak shift, demonstrating that Knl1<sup>2000-2311</sup> is unable to interact with Zw10 in the absence of Zwint-1. Together the findings that Zw10 interacted with the Knl1<sup>2000-2311</sup>/Zwint-1 complex, but neither with Knl1<sup>2000-2311</sup> nor with Zwint-1 individually argue that either a specific binding surface for Zw10 is formed by the Knl1<sup>2000-2311</sup>/Zwint-1 complex formation or that Knl1<sup>2000-2311</sup> and Zwint-1 bind cooperatively to Zw10.



## Results

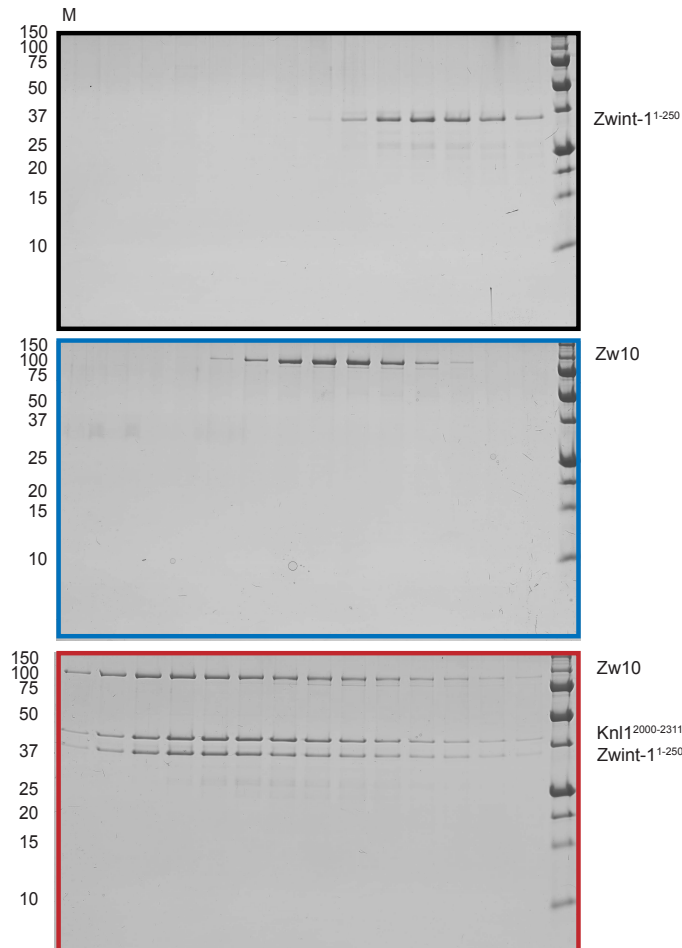
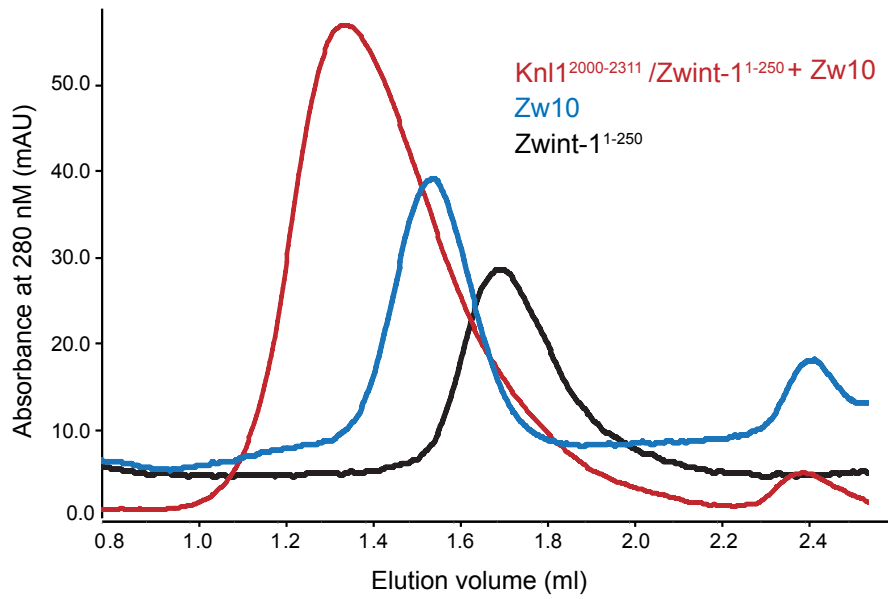


**Figure 35: Knl1/Zwint-1 does interact with Zw10**

SEC elution profiles and SDS-PAGE analyses of Zwint-1<sup>1-250</sup> (black) Zw10 (blue) and the stoichiometric combination of Knl1<sup>2000-2311</sup>/Zwint-1<sup>1-250</sup> and Zw10 (red). Co-elution of these three proteins suggested a physical interaction. The proteins were used at 5  $\mu$ M (10  $\mu$ M Zwint-1<sup>1-250</sup>) in 50  $\mu$ l and a Superose 6 5/15 column (GE Healthcare, Munich) was used.

## Results

Since Knl1/Zwint-1 interacts with the isolated Zw10 subunit, we expected that it interacted also with the RZZ. We also asked if Zw10 interacted with the entire KMN network. We tested these interactions in analytical SEC co-elution assays (Figure 36 and Figure 37). Surprisingly, Zw10 did not co-elute with the KMN network, nor did the Knl1<sup>2000-2311</sup>/Zwint-1 complex co-elute with the RZZ complex. Additionally we tested if the RZZ complex interacts with the KMN complex, but also those two complexes do not reveal any interaction. Why Zw10 binds Knl1<sup>2000-2311</sup>/Zwint-1 but not the entire KMN complex, and why Zw10 in the RZZ complex is unable to bind Knl1<sup>2000-2311</sup>/Zwint-1 is unclear. We surmise that interacting interfaces available in the Knl1<sup>2000-2311</sup>/Zwint-1/Zw10 complex become hindered in the context of the larger complexes. Perhaps phosphorylation or other modifications are required to expose these interacting interfaces. We note that it was previously reported that Aurora B and Mps1 might be involved in recruiting the RZZ complex to kinetochores. So we repeated our binding assays after adding purified Aurora B (Kasuboski *et al*, 2011) or Mps1 (Santaguida *et al*, 2010) and ATP to the samples, but also in these assays we did not detect interactions between either Zw10 with the KMN, RZZ with the KMN or RZZ with Knl1<sup>2000-2311</sup>/Zwint-1. Pull down experiments corroborated these findings (Table 3).

## Results

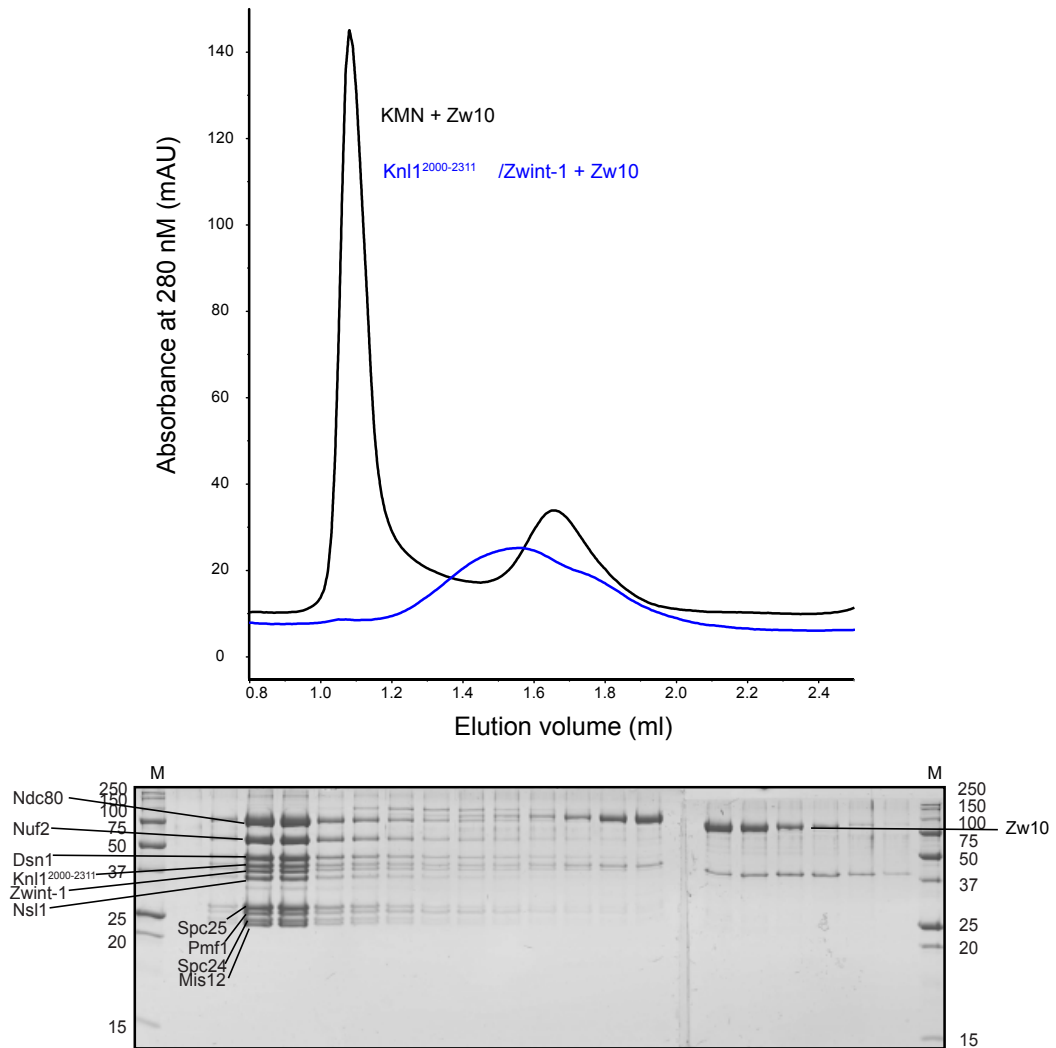


**Figure 36: Zw10 does not interact with the KMN network**

SEC elution profile and SDS-PAGE analysis of the KMN network combined with Zw10 (black) and SEC elution profile of the Kn1<sup>2000-2311</sup>/Zwint-1/Zw10 complex (blue). An interaction of the KMN network with Zw10 was not detected. The proteins were used at 5  $\mu$ M (10  $\mu$ M Zwint-1) in 50  $\mu$ l and loaded onto a Superose 6 5/15 column (GE Healthcare, Munich).

## Results

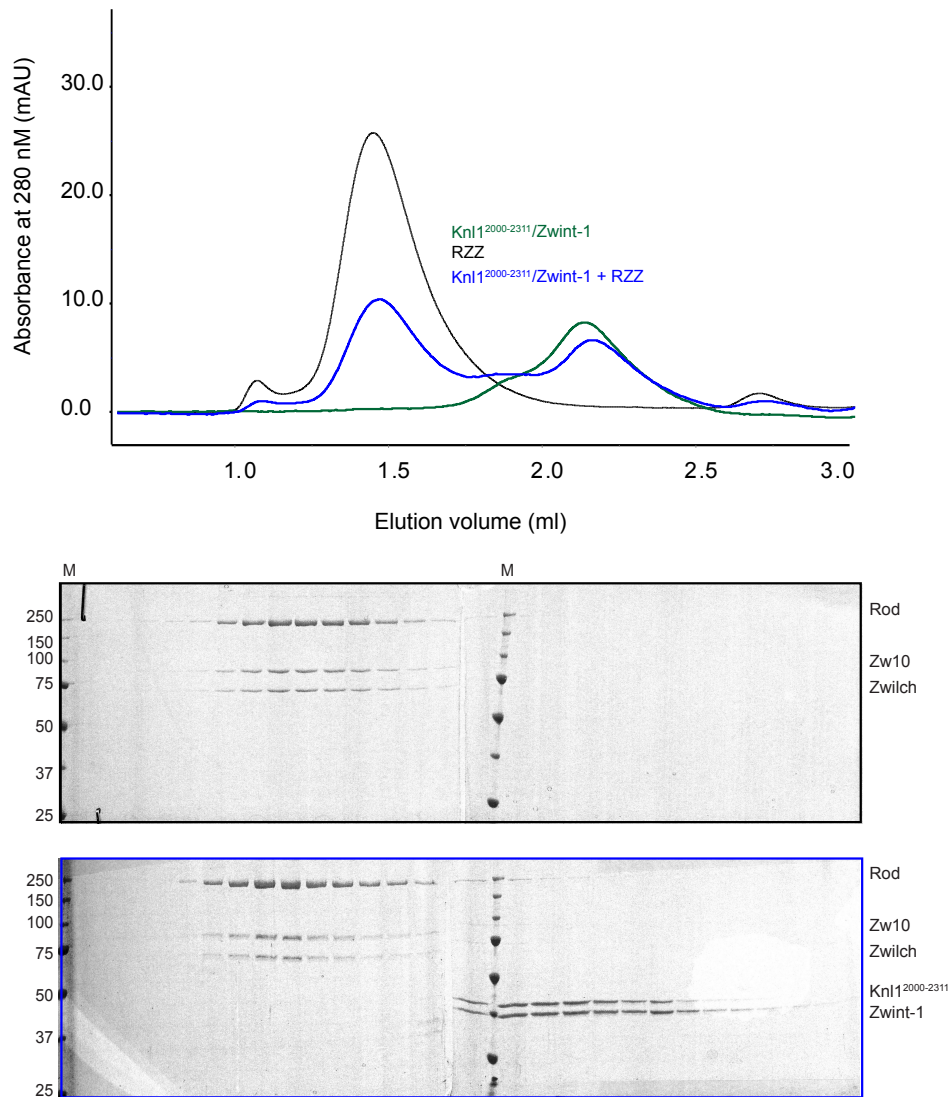


**Figure 37: KnI1/Zwint-1 does not interact with the RZZ complex**

SEC elution profile and SDS-PAGE analysis of the KnI1<sup>2000-2311</sup>/Zwint-1 complex (green), the RZZ complex (black) and a stoichiometric combination of the two complexes (blue) are shown. An interaction of the RZZ complex with the KnI1<sup>2000-2311</sup>/Zwint-1 complex was not detected. The proteins were used at 5  $\mu$ M (10  $\mu$ M Zwint-1) in 50  $\mu$ l and a Superose 6 5/15 column (GE Healthcare, Munich) was used.

## Results

### 4.3.2 Does the RZZ complex bind any kinetochore proteins?

This section is dedicated to summarize interaction experiments of the RZZ complex with other kinetochore proteins that have been proposed as RZZ binders in the literature. Regretfully, none of the binding species tested in these experiments revealed an interaction with the RZZ complex

We complemented our investigations of a potential interaction of the RZZ complex with the KMN complex with testing for Ndc80 complex binding. Interaction studies of the RZZ with checkpoint components, such as Mad1/Mad2 and Bub1/Bub3 were performed, because the RZZ complex has a crucial role in activation and inactivation of the SAC (Karess, 2005), (Barisic & Geley, 2011) (Section 2.6). As the RZZ complex putatively interacts with the protein Spindly (Barisic & Geley, 2011) and is involved in silencing the SAC by recruiting Dynein/Dynactin (Barisic & Geley, 2011) to kinetochores (Section 2.6), we performed binding studies with Spindly and Dynein and Dynactin subunits that were available in the lab. The Ska complex was also tested as a putative RZZ binder because of its role in the establishment of kinetochore microtubule attachment (see chapter 2.3) and because it is positioned in close proximity with RZZ complex on kinetochores (Maresca & Salmon, 2009), (Varma *et al*, 2013). The influence of kinases such as Aurora B, Mps1, Cdk1, and others was also tested.

All interaction studies did not detect a direct interaction (summarized in Table 3). Lack of binding might indicate that there is no direct interaction in living cells of the tested proteins, or that additional binding partners are missing, or that other physiologically relevant aspects of the reaction, including post translational modification, cannot be recapitulated *in vitro*.

Results

**Table 3: Overview of RZZ interaction trials with other kinetochore proteins or protein complexes**

| <b>RZZ construct</b> | <b>Binding partner</b>            | <b>Binding detected</b> | <b>Method</b>                                      | <b>Variations, Modifications</b>            |
|----------------------|-----------------------------------|-------------------------|----------------------------------------------------|---------------------------------------------|
| RZZ                  | Ndc80                             | No                      | MST, ITC, SEC, IP, Flow cell assay on microtubules | +/- Mps1, λ-pp                              |
| RZZ                  | Bonsai                            | No                      | MST, SEC                                           | +/- Mps1, λ-pp                              |
| RZZ                  | KMN                               | No                      | SEC, IP                                            | +/- Mps1, AuroraB, Cdk1, Plk1, λ-pp         |
| RZZ                  | Kn1 <sup>2000-2311</sup> /Zwint-1 | No                      | SEC, IP                                            | +/- Mps1, AuroraB, Cdk1, Plk1, λ-pp         |
| Zw10                 | Kn1 <sup>2000-2311</sup> /Zwint-1 | Yes                     | SEC                                                |                                             |
| Zw10                 | KMN                               | No                      | SEC                                                | +/- Mps1, AuroraB, Cdk1, Plk1, λ-pp         |
| RZZ                  | Spindly                           | No                      | SEC                                                | +/- Mps1, λ-pp                              |
| RZZ                  | Spindly, KMN                      | No                      | SEC                                                | +/- Mps1, λ-pp                              |
| RZZ                  | Spindly, Ska complex              | No                      | SEC                                                | +/- Mps1, λ-pp                              |
| RZZ                  | Spindly, Mad1/Mad2                | No                      | SEC, IP                                            | +/- Mps1, λ-pp<br>different Mad1 constructs |
| RZZ                  | Spindly, KMN, Mad1/Mad2           | No                      | SEC                                                | +/- Mps1, λ-pp                              |
| RZZ                  | Spindly, KMN, Bub1/Bub3           | No                      | SEC                                                | +/- Mps1, λ-pp                              |
| RZZ                  | Ska complex                       | No                      | SEC, IP                                            | +/- Mps1, λ-pp                              |
| RZZ                  | Ska1, Ska2                        | No                      | SEC, IP                                            | +/- Mps1, λ-pp                              |
| RZZ                  | Mad1/Mad2                         | No                      | SEC, IP                                            | +/- Mps1, λ-pp<br>different Mad1 constructs |
| RZZ                  | Mad1/Mad2, P31                    | No                      | SEC, IP                                            | +/- Mps1, λ-pp<br>different Mad1 constructs |
| RZZ                  | Mad1/Mad2, Spindly-F              | No                      | SEC                                                | +/- Mps1, Cdk1, different Mad1 constructs   |
| RZZ                  | Bub1/Bub3                         | No                      | SEC                                                | +/- Mps1, λ-pp                              |
| RZZ                  | Mps1                              | No                      | SEC                                                |                                             |

## Results

|        |                                              |    |          |                   |
|--------|----------------------------------------------|----|----------|-------------------|
| RZZ    | Cenp-T <sup>P</sup> / Mis12/<br>Ndc80        | No | SEC      | +/- Mps1,<br>λ-pp |
| Zw10   | Zwilch                                       | No | SEC      |                   |
| Zw10   | Spindly                                      | No | SEC      | Kinase cocktail   |
| Zwilch | Spindly                                      | No | SEC, ITC | Kinase cocktail   |
| RZZ    | Dynein subunits<br>Lic2, Tctex1, Lc8,<br>Rb1 | No | SEC      |                   |
| Zw10   | Dynein subunits<br>Lic2, Tctex1, Lc8,<br>Rb1 | No | SEC,     |                   |
| RZZ    | P50                                          | No | SEC      |                   |
| Zw10   | P50                                          | No | SEC,     |                   |
| RZZ    | Cenp-I                                       | No | SEC      |                   |
| RZZ    | Cenp-HIKM                                    | No | SEC      |                   |

## Results

### 4.3.3 Microinjection of the RZZ complex into human cells

To address the question whether our recombinant RZZ complex is competent for kinetochore recruitment, we injected a fluorescent version of it into mitotic HeLa cells and tested its possible recruitment to mitotic kinetochores. Cells were transfected with a vector expressing mCherry labeled CENP-A to label kinetochores. As expected, we observed that GFP did not localize at kinetochores whereas the recombinant RZZ co-localized with marker CENP-A (Figure 38). As an additional validation of the functionality of our recombinant RZZ complex we injected it into mitotic HeLa cells treated with the Mps1 inhibitor Reversine. We observed a significant reduction in the kinetochore levels of GFP-RZZ in the majority of injected cells (Figure 38), in agreement with previous reports that Mps1 activity is needed for proper RZZ recruitment to kinetochores (Santaguida *et al*, 2010). Collectively, the microinjection experiments functionally validate our recombinant RZZ complex.



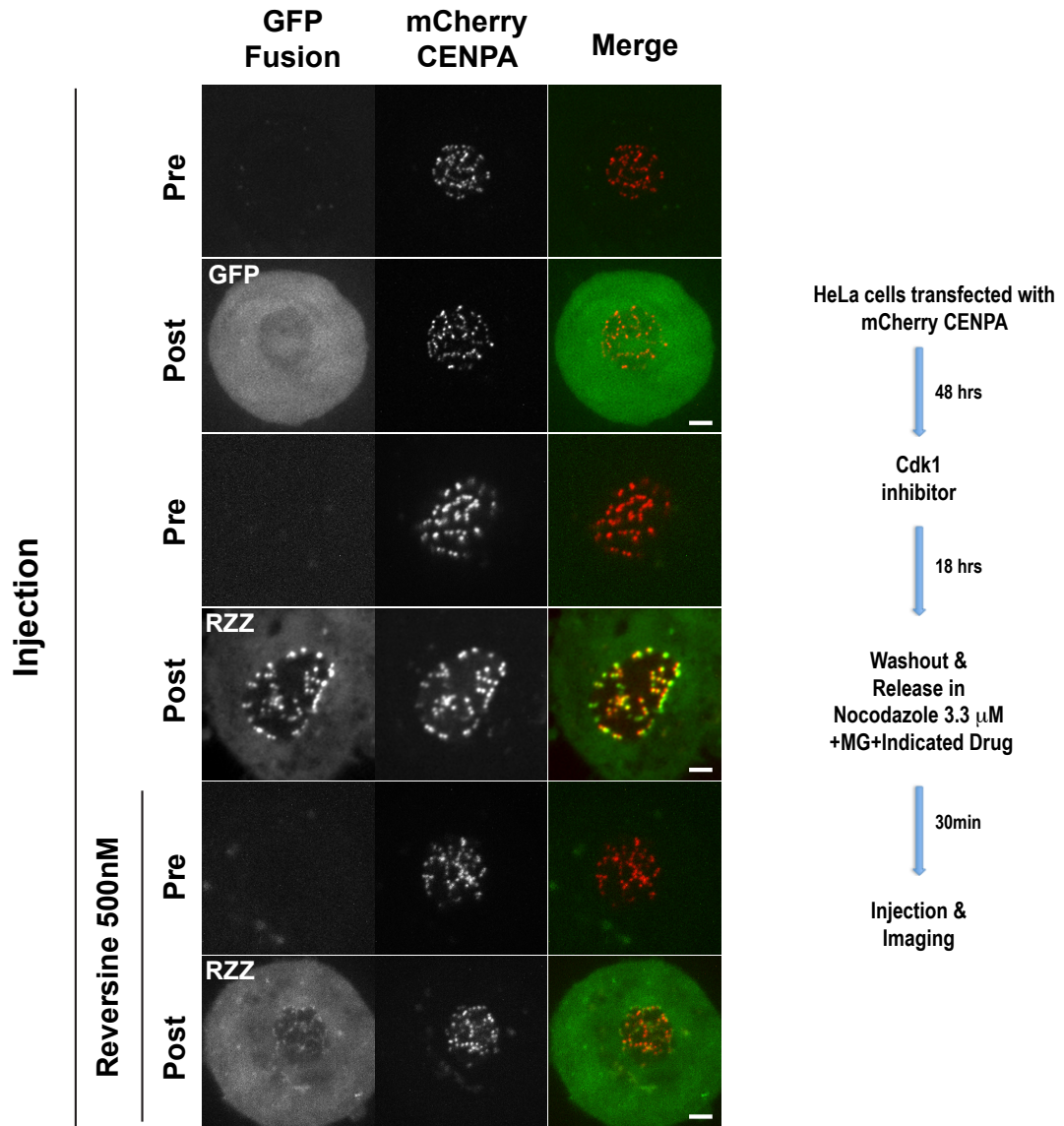


**Figure 38: Recombinant RZZ localizes to kinetochores in mitotic HeLa cells**

Representative images of the localization of recombinant GFP-RZZ complex injected in mitotic HeLa cells transiently expressing mCherry-CENPA. Cells were synchronized in G2 by treatment with the Cdk1 inhibitor RO3306 and released into mitosis in the presence of the indicated drugs. Once in mitosis, cells were live-imaged before (Pre) and after (Post) microinjection with recombinant GFP or GFP-RZZ. Scale bars = 2 μm.

## Results

### 4.3.4 Spindly interaction

#### SILAC experiment

Spindly might be a direct interaction partner of the RZZ complex (Barisic & Geley, 2011). We wanted to verify and characterize this interaction. First, we tested a possible direct interaction using recombinant proteins. Therefore, we produced the full-length Spindly in insect cells (Figure 51). Next, we investigated the Spindly-RZZ interaction using analytical size exclusion chromatography (SEC). In these experiments we could not detect binding of RZZ to Spindly (Table 3). Two independent groups have reported that Spindly co-immunoprecipitates with the RZZ complex but that this reaction is inhibited by detergents (Chan *et al*, 2009), (Gassmann *et al*, 2008). Recent evidence that the interaction of Spindly with RZZ might be mediated by farnesylation of the C-terminal region of Spindly in HeLa cells (Holland *et al*, 2015), (Moudgil *et al*, 2015) might explain this observation.

We resorted to Stable Isotope Labeling in Cell Culture (SILAC) combined with high-resolution mass-spectrometry to study the interaction of Spindly with RZZ. SILAC is a powerful method to obtain accurate relative quantifications of proteins in different samples and is particularly useful to identify potential interaction partners of a protein of interest. Briefly, two cell populations are grown for five doublings in medium containing either “light” Arginine and Lysine or “heavy” non-radioactive stable isotopes of these two amino acids. With human cells in culture, five doublings are sufficient to obtain 95% incorporation of the light or heavy. The two cell populations cannot be distinguished by eye or in their behavior, but they can be separated and quantified in the mass-spectrometer through the different mass of the corresponding proteins/peptides. The combination of SILAC with a high-resolution mass-spectrometer allows then the unbiased identification of possible interaction partners. For our experiment, we prepared mitotic “light” and “heavy” cell lysates. Then, we assembled as baits GFP-RZZ or a GFP control *in vitro* on GFP-trap beads. The beads were incubated with either “light” or “heavy” lysates to pull out interactors from SILAC lysates. We combined GFP-RZZ and GFP beads after the pull-down and washed the IPs together. Next, bound proteins were digested on beads and analyzed directly in the mass spectrometer (schematic view of the experiment: Figure 39).

## Results

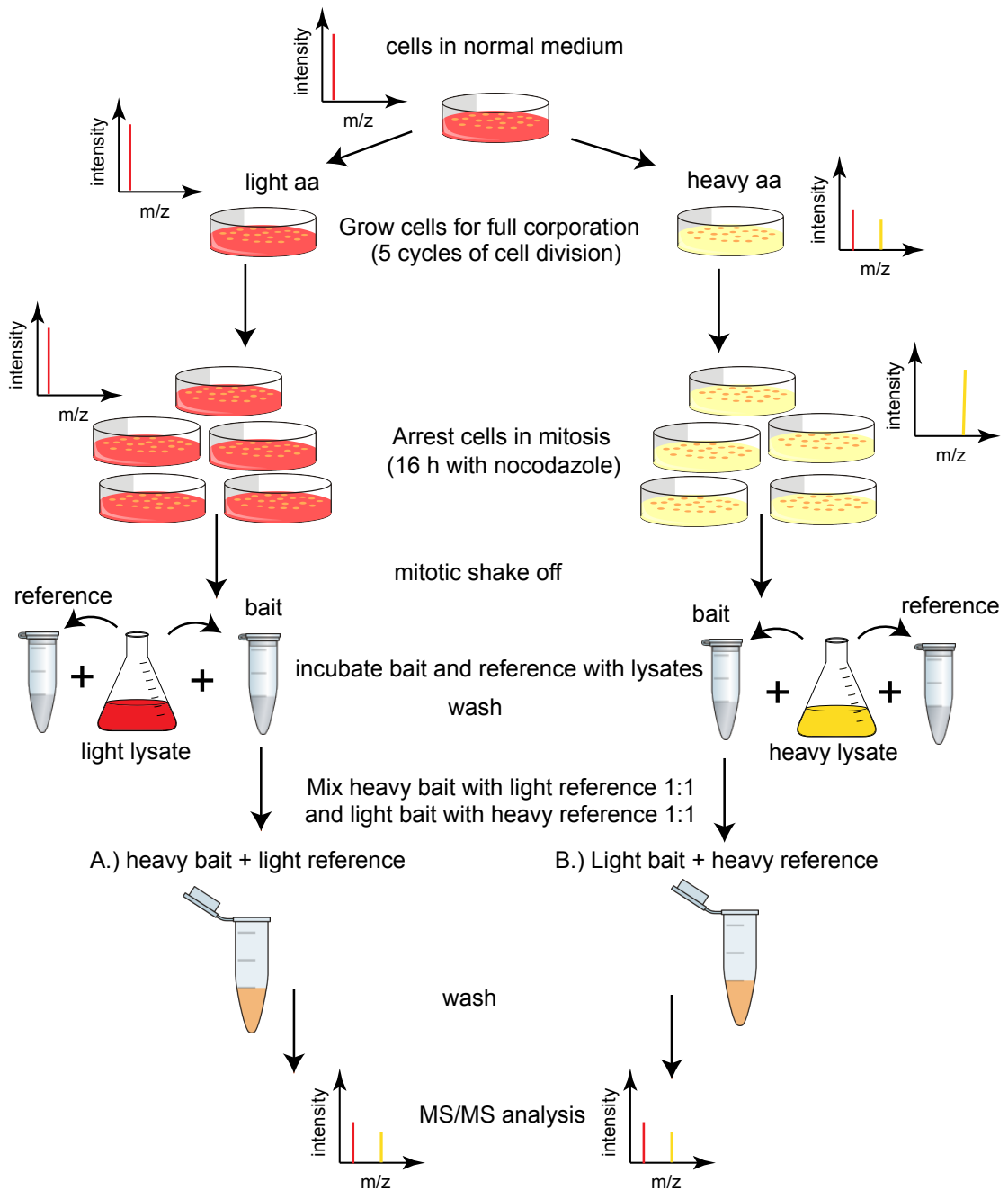


**Figure 39: Schematic view of the SILAC experiment**

HeLa cells were grown in normal light media and in heavy media where heavy versions of the amino acids lysine and arginine become incorporated. For full incorporation the cells were cultured for five divisions. Cells were arrested in mitosis by a 16 h nocodazole treatment. Cells were harvested by mitotic shake off and heavy and light cell lysates were incubated both with GFP-trap beads containing as a reference GFP alone, and with GFP-trap beads containing the bait GFP-RZZ. After three washing steps the “heavy” bait was mixed with the “light” reference 1:1 and the “light” bait was mixed with the “heavy” reference 1:1. After two more washes the immunoprecipitates were prepared for LC-MS/MS and directly analyzed.

## Results

We performed these experiments using either detergent-free buffers for cell lysis and washes, or the standard buffers containing detergents. In addition, we performed a replicate of every experiment swapping the labeled lysates. Thus, for the first experiment we incubated GFP with “light” and GFP-RZZ with “heavy” lysates and for the replica we inverted conditions and incubated GFP beads with “heavy” lysate and RZZ with “light” lysates. Repeating the experiment after inversion of labels contributed to filter out contaminants. The obtained raw data were analyzed with the MaxQuant software (Cox & Mann, 2008), using standard parameters.

We identified and quantified 944 proteins in the detergent-free experiment and 790 using detergents (data not shown). For an easier handling of the data we inverted the ratios of the GFP “heavy” and the GFP-RZZ “light” experiment (1/ H/L ratio) in the detergent-free and detergent experiment respectively. In this way the potential interaction partners of RZZ can be identified by a high ratio in both replicates (GFP “light/GFP-RZZ “heavy” and the respective label swap). To visualize potential interaction partners we plotted the logarithmized ratios ( $\log_2$ ) of all proteins of two replicates against each other (Figure 40). In this way, all background binders were centered on 0. Baits were light in both experiments and showed up in the lower left quadrant. Potential interactors should have appeared in the upper right quadrant because ratios should have been high in both experiments. Contaminant hits instead appeared in the other two quadrants. It can be clearly appreciated from these plots that Spindly was identified as an interaction partner of the RZZ complex in both experiments (detergent-free and with detergents). Of note is that no clear other potential interaction partners appeared in addition to Spindly in these experiments, supporting a direct interaction with the RZZ.

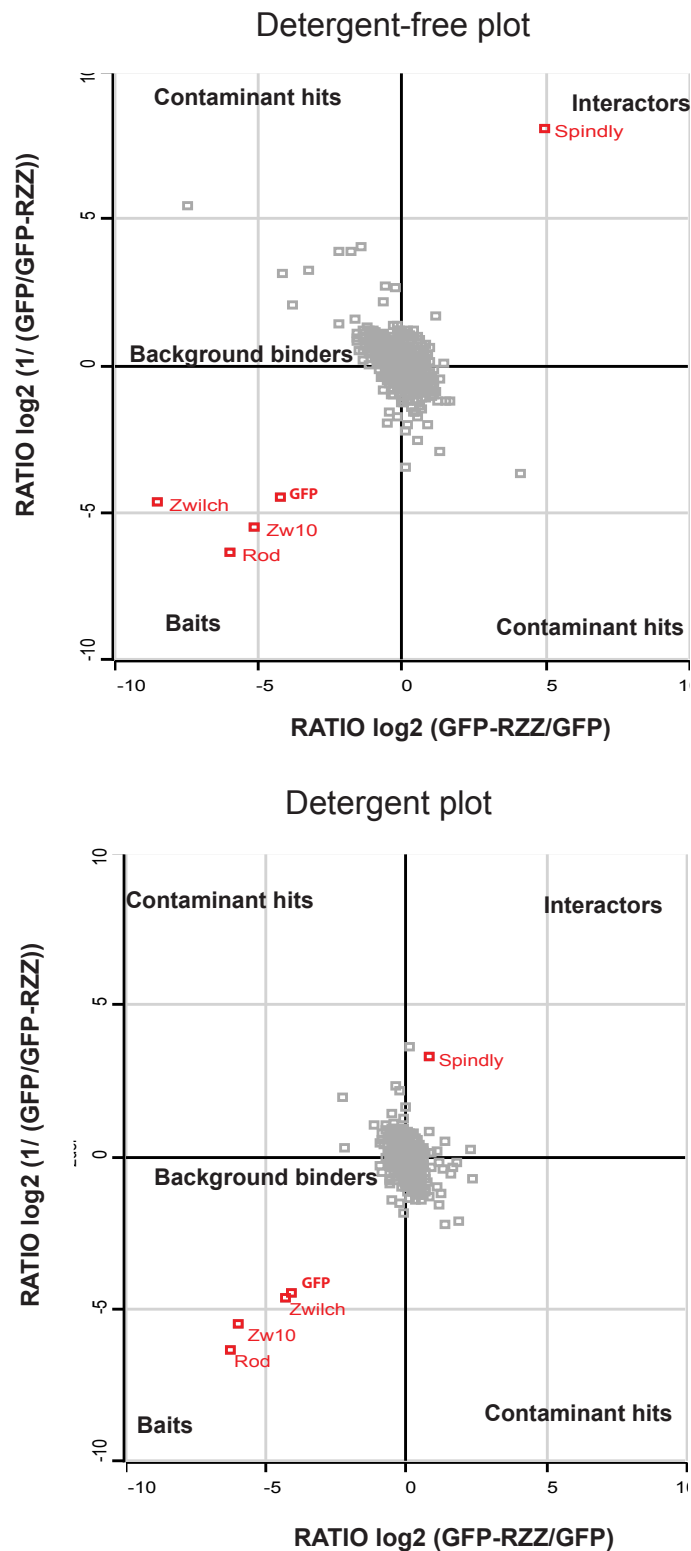


**Figure 40: Identification of RZZ interacting under the influence of detergents**

Purified GFP and GFP-RZZ were bound to GFP-trap beads. Then, light and heavy SILAC lysates from mitotic HeLa cells were incubated with the baits. Proteins bound to the beads were identified by mass spectrometry. After filtering the results, the ratios of 944 proteins (detergent-free) and 790 proteins (detergents) identified in two independent experiments with swapped labels were plotted against each other. To ensure readability, the reciprocal of the ratio of one experiment is shown. Thus the GFP-RZZ interaction partners showed up with high values.

## Results

Together, these experiments show that the RZZ complex pulls down Spindly from mitotic HeLa cell lysates. In addition, the absolute ratios of the detergent-free and detergent experiment suggest that the interaction is tighter without detergents. Since we did not perform a direct comparison between RZZ with and without detergents but “only” between GFP and GFP-RZZ, we could not directly compare the ratios of these two experiments. Thus, to get a better idea about the difference in Spindly binding with and without detergents we made use of the label-free quantification option in MaxQuant (Cox & Mann, 2008). We calculated these so called label free quantification intensities (LFQ intensities) separately for light and heavy peaks in all experiments. Afterwards, we plotted the log<sub>10</sub> of the LFQ intensities from GFP-RZZ pull-downs from the detergent-free and the detergent containing experiment against each other (Figure 41). The label-free approach showed that Spindly LFQ intensities are around a 100 fold higher in the detergent-free experiment strongly indicating that Spindly binding to RZZ is indeed substantially higher by omitting detergents in the experiment. LFQ intensities for RZZ were equal in both experiments (not shown). In sum, these results confirm a clear dependency of RZZ Spindly interaction on detergent usage and suggest that the interaction is dependent on a detergent sensitive modification.

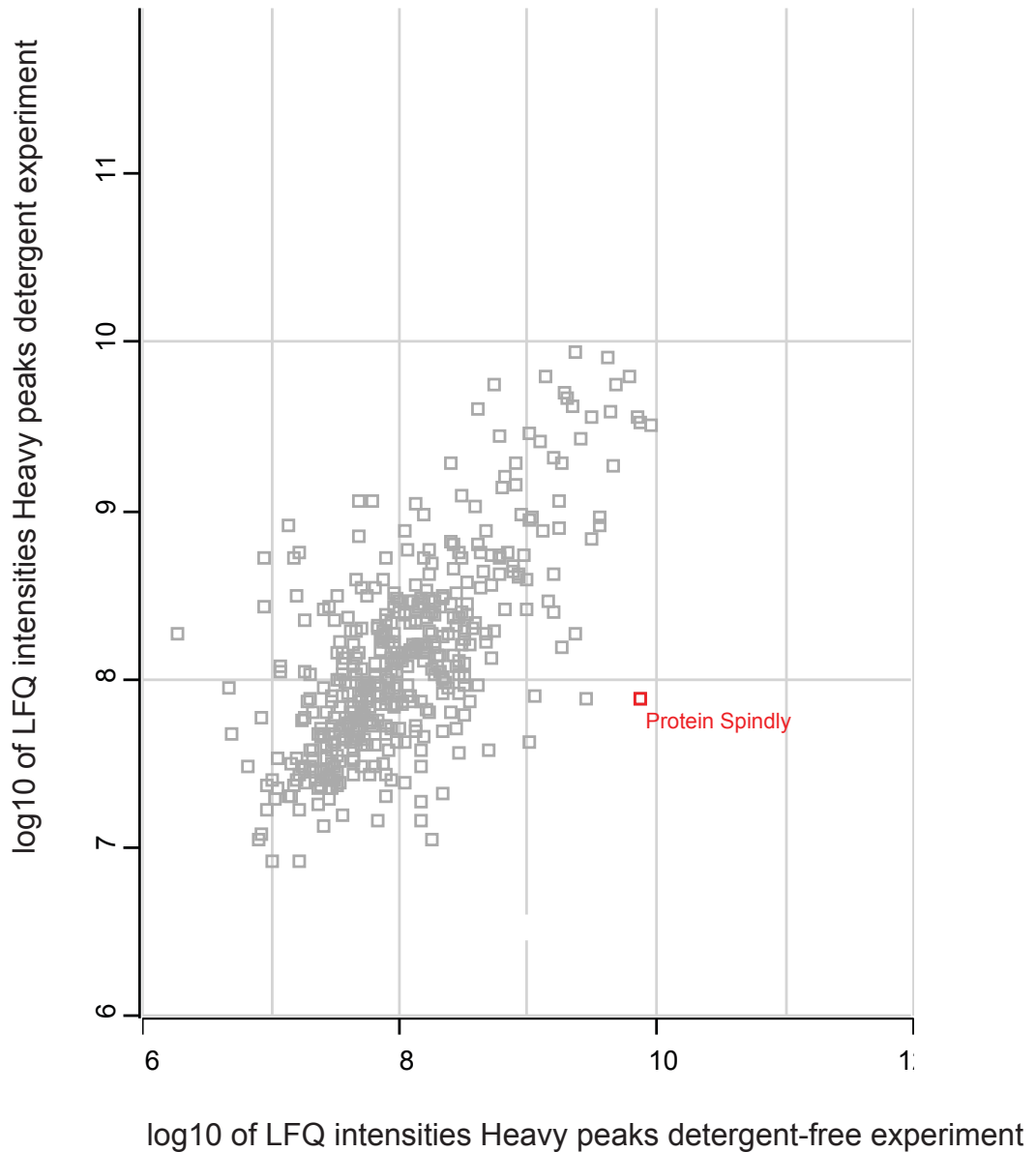


**Figure 41: LFQ intensities of heavy peaks of the detergent free and detergent-containing experiment plotted against each other**

Calculation of label free quantification intensities (LFQ) using the label-free quantification option in MaxQuant (Cox & Mann, 2008) for a direct comparison of Spindly quantities in conditions with and without detergents. The log<sub>10</sub> of the LFQ intensities from GFP-RZZ pull-downs from the detergent-free and the detergent containing experiment were plotted against each other. The label-free approach showed that Spindly LFQ intensities are around a 100 fold higher in the detergent-free experiment.

## Results

### **RZZ Spindly interaction depends on the farnesylation of the C-terminal Caax-box within Spindly**

Because the C-terminal farnesylation of Spindly is required for its localization at kinetochores, and the RZZ complex has been proposed to be the kinetochore receptor of Spindly, our data argue that the interaction of RZZ complex and farnesylated Spindly may be direct. To investigate the role of Spindly farnesylation, we performed an analytical SEC co-elution shift assay, where we incubated RZZ and Spindly together with the enzyme Farnesyltransferase (FTase) in the presence and absence of its substrate farnesylpyrophosphate (FPP) (Figure 42). Additionally, because the mentioned publications also indicated a possible role of Cdk1 phosphorylation of the C-terminus of Spindly, we also incubated Spindly and RZZ with Cdk1 and ATP in the presence and absence of Farnesyltransferase and farnesylpyrophosphate.  $MgCl_2$  was added to the SEC buffer, as it is an important cofactor for both the kinase Cdk1 and Farnesyltransferase.

We observed that RZZ and Spindly incubated with Farnesyltransferase in the absence of farnesylpyrophosphate did not co-elute, suggesting that they do not interact with high affinity (Figure 42). Conversely, in the presence of the Farnesyltransferase substrate we observed a significant shift in the elution of RZZ and Spindly and significant co-elution (Figure 43). This suggests that the RZZ/Spindly interaction depends on the farnesylation of the C-terminal CAAX box of Spindly. Fractions of the peak containing the RZZ/Spindly complex were analyzed by mass spectrometry. The analysis confirmed that within the complex Spindly was indeed farnesylated (Spindly-F) (see supplementary Figure 52).



## Results

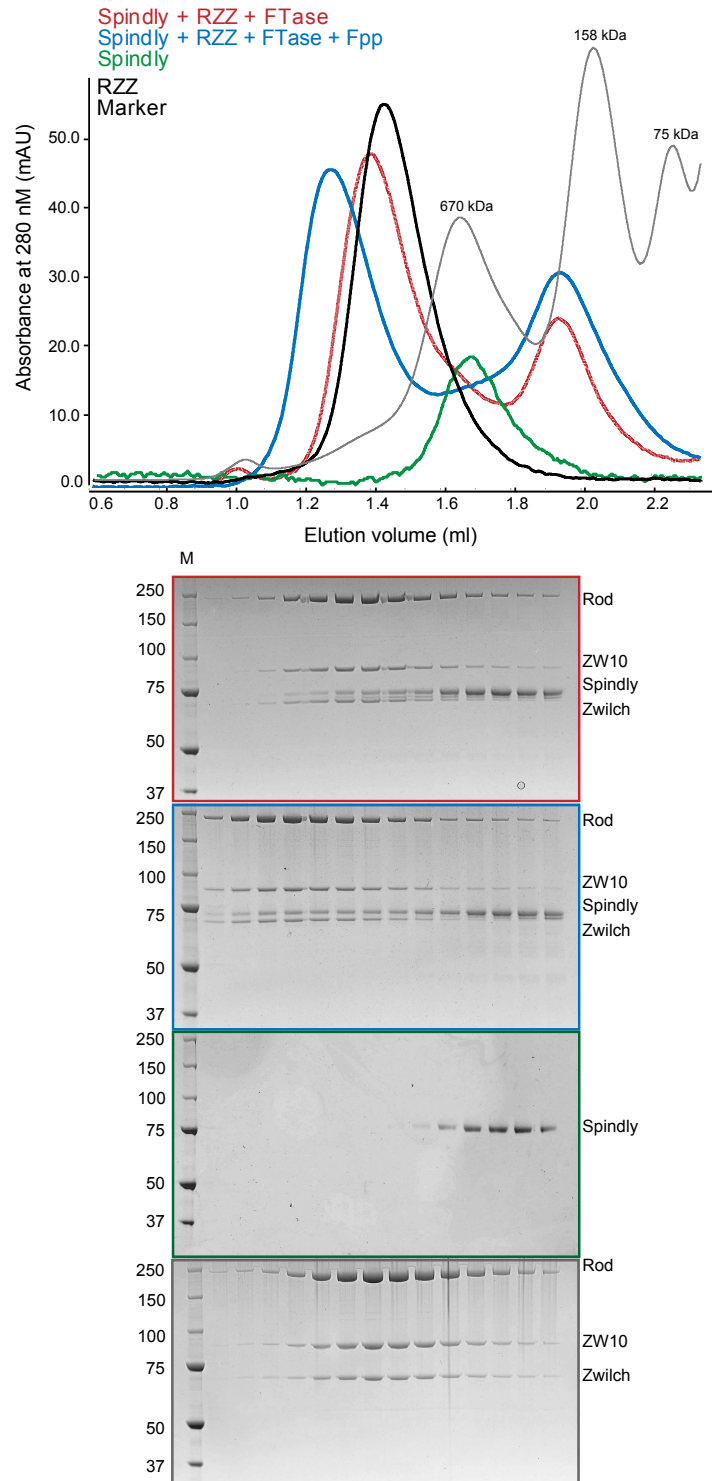


**Figure 42: The RZZ complex interacts with farnesylated Spindly**

SEC elution profile and SDS-PAGE analysis of the RZZ complex (black), Spindly (green) and a stoichiometric combination of the RZZ complex and Spindly with the Farnesyltransferase (FTase) in the absence (red) or presence of its substrate farnesylpyrophosphate (FPP) (blue) are shown. RZZ did not bind Spindly in the absence of FPP, but bound in the presence of FPP. Thus we conclude that the RZZ complex does interact with farnesylated Spindly, but not with non farnesylated Spindly. The proteins were used at 5  $\mu$ M (3  $\mu$ M FTase) in 50  $\mu$ l and incubated for 1,5 h at RT for efficient farnesylation. A Superose 6 5/15 column (GE Healthcare, Munich) was used.

## Results

Furthermore, RZZ and Spindly did not interact upon addition of Cdk1, suggesting that the interaction is most likely not Cdk1 dependent, or that Cdk1 phosphorylation is not sufficient (Figure 43). We conclude from our observations that the Spindly RZZ interaction is mainly influenced by Spindly farnesylation.

## Results

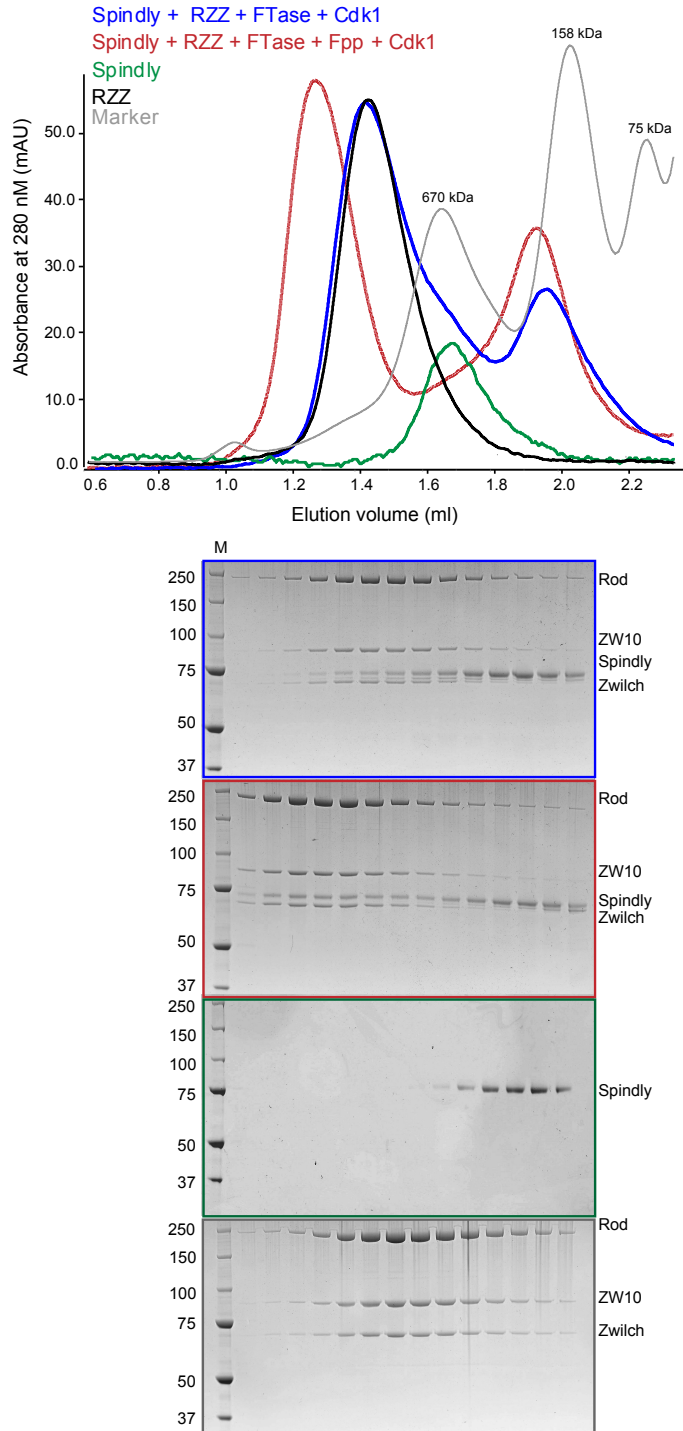


**Figure 43: Cdk1 phosphorylation does not influence the interaction of RZZ with farnesylated Spindly**

SEC elution profile and SDS-PAGE analysis of the RZZ complex (black), Spindly (green) and a stoichiometric combination of the RZZ complex and Spindly with FTase and the kinase Cdk1 and its substrate ATP in the absence (red) or presence of FPP (blue) are shown. No Cdk1 dependency of the RZZ interaction with Spindly was detected. The proteins were used at 5  $\mu$ M (3  $\mu$ M FTase) in 50  $\mu$ l and incubated for 1,5 h at RT for efficient farnesylation and phosphorylation. A Superose 6 5/15 column (GE Healthcare, Munich) was used.

## Results

### **Farnesylated Spindly does not interact with Zw10 or Zwilch individually, nor with the Mini-Rod Zwilch complex, but it binds Mini-RZZ complex**

To narrow down the binding site for Spindly-F on the RZZ complex, we repeated our analytical SEC co-migration shift assay using Zw10 and Zwilch instead of RZZ. Zw10 did not interact with farnesylated Spindly, as there was no peak shift and Zw10 and Spindly did not co-elute (Figure 44). The same is true for Zwilch (Figure 45). As it was not possible to express and purify Rod individually, we tested the interaction of farnesylated Spindly with the Mini-Rod/Zwilch complex and with the Mini-RZZ complex. The Mini-Rod/Zwilch complex, (Rod<sup>1-753-(GGSG)<sub>4</sub>-1797-2209</sup>/Zwilch) did not bind farnesylated Spindly (Figure 46). However, the Mini-RZZ complex, (Rod<sup>1-1250</sup>/Zw10/Zwilch) bound to farnesylated Spindly (Spindly-F) (Figure 47). The elution peak of Mini-RZZ shifted towards higher molecular weights and the proteins clearly co-eluted in a single peak, which demonstrated the formation of a complex (Figure 47). In isolation, Spindly-F eluted as expected for proteins of greater molecular weight (near the 670 kDa marker, see Figure 51 and Figure 43), indicating that Spindly (a 72 kDa protein) may be elongated or form multimers. When associated to the Mini-RZZ complex, the exclusion volume of Spindly-F increased, which suggests that the binding of Spindly to the Mini-RZZ complex leads to a less extended structure of Spindly. Spindly-F bound the Mini-RZZ complex, but not to the Mini-Rod/Zwilch complex and nor Zw10 or Zwilch individually. Collectively, this is compatible with at least three different possible positions for a binding site for Spindly-F on the RZZ complex. (i) Spindly-F binds the Zw10/Rod interface, (ii) Spindly-F binds the Sec39 region of Rod (amino acid 753 and 1250), or (iii) Spindly-F binds an extended region contacting all RZZ subunits.

## Results

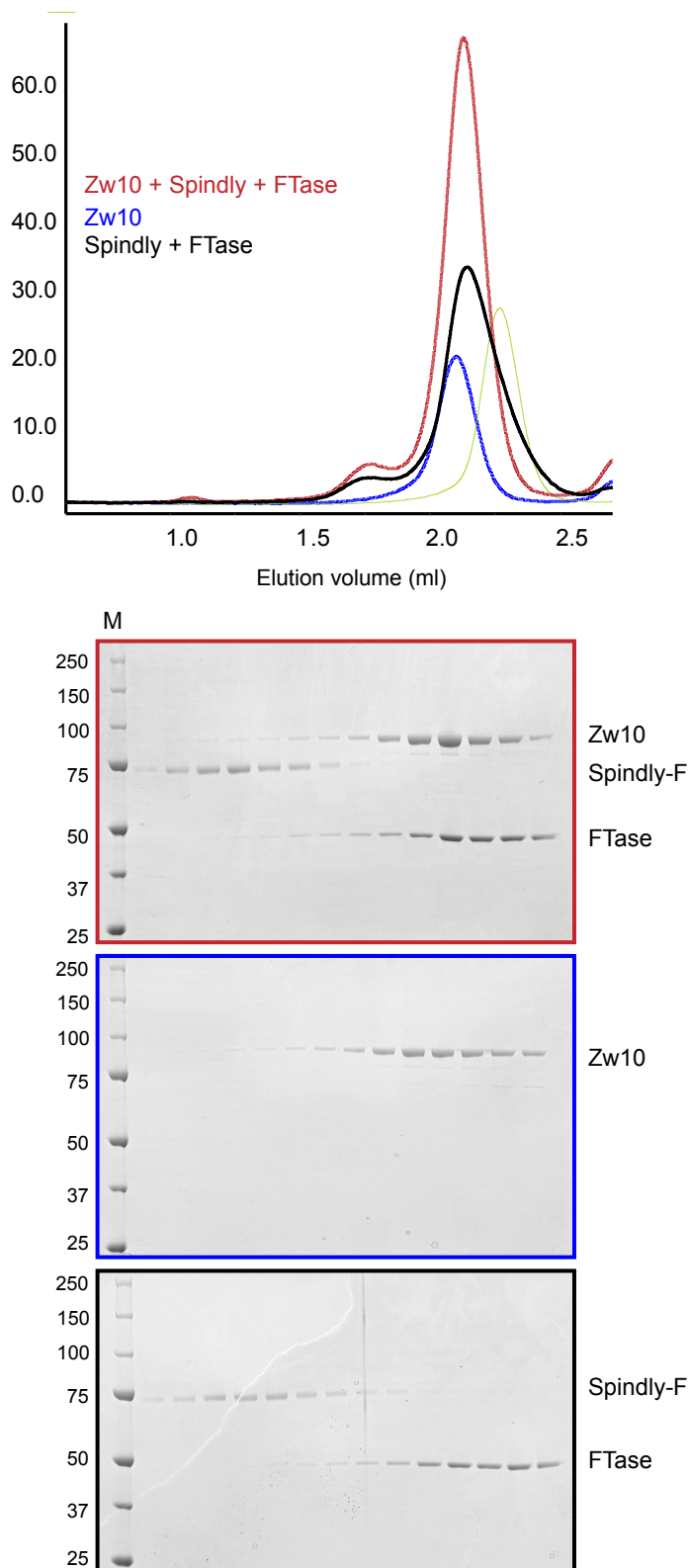


**Figure 44: Zw10 does not interact with farnesylated Spindly**

SEC elution profile and SDS-PAGE analysis of Zw10 (blue), a combination of Spindly and FTase in the presence of FPP (black) and a stoichiometric combination of them (red). An interaction of Zw10 with farnesylated Spindly was not detected. The proteins were used at 5  $\mu$ M (3  $\mu$ M FTase) in 50  $\mu$ l and incubated for 1.5 h at RT for efficient farnesylation. A Superose 6 5/15 column (GE Healthcare, Munich) was used.

## Results

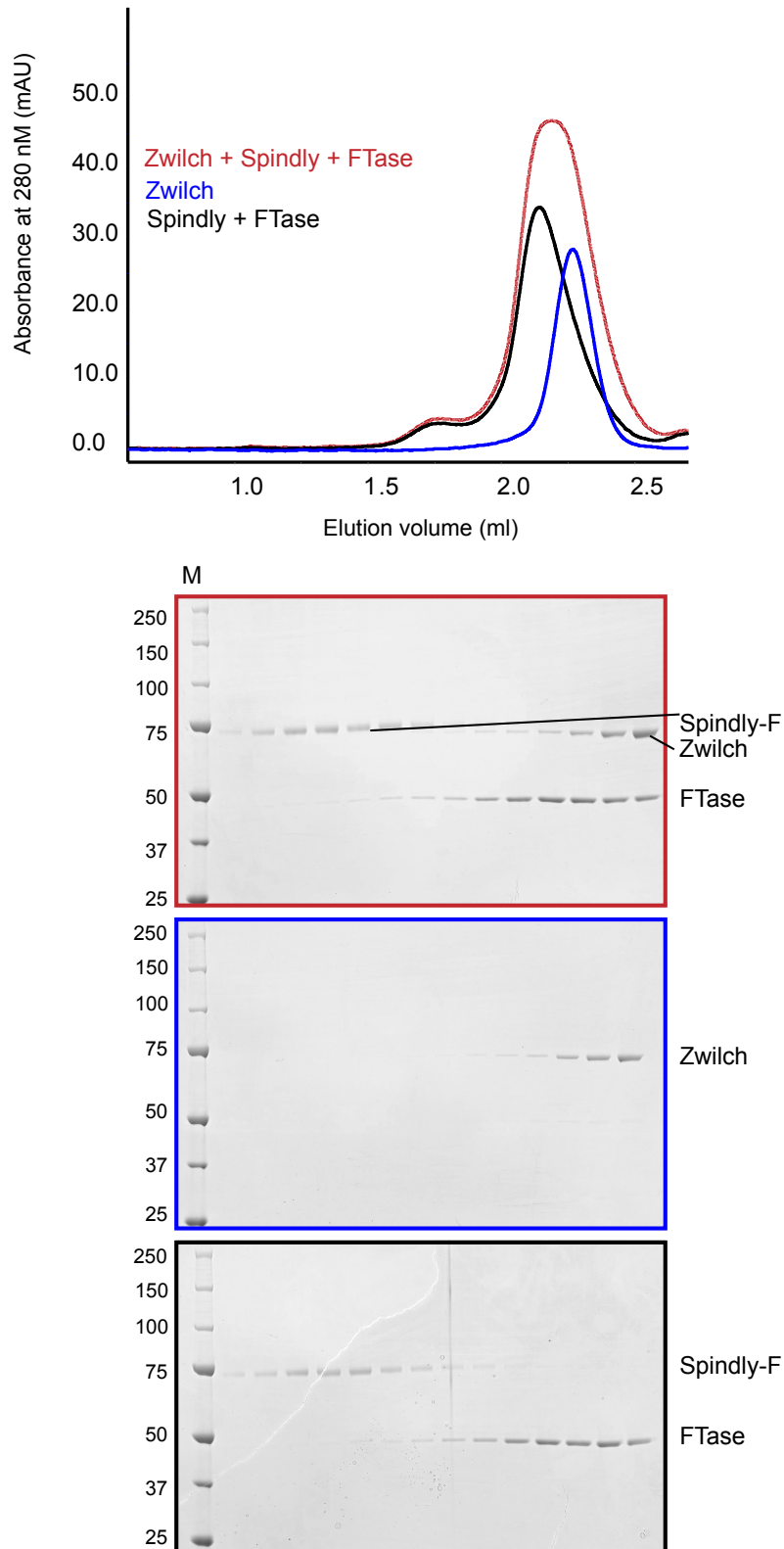


**Figure 45: Zwilch does not interact with farnesylated Spindly**

SEC elution profile and SDS-PAGE analysis of Zwilch (blue), a combination of Spindly and FTase in the presence of FPP (black) and a stoichiometric combination of them (red). An interaction of Zwilch with farnesylated Spindly was not detected. The proteins were used at 5  $\mu$ M (3  $\mu$ M FTase) in 50  $\mu$ l and incubated for 1,5 h at RT for efficient farnesylation. A Superose 6 5/15 column (GE Healthcare, Munich) was used.

## Results

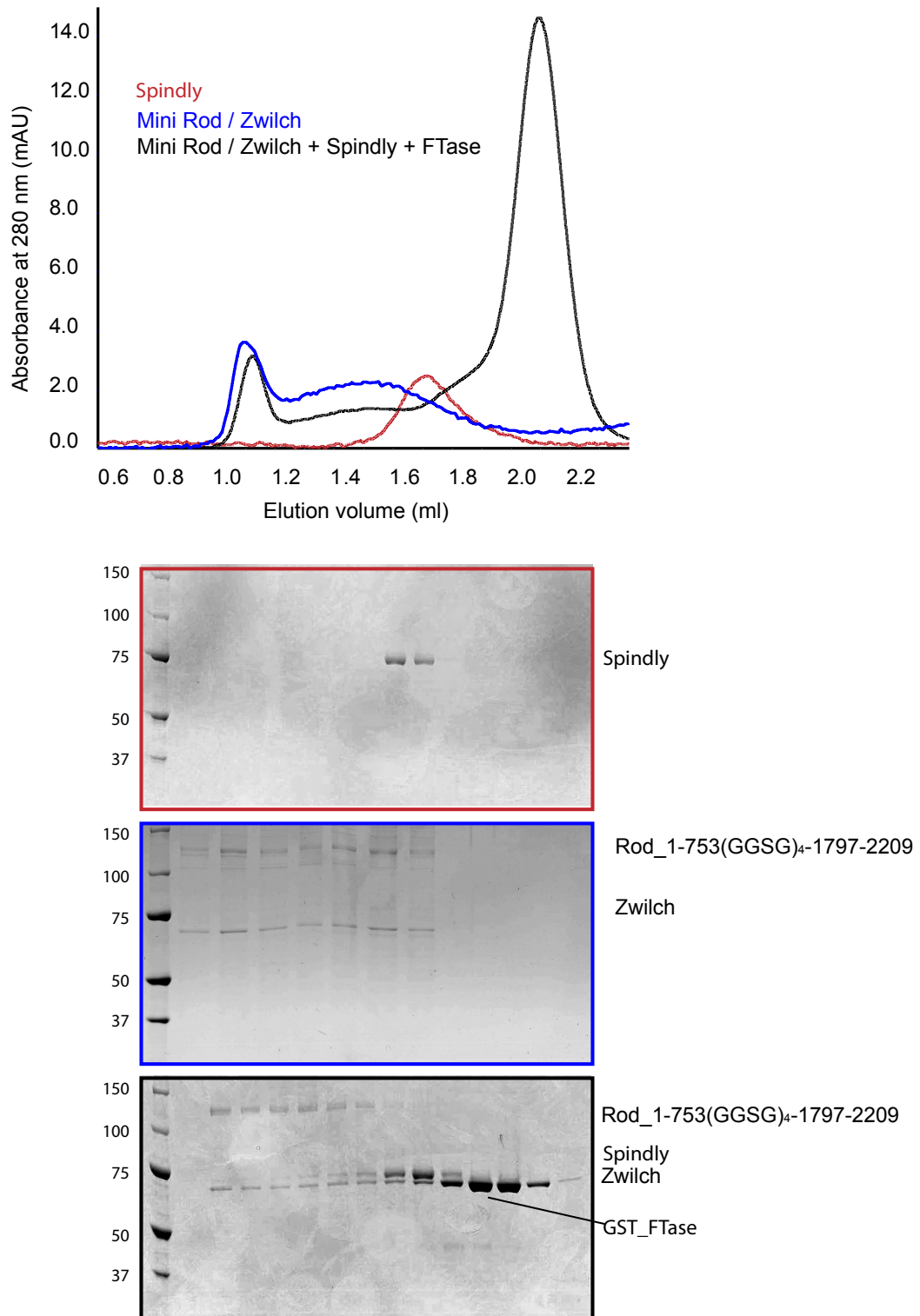


**Figure 46: The Mini-Rod/Zwilch complex does not interact with farnesylated Spindly**

SEC elution profile and SDS-PAGE analysis of Spindly (red), the Mini-Rod/Zwilch complex (blue) and a stoichiometric combination of them in the presence of FTase and FPP (black). An interaction of the Mini-Rod/Zwilch complex with farnesylated Spindly was not detected. The proteins were used at 5  $\mu$ M in 50  $\mu$ l and incubated for 1,5 h at RT for efficient farnesylation. A Superose 6 5/15 column (GE Healthcare, Munich) was used.

## Results

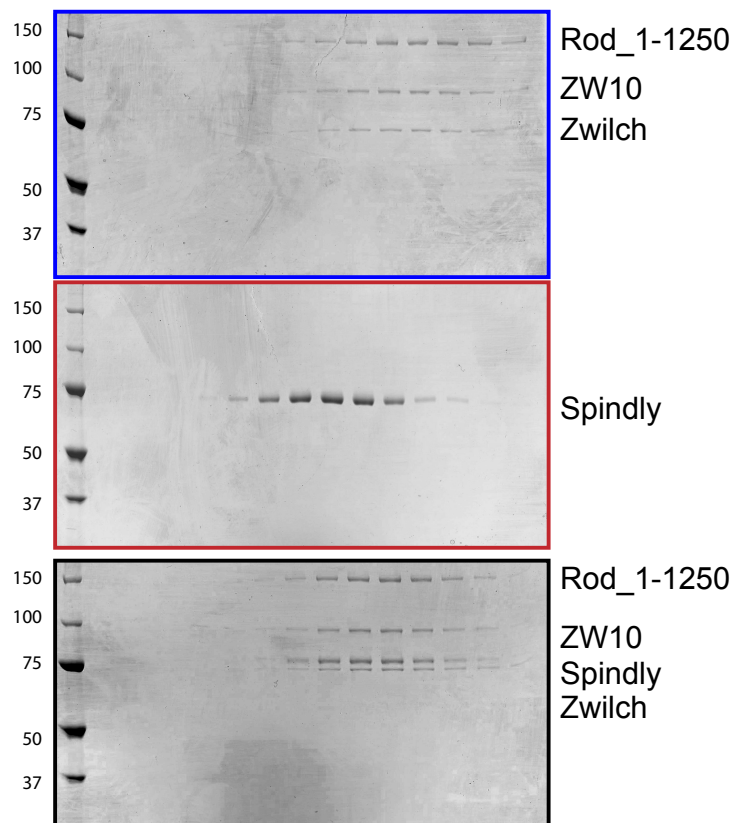
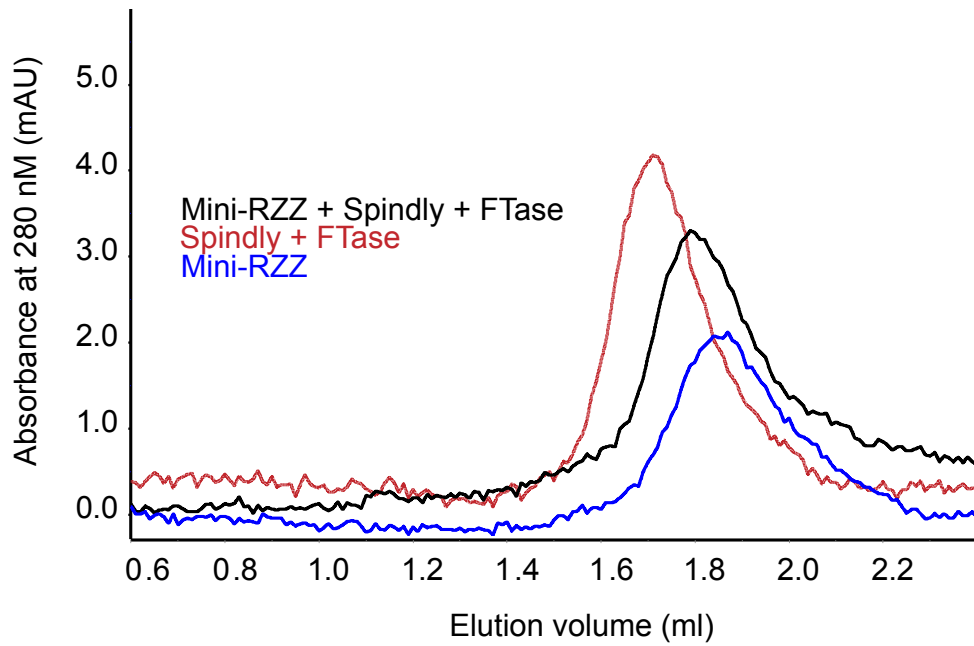


**Figure 47: The Mini RZZ complex does interact with farnesylated Spindly**

SEC elution profile and SDS-PAGE analysis of Spindly (red), the Mini-RZZ complex (blue) and a stoichiometric combination of them in the presence of FTase and FPP (black). We detected an interaction of the Mini-RZZ complex with farnesylated Spindly. The proteins were used at 5  $\mu$ M (3  $\mu$ M FTase) in 50  $\mu$ l and incubated for 1,5 h at RT for efficient farnesylation. A Superose 6 5/15 column (GE Healthcare, Munich) was used.



## 5 Discussion

The RZZ complex is a key regulator and essential functional component of the kinetochore in mitosis (Karess, 2005). Relatively little is known about the characteristics and function of the RZZ complex at the kinetochore. The work presented in this thesis contributes to gaining a better biochemical, structural and functional understanding of the RZZ complex.

### 5.1 Structural organization of the RZZ complex

To address the structural organization of the RZZ complex it was crucial to generate recombinant RZZ. For this purpose I expressed and purified full length RZZ as well as several constructs containing specific domains and/or sub-complexes. In collaboration with Sabine Wohlgemuth and Annemarie Wehenkel we were able to recombinantly reconstitute the RZZ complex for the first time (Section 4.1.1). Additionally I demonstrated that the RZZ complex could be obtained in high yield and in a grade suitable for crystallization (Section 4.1). Given the size and molecular complexity of the RZZ complex, this is an exciting achievement that paves the way to further biochemical and structural characterization of the complex. Despite extensive attempts a crystal structure could not be obtained by X-ray crystallography so far (Section 4.1.5 and 4.1.6). Future efforts will be directed towards the optimization of crystal growth to improve the diffraction limit of the generated crystals. These efforts will include the generation of loop deletion mutants, an approach that has been shown previously to have a positive effect on crystal growth and diffraction (Jakob *et al*, 2010). Remarkably these characterization studies including AUC analysis of the recombinant RZZ complex (Section 4.1.2) could already validate that the RZZ complex forms a heterodimer, as previously proposed (Scaërou *et al*, 2001), (Williams *et al*, 2003). The functional implication of RZZ dimerization will be discussed in more detail later in this section.

Aside from crystallographic attempts, 3D negative-stain and cryo-electron microscopy reconstructions, carried out in collaboration with Dr. Shyamal Mosalaganti, in the laboratory of Professor Dr. Stefan Raunser, were used to generate structural information about the RZZ complex (Section 4.2). Combining subunit labeling and cross-linking mass spectrometry experiments, we were able to identify inter-subunit contacts. We were further able to build a precise model of

## Discussion

the inter subunit organization within the RZZ complex in a 10.5 Å 3D density map of the RZZ complex. Two Rod molecules form an antiparallel dimer. In this dimer, each Zwilch molecule is trapped between the N-terminus of one Rod monomer and the C-terminus of a second monomer. Zw10 bridges the two Rod molecules in the central region of the complex. Thus, the RZZ complex comprises an extensive dimer interface (Figure 25).

Based on the model of the intersubunit organization of the RZZ complex, we were able to fit crystal structures and structure homology models of individual RZZ protein domains into the 3D EM density of the RZZ complex (Figure 26) with high confidence scores. Most importantly, we validated this model by analyzing two subcomplexes of the RZZ (Mini-RZZ and Mini-Rod/Zwilch), adding confidence to our model.

The organization of Rod, with an N-terminal  $\beta$ -propeller followed by an  $\alpha$ -solenoid, is also observed in certain transport proteins. Proteins in the nuclear pore complexes (NPCs), such as Nup145, of COPII vesicles, such as Sec31, and of clathrin-coated vesicles, such as clathrin itself, share a similar fold (Leksa & Schwartz, 2010). Rod might have evolved from these proteins. There are also clear differences between these transport complexes and the RZZ complex. First, the RZZ complex contains the protein Zwilch, which contains a novel fold (Çivril *et al.*, 2010). Secondly, it is unclear if RZZ has a tendency to form higher order structures, like the lattices built by propeller-propeller interactions within the nuclear pore complex or in COPII vesicles (Leksa & Schwartz, 2010) (Figure 48). Whether RZZ can form such structures, however, has not been investigated in detail.

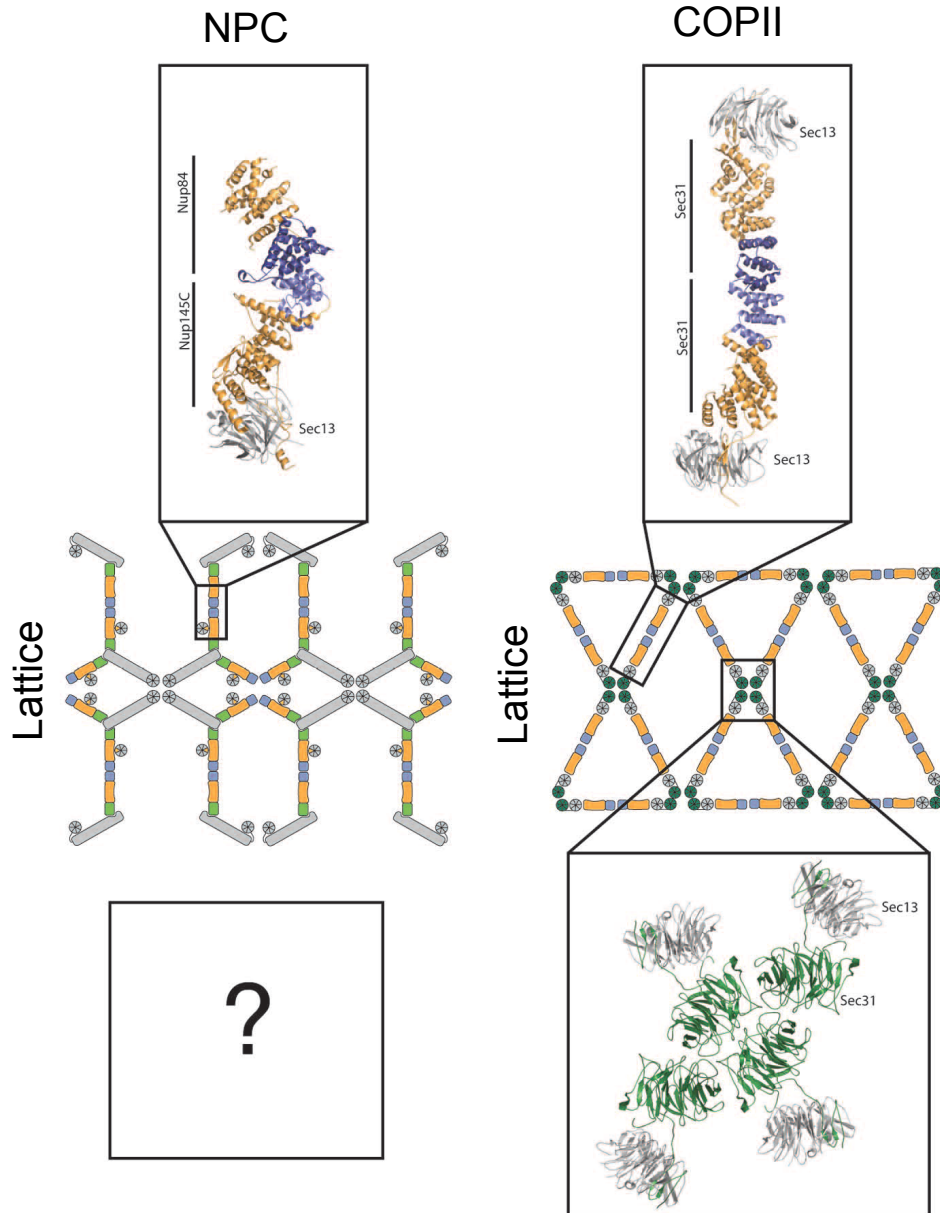


**Figure 48: Membrane-coating scaffolds of the NPC and vesicle coats**

Schematics of the lattice like assemblies of the NPC and COPII scaffolds are shown. Enlarged views of the ancestral coatamer elements are shown for both the NPC and COPII.

(Adapted from (Leksa & Schwartz, 2010))

As the RZZ complex exposes its  $\beta$ -propellers at both ends, we surmise that the RZZ complex may also be able to form higher order structures. Analysis of RZZ structures by negative stain EM after varying the pH and salt concentrations quite drastically, as has been done for the Sec13/31 COPII coat cage (Stagg *et al*, 2006), failed to identify the formation of high-order structures of RZZ (data not shown). One option is that the RZZ complex may require adaptor proteins at the kinetochore to form higher order structures. Alternatively, the RZZ complex has

## Discussion

simply evolved from transport proteins, with Rod and Nag sharing a common ancestor (Çivril *et al*, 2010), and lost the ability to form lattices. Why would we expect the RZZ complex to form higher ordered structures at kinetochores? The main reason to think that RZZ may form lattices, is that there is a conspicuous structure, called the fibrous corona, that coats kinetochores prior to microtubule attachment (Magidson *et al*, 2015). Additionally human kinetochores bind multiple microtubules (see section 2.2), and it has been reported that the RZZ complex may be involved in microtubule kinetochore attachments (Cheerambathur *et al*, 2013). If the RZZ complex formed a lattice at kinetochores it could contribute to the process of microtubule kinetochore attachment in a cooperative manner.

## 5.2 RZZ kinetochore recruitment

To study the recruitment mechanism of the RZZ complex to kinetochores, proteins proposed to be involved in this process were systematically tested for RZZ binding (Table 3). However, I did not detect any interaction between the RZZ complex and the proposed proteins. Zwint-1 has been implicated as the receptor for the RZZ complex at the kinetochore. Interestingly, we observed that Zw10 forms a tight complex with Knl1<sup>2000-2311</sup>/Zwint-1 but if either Zw10 is incorporated in the RZZ complex, or Knl1<sup>2000-2311</sup>/Zwint-1 is incorporated into the KMN network, the interaction is abolished (Section 4.3.1 and 4.3.2). While we cannot provide an explanation for this observation at this time, it might imply that the exposure of the binding interfaces in the context of the larger complexes is regulated, and that they are not available in the absence of specific modifications or additional interactions.

The KMN network produced in the studies outlined in this thesis did not contain full length Knl1 and a quite substantial part of Knl1 (residues 139-1999) was missing. Given the evidence outlined in the introduction (Section 2.5), I assume that within the KMN network Knl1 is the receptor of the RZZ complex. Therefore, either a region within the missing residues in Knl1 is required for RZZ localization, or dimerization of the KMN is required for RZZ binding and KMN dimerization is not possible without the missing region of Knl1.

Another possible reason why we failed to observe an interaction of the RZZ and the KMN network is that a post-translational modification (including modifications other than phosphorylation) of the KMN network is required to increase the binding affinity. For the RZZ complex we have demonstrated through microinjection experiments that the recombinant complex used in this study was able to localize to kinetochores in living cells (see section 4.3.3). However, we cannot rule out that the injected complex becomes modified after injection in living cells. It is also conceivable that additional proteins, which contribute to RZZ-KMN network binding, are missing.

For future investigations of RZZ kinetochore recruitment, a recombinant version of the full length Knl1 protein would be very useful. Despite extensive attempts, the production of Knl1 full-length either in bacteria or in insect cells has been so far unsuccessful. Therefore it will be necessary to tackle this expression in another system with HEK cells for instance, or in a cell free system.

### 5.3 RZZ function in SAC activation

The RZZ complex contributes to the recruitment of Mad1/Mad2 to the kinetochore. Thus, in order to study the role of the RZZ complex in SAC activation, I investigated whether there is a direct interaction of the RZZ complex with Mad1/Mad2. However, no interaction between the RZZ complex and Mad1/Mad2 could be detected (see section 4.3.2). To ensure that lack of phosphorylation did not hamper a putative direct interaction between the RZZ complex and Mad1/Mad2, the influence of different kinases was tested but binding was not detected (see section 4.3.2). Recombinant RZZ and Mad2 both localize to kinetochores in microinjection experiments (data for Mad2 not shown). However, we cannot rule out that Mad1/Mad2 requires an additional post-translational modification for RZZ binding, which is not required for its localization to kinetochores or that RZZ and Mad2 become immediately post-translational modified after being injected into HeLa cells.

Next we investigated whether the Mad1/Mad2-RZZ interaction might depend on additional kinetochore components (Table 3). As the KMN network is most likely responsible for RZZ kinetochore recruitment, we tested whether we could detect Mad1/Mad2 RZZ binding upon addition of the KMN but could not detect any interaction (Table 3) possibly due to the missing part of Knl1 (discussed in section 5.2). Mad1/Mad2, RZZ and Spindly lie in close proximity at the kinetochore, as established in super resolution microscopy mapping experiments (Varma *et al*, 2013). RZZ did not bind to Mad1/Mad2 in the presence of Spindly neither in the presence or absence of the KMN and independent of Spindly farnesylation. Thus, Mad1/Mad2 stabilization at kinetochores by RZZ is probably more indirect and requires either additional components (i.e. full length Knl1) or post-translational modifications of one of the interaction partners or additional kinetochore proteins not included in our binding assays. Another option could be that, at kinetochores, the Mad1/Mad2 interaction with RZZ is established due to an increased local concentration at kinetochores. If the RZZ formed a network-like structure, Mad1/Mad2 could interact with it in a cooperative manner. In conclusion, it remains elusive how the RZZ complex provides stable kinetochore localization of Mad1/Mad2. Dissecting the mechanism by which RZZ stabilizes at kinetochores will be an important achievement in the future.

## Discussion

### 5.3.1 RZZ function in SAC silencing

To dissect the role of RZZ in SAC silencing I aimed to gain a better understanding of how the RZZ contributes to the recruitment of Dynein/Dynactin. As neither Dynein/Dynactin nor Spindly were available as recombinant proteins in the Musacchio laboratory, I started by generating recombinant Spindly, the putative adaptor for Dynein/Dynactin, and investigated its interactions with the RZZ complex. I was able to express and purify recombinant Spindly in high purity from insect cells, which facilitated a direct test of the interactions between RZZ and Spindly. In SILAC experiments, recombinant RZZ interacted with endogenous Spindly from HeLa cell extracts in a detergent sensitive manner, as indicated previously (Section 4.3.4). Two recent publications showed that Spindly is only able to localize to kinetochores when its C-terminal CAAX-box is farnesylated (Moudgil *et al*, 2015), (Holland *et al*, 2015). This prompted me to test the direct interaction of RZZ and Spindly in the presence of FTase and its substrate FPP. Under those conditions, RZZ and Spindly interacted tightly, as shown by SEC co-elution experiments. Though these experiments I clearly showed a Farnesylation dependent interaction of RZZ and Spindly.

To determine the binding surface of Spindly-F-RZZ, we plan to examine the structure of the Spindly-F-RZZ complex by negative stain EM experiments in collaboration with Dr. Michael Saur from the Raunser laboratory. Furthermore it will be interesting to subject the Spindly-F-RZZ complex to crystallogensis. For this purpose I have created deletion mutants of Spindly that contain the C-terminal region, which has been shown to be sufficient for RZZ binding (Moudgil *et al*, 2015).

## Discussion

### 5.3.2 Dynein/Dynactin interaction

As the individual subunits of Dynein and Dynactin became available in the Musacchio laboratory, they were subjected to interaction studies with the RZZ complex as well as with Zw10. Zw10 has been proposed in the literature to be the Dynein/Dynactin anchor within the RZZ complex (Starr *et al*, 1998). Neither Zw10 nor RZZ bound to the P50 subunit of Dynactin, seemingly contradicting previous reports (Starr *et al*, 1998). Zw10 and RZZ also did not bind to the Dynein subunits Lic2, Tctex1, Lc8, Rb1 or to a combination of these subunits (Table 3). It is likely that the Dynein/Dynactin complex has to be properly assembled into an active form to interact with the RZZ complex. Moreover also Spindly-F may be required for the RZZ Dynein/Dynactin interaction and phosphorylation may play a part in this interaction. In the near future and in collaboration with the laboratory of Andrew Carter who kindly provided us with the Dynein–Dynactin holoenzyme, we will be investigating these interactions in more detail.



#### 5.4 Model of RZZ function

Based on the evidence presented in this thesis as part of my doctoral studies and on evidence discussed in literature I propose the following model for the functions of the human RZZ complex in checkpoint signaling. During mitosis and prior to all kinetochores reaching bi-orientation, the RZZ complex at kinetochores provides stable association of Mad1/Mad2 to kinetochores. The association of Mad1/Mad2 also requires an unknown factor X. Factor X could be another protein, based on my discussion either Knl1 or an as yet unknown protein. Factor X could also be a modification on Mad1/Mad2 or cooperativity resulting from RZZ oligomerization at kinetochores (Section 5.3). RZZ stabilized Mad1/Mad2 localization at kinetochore causes the SAC to be active (Figure 49 Step 1). Upon SAC activation the enzyme FTase farnesylates Spindly (Figure 49 Step 2). Spindly farnesylation allows for high affinity binding to the RZZ complex, in the course of which Spindly-F becomes recruited to kinetochores. The Spindly-F-RZZ interface then recruits the Dynein/Dynactin complex (Figure 49 Step 3). The minus-end directed motor protein Dynein transports RZZ and Spindly with factor X away from kinetochores signifying that Mad1/Mad2 are not longer stabilized by the RZZ complex (Figure 49 Step 4). Mad1/Mad2 are then removed from kinetochores via an independent silencing mechanism and ultimately the checkpoint is switched off.

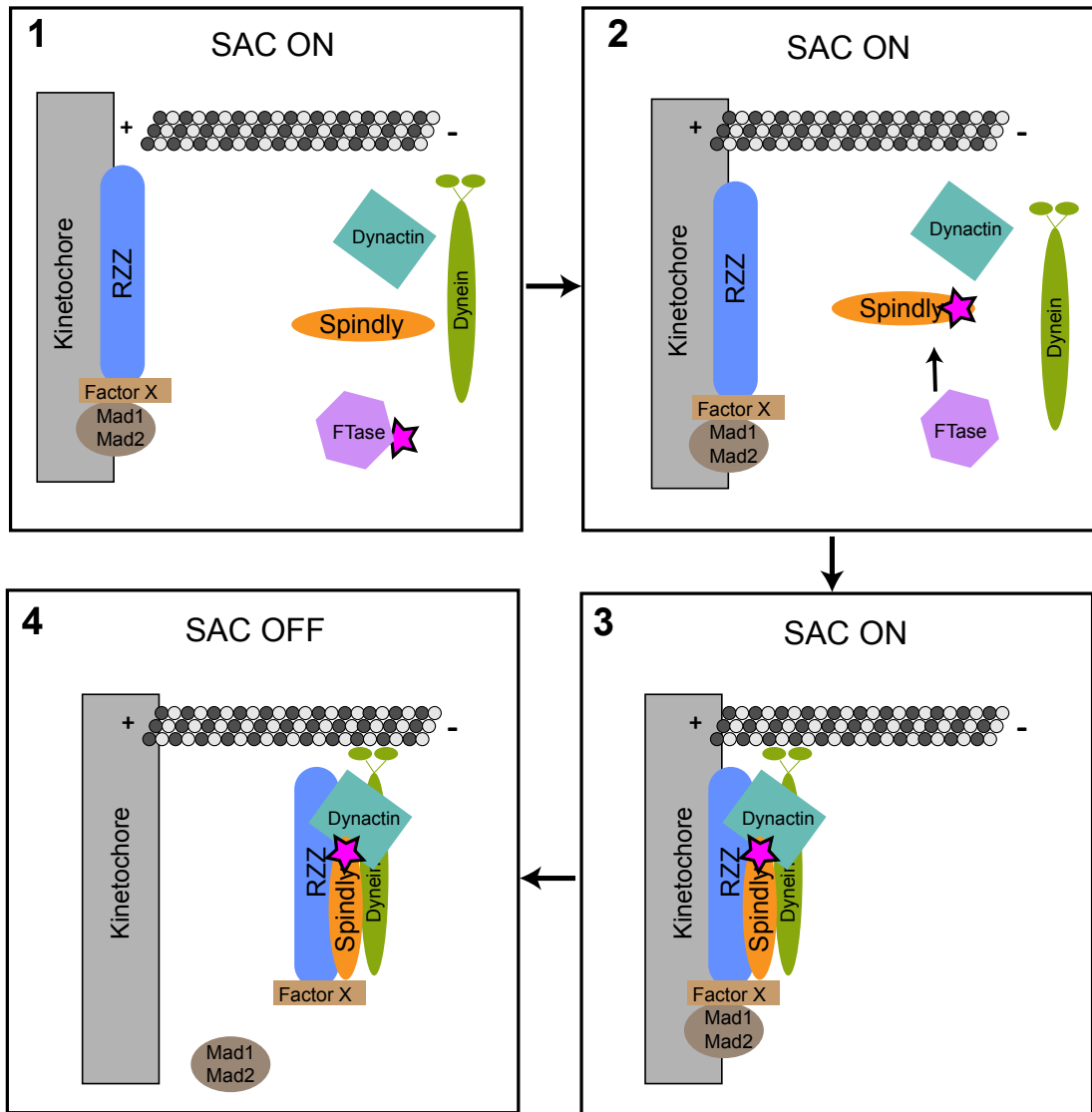


**Figure 49: Model for the functions of RZZ at kinetochores**

During mitosis and until all kinetochores have reached bi-orientation, the RZZ complex at kinetochores provides stably associated Mad1/Mad2, which requires an unknown factor X. Upon checkpoint activation the enzyme FTase farnesylates Spindly. Spindly farnesylation allows high affinity binding to the RZZ complex, in the course of which farnesylated Spindly (Spindly-F) becomes recruited to kinetochores. The Spindly-F-RZZ interface then recruits the Dynein/Dynactin complex. The minus-end directed motor protein Dynein transports RZZ, Spindly and factor X away from kinetochores destabilizing Mad1/Mad2. Mad1/Mad2 are then removed from kinetochores via an independent silencing mechanism and ultimately the checkpoint is switched off.

## 6 Materials and Methods

### 6.1 Methods

#### 6.1.1 Chemicals

Chemicals of the following companies have been used for the experiments described in this thesis:

AppliChem (Darmstadt), Boehringer (Mannheim), Difco Microbiology / Voigt Global, Fermentas (St. Leon-Rot, Deutschland), Fluka / Sigma-Aldrich (München, Deutschland), Gerbu (Gaiberg), J. T. Baker / Mallinckrodt Baker B.V. (Deventer, Niederlande), Merck (Darmstadt), Riedel de Haën (Seelze), Roche (Basel, Schweiz), Carl Roth GmbH (Karlsruhe), Serva (Heidelberg), Sigma-Aldrich (München), Thermo Fisher Scientific Inc. (Schwerte), Invitrogen / Lifetechnologies (Karlsruhe), Creative Molecules (Arizona, USA).

#### 6.1.2 Kits

**Table 4: List of all used Kits**

| Kit                                                                                                     | Company                |
|---------------------------------------------------------------------------------------------------------|------------------------|
| QIAquick Gel Extraction Kit,<br>QIAprep Spin Miniprep Kit,<br>Plasmid Midi Kit, PCR Purification<br>Kit | QIAGEN, Hilden         |
| ProQDiamond Phosphostain                                                                                | Invitrogen, Karlsruhe  |
| ECL Kit and Chemiluminescence<br>Films                                                                  | GE Healthcare, München |

## Materials and Methods

### 6.1.3 Markers

**Table 5: List of all used markers**

| Marker                                     | Company                    |
|--------------------------------------------|----------------------------|
| Gel Filtration Standard                    | Bio-Rad, München           |
| Precision Plus Protein Standard Unstained  | Bio-Rad, München           |
| Precision Plus Protein Standard Dual Color | Bio-Rad, München           |
| Gene Ruler 1 kb plus DNA ladder            | ThermoScientific, Schwerte |

## Materials and Methods

### 6.1.4 Microorganisms and cell lines

**Table 6: List of all used microorganisms**

| <i>E. coli</i> cell line          | Genotype                                                                                                                                                                                                                                             |
|-----------------------------------|------------------------------------------------------------------------------------------------------------------------------------------------------------------------------------------------------------------------------------------------------|
| TOP10                             | F- <i>mcrA</i> $\Delta(mrr-hsdRMS-mcrBC)$ $\Phi 80/lacZ\Delta M15$<br>$\Delta lacX74$<br><i>nupG recA1 araD139</i> $\Delta(ara-leu)7697 galE15$<br><i>galK16 rpsL(Str<sup>R</sup>) endA1 nupG</i> $\lambda^-$                                        |
| DH10<br>MultiBac <sup>Turbo</sup> | F- <i>mcrA</i> $\Delta(mrr-hsdRMS-mcrBC)$ $\Phi 80/lacZ\Delta M15$<br>$\Delta lacX74$<br><i>recA1 endA1 araD139</i> $\Delta(ara, leu)7697 galU galK$<br>$\lambda^- rpsL$<br><i>nupG /pMON14272 v-cath::Amp<sup>r</sup> chiA::LoxP */</i><br>pMON7124 |
| BL21 (DE3)                        | F-, <i>ompT, hsdSB(rB-, mB-), dcm, gal, <math>\lambda</math>(DE3)</i>                                                                                                                                                                                |
| Omnimax                           | F' pro AB+ <i>lacIq lacZ</i> $\Delta M15$ Tn10 (Tetr) $\Delta(ccdAB)\{fa$<br><i>mcrA</i> $\Delta(mrr-hsdRMS-mcrBC)$ $\Phi 80/lacZ\Delta M15$ $\Delta(lacZY,$<br><i>argF) U169 endA1 recA1 supE44 thi-1 gyrA96 relA1<br/><i>tonA panA</i></i>         |
| Cell line                         | Genotype                                                                                                                                                                                                                                             |
| Sf9                               | Sf21 (IPLB-SF21-AE ) based cell line from<br><i>Spodoptera frugiperda</i> ovaries (Vaughn <i>et al</i> ,<br>1977)                                                                                                                                    |
| Tna038                            | HiFive (BTI-TN-5B1-4) based cell line from cabbage<br>looper ovaries (Hashimoto <i>et al</i> , 2010)                                                                                                                                                 |

## Materials and Methods

### 6.1.5 Vectors and constructs

**Table 7: List of all used vectors and designed constructs**

| Vector / Construct    | Source                           |
|-----------------------|----------------------------------|
| pOPIN                 | DPF, Dortmund                    |
| pOPIN-NHis            | DPF, Dortmund                    |
| pOPIN-CHis            | DPF, Dortmund                    |
| pOPIN-NHis-3C         | DPF, Dortmund                    |
| pOPIN(N)-EGFP         | DPF, Dortmund                    |
| pOPIN(C)-EGFP         | DPF, Dortmund                    |
| pACEbac1              | ATG Biosynthetics,<br>Merzhausen |
| pFG                   | ATG Biosynthetics,<br>Merzhausen |
| pFH                   | ATG Biosynthetics,<br>Merzhausen |
| pACEbac1_2His_Zwilch  | ATG Biosynthetics,<br>Merzhausen |
| pACEbac1_6His_Zwilch  | ATG Biosynthetics,<br>Merzhausen |
| pOPIN(N)-EGFP_Zw10    | DPF, Dortmund                    |
| pOPIN(C)-EGFP_Zw10    | DPF, Dortmund                    |
| pOPIN-CHis_Zw10       | DPF, Dortmund                    |
| pFG_Rod               | ATG Biosynthetics,<br>Merzhausen |
| pFH_Rod               | ATG Biosynthetics,<br>Merzhausen |
| pOPIN_NHis_Rod_1-1250 | DPF, Dortmund                    |
| pOPIN_NHis_Spindly    | DPF, Dortmund                    |

## Materials and Methods

### 6.1.6 Enzymes

**Table 8: List of all used enzymes**

| Enzyme                           | Company                                    |
|----------------------------------|--------------------------------------------|
| Restriction Endonucleases        | New England Biolabs, Ipswich, USA          |
| T4 DNA Ligase                    | New England Biolabs, Ipswich, USA          |
| 2x Phusion Polymerase master mix | Biozym Scientific GmbH, Hessisch Oldendorf |
| T4 DNA Polymerase                | New England Biolabs, Ipswich, USA          |
| RecA                             | Biozym Scientific GmbH, Hessisch Oldendorf |
| ET-SSB                           | New England Biolabs, Ipswich, USA          |
| Precision Protease               | DPF, Dortmund                              |
| $\lambda$ -Phosphatase           | New England Biolabs, Ipswich, USA          |
| Fast Alkaliphosphatase           | New England Biolabs, Ipswich, USA          |

## Materials and Methods

### 6.1.7 Media, antibiotics and transfection reagents

**Table 9: List of all used media, antibiotics and transfection reagents**

| Material        | Company/Composition                                                                                                                                          |
|-----------------|--------------------------------------------------------------------------------------------------------------------------------------------------------------|
| DMEM            | PAN Biotech, Aidenbach                                                                                                                                       |
| FBS             | Invitrogen, Karlsruhe                                                                                                                                        |
| Sf-900™ III SFM | Invitrogen, Karlsruhe                                                                                                                                        |
| LB plates       | LB-Agar containing:<br>100 µg/ml Ampicillin,<br>7 µg/ml Gentamycin,<br>10 µg/ml Tetracyclin,<br>100 µg/ml X-Gal,<br>40 µg/ml IPTG                            |
| Antibiotics     | Ampicillin (100 mg/L medium)<br>Gentamycin (7 mg/L medium)<br>Tetracyclin (10 mg/L medium)<br>Streptomycin (100 µg/ml medium)<br>Penicillin( 10 U/ml medium) |



## Materials and Methods

### 6.1.8 Columns

**Table 10: List of all used columns and beads**

| Columns                                                                            | Company                                   |
|------------------------------------------------------------------------------------|-------------------------------------------|
| HisTrap Crude FF, 5ml                                                              | GE Healthcare, München                    |
| Ni-NTA Superflow beads                                                             | QIAGEN, Hilden                            |
| HiTrap SP HP, 5 ml                                                                 | GE Healthcare, München                    |
| HiTrap Q HP, 5 ml                                                                  | GE Healthcare, München                    |
| Resource Q, 5 ml                                                                   | GE Healthcare, München                    |
| Amylose beads                                                                      | GE Healthcare, München                    |
| Superdex 75 HR 10/300                                                              | GE Healthcare, München                    |
| Superdex 200 HR 10/300                                                             | GE Healthcare, München                    |
| Superose 6 HR 10/300                                                               | GE Healthcare, München                    |
| TSKgel G4000SW <sub>XL</sub> column<br>with a TSKgel SW <sub>XL</sub> guard column | TOSOH Bioscience,<br>Tessenderlo, Belgium |

## Materials and Methods

### 6.1.9 Laboratory Equipment

**Table 11: List of the laboratory equipment**

| Laboratory Equipment        | Company                             |
|-----------------------------|-------------------------------------|
| Agarose gel chamber, CRHU10 | Carl Roth GmbH, Karlsruhe           |
| Autoklave Laboklav          | SHP Steriltechnik AG, Detzel Schloß |
| Balance BP110S              | Sartorius, Göttingen                |
| Balance CPA324S             | Sartorius, Göttingen                |
| Centrifuge Avanti J-30I     | Beckman Coulter, Krefeld            |
| Centrifuge Eppendorf 3424 R | Eppendorf, Hamburg                  |
| Centrifuge Sorvall RC3BP+   | ThermoScientific, Schwerte          |
| Centrifuge Universal 320R   | Hettich, Kirchlingern               |
| Femtojet injection device   | Eppendorf, Hamburg                  |
| FPLC-System Äkta Micro      | GE Healthcare                       |
| FPLC-System Äkta Purifier   | GE Healthcare                       |
| FPLC-System Äkta Prime      | GE Healthcare                       |
| Freezer (-20°C)             | Panasonic, Hamburg                  |
| Freezer (-80°C)             | Panasonic, Hamburg                  |
| Incubator (27°C)            | WTC Binder, Tuttlingen              |
| Incubator (37°C)            | WTC Binder, Tuttlingen              |
| Incubation Shaker Multitron | Infors HT, Bottmingen, Schweiz      |
| InjectMan IN2 microinjector | Eppendorf, Hamburg                  |
| ITC 200                     | MicroCal GE Healthcare, München     |
| Magnetic Stirrer MR 2000    | Heidolph, Schwabach                 |
| Microscope Axiolab          | Carl Zeiss, Jena                    |
| Nanodrop 2000               | ThermoScientific, Schwerte          |
| Milli-Q                     | Merck Millipore, Darmstadt          |
| Micro Scale Thermophoresis  | NanoTemper Technologies, München    |

## Materials and Methods

|                                              |                                |
|----------------------------------------------|--------------------------------|
| PCR Cycler Professional TRIO                 | Biometra, Göttingen            |
| Photometer Eppendorf Biophotometer           | Eppendorf, München             |
| SDS-PAGE Gel System, Mini PROTEAN Tetra Cell | Bio-Rad, München               |
| Sonicator Sonifier Cell Disruptor            | G. Heinemann, Schwäbisch Gmünd |
| Thermomixer S436                             | Eppendorf, München             |
| Trans-Blot Semi-Dry blotter Unit             | Scie-Plas, Cambridge, UK       |
| Ultracentrifuge Optima L-80 XP               | Beckman Coulter, Krefeld       |
| Vortex Genie 2                               | Bender & Hobein, Bruchsal      |

## Materials and Methods

### 6.1.11 Frequently used buffers

**Table 12: List of frequently used buffers**

| Buffer                                                     | Composition                                                                                 |
|------------------------------------------------------------|---------------------------------------------------------------------------------------------|
| RZZ wash buffer                                            | 50 mM Hepes pH 8.5; 200 mM NaCl;<br>10 % Glycerol;<br>20 mM Imidazole; 5 mM $\beta$ -ME     |
| RZZ G4000 buffer<br>for<br>FTase and kinase<br>experiments | 25 mM Hepes pH 7.5; 250 mM NaCl; 10 mM<br>MgCl <sub>2</sub> ,<br>4 mM TCEP                  |
| RZZ S6 buffer                                              | 25 mM Hepes pH 8.5; 250 mM NaCl; 4 mM<br>TCEP                                               |
| Zw10 wash buffer                                           | 1 x PBS pH 7.4-7.6; 150 mM NaCl; 10 %<br>Glycerol;<br>20 mM Imidazole; 5 mM $\beta$ -ME     |
| Buffer A/B                                                 | 50 mM Tris pH 8.5; 100 /1000mM NaCl; 2 mM<br>DTE                                            |
| Zw10 S200 buffer                                           | 25 mM Hepes pH 8.5; 250 mM NaCl; 4 mM<br>TCEP                                               |
| TAE buffer (10x)                                           | 89 mM Tris<br>89 mM Boric Acid<br>0.9 mM EDTA                                               |
| DNA Loading dye                                            | 10 % (w/v) Ficoll<br>0.025 % (w/v) Bromphenol Blue in 1x TAE buffer                         |
| Coomassie Stain                                            | 44 % (v/v) Ethanol<br>12 % (v/v) Acedic Acid<br>0.15 % (w/v) Coomassie Brilliant Blue R 250 |
| Destain                                                    | 44 % (v/v) Ethanol<br>12 % (v/v) Acedic Acid                                                |
| SDS Runningng<br>buffer                                    | 25 mM Tris<br>190 mM Glycin                                                                 |

## Materials and Methods

|                        |                                                                                                                           |
|------------------------|---------------------------------------------------------------------------------------------------------------------------|
|                        | 0.1 % (w/v) SDS                                                                                                           |
| SDS Loadingng dye (5x) | 5 % $\beta$ -Mercaptoethanol<br>0.02 % Bromophenol blue<br>30 % Glycerol, 10 % SDS<br>25 mM Tris                          |
| Separation gel buffer  | 1.5 M Tris pH 8.8<br>0.4 % (w/v) SDS                                                                                      |
| Stacking gel buffer    | 0.5 M Tris pH 6.8<br>0.4 % (w/v) SDS                                                                                      |
| Transfer buffer        | 25 mM Tris, 200 mM glycine, 20 % methanol                                                                                 |
| TBST                   | 1.5 M NaCl, 25 mM KCl, 250 mM Tris, 0.05 % Tween-20                                                                       |
| Wash buffer 1          | 25mM $\text{NH}_4\text{HCO}_3$ 3:1 mixed with Acetonitrile                                                                |
| Wash buffer 2          | 25mM $\text{NH}_4\text{HCO}_3$ 1:1 mixed with Acetonitrile                                                                |
| Reduction solution     | 50mM DTT, 25mM $\text{NH}_4\text{HCO}_3$ (stored at $-20^\circ\text{C}$ )                                                 |
| Alkylation solution    | 55mM Iodacetamide, 25mM $\text{NH}_4\text{HCO}_3$ (stored at $-20^\circ\text{C}$ )                                        |
| Digestion solution     | 0.01 $\mu\text{g}/\mu\text{l}$ trypsin in 10 mM HCl with 25 mM $\text{NH}_4\text{HCO}_3$ (stored at $-20^\circ\text{C}$ ) |

## 6.2 Methods Molecular Biology

### 6.2.1 Plasmid Purification

All plasmids were purified after propagation in *E. coli* Omnimax cells using the QIAGEN Plasmid Mini Kit.

### 6.2.2 Polymerase Chain Reaction

The polymerase chain reaction (PCR) is a method for in vitro amplification of deoxyribonucleic acids (DNA) for further processing (Quelle/Caro66). The method includes repetitive cycles of denaturation of double stranded DNA (dsDNA), hybridization of oligonucleotides (oligos) and enzymatic elongation of these oligos. During denaturation (94-98°C) the hydrogen bonds between base pairs are melted resulting in single stranded DNA (ssDNA). In the following hybridization the oligos (short single stranded DNA) anneal to complementary ssDNA serving as a starting point for the enzymatic synthesis of new DNA. For efficient annealing the temperature is decreased below the melting temperature of the oligo. DNA polymerases are utilized for the DNA elongation. The elongation temperature depends on the temperature optimum of the chosen DNA polymerase. The duration of the elongation depends on the length of the fragment to be amplified and the efficacy of the used polymerase. Here the Phusion Flash HF PCR Master Mix was used.

The following tables show the details for the PCRs.

**Table 13: PCR pipetting scheme**

| <b>Components</b>                  | <b>Quantity</b> |
|------------------------------------|-----------------|
| dsDNA template                     | 25 – 100 ng     |
| Oligo, forward (10 pM)             | 1 µl            |
| Oligo, reverse (10 pM)             | 1 µl            |
| 2x Phusion Flash HF PCR Master Mix | 12.5 µl         |
| H <sub>2</sub> O                   | Add up to 25 µl |

**Table 14: PCR program**

|                  |         |               |
|------------------|---------|---------------|
| Denaturation     | 95°C    | 2 min         |
| Denaturation     | 95°C    | 10 s          |
| Annealing        | 50-65°C | 30 s          |
| Elongation       | 72°C    | 1 min/1000 bp |
| Final elongation | 72°C    | 8 min         |

} 25-35 cycles

### 6.2.3 Agarose Gel Electrophoresis

The agarose gel electrophoresis is a biochemical method to separate DNA fragments. Based on their negatively charged phosphate backbone DNA molecules migrate in an electric field corresponding to their size, which enables separation. Depending on the DNA fragments that were to be separated 0.9 % or 2% Agarose gels (in TAE buffer) were used. An electric field of 120 V was applied for 45min to 60 min.

### 6.2.4 Restriction Digest

Restriction enzymes recognize specific DNA sequences and hydrolyze the phosphodiester bonds of dsDNA within or near this sequence (Pingoud & Jeltsch, 2001). Restriction enzymes are endonucleases of bacterial origins with the physiological role to digest foreign DNA. They can produce either sticky ends, which have short single stranded DNA overhangs, or blunt ends. In this thesis exclusively sticky end producing restriction enzymes from NEB were used. For the digest, DNA was mixed with a relevant enzyme and its corresponding buffer following the NEB manual and incubated at 37°C for 1-3 h.

### 6.2.5 Ligation

Ligation is the process of coupling 2 DNA fragments using the T4 DNA ligase. In order to produce a plasmid in a 20 µl reaction volume, 250 ng of dephosphorylated vector and a five fold molar excess of insert and 1 µl T4 DNA ligase were overnight incubated at 4°C.

## Materials and Methods

### 6.2.6 Transformation of DNA into *E. coli* cells

The plasmid DNA was transformed into chemical competent *E. coli* cells. Therefore 50–100 ng of DNA was mixed with 50 µl of chemical competent cells and incubated for 30 min on ice. This was followed by a heat shock, which opened shortly the cell membrane, allowing the DNA to enter the cell. This was achieved by a 45 s incubation at 42°C, followed by 2 min on ice, allowing the cell membrane pores to close again. The cells were then grown in 200 µl LB medium for 1 h at 37°C. To grow cells containing the desired DNA selectively, 200 µl were plated on LB- plates supplemented with the corresponding antibiotic.

### 6.2.7 Colony PCR

For a quick identification of potential positive colonies (vector harboring the desired insert) some colonies were picked from the LB-Agar plate with a 10 µl pipette tip and part of this material was immersed into a 25 µl PCR mixture (**Table 15**). A PCR was carried out using the protocol depicted in table **Table 16**. Oligos binding specifically upstream and downstream of the insert were used. 10 µl of the PCR product were analyzed using a 0.9% agarose gel.

**Table 15: Colony-PCR pipetting scheme**

| Components              | Quantity        |
|-------------------------|-----------------|
| Chrimson Taq buffer 5x  | 5 µl            |
| Oligo, forward (10 pM)  | 0.5 µl          |
| Oligo, reverse (10 pM)  | 0.5 µl          |
| Chrimson Taq polymerase | 0.125 µl        |
| H <sub>2</sub> O        | Add up to 25 µl |

**Table 16: Colony-PCR program**

|                  |         |               |             |
|------------------|---------|---------------|-------------|
| Denaturation     | 95°C    | 30 s          | } 29 cycles |
| Denaturation     | 95°C    | 30 s          |             |
| Annealing        | 50-65°C | 1 min         |             |
| Elongation       | 68°C    | 1 min/1000 bp |             |
| Final elongation | 68°C    | 8 min         |             |



## Materials and Methods

### 6.2.8 DNA sequencing

Positive clones (judged by colony PCR or analytical restriction digest) were sequenced in order to verify the DNA sequence integrity of the insert. Sequencing was performed by an external company (Beckmann Counter Genomics, Takeley, UK), which is using the Sanger-Method (Sanger, 1975), (Sanger *et al*, 1977).

## Materials and Methods

### 6.2.9 Baculo-Transfection and Virus Amplification in sf9 cells

#### Bacmid Recombination

Due to the inability of plasmid DNA to be propagated in insect cells it is necessary to utilize Bacmid DNA as a shuttle vector, since Bacmid DNA can be propagated both in insect cells and in *E. coli*. Thus, the plasmid DNA gets recombined with the Bacmid DNA. Correct insertion of the plasmid DNA into the Bacmid is tested via a so-called blue/white screening. In this blue/white screening white colonies indicate that the plasmid DNA was inserted into the Bacmid, because the transposition site within DH10EMBacY cells is harbored within the lac Z gene. If the lac Z gene was destroyed, so the plasmid DNA was integrated, the cells were not able anymore to metabolize 5-bromo-4-chloro-indolyl- $\beta$ -D-galactopyranoside (x-gal) into 5,5'-dibromo-4,4'-dichloro-indigo which is blue.

In order to create recombinant Bacmid DNA the plasmid DNA was transformed into chemical competent DH10EMBacY cells following the protocol from chapter 6.2.6. The 37°C incubation step was extended to 6 h. Cells were plated on Kan/Tet/Gent/IPTG/X-Gal plates in 1:1, 1:10 and 1:50 dilutions and subsequently incubated for 2 days @ 37°C. For verification, a couple of putative positive colonies (white) were streaked out again on a Kan/Tet/Gent/IPTG/X-Gal plate and incubate for 2 days.

#### Bacmid-DNA Preparation and Transfection

For each construct 2-3 white colonies were inoculated in 3 ml LB (Kan/Tet/Gent) and incubated over night at 37°C. The cultures were centrifuged for 10 min. at 4000 rpm and the supernatants were discarded. 300  $\mu$ l of resuspension buffer P1 (Qiagen Miniprep Kit) were added, the pellets were resuspended and transferred into 2 ml Eppendorf tubes. Then 300  $\mu$ l lysis buffer P2 (Qiagen Miniprep Kit) was added and inverted carefully. Next 300  $\mu$ l neutralization buffer N3 (Qiagen Miniprep Kit) was added and gently mixed. The tubes were centrifuged for 10 min at maximum speed and RT. Supernatants were transferred into fresh tubes and centrifuged again for 5 min at max speed and RT. Supernatants were transferred into new tubes containing 700  $\mu$ l isopropanol and incubated over night at -20°C. The tubes were then centrifuged for 10 min at 13500 rpm and 4°C and the supernatants were discarded. Then 200  $\mu$ l of 70 % EtOH was added and again centrifuged for 10 min, 13500 rpm, 4°C. The EtOH was removed and another 50  $\mu$ l 70% EtOH was added. Then the tubes were transferred to the clean bench where

## Materials and Methods

the EtOH was removed again and the pellets were dried.. Then 40  $\mu$ l sterile TE-buffer was added to the dry pellets and the Bacmid-DNA was resuspended.

In the meantime 2 ml of Sf9 cells at a density of  $1 \times 10^6$  cells/ml in fresh SF900 III media were transferred into each well of a 6 well plate. 200  $\mu$ l SF900 III media was supplemented with 10  $\mu$ l FuGENE, added to 20  $\mu$ l of Bacmid-DNA and incubated for 15 min at RT (the remaining 20  $\mu$ l Bacmid DNA were stored for future transfection at  $-20^\circ\text{C}$ ). These transfections mixtures were added carefully to the cells and mixed by slowly moving the plates back and forth. Cells were incubated for 3 days at  $27^\circ\text{C}$ .

### Amplification ( $V_0$ )

To generate the first virus stock ( $V_0$ ),  $10 \times 10^6$  cells were seeded in a 10cm plate in 10 ml SF900 III media (10 ml with  $1 \times 10^6$  cells/ml). The supernatant from one well from the transfection plate (6-well plate) was transferred completely to the 10 cm plate. The virus amplification was incubated for 4 days at  $27^\circ\text{C}$ . Then the supernatants were sterile filtered into a 15ml Falcon tube and FBS to a final concentration of 10% was added. Viruses were stored at  $4^\circ\text{C}$ .

### Virus Amplification ( $V_1$ )

To amplify into the subsequent virus stocks ( $V_1, V_2, \dots$ ),  $1 \times 10^6$  Sf9 cells/ml were incubated with 1/100 volume  $V_0$  and incubated for 4 days at  $27^\circ\text{C}$ . Then cells were centrifuged at 250g for 15 min at RT and the supernatant was sterile filtered and FCS was added to a final concentration of 10%. Viruses were stored at  $4^\circ\text{C}$ .

## Materials and Methods

### 6.3 Methods Biochemistry

#### 6.3.1 Protein Expression test (insect cells)

Based on this analysis it was decided for each construct individually which virus concentration to use and how long to wait for all following expressions. For each construct 3 flasks containing 50 ml of TnaO38 cells (between  $0.5 \times 10^6$  and  $1 \times 10^6$  cells/ml) were infected with  $V_0$  or  $V_1$  at 1/50, 1/100, 1/200. The cells were incubated at 27°C in a shaker (110 rpm). 1 ml samples were taken after 48 h and 72 h (centrifuge at 250g for 2 min and use pellets). The pellets were resuspended in 500  $\mu$ l lysis buffer (RZZ wash buffer supplemented with a protease inhibitor mix) and sonicated twice for 10 sec. (intensity 30 %, output 3). A sample was taken for SDS gel analysis. The cell lysates were centrifuged for 10 min at 13500 rpm and 4°C. A sample was taken for SDS gel analysis. To each cleared lysate 50  $\mu$ l equilibrated beads (RZZ wash buffer) were added and incubated for 1h at 4°C while gently rotating. The beads were washed five times with 1ml of a washing buffer. The buffer was taken off completely and 40 $\mu$ l SDS-loading buffer was added. The samples were boiled at 95°C for 5 min and analyzed by SDS-PAGE.

#### 6.3.2 Protein Expression

The desired amount of TnaO38 cell suspension (between  $0.5 \times 10^6$  and  $1 \times 10^6$  cells/ml) was infected with the desired virus stock at the concentration and for expression duration recommended by the protein expression test (Section 6.3.1). After the protein expression cells were centrifuged at 250 g for 20 min. The pellets were washed once with PBS buffer and either processed immediately or flash frozen in liquid nitrogen and stored at -80°C.

#### 6.3.3 Cell lysis

A pellet of 500-800 ml insect cell culture was resuspended in 100 ml wash buffer supplemented with 1 mM PMSF (Phenylmethylsulfonylfluorid) and 1mM protease inhibitor cocktail (Serva). The cells were lysed using sonication for 3 times 45 pulses (intensity 60 %, output 6). Cell membranes and other insoluble components were separated from the cleared lysate by centrifugation at 100,000g for 1h at 4°C followed by filtration.

## Materials and Methods

### 6.3.4 Immobilized Metal Ion Affinity Chromatography (IMAC)

The immobilized metal ion affinity chromatography (IMAC) allows the separation of proteins carrying an exposed His<sub>6</sub>-tag from a biochemical mixture based on the highly specific and reversible interaction between the resin material of the column, Ni<sup>2+</sup>-nitriloacetic acid (Ni-NTA) and histidin. In order to purify proteins carrying a His<sub>6</sub>-tag the cleared cell lysate was loaded on a HisTrap FF column that was equilibrated with the wash buffer using a peristaltic pump at 4°C and a flow rate of 2 ml/min. To remove unspecific bound proteins the column was washed with 500 ml of wash buffer. Then the protein of interest was either eluted using an elution buffer, containing 250 mM imidazole competing with the Histidins for the binding sites of the Ni-NTA or incubated over night with Prescission protease, which specifically cleaves between the His<sub>6</sub>-tag and the protein of interest. The respective fractions were analyzed by SDS-PAGE.

### 6.3.5 Ion Exchange Chromatography

Ion exchange chromatography relies on reversible charge-charge interactions between the protein of interest and the charges of the resin of choice. In order to allow binding of the protein to the ion exchange column (Resource Q or HiTrap Q from GE Healthcare) the protein samples were diluted 1:5 in buffer A before loading. The diluted sample was loaded onto the column applying a flow rate of 1 ml/min and washed for 3 column volumes with buffer A. This was followed by a gradient from 0% buffer B till 50 % buffer B (containing 1M NaCl) for a length of 20 column volumes. Peak fractions containing putatively the protein of interest were analyzed by SDS-PAGE.

### 6.3.6 Concentration of protein samples

In order to concentrate fractions containing the protein of interest ultrafiltration units (Millipore) were used. The molecular weight cut off (MWCO) was chosen respectively to the size of the smallest protein of interest in the solution. The units were washed once with ddH<sub>2</sub>O and equilibrated with the respective buffer from the last purification step. Then the protein solution was applied to the concentrators centrifuged for several rounds at 2000-4000 rpm.

## Materials and Methods

### 6.3.7 Dialysis of protein samples

To exchange the buffer of the POI, we dialyzed either for 3 h against a 500 fold volume (dialysis buffer over sample volume) or overnight against a 100 fold volume.

### 6.3.8 Determination of protein concentrations

Protein concentrations were determined using the Nanodrop spectrometer measuring the absorbance at 280 nm and considering the molecular weight and the extinction coefficient of the respective proteins.

### 6.3.9 Size Exclusion Chromatography (SEC)

Size exclusion chromatography is a method that separates molecules based on their size and shape. The column serves as a stationary pore system where larger molecules pass through earlier than smaller molecules, because they penetrate less with the pore system. This method is frequently used as the final step during protein purification. For the purification of different proteins or protein complexes the column types Superdex 200 10/300 and Superose 6 10/300 were used. All samples were injected at a volume of 500  $\mu$ l and eluted under isocratic conditions at 4°C with the respective buffer over 1.5 column volumes at a flow rate of 0.3 ml/min.

### 6.3.10 Sodiumdodecylsulfate-Polyacrylamide Gelelectrophoresis (SDS-PAGE)

The Sodiumdodecylsulfate-Polyacrylamidegelelectrophoresis (SDS-PAGE) is a method that separates proteins in a gel based on their molecular weights. Therefore the proteins are denatured by sodiumdodecylsulfate before loading onto the gel. Due to the negative charges resulting from the bound sodiumdocedylsulfate, the proteins migrate in the gel during the electrophoresis. This way the proteins get separated based on their molecular weight, because smaller molecules migrate faster than bigger ones. Depending on the molecular

## Materials and Methods

weight range of proteins that have to be separated in the gel, different acrylamide concentrations can be used.

**Table 17: Pipetting scheme for 4 SDS gels**

|                          | Running gel<br>10 % | Running gel<br>12 % | Running gel<br>15 % | Stacking gel<br>7 % |
|--------------------------|---------------------|---------------------|---------------------|---------------------|
| ddH <sub>2</sub> O       | 12.3 ml             | 10.2 ml             | 7.2 ml              | 6.7 ml              |
| 30 % (w/v)<br>Acrylamide | 9.9 ml              | 12.0 ml             | 15. ml              | 1,33 ml             |
| Running buffer           | 7.5 ml              | 7.5 ml              | 7.5 ml              | –                   |
| Stacking buffer          | –                   | –                   | –                   | 2.5 ml              |
| 10 % (w/v) SDS           | 150 µl              | 150 µl              | 150 µl              | 50 µl               |
| TEMED                    | 20 µl               | 20 µl               | 20 µl               | 5 µl                |
| 10 % (w/v) APS           | 150 µl              | 150 µl              | 150 µl              | 50 µl               |

The electrophoresis was performed at 46 mA for one gel, 86 mA for two gels or at 180V for 30-40 min. The gels were stained with a coomassie staining solution and destained with a destaining solution (Section 6.1.11).

## Materials and Methods

### 6.3.11 Western Blot Analysis

Western blot analysis is a more sensitive staining technique for proteins than SDS-PAGE analysis. It allows the detection of specific proteins as it is based on specific interactions between the protein of interest and its specific antibody.

In practice, the electrophoretically separated proteins were transferred from the polyacrylamide gel to a methanol-activated polyvinylidene fluoride (PVDF) membrane in transfer buffer at 90 V and 4°C for 100 minutes. To reduce unspecific binding the membrane was incubated on a shaker in 10 ml TBST buffer with 5% milk powder for 1 h at RT. Next the membrane was incubated on a shaker with TBST supplemented with 5 % milk and the primary antibody over night at 4°C. The membrane was washed three times with 10 ml TBST with 5% milk powder for 10 min at RT. Then the secondary antibody in 5 ml TBST with 5% milk powder was applied to the membrane for 1 h at RT. For detection of secondary antibodies that are conjugated to horseradish peroxidase (HRP), ECL Prime Western Blotting Detection reagent and High Performance Chemiluminescence Films were used following the company's instructions.

### 6.3.12 Expression and purification of Zw10

For a pellet of 800 ml CHis-POPIN-Zw10 expression culture (insect cell expression in TnaO38 cells V1 Zw10 full length 1:30) cell lysis was performed in 100 ml lysis buffer by 3 x 45 pulses sonication (Section 6.3.3). The cleared lysate was loaded onto an equilibrated 5 ml Ni-NTA column using the peristaltic pump (Section 6.3.4) and the flow through was reloaded one more time (2 ml/min flow rate). The column was washed with 500 ml wash buffer and the elution was done with 250 mM imidazole added to the wash buffer collecting 2 ml fractions. The fractions were analyzed by SDS-PAGE and the fractions containing Zw10 were concentrated up to a volume of 10 ml. Afterwards the protein solution was diluted 5 times with buffer A and subsequently purified with a Resource Q anion exchange (Section 6.3.5). Peak fractions were analyzed by SDS-PAGE and the ones containing Zw10 were concentrated up to 500 µl, and applied to a Superdex 200 10/300 column (Section 6.3.9). The peak fractions were again analyzed by SDS-PAGE and the fractions containing pure Zw10 were concentrated up to 10 mg/ml and flash frozen in liquid nitrogen in aliquots of 20 µl volume and stored at -80°C.



## Materials and Methods

### 6.3.13 Expression and purification of Spindly

For a pellet of 500 ml NHis-POPIN-Spindly expression culture (insect cell expression in TnaO38 cells V<sub>1</sub> Spindly full length 1:50) cell lysis was performed in 100 ml lysis buffer RZZ by 3 x 45 pulses sonication (Section 6.3.3). The cleared lysate was loaded onto an equilibrated 5 ml Ni-NTA column using the peristaltic pump (Section 6.3.4) and the flow through was reloaded one more time (2 ml/min flow rate). The column was washed with 500 ml wash buffer RZZ and the elution was done with 250 mM imidazole added to the wash buffer RZZ collecting 2 ml fractions. The fractions were analyzed by SDS-PAGE and the fractions containing Spindly were concentrated up to a volume of 10 ml. Afterwards the protein solution was diluted 5 times with buffer A and subsequently purified with a Resource Q anion exchange (Section 6.3.5). Peak fractions were analyzed by SDS-PAGE and the ones containing Spindly were concentrated up to 500  $\mu$ l, and applied to a Superose 6 10/300 column (Section 6.3.9). The peak fractions were again analyzed by SDS-PAGE and the fractions containing pure Spindly were concentrated up to 20 mg/ml and flash frozen in liquid nitrogen in aliquots of 20  $\mu$ l volume and stored at -80°C.

### 6.3.14 Expression and purification of RZZ

For the expression of RZZ it was essential to generate fresh virus stocks that expressed Zw10 and Zwi1c in stoichiometric amounts. Typically, we generated and tested two virus stocks infected either with 1:2 or 1:4 ratio of Zw10 vs. Zwi1c. This fresh virus was used for a large expression culture. Usually, 500 ml of Tna038 cells at  $1 \times 10^6$  cells/ml were infected with 5 ml of the chosen pre-virus and 7 ml of a virus stock of pACEbac1\_6His-Rod.

For a pellet of 500 ml RZZ expression culture the cell lysis was performed in 100 ml lysis buffer RZZ by 3 x 45 pulses sonication (Section 6.3.3). The cleared lysate was loaded onto an equilibrated 5 ml Ni-NTA column using the peristaltic pump (Section 6.3.4) and the flow through was reloaded one more time (2 ml/min flow rate). The column was washed with 500 ml wash buffer RZZ and the elution was done by Precision digest on the column using the Precision protease 1:10 and circulating in a buffer volume of 20 ml over night with a flow rate of 1 ml/min. In case the aim was to purify dephosphorylated RZZ, in this step  $\lambda$ -phosphatase was added in a molar ratio of 1:10. The eluate was analyzed by SDS-PAGE and

## Materials and Methods

concentrated up to a volume of 500  $\mu$ l. Then a SEC using a Superose 6 10/300 column was performed (Section 6.3.9). The peak fractions were again analyzed by SDS-PAGE and the fractions containing pure RZZ were concentrated up to 8-10 mg/ml and flash frozen in liquid nitrogen in aliquots of 20  $\mu$ l volume and stored at -80°C.

### 6.3.15 Expression and purification of Mini-RZZ

The expression and purification of Mini-RZZ was essentially performed as for the RZZ complex. Instead of the full length His<sub>6</sub>\_Rod virus the His<sub>6</sub>\_Rod\_1-1250 virus was used for the co expression and the purification had to be performed within one day due to the low stability of the complex, thus the elution from the Ni-NTA column was done by step elution using 250 mM Imidazole.

### 6.3.16 Expression and purification of Mini-Rod/Zwilch

For a pellet of 500 ml Mini-Rod (His6-POPIN-Rod\_1-753\_(GGG)4\_1797-2209)/His2-Zwilch co expression culture (insect cell expression in TnaO38 cells both viruses 1:100) cell lysis was performed in 100 ml lysis buffer RZZ by 3 x 45 pulses sonication (Section 6.3.3). The cleared lysate was loaded onto an equilibrated 5 ml Ni-NTA column using the peristaltic pump (Section 6.3.4) (2 ml/min flow rate). The column was washed with 500 ml wash buffer RZZ and the elution was done with 250 mM imidazole added to the wash buffer RZZ collecting 1.5 ml fractions. The fractions were analyzed by SDS-PAGE and the fractions containing the Mini-Rod/Zwilch complex were concentrated up to 500  $\mu$ l, and applied to a Superose 6 10/300 column (Section 6.3.9). The peak fractions were again analyzed by SDS-PAGE and the fractions containing the pure Min-Rod/Zwilch complex were concentrated up to 5 mg/ml and flash frozen in liquid nitrogen in aliquots of 20  $\mu$ l volume and stored at -80°C.

### 6.3.17 Analytical SEC migration shift assay

Analytical SEC migration shift assays were performed to investigate interactions between proteins or protein complexes. If the proteins or protein complexes comigrate in SEC and reveal a longer retention time in SEC an interaction is indicated. In practice 5  $\mu$ M of the putative interaction partners were mixed and incubated for 2-3 h on ice in a sample volume of 60  $\mu$ l before being subjected to analytical SEC. Each of the putative interaction partners was also analyzed

## Materials and Methods

individually. The analytical SEC experiments were performed on an equilibrated Superose 6 5/150 column (GE Healthcare). All samples were injected in a volume of 50  $\mu$ l and eluted under isocratic conditions in the RZZ S6 buffer at 4°C and a flow rate of 0.08 ml/min. 50  $\mu$ l fractions were collected and analyzed by SDS-PAGE analysis.

### 6.3.18 Limited proteolysis

Limited proteolysis is a frequently used method to analyze the stability of recombinant proteins. 4  $\mu$ g of the recombinant protein was mixed in a 20  $\mu$ l volume with different proteases in a 1:100 ratio and incubated at either 30°C or 37°C for one hour in total. Protein samples were taken after several time points by adding 5  $\mu$ l SDS loading buffer and boiling for 5 minutes. The samples were first visualized by SDS-PAGE and afterwards analyzed by Petra Janning using limited in-gel digest, a mass spectrometry analysis described in Section 6.3.19.

### 6.3.19 In-gel digestion for mass spectrometric characterization of proteins

Typically, after the first purification of a protein construct, an in-gel digestion for mass spectrometric characterization of proteins was applied to check for the protein identity. Bands were cut from a polyacrylamide gel using a scalpel. The scalpel was cleaned after every protein with Ethanol. Gel pieces were cut in tiny pieces (1mm x 1mm). The gel pieces were incubated with 200  $\mu$ l of wash buffer 1 for 30 min at 37°C and 350 rpm. All remaining liquid was removed completely and 200  $\mu$ l of wash buffer 2 was added and incubated at 37°C, 350 rpm for 15 min. Wash solution 2 was replaced with 100  $\mu$ l of the reduction solution and incubated at 37°C, 350 rpm for 45 min. Afterwards the reduction solution was replaced by 100  $\mu$ l of the alkylation solution and incubated for 1h at 22°C in the dark. The alkylation solution was discarded and the gel pieces were two times washed with wash buffer 2 for 15 min. at RT and 350 rpm. To dry the gel the wash buffer was removed as complete as possible and dehydrated by addition of 10  $\mu$ l Acetonitrile. After 10 min. the Acetonitrile was removed and the eppendorf tube containing the gel pieces were kept under the fume hood for 10 min. 10-15  $\mu$ l of the digest solution were added and incubated for 15 min at RT. After addition of 20  $\mu$ l of 25mM  $\text{NH}_4\text{HCO}_3$  the tube is incubated at 30°C and 350 rpm over night.

## Materials and Methods

The peptides are extracted from the gel pieces by incubation with 3,5  $\mu$ l of 10% Trifluoroacetic acid for 30 min on ice in a sonication bath. After this the samples were dried using a speedvaccum centrifuge. Petra Janning performed the LC/MS-MS analysis.

### 6.3.20 Analytical Ultracentrifugation

Analytical ultracentrifugation (AUC) is a versatile and powerful method for the quantitative analysis of macromolecules in solution. In sedimentation velocity, the movement of molecules in high centrifugal fields is interpreted using hydrodynamic theory to define the size, shape and interactions of macromolecules. Sedimentation equilibrium is a thermodynamic method where equilibrium concentration gradients at lower centrifugal fields are analyzed to define molecule mass, assembly stoichiometry, association constants and solution nonideality (Cole *et al*, 2008).

Sedimentation velocity experiments were performed at 20 °C using a ProteomeLab XL-I analytical ultracentrifuge (Beckman Coulter) equipped with double-UV and Rayleigh interference detection. The samples were used immediately dialysis 25 mM Hepes pH 8.5, 150 mM NaCl and 2 mM DTT. The RZZ complex in concentrations (ranging from 0.1 mg/ml to 0.6 mg/ml) were spun at 42,000 rpm using an AN60-Ti rotor and 3 mm or 12 mm thick epon double sector centerpieces. Absorbance and interference profiles were recorded every 1 min. Detection of concentrations as a function of radial position and time was performed by optical density measurements at wavelengths of 280 nm. Buffer viscosity ( $\eta=0.01034$  P) and density ( $\rho=1.00641$  g.mL<sup>-1</sup>) at 20 °C were estimated with the online software Sednterp (<http://www.rasmb.bbri.org>). Data were analyzed with Sedfit 12.1 (Schuck, 2000) using a continuous size distribution c(S) model.

### 6.3.21 Thermofluor Assay

The thermofluor assay offers a rapid technique to determine the thermal stability of proteins and to investigate factors affecting this stability. An environmentally sensitive fluorescent dye is used to monitor temperature dependent protein unfolding. Melting curve analysis determines the melting temperature,  $T_m$ . For monitoring real-time PCR machines, which have sensitive thermal control and

## Materials and Methods

fluorescent detection capabilities are used. The fluorescence signal is then used to determine the protein melting point ( $T_m$ ) which corresponds to middle point (50% protein unfolded).

For analyzing the thermal stability of RZZ and Mini-RZZ, a 10 x stock solution of the Sypro Orange dye was freshly prepared in H<sub>2</sub>O and stored on ice. The protein in a final concentration of 2  $\mu$ M, diluted in its storage buffer, was pipetted into a 96-well PCR plate and 2  $\mu$ l of the 10x Sypro Orange stock solution was added. The PCR-plate was sealed with Optically clear plate seals (Microseal "B" Film, Bio-Rad). The PCR plate was placed in the RT-PCR machine and a thermal denaturation analysis was performed applying a gradient of 1.5°C/min from 5°C to 95°C.

### 6.3.22 Cross-linking Analysis coupled with mass spectrometry

Combination of protein cross-linking and mass spectrometry can reveal important inter and intra molecular interaction of within protein complexes. Therefore the proteins are first cross-linked using a bi-functional cross linker, such as Disuccinimidyl Suberate (DSS), which contains two functional groups that form covalent bonds with the free amine groups of exposed lysines. If two lysines are close to each other both lysines are covalent bound to the same cross linker molecule, and will be found after a digest and LC/MS analysis in the same fragment.

The protein samples were cross linked with the cross linker DSS as follows (Maiolica *et al*, 2007). First, 1 mg of DSS was dissolved in 53  $\mu$ l DMSO. Then 20  $\mu$ l of this was mixed with 230  $\mu$ l of RZZ Gefi buffer. 100  $\mu$ g of RZZ or another protein sample were incubated with the cross linker in ratios 1:1, 1:5 and 1:10 of protein to cross linker for 30 min at 37°C or at 4°C over night. To stop the reaction 22  $\mu$ l NH<sub>4</sub>CO<sub>3</sub> were added and incubated for 15 min at 37°C. Then the samples were shipped on ice to our collaborator Franz Herzog who performed the tryptic digest and the LC/MS analysis as described in (Maiolica *et al*, 2007).

### 6.3.23 SILAC Immunoprecipitation experiments

For SILAC light cells were grown under normal conditions in DMEM w/o lysine and arginine, supplemented with 10 % FCS, 1 % penicillin/streptomycin (pen/strep). In order to remove all kinds of small molecules, especially amino acids that could be used as an external amino acids source, FCS was dialyzed against a 10 kDa cut

## Materials and Methods

off filter before and thus ensuring efficient labeling. Heavy labeled cells were grown in DMEM, which contained in contrast to the light cells 15N213C6-lysine and 15N413C6-arginine. To ensure the complete incorporation of the labeled amino acids into all cellular proteins cells were passaged at least 5 times in the corresponding medium.

To generate mitotic populations for immunoprecipitation experiments, cells were treated with 330nM nocodazole for 16 hours. Mitotic cells were then harvested by shake off and lysed by sonication in lysis buffer [150 mM KCl, 75 mM Hepes, pH 7.5, 1.5 mM EGTA, 1.5 mM MgCl<sub>2</sub>, 10 % glycerol, and 0.075 % NP-40] or in lysis buffer without detergents [20 mM Hepes-KOH pH 7.5, 10 mM KCl, 1 mM MgCl<sub>2</sub>, 1 mM EGTA, 1 mM EDTA] supplemented with protease inhibitor cocktail (Serva) and PhosSTOP phosphatase inhibitors (Roche)].

Extracts were pre-cleared with a mixture of protein A–Sepharose (CL-4B; GE Healthcare) and protein G–Sepharose (rec-Protein G Sepharose 4B; Invitrogen) for 1 hour at 4 °C.

Extracts were incubated with GFP-trap beads (ChromoTek; 3 µl/mg of extract), which have been previously bound with GFP-RZZ (2 µg) or GFP (equimolar to 2 µg GFP-RZZ) over night at 4°C. After three washing steps the “heavy” immunoprecipitate of the reference (GFP alone) was mixed with the “light” immunoprecipitate of the bait (GFP-RZZ) in a 1:1 ratio. And the “light” immunoprecipitate of the reference (GFP alone) was mixed with the “heavy” immunoprecipitate of the bait (GFP-RZZ) in a 1:1 ratio. After two more washes the combined immunoprecipitates were analyzed by LC-MS/MS by Tanja Bange.

### 6.3.24 Microinjection of human cells with recombinant proteins

HeLa cells were grown in Dulbecco’s Modified Eagle’s Medium (DMEM; PAN Biotech) supplemented with 10 % tetracycline-free FBS (PAN Biotech), penicillin and streptomycin (GIBCO) and L-Glutamine (PAN Biotech). Cells were grown at 37°C in the presence of 5 % CO<sub>2</sub>. Cdk1 inhibitor, microinjections and live imaging were performed in complemented CO<sub>2</sub>-independent media (GIBCO) at 37°C. A cDNA segment encoding human CENP-A was cloned in a pcDNA5/FRT/TO-IRES-mCherry vector, a modified version of pcDNA5/FRT/TO vector (Invitrogen) generated in house as a C-terminal fusion to mCherry. (Marta Mattiuzzo and Anna De Antoni). Transient transfections of pcDNA5/FRT/TO-IRES-mCherry were performed with Lipofectamine2000 (Invitrogen) according to the manufacturer’s

## Materials and Methods

instructions and the mCherry-CENPA fusion was expressed by addition of 200 ng/ml doxycycline (Sigma) for 48 hours.

Where indicated, Nocodazole (Sigma) was used at 3.3  $\mu$ M, RO-3306 (Calbiochem) was used at 9  $\mu$ M for 18 hours, MG-132 (Calbiochem) at 10  $\mu$ M and Reversine (Cayman) at 500nM. Microinjections were performed using a combination of FemtoJet, InjectMan-NI2 and Femtotip-II, all purchased by Eppendorf. Recombinant GFP and GFP-RZZ complex were injected at a concentration of 4 $\mu$ M and 10 $\mu$ M respectively. N (Number of cells injected): for GFP N=2; for GFP-RZZ N=8; for GFP in Reversine treated cells N=2 (data not shown); for GFP-RZZ in Reversine treated cells N=8. Live-cell images were taken before injection and 1 to 3 minutes after injection using the spinning disk confocal microscopy of a 3i Marianas™ system (Intelligent Imaging Innovations, Denver, CO, USA) equipped with an Axio Observer Z1 microscope (Zeiss, Germany), a CSU-X1 confocal scanner unit (Yokogawa Electric Corporation, Japan), Plan-Apochromat 63x or 100x/1.4NA objectives (Zeiss) and Orca Flash 4.0 sCMOS Camera (Hamamatsu, Japan). Images were acquired as Z-sections (using Slidebook Software 5.5 from Intelligent Imaging Innovations or using LCS 3D software from Leica) and converted into maximal intensity projections TIFF files for illustrative purposes.

### 6.3.25 Crystallogenesis

Initially commercial Crystallogenesis Screens from Qiagen and Hampton were applied to the purified RZZ complex using different protein concentrations and Protein:reservoir ratios. Crystals were obtained with condition 69 (1 M (NH<sub>4</sub>)<sub>2</sub>SO<sub>4</sub>, 0.1 M MES pH 6.5) of the ProComplex Screen (Qiagen, Hilden, Germany) and with the sitting-drop vapour-diffusion method as described in Table 5.2.20. Table 5.2.20 describes initial optimisation attempts, including interventions aiming to reduce the potential biochemical heterogeneity of the sample. A first attempt was the removal of the hexahistidine tag from Rod using Prescission protease during the elution from a Ni-NTA column. In addition, evidence from mass spectrometry analyses, that the RZZ complex is phosphorylated during expression in insect cells, prompted us to attempt dephosphorylation using  $\lambda$ -phosphatase (data not shown). As post-crystallisation treatments, we tried to anneal the crystals by briefly interrupting the liquid nitrogen stream that usually keeps crystals at 100 K. Data collection experiments at room temperature were also performed. As an additional approach, dehydration of the crystals was

## Materials and Methods

attempted by either serial addition of glycerol to the reservoir solution or by increasing the precipitant concentration in 2-5 % steps every 2 days.



**Table 18: Overview crystallogensis attempts**

| Method                                            | Initial Screening                                                                        | Optimisation Screening                                                                                                                                  | Additive Screening                                                                                  | Seeding                                                                                                                                         | In-Situ Proteolysis                                                                                                                                     |
|---------------------------------------------------|------------------------------------------------------------------------------------------|---------------------------------------------------------------------------------------------------------------------------------------------------------|-----------------------------------------------------------------------------------------------------|-------------------------------------------------------------------------------------------------------------------------------------------------|---------------------------------------------------------------------------------------------------------------------------------------------------------|
| Plate type                                        | 96-well                                                                                  | 24-well                                                                                                                                                 | 96-well                                                                                             | 24-well                                                                                                                                         | 96-well, 24-well                                                                                                                                        |
| Temperature (K)                                   | 277.15, 293.15                                                                           | 277.15, 285.15, 293.15                                                                                                                                  | 293.15                                                                                              | 293.15                                                                                                                                          | 285.15, 293,15                                                                                                                                          |
| Protein concentration                             | 5-10 mg/ml                                                                               | 5-10 mg/ml                                                                                                                                              | 5-10 mg/ml                                                                                          | 5-10 mg/ml                                                                                                                                      | 5-10 mg/ml                                                                                                                                              |
| Buffer composition of protein solution            | 25 mM HEPES pH 8.5<br>250 mM NaCl<br>2 mM TCEP                                           | Unchanged                                                                                                                                               | Unchanged                                                                                           | Unchanged                                                                                                                                       | Unchanged                                                                                                                                               |
| Composition of reservoir solution / Screening Kit | JSCG Core 1-4, ProComplex, Anions, Cations, Cryo, PEG1, PEG2, AmSO <sub>4</sub> (Qiagen) | Buffer, pH, salt and glycerol were varied systematically around condition 69 of the ProComplex Screen as well as other conditions identified by initial | The Additive Screen (Hampton) was applied to various conditions obtained after initial optimisation | In drops with various conditions obtained after initial optimisation but with precipitant concentrations reduced to 75 % of original condition. | Based on various conditions obtained after initial optimisation, performed as in (Dong <i>et al.</i> , 2007) Trypsin and Elastase dilutions from 1:100- |

## Materials and Methods

|                          |                       |                                                                                 |                       |                                                                                                                                                                                                                                 |                                                                           |
|--------------------------|-----------------------|---------------------------------------------------------------------------------|-----------------------|---------------------------------------------------------------------------------------------------------------------------------------------------------------------------------------------------------------------------------|---------------------------------------------------------------------------|
|                          |                       | screening of RZZ complex devoid of His <sub>6</sub> tag and/or dephosphorylated |                       | Seed stock preparation : Crystals from a similar condition were typically mixed with 100-200 $\mu$ l of the reservoir solution and smashed by adding a glass bead and vortexing followed by serial streaking with a cat whisker | 1:20000                                                                   |
| Volume and ratio of drop | 300 nl, 1:1, 1:2, 2:1 | 1-8 $\mu$ l, 1:1, 1:2, 2:1                                                      | 300 nl, 1:1, 1:2, 2:1 | 1-2 $\mu$ l, 1:1, 1:2, 2:1                                                                                                                                                                                                      | 300 nl, 1:1, 1:2, 2:1 for 96-well<br>1 $\mu$ l, 1:1, 1:2, 2:1 for 24-well |
| Volume of reservoir      | 70 $\mu$ l            | 500 $\mu$ l                                                                     | 70 $\mu$ l            | 500 $\mu$ l                                                                                                                                                                                                                     | 70 $\mu$ l for 96-well,<br>500 $\mu$ l for 24-well                        |

## Materials and Methods

### 6.3.26 Data Collection and Processing

In order to choose a suitable cryoprotectant, crystals were harvested in the reservoir buffer and soaked directly or serially (in 2-5 % steps) in reservoir buffer supplemented with 5-20 % of Ethyleneglycol, Glycerol or PEG 400, flash frozen in liquid nitrogen, and tested in a cryo-beam for ice rings. Diffraction data were collected at 100 K at beamline X10SA at the Swiss Light Source (SLS), Villigen, Switzerland using a PILATUS 6 M detector at a wavelength of 0.9789 Å. Data were indexed and integrated using XDS and scaled using XSCALE (Kabsch, 2010).

## 7 References

- Akiyoshi B, Sarangapani KK, Powers AF, Nelson CR, Reichow SL, Arellano-Santoyo H, Gonen T, Ranish JA, Asbury CL & Biggins S (2010) Tension directly stabilizes reconstituted kinetochore-microtubule attachments. *Nature* **468**: 576–579
- Alushin GM, Musinipally V, Matson D, Tooley J, Stukenberg PT & Nogales E (2012) Multimodal microtubule binding by the Ndc80 kinetochore complex. *Nature Structural & Molecular Biology* **19**: 1161–1167
- Alushin GM, Ramey VH, Pasqualato S, Ball DA, Grigorieff N, Musacchio A & Nogales E (2010) The Ndc80 kinetochore complex forms oligomeric arrays along microtubules. *Nature* **467**: 805–810
- Andag U & Schmitt HD (2003) Dsl1p, an essential component of the Golgi-endoplasmic reticulum retrieval system in yeast, uses the same sequence motif to interact with different subunits of the COPI vesicle coat. *J. Biol. Chem.* **278**: 51722–51734
- Aoki T, Ichimura S, Itoh A, Kuramoto M, Shinkawa T, Isobe T & Tagaya M (2009) Identification of the neuroblastoma-amplified gene product as a component of the syntaxin 18 complex implicated in Golgi-to-endoplasmic reticulum retrograde transport. *Molecular Biology of the Cell* **20**: 2639–2649
- Barisic M & Geley S (2011) Spindly switch controls anaphase: Spindly and RZZ functions in chromosome attachment and mitotic checkpoint control. *cc* **10**: 449–456
- Barisic M, Sohm B, Mikolcevic P, Wandke C, Rauch V, Ringer T, Hess M, Bonn G & Geley S (2010) Spindly/CCDC99 is required for efficient chromosome congression and mitotic checkpoint regulation. *Molecular Biology of the Cell* **21**: 1968–1981
- Basilico F, Maffini S, Weir JR, Prumbaum D, Rojas AM, Zimniak T, De Antoni A, Jeganathan S, Voss B, van Gerwen S, Krenn V, Massimiliano L, Valencia A, Vetter IR, Herzog F, Raunser S, Pasqualato S & Musacchio A (2014) The pseudo GTPase CENP-M drives human kinetochore assembly. *Elife* **3**: e02978
- Basto R, Scaerou F, Mische S, Wojcik E, Lefebvre C, Gomes R, Hays T & Karess R (2004) In Vivo Dynamics of the Rough Deal Checkpoint Protein during Drosophila Mitosis. *Current Biology* **14**: 56–61
- Bischof JC & He X (2005) Thermal stability of proteins. *Ann. N. Y. Acad. Sci.* **1066**: 12–33
- Boivin S, Kozak S & Meijers R (2013) Optimization of protein purification and characterization using Thermofluor screens. *Protein Expr. Purif.* **91**: 192–206
- Buffin E, Lefebvre C, Huang J, Gagou ME & Karess RE (2005) Recruitment of Mad2 to the kinetochore requires the Rod/Zw10 complex. *Current Biology* **15**: 856–861

## Supplementary Information

- Burton JL & Solomon MJ (2007) Mad3p, a pseudosubstrate inhibitor of APCCdc20 in the spindle assembly checkpoint. *Genes & Development* **21**: 655–667
- Carmena M, Wheelock M, Funabiki H & Earnshaw WC (2012) The chromosomal passenger complex (CPC): from easy rider to the godfather of mitosis. *Nat Rev Mol Cell Biol* **13**: 789–803
- Carroll CW, Silva MCC, Godek KM, Jansen LET & Straight AF (2009) Centromere assembly requires the direct recognition of CENP-A nucleosomes by CENP-N. *Nat Cell Biol* **11**: 896–902
- Chan GK, Jablonski SA, Starr DA, Goldberg ML & Yen TJ (2000) Human Zw10 and ROD are mitotic checkpoint proteins that bind to kinetochores. *Nat Cell Biol* **2**: 944–947
- Chan YW (2009) Mitotic control of kinetochore-associated dynein and spindle orientation by human Spindly. *J. Cell Biol.* **185**: 859–874
- Chan YW, Fava LL, Uldschmid A, Schmitz MHA, Gerlich DW, Nigg EA & Santamaria A (2009) Mitotic control of kinetochore-associated dynein and spindle orientation by human Spindly. *J. Cell Biol.* **185**: 859–874
- Chan YW, Jeyaprakash AA, Nigg EA & Santamaria A (2012) Aurora B controls kinetochore-microtubule attachments by inhibiting Ska complex-KMN network interaction. *J. Cell Biol.* **196**: 563–571
- Chang L, Zhang Z, Yang J, McLaughlin SH & Barford D (2015) Atomic structure of the APC/C and its mechanism of protein ubiquitination. *Nature* **522**: 450–454
- Chao WCH, Kulkarni K, Zhang Z, Kong EH & Barford D (2012) Structure of the mitotic checkpoint complex. *Nature* **484**: 208–213
- Cheerambathur DK, Gassmann R, Cook B, Oegema K & Desai A (2013) Crosstalk Between Microtubule Attachment Complexes Ensures Accurate Chromosome Segregation. *Science* **342**: 1239–1242
- Cheeseman IM (2014) The kinetochore. *Cold Spring Harb Perspect Biol* **6**: a015826
- Cheeseman IM & Desai A (2008) Molecular architecture of the kinetochore-microtubule interface. *Nat Rev Mol Cell Biol* **9**: 33–46
- Cheeseman IM, Chappie JS, Wilson-Kubalek EM & Desai A (2006) The conserved KMN network constitutes the core microtubule-binding site of the kinetochore. *Cell* **127**: 983–997
- Ciferri C, De Luca J, Monzani S, Ferrari KJ, Ristic D, Wyman C, Stark H, Kilmartin J, Salmon ED & Musacchio A (2005) Architecture of the human ndc80-hec1 complex, a critical constituent of the outer kinetochore. *J. Biol. Chem.* **280**: 29088–29095
- Ciferri C, Pasqualato S, Screpanti E, Varetto G, Santaguida S, Reis Dos G, Maiolica A, Polka J, De Luca JG, De Wulf P, Salek M, Rappsilber J, Moores

## Supplementary Information

- CA, Salmon ED & Musacchio A (2008) Implications for kinetochore-microtubule attachment from the structure of an engineered Ndc80 complex. *Cell* **133**: 427–439
- Cimini D, Wan X, Hirel CB & Salmon ED (2006) Aurora kinase promotes turnover of kinetochore microtubules to reduce chromosome segregation errors. *Current Biology* **16**: 1711–1718
- Cleveland DW, Mao Y & Sullivan KF (2003) Centromeres and kinetochores: from epigenetics to mitotic checkpoint signaling. *Cell* **112**: 407–421
- Cole JL, Lary JW, P Moody T & Laue TM (2008) Analytical ultracentrifugation: sedimentation velocity and sedimentation equilibrium. *Methods Cell Biol.* **84**: 143–179
- Cox J & Mann M (2008) MaxQuant enables high peptide identification rates, individualized p.p.b.-range mass accuracies and proteome-wide protein quantification. *Nat. Biotechnol.* **26**: 1367–1372
- Çivril F, Wehenkel A, Giorgi FM, Santaguida S, Di Fonzo A, Grigorean G, Ciccarelli FD & Musacchio A (2010) Structural Analysis of the RZZ Complex Reveals Common Ancestry with Multisubunit Vesicle Tethering Machinery. *Structure/Folding and Design* **18**: 616–626
- Davenport J, Harris LD & Goorha R (2006) Spindle checkpoint function requires Mad2-dependent Cdc20 binding to the Mad3 homology domain of BubR1. *Exp. Cell Res.* **312**: 1831–1842
- De Antoni A, Pearson CG, Cimini D, Canman JC, Sala V, Nezi L, Mapelli M, Sironi L, Faretta M, Salmon ED & Musacchio A (2005) The Mad1/Mad2 complex as a template for Mad2 activation in the spindle assembly checkpoint. *Current Biology* **15**: 214–225
- DeLuca JG, Gall WE, Ciferri C, Cimini D, Musacchio A & Salmon ED (2006) Kinetochore microtubule dynamics and attachment stability are regulated by Hec1. *Cell* **127**: 969–982
- DeLuca JG, Howell BJ, Canman JC, Hickey JM, Fang G & Salmon ED (2003) Nuf2 and Hec1 are required for retention of the checkpoint proteins Mad1 and Mad2 to kinetochores. *Current Biology* **13**: 2103–2109
- Desai A & Mitchison TJ (1997) Microtubule polymerization dynamics. *Annu. Rev. Cell Dev. Biol.* **13**: 83–117
- Dewar H, Tanaka K, Nasmyth K & Tanaka TU (2004) Tension between two kinetochores suffices for their bi-orientation on the mitotic spindle. *Nature* **428**: 93–97
- Ditchfield C, Johnson VL, Tighe A, Ellston R, Haworth C, Johnson T, Mortlock A, Keen N & Taylor SS (2003) Aurora B couples chromosome alignment with anaphase by targeting BubR1, Mad2, and Cenp-E to kinetochores. *J. Cell Biol.* **161**: 267–280

## Supplementary Information

Dupeux F, Röwer M, Seroul G, Blot D & Márquez JA (2011) A thermal stability assay can help to estimate the crystallization likelihood of biological samples. *Acta Crystallogr. D Biol. Crystallogr.* **67**: 915–919

Emanuele MJ, Lan W, Jwa M, Miller SA, Chan CSM & Stukenberg PT (2008) Aurora B kinase and protein phosphatase 1 have opposing roles in modulating kinetochore assembly. *J. Cell Biol.* **181**: 241–254

Espeut J, Cheerambathur DK, Krenning L, Oegema K & Desai A (2012a) Microtubule binding by KNL-1 contributes to spindle checkpoint silencing at the kinetochore. *J. Cell Biol.* **196**: 469–482

Espeut J, Cheerambathur DK, Krenning L, Oegema K & Desai A (2012b) Microtubule binding by KNL-1 contributes to spindle checkpoint silencing at the kinetochore. *J. Cell Biol.* **196**: 469–482

Euteneuer U & McIntosh JR (1981) Structural polarity of kinetochore microtubules in PtK1 cells. *J. Cell Biol.* **89**: 338–345

Famulski JK & Chan GK (2007) Aurora B Kinase-Dependent Recruitment of hZW10 and hROD to Tensionless Kinetochores. *Current Biology* **17**: 2143–2149

Famulski JK, Vos L, Sun X & Chan G (2008) Stable hZW10 kinetochore residency, mediated by hZwint-1 interaction, is essential for the mitotic checkpoint. *J. Cell Biol.* **180**: 507–520

Fang G (2002) Checkpoint protein BubR1 acts synergistically with Mad2 to inhibit anaphase-promoting complex. *Molecular Biology of the Cell* **13**: 755–766

Foley EA & Kapoor TM (2013) Microtubule attachment and spindle assembly checkpoint signalling at the kinetochore. *Nat Rev Mol Cell Biol* **14**: 25–37

Foley EA, Maldonado M & Kapoor TM (2011) Formation of stable attachments between kinetochores and microtubules depends on the B56-PP2A phosphatase. *Nat Cell Biol* **13**: 1265–1271

Foltz DR, Jansen LET, Black BE, Bailey AO, Yates JR & Cleveland DW (2006) The human CENP-A centromeric nucleosome-associated complex. *Nat Cell Biol* **8**: 458–469

Funabiki H & Wynne DJ (2013) Making an effective switch at the kinetochore by phosphorylation and dephosphorylation. *Chromosoma* **122**: 135–158

Gaitanos TN, Santamaria A, Jeyaprakash AA, Wang B, Conti E & Nigg EA (2009) Stable kinetochore-microtubule interactions depend on the Ska complex and its new component Ska3/C13Orf3. *EMBO J.* **28**: 1442–1452

Gascoigne KE, Takeuchi K, Suzuki A, Hori T, Fukagawa T & Cheeseman IM (2011) Induced ectopic kinetochore assembly bypasses the requirement for CENP-A nucleosomes. *Cell* **145**: 410–422

## Supplementary Information

Gassmann R, Essex A, Hu JS, Maddox PS, Motegi F, Sugimoto A, O'Rourke SM, Bowerman B, McLeod I, Yates JR, Oegema K, Cheeseman IM & Desai A (2008) A new mechanism controlling kinetochore-microtubule interactions revealed by comparison of two dynein-targeting components: SPDL-1 and the Rod/Zwilch/Zw10 complex. *Genes & Development* **22**: 2385–2399

Gassmann R, Holland AJ, Varma D, Wan X, Civril F, Cleveland DW, Oegema K, Salmon ED & Desai A (2010) Removal of Spindly from microtubule-attached kinetochores controls spindle checkpoint silencing in human cells. *Genes & Development* **24**: 957–971

Griffis ER, Stuurman N & Vale RD (2007) Spindly, a novel protein essential for silencing the spindle assembly checkpoint, recruits dynein to the kinetochore. *J. Cell Biol.* **177**: 1005–1015

Grimm M, Zimniak T, Kahraman A & Herzog F (2015) xVis: a web server for the schematic visualization and interpretation of crosslink-derived spatial restraints. *Nucleic Acids Res.*

Han JS, Holland AJ, Fachinetti D, Kulukian A, Cetin B & Cleveland DW (2013) Catalytic assembly of the mitotic checkpoint inhibitor BubR1-Cdc20 by a Mad2-induced functional switch in Cdc20. *Mol. Cell* **51**: 92–104

Hardwick KG, Johnston RC, Smith DL & Murray AW (2000) MAD3 encodes a novel component of the spindle checkpoint which interacts with Bub3p, Cdc20p, and Mad2p. *J. Cell Biol.* **148**: 871–882

Harp JM, Hanson BL, Timm DE & Bunick GJ (1999) Macromolecular crystal annealing: evaluation of techniques and variables. *Acta Crystallogr. D Biol. Crystallogr.* **55**: 1329–1334

Hartwell L (1992) Defects in a cell cycle checkpoint may be responsible for the genomic instability of cancer cells. *Cell* **71**: 543–546

Hashimoto Y, Zhang S & Blissard GW (2010) Ao38, a new cell line from eggs of the black witch moth, *Ascalapha odorata* (Lepidoptera: Noctuidae), is permissive for AcMNPV infection and produces high levels of recombinant proteins. *BMC Biotechnol.* **10**: 50

Hauf S, Cole RW, LaTerra S, Zimmer C, Schnapp G, Walter R, Heckel A, van Meel J, Rieder CL & Peters J-M (2003) The small molecule Hesperadin reveals a role for Aurora B in correcting kinetochore-microtubule attachment and in maintaining the spindle assembly checkpoint. *J. Cell Biol.* **161**: 281–294

Hayden JH, Bowser SS & Rieder CL (1990) Kinetochores capture astral microtubules during chromosome attachment to the mitotic spindle: direct visualization in live newt lung cells. *J. Cell Biol.* **111**: 1039–1045

Heras B & Martin JL (2005) Post-crystallization treatments for improving diffraction quality of protein crystals. *Acta Crystallogr. D Biol. Crystallogr.* **61**: 1173–1180

Hewitt L, Tighe A, Santaguida S, White AM, Jones CD, Musacchio A, Green S & Taylor SS (2010) Sustained Mps1 activity is required in mitosis to recruit O-Mad2 to the Mad1-C-Mad2 core complex. *J. Cell Biol.* **190**: 25–34



## Supplementary Information

Hirokawa N, Noda Y & Okada Y (1998) Kinesin and dynein superfamily proteins in organelle transport and cell division. *Curr. Opin. Cell Biol.* **10**: 60–73

Holland AJ, Reis RM, Niessen S, Pereira C, Andres DA, Spielmann HP, Cleveland DW, Desai A & Gassmann R (2015) Preventing farnesylation of the dynein adaptor Spindly contributes to the mitotic defects caused by farnesyltransferase inhibitors. *Molecular Biology of the Cell* **26**: 1845–1856

Hori T & Fukagawa T (2012) Establishment of the vertebrate kinetochores. *Chromosome Res.* **20**: 547–561

Hori T, Amano M, Suzuki A, Backer CB, Welburn JP, Dong Y, McEwen BF, Shang W-H, Suzuki E, Okawa K, Cheeseman IM & Fukagawa T (2008a) CCAN makes multiple contacts with centromeric DNA to provide distinct pathways to the outer kinetochore. *Cell* **135**: 1039–1052

Hori T, Okada M, Maenaka K & Fukagawa T (2008b) CENP-O class proteins form a stable complex and are required for proper kinetochore function. *Molecular Biology of the Cell* **19**: 843–854

Howell BJ (2001) Cytoplasmic dynein/dynactin drives kinetochore protein transport to the spindle poles and has a role in mitotic spindle checkpoint inactivation. *J. Cell Biol.* **155**: 1159–1172

Hoyt MA, Totis L & Roberts BT (1991) *S. cerevisiae* genes required for cell cycle arrest in response to loss of microtubule function. *Cell* **66**: 507–517

Höök P & Vallee RB (2006) The dynein family at a glance. *J Cell Sci* **119**: 4369–4371

Hwang LH, Lau LF, Smith DL, Mistrot CA, Hardwick KG, Hwang ES, Amon A & Murray AW (1998) Budding yeast Cdc20: a target of the spindle checkpoint. *Science* **279**: 1041–1044

Inoue M, Arasaki K, Ueda A, Aoki T & Tagaya M (2008) N-terminal region of ZW10 serves not only as a determinant for localization but also as a link with dynein function. *Genes Cells* **13**: 905–914

Izawa D & Pines J (2015) The mitotic checkpoint complex binds a second CDC20 to inhibit active APC/C. *Nature* **517**: 631–634

Izuta H, Ikeno M, Suzuki N, Tomonaga T, Nozaki N, Obuse C, Kisu Y, Goshima N, Nomura F, Nomura N & Yoda K (2006) Comprehensive analysis of the ICEN (Interphase Centromere Complex) components enriched in the CENP-A chromatin of human cells. *Genes Cells* **11**: 673–684

Jakob RP, Zierer BK, Weininger U, Hofmann SD, Lorenz SH, Balbach J, Dobbek H & Schmid FX (2010) Elimination of a cis-proline-containing loop and turn optimization stabilizes a protein and accelerates its folding. *J. Mol. Biol.* **399**: 331–346

Kabsch W (2010) Integration, scaling, space-group assignment and post-refinement. *Acta Crystallogr. D Biol. Crystallogr.* **66**: 133–144

## Supplementary Information

- Kantardjieff KA & Rupp B (2003) Matthews coefficient probabilities: Improved estimates for unit cell contents of proteins, DNA, and protein-nucleic acid complex crystals. *Protein Sci.* **12**: 1865–1871
- Kardon JR & Vale RD (2009) Regulators of the cytoplasmic dynein motor. *Nat Rev Mol Cell Biol* **10**: 854–865
- Karess R (2005) Rod–Zw10–Zwilch: a key player in the spindle checkpoint. *Trends in Cell Biology* **15**: 386–392
- Karess RE & Glover DM (1989) rough deal: a gene required for proper mitotic segregation in *Drosophila*. *J. Cell Biol.* **109**: 2951–2961
- Karsenti E & Vernos I (2001) The mitotic spindle: a self-made machine. *Science* **294**: 543–547
- Kasuboski JM, Bader JR, Vaughan PS, Tauhata SBF, Winding M, Morrissey MA, Joyce MV, Boggess W, Vos L, Chan GK, Hinchcliffe EH & Vaughan KT (2011) Zwint-1 is a novel Aurora B substrate required for the assembly of a dynein-binding platform on kinetochores. *Molecular Biology of the Cell* **22**: 3318–3330
- Kato H, Jiang J, Zhou B-R, Rozendaal M, Feng H, Ghirlando R, Xiao TS, Straight AF & Bai Y (2013) A conserved mechanism for centromeric nucleosome recognition by centromere protein CENP-C. *Science* **340**: 1110–1113
- Kelley LA, Mezulis S, Yates CM, Wass MN & Sternberg MJE (2015) The Phyre2 web portal for protein modeling, prediction and analysis. *Nat Protoc* **10**: 845–858
- King EMJ, van der Sar SJA & Hardwick KG (2007) Mad3 KEN boxes mediate both Cdc20 and Mad3 turnover, and are critical for the spindle checkpoint. *PLoS ONE* **2**: e342
- King JM, Hays TS & Nicklas RB (2000) Dynein is a transient kinetochore component whose binding is regulated by microtubule attachment, not tension. *J. Cell Biol.* **151**: 739–748
- Kingwell B & Rattner JB (1987) Mammalian kinetochore/centromere composition: a 50 kDa antigen is present in the mammalian kinetochore/centromere. *Chromosoma* **95**: 403–407
- Kolodner RD, Cleveland DW & Putnam CD (2011) Cancer. Aneuploidy drives a mutator phenotype in cancer. *Science* **333**: 942–943
- Kops GJPL (2005) ZW10 links mitotic checkpoint signaling to the structural kinetochore. *J. Cell Biol.* **169**: 49–60
- Kwiatkowski N, Jelluma N, Filippakopoulos P, Soundararajan M, Manak MS, Kwon M, Choi HG, Sim T, Deveraux QL, Rottmann S, Pellman D, Shah JV, Kops GJPL, Knapp S & Gray NS (2010) Small-molecule kinase inhibitors provide insight into Mps1 cell cycle function. *Nat. Chem. Biol.* **6**: 359–368

## Supplementary Information

- Lampert F, Hornung P & Westermann S (2010) The Dam1 complex confers microtubule plus end-tracking activity to the Ndc80 kinetochore complex. *J. Cell Biol.* **189**: 641–649
- Lampson MA & Cheeseman IM (2011) Sensing centromere tension: Aurora B and the regulation of kinetochore function. *Trends in Cell Biology* **21**: 133–140
- Lampson MA, Renduchitala K, Khodjakov A & Kapoor TM (2004) Correcting improper chromosome-spindle attachments during cell division. *Nat Cell Biol* **6**: 232–237
- Lara-Gonzalez P, Scott MIF, Diez M, Sen O & Taylor SS (2011) BubR1 blocks substrate recruitment to the APC/C in a KEN-box-dependent manner. *J Cell Sci* **124**: 4332–4345
- Lara-Gonzalez P, Westhorpe FG & Taylor SS (2012) The spindle assembly checkpoint. *Curr. Biol.* **22**: R966–80
- Leitner A, Walzthoeni T, Kahraman A, Herzog F, Rinner O, Beck M & Aebersold R (2010) Probing native protein structures by chemical cross-linking, mass spectrometry, and bioinformatics. *Mol. Cell Proteomics* **9**: 1634–1649
- Leksa NC & Schwartz TU (2010) Membrane-coating lattice scaffolds in the nuclear pore and vesicle coats: commonalities, differences, challenges. *Nucleus* **1**: 314–318
- Li R & Murray AW (1991) Feedback control of mitosis in budding yeast. *Cell* **66**: 519–531
- Li X & Nicklas RB (1995) Mitotic forces control a cell-cycle checkpoint. *Nature* **373**: 630–632
- Lin Y-T, Chen Y, Wu G & Lee W-H (2006) Hec1 sequentially recruits Zwint-1 and ZW10 to kinetochores for faithful chromosome segregation and spindle checkpoint control. *Oncogene* **25**: 6901–6914
- Liu D, Vader G, Vromans MJM, Lampson MA & Lens SMA (2009) Sensing chromosome bi-orientation by spatial separation of aurora B kinase from kinetochore substrates. *Science* **323**: 1350–1353
- Liu S-T, Rattner JB, Jablonski SA & Yen TJ (2006) Mapping the assembly pathways that specify formation of the trilaminar kinetochore plates in human cells. *J. Cell Biol.* **175**: 41–53
- London N, Ceto S, Ranish JA & Biggins S (2012) Phosphoregulation of Spc105 by Mps1 and PP1 regulates Bub1 localization to kinetochores. *Curr. Biol.* **22**: 900–906
- Luo X, Fang G, Coldiron M, Lin Y, Yu H, Kirschner MW & Wagner G (2000) Structure of the Mad2 spindle assembly checkpoint protein and its interaction with Cdc20. *Nat. Struct. Biol.* **7**: 224–229

## Supplementary Information

- Luo X, Tang Z, Rizo J & Yu H (2002) The Mad2 spindle checkpoint protein undergoes similar major conformational changes upon binding to either Mad1 or Cdc20. *Mol. Cell* **9**: 59–71
- Luo X, Tang Z, Xia G, Wassmann K, Matsumoto T, Rizo J & Yu H (2004) The Mad2 spindle checkpoint protein has two distinct natively folded states. *Nature Structural & Molecular Biology* **11**: 338–345
- Maciejowski J, George KA, Terret M-E, Zhang C, Shokat KM & Jallepalli PV (2010) Mps1 directs the assembly of Cdc20 inhibitory complexes during interphase and mitosis to control M phase timing and spindle checkpoint signaling. *J. Cell Biol.* **190**: 89–100
- Magidson V, Paul R, Yang N, Ault JG, O'Connell CB, Tikhonenko I, McEwen BF, Mogilner A & Khodjakov A (2015) Adaptive changes in the kinetochore architecture facilitate proper spindle assembly. *Nat Cell Biol* **17**: 1134–1144
- Maiolica A, Cittaro D, Borsotti D, Sennels L, Ciferri C, Tarricone C, Musacchio A & Rappsilber J (2007) Structural analysis of multiprotein complexes by cross-linking, mass spectrometry, and database searching. *Mol. Cell Proteomics* **6**: 2200–2211
- Mapelli M, Massimiliano L, Santaguida S & Musacchio A (2007) The Mad2 conformational dimer: structure and implications for the spindle assembly checkpoint. *Cell* **131**: 730–743
- Maresca TJ & Salmon ED (2009) Intrakinetochore stretch is associated with changes in kinetochore phosphorylation and spindle assembly checkpoint activity. *J. Cell Biol.* **184**: 373–381
- Martin-Lluesma S, Stucke VM & Nigg EA (2002) Role of Hec1 in spindle checkpoint signaling and kinetochore recruitment of Mad1/Mad2. *Science* **297**: 2267–2270
- Matson DR & Stukenberg PT (2014) CENP-I and Aurora B act as a molecular switch that ties RZZ/Mad1 recruitment to kinetochore attachment status. *J. Cell Biol.* **205**: 541–554
- Matthews BW (1968) Solvent content of protein crystals. *J. Mol. Biol.* **33**: 491–497
- McAinsh AD, Tytell JD & Sorger PK (2003) Structure, function, and regulation of budding yeast kinetochores. *Annu. Rev. Cell Dev. Biol.* **19**: 519–539
- McEwen BF, Hsieh CE, Mattheyses AL & Rieder CL (1998) A new look at kinetochore structure in vertebrate somatic cells using high-pressure freezing and freeze substitution. *Chromosoma* **107**: 366–375
- Menant A & Karess R (2010) RZZ Finds Its Ancestral Roots. *Structure/Folding and Design* **18**: 549–550
- Meppelink A, Kabeche L, Vromans MJM, Compton DA & Lens SMA (2015) Shugoshin-1 balances Aurora B kinase activity via PP2A to promote chromosome bi-orientation. *Cell Rep* **11**: 508–515

## Supplementary Information

- Minshull J, Sun H, Tonks NK & Murray AW (1994) A MAP kinase-dependent spindle assembly checkpoint in *Xenopus* egg extracts. *Cell* **79**: 475–486
- Monda JK & Cheeseman IM (2015) Chromosome Segregation: A Spatial Code to Correct Kinetochore-Microtubule Attachments. *Curr. Biol.* **25**: R601–3
- Morgan DO (2007) *The Cell Cycle* New Science Press
- Moudgil DK, Westcott N, Famulski JK, Patel K, Macdonald D, Hang H & Chan GKT (2015) A novel role of farnesylation in targeting a mitotic checkpoint protein, human Spindly, to kinetochores. *J. Cell Biol.* **208**: 881–896
- Musacchio A & Salmon ED (2007) The spindle-assembly checkpoint in space and time. *Nat Rev Mol Cell Biol* **8**: 379–393
- Nasmyth K (2011) Cohesin: a catenase with separate entry and exit gates? *Nat Cell Biol* **13**: 1170–1177
- Nicklas RB (1997) How cells get the right chromosomes. *Science* **275**: 632–637
- Nicklas RB & Koch CA (1969) Chromosome micromanipulation. 3. Spindle fiber tension and the reorientation of mal-oriented chromosomes. *J. Cell Biol.* **43**: 40–50
- Nigg EA (2001) Mitotic kinases as regulators of cell division and its checkpoints. *Nat Rev Mol Cell Biol* **2**: 21–32
- Nishino T, Rago F, Hori T, Tomii K, Cheeseman IM & Fukagawa T (2013) CENP-T provides a structural platform for outer kinetochore assembly. *EMBO J.* **32**: 424–436
- Obuse C, Yang H, Nozaki N, Goto S, Okazaki T & Yoda K (2004) Proteomics analysis of the centromere complex from HeLa interphase cells: UV-damaged DNA binding protein 1 (DDB-1) is a component of the CEN-complex, while BMI-1 is transiently co-localized with the centromeric region in interphase. *Genes Cells* **9**: 105–120
- Oliveira RA & Nasmyth K (2010) Getting through anaphase: splitting the sisters and beyond. *Biochem. Soc. Trans.* **38**: 1639–1644
- Overlack K, Primorac I, Vleugel M, Krenn V, Maffini S, Hoffmann I, Kops GJPL & Musacchio A (2015) A molecular basis for the differential roles of Bub1 and BubR1 in the spindle assembly checkpoint. *Elife* **4**: e05269
- Pagliuca C, Draviam VM, Marco E, Sorger PK & De Wulf P (2009) Roles for the conserved spc105p/kre28p complex in kinetochore-microtubule binding and the spindle assembly checkpoint. *PLoS ONE* **4**: e7640
- Paweletz N (2001) Walther Flemming: pioneer of mitosis research.
- Perpelescu M & Fukagawa T (2011) The ABCs of CENPs. *Chromosoma* **120**: 425–446

## Supplementary Information

- Petrovic A, Mosalaganti S, Keller J, Mattiuzzo M, Overlack K, Krenn V, De Antoni A, Wohlgemuth S, Cecatiello V, Pasqualato S, Raunser S & Musacchio A (2014) Modular assembly of RWD domains on the Mis12 complex underlies outer kinetochore organization. *Mol. Cell* **53**: 591–605
- Pingoud A & Jeltsch A (2001) Structure and function of type II restriction endonucleases. *Nucleic Acids Res.* **29**: 3705–3727
- Pinsky BA, Nelson CR & Biggins S (2009) Protein phosphatase 1 regulates exit from the spindle checkpoint in budding yeast. *Curr. Biol.* **19**: 1182–1187
- Pomerening JR, Sontag ED & Ferrell JE (2003) Building a cell cycle oscillator: hysteresis and bistability in the activation of Cdc2. *Nat Cell Biol* **5**: 346–351
- Primorac I & Musacchio A (2013) Panta rhei: the APC/C at steady state. *J. Cell Biol.* **201**: 177–189
- Primorac I, Weir JR, Chiroli E, Gross F, Hoffmann I, van Gerwen S, Ciliberto A & Musacchio A (2013) Bub3 reads phosphorylated MELT repeats to promote spindle assembly checkpoint signaling. *Elife* **2**: e01030
- Reddy SK, Rape M, Margansky WA & Kirschner MW (2007) Ubiquitination by the anaphase-promoting complex drives spindle checkpoint inactivation. *Nature* **446**: 921–925
- Ren Y, Yip CK, Tripathi A, Huie D, Jeffrey PD, Walz T & Hughson FM (2009) A Structure-Based Mechanism for Vesicle Capture by the Multisubunit Tethering Complex Dsl1. *Cell* **139**: 1119–1129
- Rieder CL & Alexander SP (1990) Kinetochores are transported poleward along a single astral microtubule during chromosome attachment to the spindle in newt lung cells. *J. Cell Biol.* **110**: 81–95
- Rischitor PE, May KM & Hardwick KG (2007) Bub1 is a fission yeast kinetochore scaffold protein, and is sufficient to recruit other spindle checkpoint proteins to ectopic sites on chromosomes. *PLoS ONE* **2**: e1342
- Rosenberg JS, Cross FR & Funabiki H (2011) KNL1/Spc105 recruits PP1 to silence the spindle assembly checkpoint. *Curr. Biol.* **21**: 942–947
- Sanger F (1975) The Croonian Lecture, 1975. Nucleotide sequences in DNA. *Proc. R. Soc. Lond., B, Biol. Sci.* **191**: 317–333
- Sanger F, Nicklen S & Coulson AR (1977) DNA sequencing with chain-terminating inhibitors. *Proc. Natl. Acad. Sci. U.S.A.* **74**: 5463–5467
- Santaguida S & Musacchio A (2009) Focus Review The life and miracles of kinetochores. **28**: 2511–2531
- Santaguida S, Tighe A, D'Alise AM, Taylor SS & Musacchio A (2010) Dissecting the role of MPS1 in chromosome biorientation and the spindle checkpoint through the small molecule inhibitor reversine. *J. Cell Biol.* **190**: 73–87

## Supplementary Information

- Santaguida S, Vernieri C, Villa F, Ciliberto A & Musacchio A (2011) Evidence that Aurora B is implicated in spindle checkpoint signalling independently of error correction. *EMBO J.* **30**: 1508–1519
- Scaërou F, Aguilera I, Saunders R, Kane N, Blottière L & Karess R (1999) The rough deal protein is a new kinetochore component required for accurate chromosome segregation in *Drosophila*. *J Cell Sci* **112** ( Pt **21**): 3757–3768
- Scaërou F, Starr DA, Piano F, Papoulas O, Karess RE & Goldberg ML (2001) The ZW10 and Rough Deal checkpoint proteins function together in a large, evolutionarily conserved complex targeted to the kinetochore. *J Cell Sci* **114**: 3103–3114
- Schleiffer A, Maier M, Litos G, Lampert F, Hornung P, Mechtler K & Westermann S (2012) CENP-T proteins are conserved centromere receptors of the Ndc80 complex. *Nat Cell Biol* **14**: 604–613
- Schmidt JC, Arthanari H, Boeszoermyeni A, Dashkevich NM, Wilson-Kubalek EM, Monnier N, Markus M, Oberer M, Milligan RA, Bathe M, Wagner G, Grishchuk EL & Cheeseman IM (2012) The kinetochore-bound Ska1 complex tracks depolymerizing microtubules and binds to curved protofilaments. *Dev. Cell* **23**: 968–980
- Schuck P (2000) Size-distribution analysis of macromolecules by sedimentation velocity ultracentrifugation and lamm equation modeling. *Biophys. J.* **78**: 1606–1619
- Shepherd LA, Meadows JC, Sochaj AM, Lancaster TC, Zou J, Buttrick GJ, Rappalber J, Hardwick KG & Millar JBA (2012) Phosphodependent recruitment of Bub1 and Bub3 to Spc7/KNL1 by Mph1 kinase maintains the spindle checkpoint. *Curr. Biol.* **22**: 891–899
- shyamal (2014) Structural studies on human RZZ and Cln3p. : 1–145
- Sironi L, Mapelli M, Knapp S, De Antoni A, Jeang K-T & Musacchio A (2002) Crystal structure of the tetrameric Mad1-Mad2 core complex: implications of a 'safety belt' binding mechanism for the spindle checkpoint. *EMBO J.* **21**: 2496–2506
- Sivaram MVS, Wadzinski TL, Redick SD, Manna T & Doxsey SJ (2009) Dynein light intermediate chain 1 is required for progress through the spindle assembly checkpoint. *EMBO J.* **28**: 902–914
- Smith DA, Baker BS & Gatti M (1985) Mutations in genes encoding essential mitotic functions in *Drosophila melanogaster*. *Genetics* **110**: 647–670
- Stagg SM, Gürkan C, Fowler DM, LaPointe P, Foss TR, Potter CS, Carragher B & Balch WE (2006) Structure of the Sec13/31 COPII coat cage. *Nature* **439**: 234–238
- Starr DA, Saffery R, Li Z, Simpson AE, Choo KH, Yen TJ & Goldberg ML (2000) HZWint-1, a novel human kinetochore component that interacts with HZW10. *J Cell Sci* **113** ( Pt **11**): 1939–1950

## Supplementary Information

- Starr DA, Williams BC, Hays TS & Goldberg ML (1998) ZW10 Helps Recruit Dynactin and Dynein to the Kinetochore. : 1–12
- Starr DA, Williams BC, Li Z, Etemad-Moghadam B, Dawe RK & Goldberg ML (1997) Conservation of the centromere/kinetochore protein ZW10. *J. Cell Biol.* **138**: 1289–1301
- Stucke VM, Baumann C & Nigg EA (2004) Kinetochore localization and microtubule interaction of the human spindle checkpoint kinase Mps1. *Chromosoma* **113**: 1–15
- Sudakin V, Chan GK & Yen TJ (2001) Checkpoint inhibition of the APC/C in HeLa cells is mediated by a complex of BUBR1, BUB3, CDC20, and MAD2. *J. Cell Biol.* **154**: 925–936
- Tanaka K (2013) Regulatory mechanisms of kinetochore-microtubule interaction in mitosis. *Cell. Mol. Life Sci.* **70**: 559–579
- Tanaka TU (2010) Kinetochore-microtubule interactions: steps towards bi-orientation. *EMBO J.* **29**: 4070–4082
- Tien JF, Umbreit NT, Gestaut DR, Franck AD, Cooper J, Wordeman L, Gonen T, Asbury CL & Davis TN (2010) Cooperation of the Dam1 and Ndc80 kinetochore complexes enhances microtubule coupling and is regulated by aurora B. *J. Cell Biol.* **189**: 713–723
- Tripathi A, Ren Y, Jeffrey PD & Hughson FM (2009) Structural characterization of Tip20p and Dsl1p, subunits of the Dsl1p vesicle tethering complex. *Nature Structural & Molecular Biology* **16**: 114–123
- Vanoosthuyse V & Hardwick KG (2009) A novel protein phosphatase 1-dependent spindle checkpoint silencing mechanism. *Curr. Biol.* **19**: 1176–1181
- Vanoosthuyse V, Valsdottir R, Javerzat J-P & Hardwick KG (2004) Kinetochore targeting of fission yeast Mad and Bub proteins is essential for spindle checkpoint function but not for all chromosome segregation roles of Bub1p. *Mol. Cell. Biol.* **24**: 9786–9801
- Varma D, Monzo P, Stehman SA & Vallee RB (2008) Direct role of dynein motor in stable kinetochore-microtubule attachment, orientation, and alignment. *J. Cell Biol.* **182**: 1045–1054
- Varma D, Wan X, Cheerambathur D, Gassmann R, Suzuki A, Lawrimore J, Desai A & Salmon ED (2013) Spindle assembly checkpoint proteins are positioned close to core microtubule attachment sites at kinetochores. *J. Cell Biol.* **202**: 735–746
- Vaughn JL, Goodwin RH, Tompkins GJ & McCawley P (1977) The establishment of two cell lines from the insect *Spodoptera frugiperda* (Lepidoptera; Noctuidae). *In Vitro* **13**: 213–217
- Wang H, Hu X, Ding X, Dou Z, Yang Z, Shaw AW, Teng M, Cleveland DW, Goldberg ML, Niu L & Yao X (2004) Human Zwint-1 specifies localization of Zeste White 10 to kinetochores and is essential for mitotic checkpoint signaling. *J. Biol. Chem.* **279**: 54590–54598



## Supplementary Information

- Wang Z (2004) Three Classes of Genes Mutated In Colorectal Cancers with Chromosomal Instability. *Cancer Research* **64**: 2998–3001
- Warburton PE, Cooke CA, Bourassa S, Vafa O, Sullivan BA, Stetten G, Gimelli G, Warburton D, Tyler-Smith C, Sullivan KF, Poirier GG & Earnshaw WC (1997) Immunolocalization of CENP-A suggests a distinct nucleosome structure at the inner kinetochore plate of active centromeres. *Current Biology* **7**: 901–904
- Weaver BAA & Cleveland DW (2006) Does aneuploidy cause cancer? *Curr. Opin. Cell Biol.* **18**: 658–667
- Wei RR, Al-Bassam J & Harrison SC (2007) The Ndc80/HEC1 complex is a contact point for kinetochore-microtubule attachment. *Nature Structural & Molecular Biology* **14**: 54–59
- Welburn JPI, Grishchuk EL, Backer CB, Wilson-Kubalek EM, Yates JR & Cheeseman IM (2009) The human kinetochore Ska1 complex facilitates microtubule depolymerization-coupled motility. *Dev. Cell* **16**: 374–385
- Welburn JPI, Vleugel M, Liu D, Yates JR, Lampson MA, Fukagawa T & Cheeseman IM (2010) Aurora B phosphorylates spatially distinct targets to differentially regulate the kinetochore-microtubule interface. *Mol. Cell* **38**: 383–392
- Westhorpe FG, Tighe A, Lara-Gonzalez P & Taylor SS (2011) p31 comet-mediated extraction of Mad2 from the MCC promotes efficient mitotic exit. *J Cell Sci* **124**: 3905–3916
- Whyte J, Bader JR, Tauhata SBF, Raycroft M, Hornick J, Pfister KK, Lane WS, Chan GK, Hinchcliffe EH, Vaughan PS & Vaughan KT (2008) Phosphorylation regulates targeting of cytoplasmic dynein to kinetochores during mitosis. *J. Cell Biol.* **183**: 819–834
- Williams BC, Karr TL, Montgomery JM & Goldberg ML (1992) The Drosophila l(1)zw10 gene product, required for accurate mitotic chromosome segregation, is redistributed at anaphase onset. *J. Cell Biol.* **118**: 759–773
- Williams BC, Li Z, Liu S, Williams EV, Leung G, Yen TJ & Goldberg ML (2003) Zwilch, a new component of the ZW10/ROD complex required for kinetochore functions. *Molecular Biology of the Cell* **14**: 1379–1391
- Winn MD, Ballard CC, Cowtan KD, Dodson EJ, Emsley P, Evans PR, Keegan RM, Krissinel EB, Leslie AGW, McCoy A, McNicholas SJ, Murshudov GN, Pannu NS, Potterton EA, Powell HR, Read RJ, Vagin A & Wilson KS (2011) Overview of the CCP4 suite and current developments. *Acta Crystallogr. D Biol. Crystallogr.* **67**: 235–242
- Wojcik E, Basto R, Serr M, Scaërrou F, Karess R & Hays T (2001) Kinetochore dynein: its dynamics and role in the transport of the Rough deal checkpoint protein. *Nat Cell Biol* **3**: 1001–1007
- Yamagishi Y, Yang C-H, Tanno Y & Watanabe Y (2012) MPS1/Mph1 phosphorylates the kinetochore protein KNL1/Spc7 to recruit SAC components. *Nat Cell Biol* **14**: 746–752

## Supplementary Information

Yeh JI & Hol WG (1998) A flash-annealing technique to improve diffraction limits and lower mosaicity in crystals of glycerol kinase. *Acta Crystallogr. D Biol. Crystallogr.* **54**: 479–480

Zhang G, Lischetti T, Hayward DG & Nilsson J (2015) Distinct domains in Bub1 localize RZZ and BubR1 to kinetochores to regulate the checkpoint. *Nat Commun* **6**: 7162

Zinkowski RP, Meyne J & Brinkley BR (1991) The centromere-kinetochore complex: a repeat subunit model. *J. Cell Biol.* **113**: 1091–1110

## 8 Supplementary Information

**Table 19: List of all crosslinks within the RZZ complex**

| <b>Protein 1</b> | <b>Protein 2</b> | <b>aa position<br/>in protein 1</b> | <b>aa position<br/>in protein 2</b> |
|------------------|------------------|-------------------------------------|-------------------------------------|
| Rod              | Zw10             | 859                                 | 130                                 |
| Rod              | Zw10             | 946                                 | 74,149                              |
| Zw10             | Rod              | 390                                 | 1307                                |
| Zwilch           | Rod              | 191                                 | 240                                 |
| Rod              | Zwilch           | 2189                                | 527                                 |
| Zw10             | Rod              | 624                                 | 1031                                |
| Rod              | Zw10             | 946                                 | 152                                 |
| Rod              | Zw10             | 1665                                | 130                                 |
| Zw10             | Rod              | 528                                 | 1081                                |
| Rod              | Zw10             | 916                                 | 777                                 |
| Zwilch           | Rod              | 191                                 | 239                                 |
| Zw10             | Rod              | 45                                  | 859                                 |
| Zw10             | Rod              | 444                                 | 1413                                |
| Rod              | Zwilch           | 437                                 | 190                                 |
| Zwilch           | Rod              | 326                                 | 739                                 |
| Zw10             | Rod              | 35                                  | 1430                                |
| Rod              | Zw10             | 1029                                | 624                                 |
| Rod              | Zw10             | 870                                 | 157                                 |
| Rod              | Zw10             | 1031                                | 624                                 |
| Rod              | Zw10             | 946                                 | 143                                 |
| Zwilch           | Rod              | 201                                 | 946                                 |
| Zwilch           | Rod              | 326                                 | 705                                 |
| Zw10             | Rod              | 129                                 | 859                                 |
| Zw10             | Rod              | 624                                 | 1092                                |
| Zw10             | Rod              | 624                                 | 1063                                |
| Rod              | Zwilch           | 1814                                | 326                                 |
| Zwilch           | Zwilch           | 317                                 | 341                                 |
| Rod              | Rod              | 1653                                | 1646                                |
| Rod              | Rod              | 1653                                | 1648                                |
| Rod              | Rod              | 1731                                | 1738                                |
| Zw10             | Zw10             | 758                                 | 777                                 |
| Zw10             | Zw10             | 35                                  | 74,149                              |
| Rod              | Rod              | 1307                                | 1316                                |
| Rod              | Rod              | 1307                                | 1318                                |
| Rod              | Rod              | 240                                 | 406                                 |
| Zwilch           | Zwilch           | 326                                 | 341                                 |
| Zwilch           | Zwilch           | 176                                 | 527                                 |
| Rod              | Rod              | 831                                 | 1648                                |
| Zw10             | Zw10             | 35                                  | 152                                 |
| Zw10             | Zw10             | 597                                 | 484                                 |
| Zwilch           | Zwilch           | 318                                 | 341                                 |

Supplementary Information

|        |        |      |        |
|--------|--------|------|--------|
| Rod    | Rod    | 1021 | 1051   |
| Rod    | Rod    | 946  | 1051   |
| Rod    | Rod    | 24   | 406    |
| Zw10   | Zw10   | 96   | 17     |
| Rod    | Rod    | 2093 | 2135   |
| Zwilch | Zwilch | 326  | 341    |
| Zw10   | Zw10   | 152  | 74,149 |
| Rod    | Rod    | 1081 | 1086   |
| Rod    | Rod    | 1031 | 1081   |
| Rod    | Rod    | 1031 | 1051   |
| Rod    | Rod    | 1021 | 1076   |
| Rod    | Rod    | 1731 | 1738   |
| Rod    | Rod    | 1665 | 1646   |
| Rod    | Rod    | 971  | 1493   |
| Rod    | Rod    | 430  | 406    |
| Rod    | Rod    | 1092 | 1081   |
| Rod    | Rod    | 971  | 1493   |
| Zwilch | Zwilch | 201  | 540    |
| Rod    | Rod    | 1653 | 1645   |
| Rod    | Rod    | 1029 | 1051   |
| Zw10   | Zw10   | 160  | 74,149 |
| Rod    | Rod    | 1493 | 1560   |
| Rod    | Rod    | 1092 | 1085   |
| Rod    | Rod    | 1665 | 1653   |
| Rod    | Rod    | 1731 | 1738   |
| Rod    | Rod    | 1333 | 1367   |
| Rod    | Rod    | 1101 | 1076   |
| Rod    | Rod    | 1493 | 1560   |
| Rod    | Rod    | 1665 | 831    |
| Rod    | Rod    | 1031 | 1081   |
| Rod    | Rod    | 1029 | 1085   |
| Rod    | Rod    | 1031 | 1076   |
| Rod    | Rod    | 1029 | 1081   |
| Rod    | Rod    | 1658 | 701    |
| Zw10   | Zw10   | 96   | 74     |
| Zw10   | Zw10   | 719  | 597    |
| Zwilch | Zwilch | 201  | 540    |
| Rod    | Rod    | 1029 | 1081   |
| Rod    | Rod    | 1031 | 1081   |
| Rod    | Rod    | 377  | 43     |
| Rod    | Rod    | 2093 | 2135   |
| Rod    | Rod    | 1756 | 1658   |
| Rod    | Rod    | 116  | 43     |
| Rod    | Rod    | 1640 | 1648   |
| Rod    | Rod    | 24   | 328    |
| Rod    | Rod    | 964  | 977    |

Supplementary Information

|        |        |      |      |
|--------|--------|------|------|
| Rod    | Rod    | 1092 | 1081 |
| Rod    | Rod    | 1021 | 1086 |
| Rod    | Rod    | 1031 | 1051 |
| Rod    | Rod    | 1768 | 1737 |
| Zwilch | Zwilch | 201  | 530  |
| Rod    | Rod    | 513  | 1031 |
| Rod    | Rod    | 2093 | 2136 |
| Rod    | Rod    | 1031 | 946  |
| Rod    | Rod    | 464  | 430  |
| Rod    | Rod    | 1413 | 1493 |
| Rod    | Rod    | 2093 | 2136 |
| Rod    | Rod    | 971  | 1493 |
| Rod    | Rod    | 1031 | 946  |
| Zwilch | Zwilch | 45   | 24   |
| Rod    | Rod    | 859  | 843  |
| Rod    | Rod    | 1031 | 1085 |
| Rod    | Rod    | 2016 | 503  |
| Zw10   | Zw10   | 390  | 402  |
| Zw10   | Zw10   | 35   | 152  |
| Rod    | Rod    | 946  | 957  |
| Zw10   | Zw10   | 719  | 597  |
| Rod    | Rod    | 2106 | 2145 |
| Rod    | Rod    | 946  | 1021 |
| Zwilch | Zwilch | 201  | 540  |
| Rod    | Rod    | 726  | 705  |
| Zwilch | Zwilch | 326  | 341  |
| Zw10   | Zw10   | 44   | 157  |
| Zwilch | Zwilch | 201  | 530  |
| Rod    | Rod    | 377  | 328  |
| Rod    | Rod    | 1640 | 1731 |
| Rod    | Rod    | 829  | 1648 |
| Rod    | Rod    | 1029 | 946  |
| Rod    | Rod    | 1728 | 1738 |
| Zwilch | Zwilch | 326  | 317  |
| Zw10   | Zw10   | 215  | 130  |
| Rod    | Rod    | 2016 | 503  |
| Rod    | Rod    | 1413 | 1493 |
| Rod    | Rod    | 1728 | 1738 |
| Zw10   | Zw10   | 143  | 130  |
| Rod    | Rod    | 739  | 1658 |
| Rod    | Rod    | 1029 | 1076 |
| Rod    | Rod    | 1728 | 1737 |
| Zwilch | Zwilch | 201  | 527  |
| Rod    | Rod    | 916  | 971  |
| Rod    | Rod    | 1031 | 1076 |
| Rod    | Rod    | 838  | 859  |

Supplementary Information

|        |        |      |      |
|--------|--------|------|------|
| Rod    | Rod    | 2135 | 2143 |
| Zwilch | Zwilch | 52   | 527  |
| Rod    | Rod    | 739  | 701  |
| Rod    | Rod    | 829  | 1646 |
| Rod    | Rod    | 957  | 1051 |
| Rod    | Rod    | 1081 | 1051 |
| Zwilch | Zwilch | 176  | 191  |
| Rod    | Rod    | 1063 | 1031 |
| Rod    | Rod    | 1768 | 1738 |
| Rod    | Rod    | 2093 | 2135 |
| Zw10   | Zw10   | 430  | 484  |
| Rod    | Rod    | 829  | 1665 |
| Rod    | Rod    | 1029 | 1063 |
| Zwilch | Zwilch | 318  | 341  |
| Rod    | Rod    | 1051 | 1086 |
| Zw10   | Zw10   | 705  | 424  |
| Zwilch | Zwilch | 52   | 540  |
| Rod    | Rod    | 770  | 843  |
| Zw10   | Zw10   | 705  | 424  |
| Rod    | Rod    | 127  | 240  |
| Zw10   | Zw10   | 528  | 634  |
| Zwilch | Zwilch | 52   | 201  |
| Rod    | Rod    | 521  | 513  |
| Zwilch | Zwilch | 527  | 540  |
| Zw10   | Zw10   | 44   | 634  |
| Zw10   | Zw10   | 215  | 188  |
| Zwilch | Zwilch | 201  | 540  |
| Zwilch | Zwilch | 201  | 540  |
| Zw10   | Zw10   | 35   | 152  |
| Zwilch | Zwilch | 201  | 540  |
| Rod    | Rod    | 1031 | 1051 |
| Rod    | Rod    | 2093 | 2135 |
| Rod    | Rod    | 1307 | 1316 |
| Zwilch | Zwilch | 326  | 341  |
| Zwilch | Zwilch | 176  | 527  |
| Zwilch | Zwilch | 326  | 341  |
| Rod    | Rod    | 1731 | 1738 |
| Rod    | Rod    | 1653 | 1648 |
| Rod    | Rod    | 1650 | 1645 |
| Rod    | Rod    | 831  | 1650 |
| Rod    | Rod    | 1029 | 1051 |
| Rod    | Rod    | 1731 | 1738 |
| Rod    | Rod    | 1731 | 1738 |
| Rod    | Rod    | 971  | 977  |
| Rod    | Rod    | 1756 | 1658 |
| Rod    | Rod    | 971  | 1493 |

Supplementary Information

|        |        |      |      |
|--------|--------|------|------|
| Rod    | Rod    | 1307 | 1318 |
| Rod    | Rod    | 1658 | 1650 |
| Rod    | Rod    | 946  | 1051 |
| Zwilch | Zwilch | 326  | 317  |
| Rod    | Rod    | 726  | 701  |
| Rod    | Rod    | 1031 | 1081 |
| Rod    | Rod    | 726  | 705  |
| Zw10   | Zw10   | 96   | 74   |
| Rod    | Rod    | 770  | 843  |
| Zwilch | Zwilch | 201  | 540  |
| Rod    | Rod    | 377  | 43   |
| Rod    | Rod    | 24   | 406  |
| Zw10   | Zw10   | 705  | 708  |
| Rod    | Rod    | 829  | 1653 |
| Rod    | Rod    | 1029 | 1081 |
| Rod    | Rod    | 1728 | 1737 |
| Rod    | Rod    | 1665 | 831  |
| Rod    | Rod    | 377  | 328  |
| Rod    | Rod    | 1021 | 1076 |
| Rod    | Rod    | 1731 | 1738 |
| Rod    | Rod    | 726  | 705  |
| Rod    | Rod    | 829  | 1650 |
| Rod    | Rod    | 2016 | 503  |
| Rod    | Rod    | 1756 | 1658 |
| Zwilch | Zwilch | 318  | 341  |
| Rod    | Rod    | 1021 | 1051 |
| Zw10   | Zw10   | 35   | 152  |
| Rod    | Rod    | 1728 | 1738 |
| Rod    | Rod    | 464  | 430  |
| Zw10   | Zw10   | 65   | 17   |
| Zwilch | Zwilch | 308  | 326  |
| Rod    | Rod    | 1031 | 946  |
| Zw10   | Zw10   | 430  | 705  |
| Rod    | Rod    | 2016 | 503  |
| Zw10   | Zw10   | 35   | 157  |
| Zwilch | Zwilch | 561  | 176  |
| Zw10   | Zw10   | 390  | 402  |
| Rod    | Zw10   | 916  | 777  |
| Rod    | Zw10   | 946  | 152  |
| Rod    | Zw10   | 2106 | 17   |
| Zw10   | Rod    | 65   | 1948 |
| Rod    | Zw10   | 859  | 130  |
| Rod    | Zw10   | 870  | 157  |
| Zw10   | Rod    | 624  | 1031 |
| Rod    | Zw10   | 1092 | 634  |
| Rod    | Zw10   | 1031 | 624  |

|     |      |      |     |
|-----|------|------|-----|
| Rod | Zw10 | 1029 | 624 |
|-----|------|------|-----|

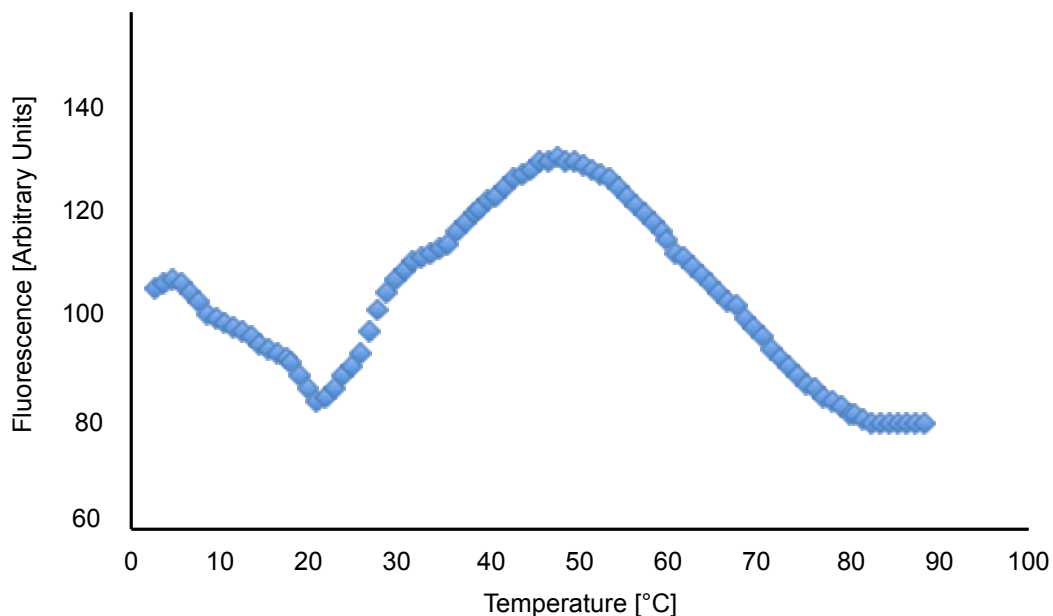


**Figure 50: Thermofluor analysis of the Mini-RZZ complex**

Thermofluor based protein-unfolding curve of the Mini-RZZ complex (Boivin *et al*, 2013). This assay was performed in the RZZ gelfiltration buffer (25 mM Hepes pH 8.5, 250 mM NaCl, 2 mM TCEP). The resulting melting curve is not interpretable.

**Table 20: Confidence values for structural models of RZZ domains**

| Construct                             | C-score (Phyre) | Confident score for rigid fit into the 3D density map EM |
|---------------------------------------|-----------------|----------------------------------------------------------|
| N-ter. ZW10 (73-388)                  | 100%            | 0.82                                                     |
| C-ter. ZW10 (475-779)                 | 100%            | 0.96                                                     |
| Zwilch                                | /               | 0.94                                                     |
| N-ter. $\beta$ -propeller of (49-365) | 96%             | 0.94                                                     |
| NRH domain of Rod (39                 | 75%             | 0.97                                                     |
| Sec39 segment of Rod (1174)           | 100%            | 0.92                                                     |
| C-ter. Rod (1798-2192)                | 86%             | 0.85                                                     |



Supplementary Information

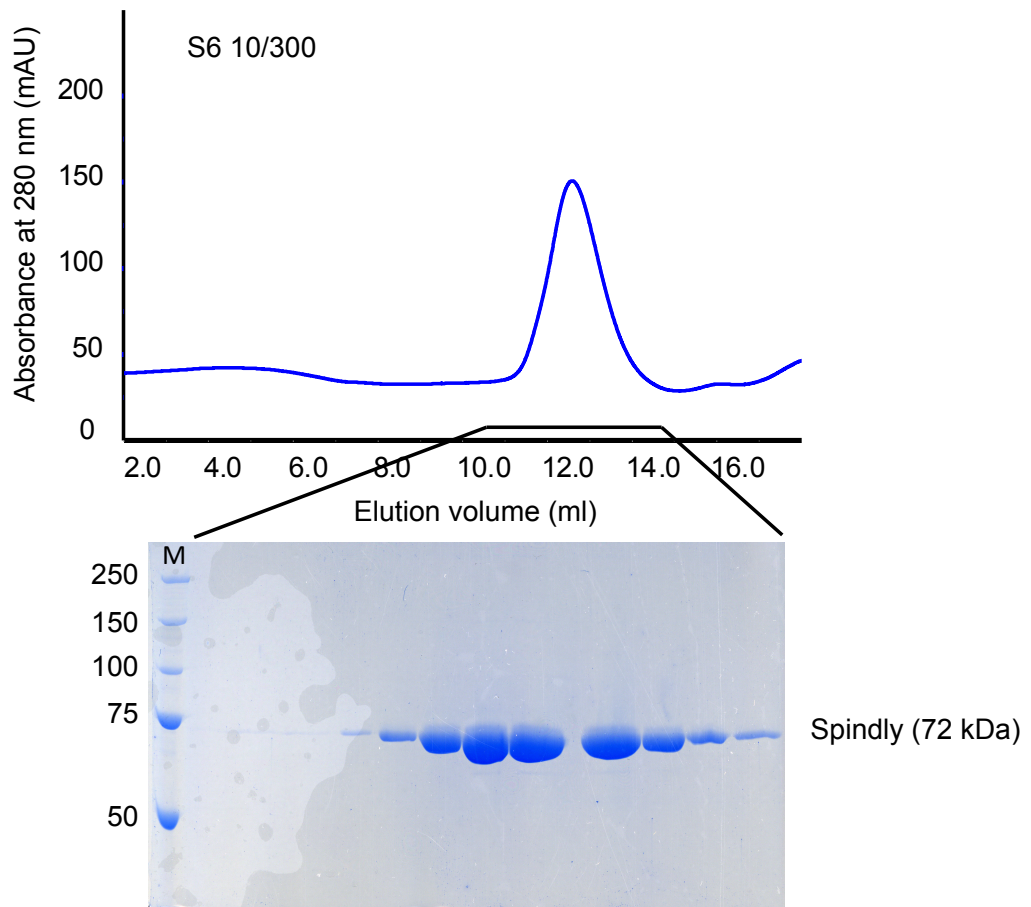


**Figure 51: Final step of Spindly purification**

Size exclusion chromatography of Spindly using a Superose 6 10/300 column (GE Healthcare, Germany).

# Supplementary Information

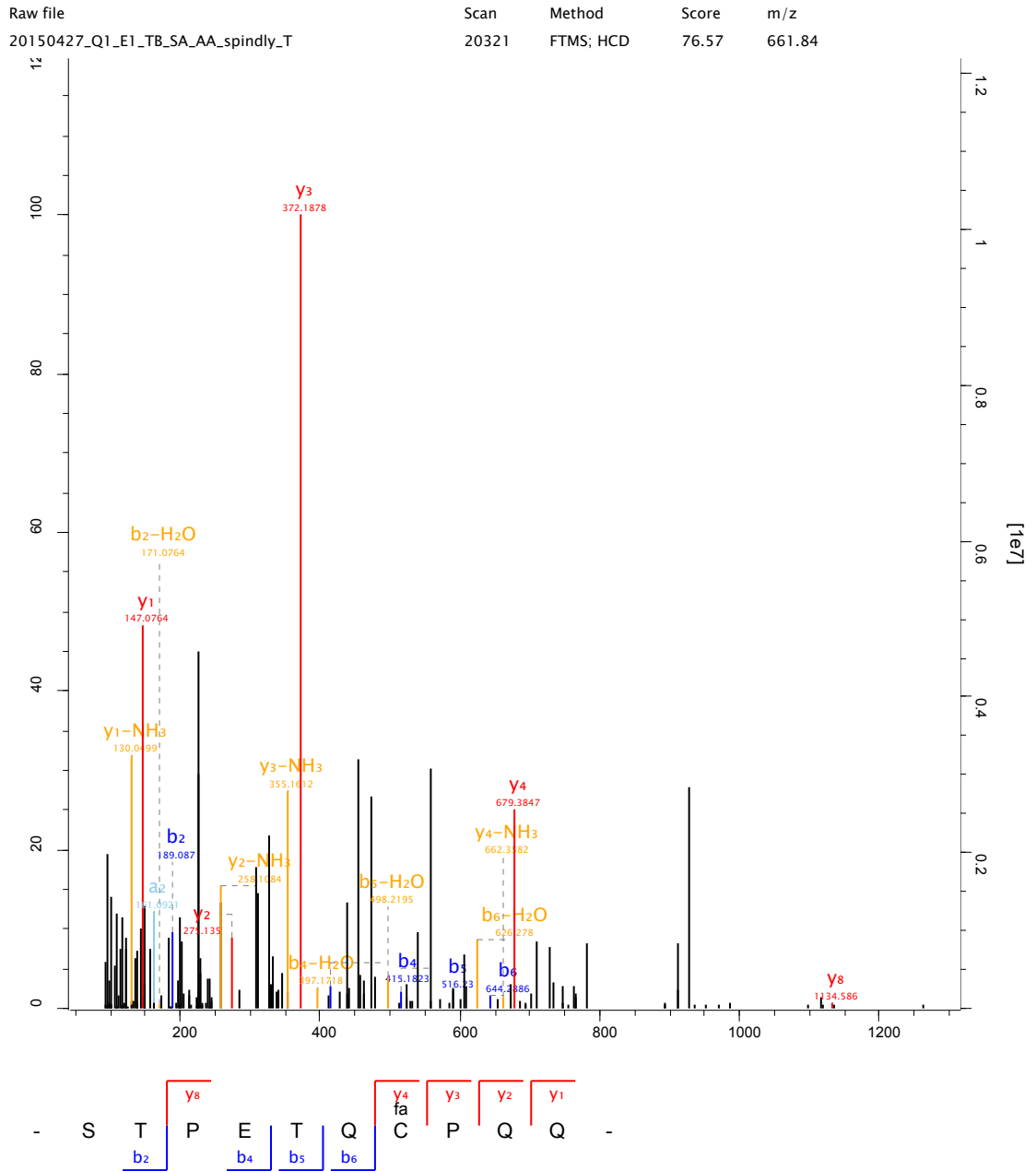


**Figure 52: Spindly farnesylation after FTase and FPP incubation**

LC-MS/MS analysis of a fraction from SEC containing putatively farnesylated Spindly upon 1,5 h RT incubation with FTase and FPP.

## **Acknowledgements**

I want to owe my deepest gratitude to Professor Andrea Musacchio for a highly interesting and challenging topic and for his excellent guidance and support.

Special thanks also go to Professor Roland Winter as my second supervisor.

Thanks to all the people that contributed to this project either by collaborations or by providing proteins: Dr. Ingrid Vetter, Dr. Jenny Keller, Annemarie Wehenkel, Sabine Wohlgemuth, Dr. Shyamal Mosalaganti, Dr. Franz Herzog, Dr. Stefano Maffini, Dr. Tanja Bange, Franziska Müller, Dr. John Weir, Dr. Petra Janning, Dr. Charlotte Smith, Dr. Siva Jeganathan, Dr. Arsen Petrovic, Claudia Breit, Dr. Maria Thanasoula Dr, Marta Matuzzi and Dr. Alex Faesen.

I am especially very grateful to Dr. Jenny Keller, Dr. Stefano Maffini, Dr. Tanja Bange and Dr. Alex Faesen for support with experiments and fruitful discussions.

Thanks to the DPF for cloning many constructs.

I am very grateful to my TAC supervisors Prof. Dr. Roger Goody, Dr. Ingrid Vetter and Prof. Geert Kops for helpful discussions and support.

Thanks to the IMPRS and especially to Christa Hornemann for numerous advanced training possibilities and her warm support.

I want to thank all previous and present colleagues for their support, helpful discussions and creating a nice working atmosphere.

Especially, I want to thank Patricia Stege, Carolin Anders, Dr, Shehab Ismail, Jana Seidel and Dr. Ann Katrin Greifenberg for making this institute a better place.

I am especially grateful to Frederik, my parents and my brother for their patience and for supporting and encouraging me any time.

## **Affirmation**

I hereby declare that this thesis and the work reported herein with the title was composed by and originated entirely from me.

Information derived from the published and unpublished work of others has been acknowledged in the text and references are given.

The presented work has not been submitted to another examination board.

## **Eidesstattliche Erklärung**

Hiermit versichere ich, dass ich die vorliegende Arbeit selbstständig und nur unter Verwendung der angegebenen Hilfsmittel angefertigt habe.

Alle wörtlichen oder inhaltlichen Zitate sind als solche gekennzeichnet und im Literaturverzeichnis aufgeführt.

Diese Arbeit wurde noch keiner Prüfungskommission zur Begutachtung vorgelegt.

Dortmund, September 2015

---

Anika Altenfeld